NITRATE, PHOSPHATE AND FLUORIDE REMOVAL FROM WATER USING ADSORPTION PROCESS

By

TANJINA NUR

A Thesis submitted in fulfilment for the degree of

Doctoral of Philosophy

School of Civil and Environmental Engineering

Faculty of Engineering & Information Technology

University of Technology, Sydney

New South Wales, Australia

June 2014.

CERTIFICATE OF AUTHORSHIP/ ORIGINALITY

I certify that the work in this thesis has not previously been submitted for a degree nor has it been submitted as part of requirements for a degree except as fully acknowledged within the text.

I also certify that the thesis has been written by me. Any help that I have received in my research work and the preparation of the thesis itself has been acknowledged. In addition, I certify that all information sources and literature used are indicated in the thesis.

Signature of Candidate:

Tanjina Nur

June 2014.

Acknowledgement

I would like to say my whole-heartily thanks to several individuals who in one way or another contributed and extended their valuable support for the preparation and completion of this dissertation.

Atfirst I would like to express my deep appreciation and gratitude to my principle supervisor, Professor Saravanamuth Vigneswaran, for the patient guidance and unwearying mentorship and consideration he provided to me, all the way from the start of the PhD degree through to completion of this degree. I am sure that this dissertation would not have been possible without his support, understanding and encouragement. My second deepest thanks go to my co-supervisor, Dr. Paripurnanda Loganathan for his tremendous help and support through my whole PhD study. I would also like to thank my co- supervisors Drs Jaya Kandasamy and Vinh Nguyen for their help and support. I would also like to thank my colleagues and lab mates Dr. Jeong, Danious, Sukanya, Gayathri, Chung in CTWW. I had a wonderful time with these guys. I would like to give a special mention to my team member and Senior Technical Officer of Environmental Engineering Laboratories, Md Abu Hasan Johir who had always been supportive in sharing his valuable time and ideas for my research.

I would like to thank the Australian Federal Government for the Australian Postgraduate Award (APA) to support my study.

My most profound thanks, my most heartfelt appreciation; my deepest gratitude goes to my family, without whom none of this could have been accomplished. At first, I heartily thank my mother Monju Monowara for her blessings, love, care, sacrifices, suggestions, help and support not only for my PhD study for my whole life. She spent almost 7 months in Sydney and looked after my son and solved all problems, so that I

could concentrate on my study. It was my parents dream for me to get Doctorate degree and today I am going to get this degree because of them. It is my bad luck that my father Late Md. Nurullah could not able to see this day, but I believed his blessings were always with me at every step.

I will never be able to thank my loving husband Noore Alam Patwary, who made me believe in myself and encouraged me through the whole process of research and always stayed beside me during my struggling periods. Thank you my dear husband for your selfless support in sharing the parenting and household burdens and for loving me the way you do. I would like to thank my cutest and dearest son, Aarshan Wajdi Noor who gave me every reason to complete this PhD through all hardships with happy and smiley face. He is my sunshine and great motivation for my life and study. I would also like to thank my father in law, Emdad Ullah Patwary and mother in law, Setera Begum for their love and blessings. My heartily thanks goes to my sweet brother Maruf Hasan and lovely sister Tahsiba Nur for their unconditional love and support and let my mother to stay with me and bear all the difficulties alone.

Last but not least, I would like to thank my sister in law, Eshita Mahmood, my whole in laws family and my uncle Shakwat Ullah Chowdhury for their love and support all the time.

Dedication

To my father Late Md. Nurullah and mother Monju Monowara

Journal papers Published

1. **T. Nur**, M.A.H. Johir, P. Loganathan, S. Vigneswaran, J. Kandasamy. (2012). Effectiveness of purolite A500PS and A520E ion exchange resins on the removal of nitrate and phosphate from synthetic water, Desalination and Water Treatment 47: 50 - 58.

2. **T. Nur**, W.G. Shim, M.A.H. Johir, S. Vigneswaran & J. Kandasamy. (2013). Modelling of phosphorus removal by ion-exchange resin (Purolite FerrIX A33E) in fixed-bed column experiments, Desalination and Water Treatment 52: 784 - 790.

3. **T. Nur**, M.A.H. Johir, P. Loganathan, T. Nguyen, S. Vigneswaran, J. Kandasamy. (2014). Phosphate removal from water using an iron oxide impregnated strong base anion exchange resin, Journal of Industrial and Engineering Chemistry 20: 1301 - 1307.

4. **T. Nur**, W.G.Shim, P. Loganathan, S. Vigneswaran, J. Kandasamy. (2014). Nitrate removal using Purolite A520E ion exchange resin: Batch and fixed-bed column adsorption modelling, International Journal of Environmental Science and Technology, doi 10.1007/s13762-014-0510-6.

5. **T. Nur**, P. Loganathan, T.C. Nguyen, S. Vigneswaran, J. Kandasamy. (2014). Batch and column adsorption and desorption of fluoride using hydrous ferric oxide: Solution chemistry and modeling, Chemical Engineering Journal 247: 93 - 102.

Conference papers and presentation

1. **T. Nur**, S. Vigneswaran, J. Kandasamy (2011). Treatment performance for stormwater harvesting and reuse, 8th IWA International Conference on Water Reclamation & Reuse , Barcelona, Spain,26-29 September, 2011.

2. M.A.H. Johir, **T. Nur**, Saravanamuthu Vigneswaran, Jaya Kandasamy and Chia-Yuan Chang (2011). Recovery of nutrients (P and N) as valuable material from wastewater by ion exchange resin, CESE Conference, Taiwan, 25-30 September, 2011.

3. **T. Nur**, W.G. Shim, M.A.H. Johir, S. Vigneswaran, J. Kandasamy (2012). Modelling of phosphorus removal by ion exchange resin (purolite FerrIX A33E) in column experiments, 5th CESE Conference, Melbourne, Australia, 9 - 13 September, 2012.

4. T. Nur, P. Loganathan, S. Vigneswaran, J. Kandasamy (2013). Removal of fluoride from water using Ferric hydroxide oxide (HFO) in batch and fixed-bed column experiments, 6th CESE Conference, Daegu, South Korea, 29th October -2nd November, 2013.

TABLE OF CONTENTS

LIST OF FIGURES

CHAPTER 2

CHAPTER 3

CHAPTER 6

CHAPTER 8

LIST OF TABLES

CHAPTER 2

CHAPTER 3

CHAPTER 6

CHAPTER 8

Nomenclature

C = the bulk phase concentration (mg/L)

Ca (OH) $_2$) = Calcium hydroxide

C_e = equilibrium concentration of adsorbate (mg/L)

C_0 = initial concentration of adsorbate (mg/L)

C_o = inlet adsorbate concentration (mg/L)

C_s = the concentration on the external surface (mg/L)

C_t = concentration of adsorbate at time t (mg/L)

C_t = outlet adsorbate concentration at time t (mg /L)

Ca^{2+} = Calcium

Cl^- = chloride

CO_3^{2-} = carbonate

COD = chemical oxygen demand

CR = Chemical reduction

D_L = the axial dispersion coefficient (m^2/s)

D_m = molecular diffusion coefficient

D_s = the surface diffusion coefficient (m^2/s)

Dowex 21k XLT = strong base anion exchange resin composed of Styrene-DVB

EDR = electrodialysis reversal

ϵ_b = the bed voidage

F = Fluoride

F = linear velocity calculated by dividing the filtration velocity by the column section area (cm/min)

Fe^{3+} = iron (III)

FTIR = Fourier transform infrared spectroscopy

FeO = zero-valent iron

g/L = gram per litre

$H_2PO_4^-$=dihydrogen phosphate ion

HCl = hydrochloric acid

HCO_3^- = bicarbonate

HFO = iron (iii) oxide

HSDM = Homogeneous surface diffusion model

H_4O_4Zr = Zirconium (IV) hydroxide

HNO_3 = Nitric acid

hr = hours

K^+ = Potassium

k_f = the external mass transfer coefficient (m/s)

K_F = Freundlich constants (mg/g)

K_L = Langmuir constant related to the energy of adsorption (L/mg)

k_{Th} = Thomas rate constant (mL/min.mg)

k_{YN} = rate velocity constant (1/min)

k_1 = equilibrium rate constant of pseudo-first-order sorption (1/min)

k_2 = equilibrium rate constant of pseudo-second-order (1/min)

k_{AB} = kinetic constant, (L/mg.min)

KNO_3 = Potassium nitrate

KH_2PO_4 = Monopotassium phosphate

KCl = Potassium chloride

LDHs = layered double hydroxides

M = mass of dry adsorbent (g)

MBR = membrane bioreactor

mg N/L = milligram nitrogen per litre

mg NO_3^- / L = mg nitrate per litre

mg N/g = milligram nitrogen per gram

mg P/L = milligram phosphorus per litre

mg PO_4^{3-} / g = mg phosphate per gram

mg P/g = milligram phosphorus per gram

mg F/L = milligram fluoride per litre

mg F/g = milligram fluoride per gram

min = minutes

mL/min = millilitre per minute

m/h = meter per hour

$MgCl_2.6H_2O$ = Magnesium Chloride Hexahydrate

Mg0 = zero-valent magnesium

μ = Solution viscosity

N = nitrogen

Na^+ = sodium

NaCl = sodium chloride

NaF = sodium fluoride

NaOH = sodium hydroxide

Na_2SO_4 = sodium sulphate

Na_2CO_3= sodium carbonate

$NaHCO_3$ = sodium bicarbonate

$NaNO_3$ = sodium nitrate

NO_3^- = nitrate

$(NH_4)_2SO_4$ = ammonium sulphate

N_o = saturation adsorbate concentration (mg/L)

n = Freundlich constant

Pe_L = Peclet number for axial dispersion

Pe_m = Peclet number for particle

ρ_p = the apparent density of the adsorbent, kg/m^3

P = phosphorus

pH = measure of the acidity or basicity of an aqueous solution

Purolite A520E = macroporous strong base anion exchange resin

Purolite A500PS = macroporous strong base anion exchanger onsists of styrene–divinylbenzene with a trimethylamine functional group

Purolite FerrIX A33E = hybrid strong base anion exchange resin with quaternary ammonium functional groups blended with hydrous iron oxide

PZC = point of zero charge

Q = Flow rate (cm3/s)

q = surface concentration at any radial distance (r) (mg /g)

q_e = amount of adsorbate adsorbed per unit mass of adsorbent (mg/g)

q_{max} = maximum amount of adsorbate adsorbed per unit mass of adsorbent (mg/g)

q_o= equilibrium adsorbate uptake per g of adsorbent (mg/g)

R = the particle radius of adsorbent (m)

RO = reverse osmosis

rpm = Revolutions per minute

Sc = Schmidt number and

SEM = Scanning electron microscopy

SO_4^{2-} = sulphate

t = filtration time (min).

τ = the time required for 50% adsorbate breakthrough (min)

t = the time (min)

τ = the tortuosity

V = volume of the solution (L)

V = the interstitial velocity (m/s)

V_s = superficial velocity (m/s)

z = the axial coordinate (m)

XRD = X-ray diffraction

XPS = X-ray photoelectron spectroscopy

Z = bed depth of column (cm)

ZVI = Zero-valent iron

Abstract

The wastewater treatment industry has identified the discharge of inorganic anions such as nitrate, phosphate and fluoride into waterways as a risk to the natural environment and human health. Of the various methods for removing these anions, adsorption/ion exchange methods are promising because they are simple, efficient, economical and result in less sludge production and therefore experience minimal disposal problems.

Of the four ion exchange resins tested (Purolite A520E, Purolite A500PS, Purolite FerrIX A33E and Dowex 21k XLT), Purolite A520E emerged as the most efficient adsorbent, having a high adsorption capacity for the removal of nitrate from water. Purolite A520E proved to be the most efficient at removing nitrate (84%) followed by Dowex 21k (81%), and Purolite A500PS (75%) within 120 min. The lowest removal efficiency was found for Purolite FerrIX A33E (48%).The Langmuir adsorption capacity was 33 mg N/g for this resin and the highest column adsorption capacity was 21.3 mg N/g at an inlet concentration of 20 mg N/L, 12 cm bed height and 2.5 m/h filtration velocity. The kinetics of nitrate adsorption by Purolite A520E in the batch study was satisfactorily described using pseudo-first-order, pseudo-second-order and HSDM models. The experimental and Thomas models predicted breakthrough adsorption capacities (12.0-13.5 mg N/g and 8.2-9.7 mg N/g, respectively) agreed fairly well. The presence of other co-ions such as SO_4^{2-}, F^- , Cl^- and PO_4^{3-} did not compete much with nitrate at equal concentrations for adsorption on Purolite A520E; only high concentrations reduced the effectiveness of this resin's ability to adsorb nitrate. Moreover, at all nitrate to phosphate ratios in solution, the ratio of nitrate to phosphate adsorbed was higher for Purolite A520E which suggested that the nitrate selectivity for adsorption was higher than phosphate. It was found that solution pH had little effect on nitrate adsorption in the pH

range 5-8. Moreover, Purolite A520E was regenerated and used at least three times without significantly reducing the adsorption capacity.

Of the six adsorbents tested in a batch study(Purolite A520E, Purolite A500PS, Purolite FerrIX A33E, Dowex 21k XLT, HFO (iron (iii) oxide $HFeO_2$) and Zirconium (IV) hydroxide (H_4O_4Zr)), Purolite FerrIX A33E had the highest phosphate removal efficiency (98%) followed by Dowex 21k (91%), Zirconium (IV) hydroxide (89%), Purolite A500PS (75%) and Purolite A520E (69%) within 240 min. HFO was found to have the least removal efficiency (36%). The batch adsorption isotherm data for Purolite FerrIX A33E was satisfactorily explained using the Langmuir, Freundlich and Tempkin isotherm models. Meanwhile the kinetic adsorption data fitted reasonably well to the pseudo-second-order, Elovich and intraparticle diffusion models. The Langmuir maximum adsorption capacity of Purolite FerrIX A33E was 48 mg P/g which constituted one of the highest phosphorus adsorption capacities reported in the literature. Three empirical models - Bohart-Adams, Thomas and Yoon-Nelson - and a numerical model based on the advection-dispersion equation satisfactorily described phosphate adsorption behaviour in a fixed-bed column containing Purolite FerrIX A33E. The phosphate adsorption capacity of the column was estimated by: firstly, the Thomas model to be 22.7 mg P/g; and secondly, the breakthrough curve calculation to be 16.3 mg/g at the inlet concentration of 30 mg P/L, 12 cm bed height and 10 m/h filtration velocity. pH had little effect on phosphate adsorption by Purolite FerrIX in the pH range 4 – 10.

The decreasing order of the anions' competition with phosphate was as follows: $SO_4^{2-} > Cl^- > NO_3^- > F^-$. The Purolite FerrIX A33E resin was regenerated by leaching the adsorbed phosphate with 1 M NaOH solution and reused at least four times without significantly reducing the adsorption capacity. This phosphorus desorbed was recovered as struvite by adding magnesium chloride ($MgCl_2.6H_2O$) and ammonium sulphate

$(NH_4)_2SO_4$ at the molar ratio of phosphate, ammonium and magnesium of 1:1:1. Calcium hydroxide (Ca (OH) $_2$) was added to the desorbed solution to recover phosphorus as hydroxyapatite at the molar ratio of phosphate and calcium of 1:0.5 and 1:2. The XRD and FTIR analyses confirmed the recovered compounds were struvite and hydroxyapatite. These compounds' phosphorous content was 12-14% which was similar to the phosphorus content of struvite and hydroxyapatite.

Hydrous ferric oxide (HFO) had the highest fluoride adsorption capacity of seven adsorbents tested (Purolite A520E, Purolite A500PS, Purolite FerrIX A33E, Dowex 21k, HFO (iron (iii) oxide $HFeO_2$), Zirconium (IV) hydroxide (H_4O_4Zr) and α-Alumina (Al_2O_3)). Among the seven adsorbents, HFO had the highest fluoride removal efficiency (56%) followed by Dowex 21k (52%), Zirconium (IV) hydroxide (38%), Purolite A502PS (35%), Purolite FerrIX A33E (29%) and Purolite A520E (25%) within 120 min. The lowest removal efficiency was found for α-Alumina (4%). The batch adsorption of fluoride on HFO was satisfactorily explained using both the Langmuir and Freundlich isotherms while the column adsorption data fitted reasonably well to the Thomas model. However, by using an artificial neural network approach the model's capability did improve. The Langmuir maximum adsorption capacity at pH 6.5 was 6.71 mg F/g and the highest column breakthrough adsorption capacity was 7.06 mg F/g at the inlet concentration of 30 mg F/L, 12 cm bed height, pH 5 and 2.5 m/h filtration velocity. The adsorption capacity predicted by the Thomas model was also highest (12.7 mg F/g) for these experimental conditions. The kinetic data concerning the fluoride adsorption on HFO was better described with the pseudo-second-order model compared to the pseudo-first-order model. The HFO was regenerated by leaching the adsorbed fluoride with 0.1 M NaOH solution and reused for at least three times. However, the fluoride adsorption capacity declined with repeated use.

CHAPTER 1

INTRODUCTION

Chapter 1

Introduction

1.1. Background of research

As the global supplies of clean water diminish and people's demand for water rises, advanced wastewater treatment is becoming an international focus for the rational use of scarce water resources and as a means of safeguarding aquatic environments from the harm caused by wastewater disposal. Reclamation and reuse of treated wastewater have become important topics in the sustainable management of water because high quality water resources are becoming increasingly limited. In recent decades the wastewater treatment industry has identified the discharge of inorganic anions such as nitrate, phosphate and fluoride into waterways as posing a major risk to the natural environment and also proving dangerous to humans. On the other hand, the recovery of phosphorus from wastewaters is very important to minimise the future global phosphorus scarcity that is likely to be one of the greatest challenges of the twenty-first century. It is necessary to find appropriate and cost effective methods to remove phosphorus from water as well as recover it so that it can be used for fertilisers and to compensate the global exhaustion of high-grade phosphate ores.

1.1.1. Adverse effects of nitrate, phosphate and fluoride

Nitrate and phosphate are essential nutrients for the growth of plants and micro-organisms. High concentrations of these nutrients in water, however, can cause

eutrophication which is a serious environmental problem as it can lead to abundant development of aquatic plants, growth of algae, harm fish and other aquatic life and disturb the ecological balance of organisms present in water (Jorgensen and Williams, 2001). Furthermore, the presence of excessive nitrate ions in drinking water is a potential public health hazard because it can cause infant methemoglobinemia, otherwise known as “blue baby” syndrome (Fewtrell, 2004). It has been noted that the formation of nitrate compounds in the stomach is potentially carcinogenic (Chiu et al., 2007). (Chinoy, 1991; Harrison, 2005; Kumar et al., 2009; Meenakshi, 2006). Due to the above problems the three anions need to be removed from water using the appropriate methods.

1.1.2. Removal technologies for these contaminants

Of the various methods for removing nitrate, phosphate and fluoride, adsorption/ion exchange methods are promising because they are simple and economical, result in less sludge production and therefore experience minimal disposal problems. These methods are also able to handle shock loadings and operate over a wide range of temperatures. Furthermore, these methods seem to be the most suitable for the following scenarios: small water supplies contaminated by these contaminants because of its simplicity and effectiveness; selective removal in the presence of other ions when adsorbents with selectivity for the contaminant are used; and easy regeneration of adsorbents for multiple reuse and consequently reducing operational costs.

1.1.3. Adsorbents

Several adsorbents such as ion exchange resins, carbon-based compounds, naturally occurring, agricultural wastes, zeolites, metal oxides and hydroxides, layered double hydroxides (LDHs), industrial wastes, biosorbents and other synthetic organic and inorganic compounds have been used by previous researchers to remove nitrate phosphate, and fluoride from water (Canter, 1997; Kapoor and Viraraghavan, 1997; Bhatnagar and Sillanpää, 2011a; Bhatnagar and Sillanpää, 2011b; Loganathan et al., 2013a; Loganathan et al., 2013b; Loganathan et al., 2014). However, most studies have not comprehensively covered the chemical mechanisms and solution factors such as pH. Neither have they investigated the presence of other anions that may influence the adsorption processes and modelling of adsorption.

1.1.4. Recovery of phosphorus

Phosphorus is an essential nutrient and makes a major contribution to agricultural and industrial development. The natural resources that can be exploited as phosphorus resources are gradually diminishing and it is stated that all reserves of phosphorus rock will be exhausted by 2035 (Cordell et al., 2009). Thus, in order to avoid exhausting the earth's phosphorus resources, it is necessary to explore alternative renewable phosphorus resources. Phosphates recovered from wastewater plants might be a viable source of industrial raw material for the manufacture of phosphate fertilisers. The emerging technology of struvite crystallisation ($(MgNH_4PO_4 \cdot 6H_2O)$) and hydroxyapatite [$(Ca_{10}(PO_4)_6(OH)_2$], as an alternative phosphorus removal technology may serve as a catalyst for removing phosphorus as a recyclable product. However, more research needs to be conducted to optimise the production variables such as pH, amounts of salts that

need to be added in relation to the concentration of phosphate removed from water by the adsorptive process, duration of the reactions and the type and concentration of reagents that must be utilised to quantitatively desorb the phosphate adsorbed before its conversion into phosphate compounds.

1.2. Research needs

Nitrate, phosphate and fluoride in wastewater sources must be removed or reduced to avoid environmental and health hazards that can be a by-product of the adsorption process. Several materials have been investigated as adsorbents for the removal of nitrate, phosphate and fluoride, yet the selectively of these adsorbents needs to be employed to effectively remove these anions. The methods reported for the removal of nitrate and phosphate using ion exchange resins were specific only for one of these nutrients. Very few studies have considered the effect of ion exchange resins in the simultaneous removal of both nitrate and phosphate. The effects of different concentrations and ratios of nitrate and phosphate on their removal by ion exchange resins were also not investigated in previous studies. Ion exchange resins which can simultaneously remove the two ions can be cost-effective. However, there may be competition for adsorption between the two anions and this needs to be investigated.

Most studies on nitrate, phosphate and fluoride removal by adsorbents have been performed in batch experiments and only a few have been reported in fixed bed column systems which are more relevant to real operating systems in natural waters. Moreover, many previous studies on adsorptive removal of these inorganic anions have not considered desorption after the adsorbent is saturated with anions. Easy desorption is important for multiple reuse of the adsorbent as this reduces operational costs. It is

important to explore highly efficient, low cost adsorbents that can be easily regenerated for reuse over several operational cycles without significant loss of adsorptive capacity. The adsorbents selected should have good hydraulic conductivity to prevent filters clogging during a fixed-bed treatment process.

The mathematical modelling of column data is important for designing treatment plants for the removal of nitrate, phosphate and fluoride from water and wastewaters. A suitable numerical solution can help to reduce the number of experiments associated with new operating conditions and a novel and well-researched model can be used as a reliable solution to design, optimise and predict the breakthrough curves of fixed bed columns in real water treatment processes. These have not been studied in great detail in previous research studies.

Recovery of phosphorus from phosphorus containing wastewater is essential for developing an alternative source of phosphorus to overcome its global scarcity. The technology to help remove phosphorus from wastewater consists of reusable compounds such as struvite and hydroxyapatite; of which interest in both is increasing as they have been identified as fertilisers. The methods currently available for struvite and hydroxyapatite derive directly from wastewater but very few studies have been conducted on phosphate recovered by the adsorption process.

1.3. Objectives of the research

The objectives of this study are as follows:

- Investigation of the competitive adsorption of nitrate and phosphate on ion exchange resins when they are present at different concentration ratios in synthetic water.
- Compare the nitrate, phosphate and fluoride removal efficiencies of different adsorbents in batch and column study.
- Analysis of the kinetic and equilibrium adsorption of these contaminants on different adsorbents.
- Study the effects of bed height, initial concentration and filtration velocity in the column studies for the adsorption of nitrate, phosphate and fluoride.
- Determine the effect of pH and complementary anions on the adsorption of these ions.
- Modelling of batch equilibrium adsorption data using Langmuir, Freundlich and Tempkin models.
- Model batch adsorption kinetic data using pseudo-first-order, pseudo-second-order, Elovich, intraparticle diffusion and homogeneous surface diffusion models (HSDM).
- Modelling of column adsorption data using the empirical models of Bohart-Adams, Thomas and Yoon-Nelson.
- Develop a numerical model based on advection-dispersion equation and simulate the equilibrium and model parameters to describe the column adsorption data of nitrate and phosphate.
- Develop a suitable method to regenerate the adsorbents for reuse so that the adsorbent becomes cost-effective.

- Develop a suitable method to recover phosphorus as struvite and hydroxyapatite.

1.4. Outline (structure) of this thesis

A brief description of the contents of each chapter is presented below.

Chapter 2 (Literature review) presents: (i) a detailed review of the inorganic anion contaminants (nitrate, phosphate and fluoride) in water; (ii) different technologies for the removal of these contaminants from water; (iii) adsorption process with mechanism and factors affecting adsorption; (iv) detailed description of the type of adsorption studies (batch and column studies); (v) specific description of batch and column adsorption modelling; (vi) characteristics of various nitrate, phosphate and fluoride adsorbents; (vii) desorption of anions and adsorbent regeneration; and (viii) the processes involved in phosphorus recovery.

Chapter 3 investigates the competitive adsorption of nitrate and phosphate using two ion exchange resins, Purolite A520E and Purolite A500PS in batch and column study. It also includes batch and column modelling for nitrate and phosphate adsorption and regeneration of these ion exchange resins.

Chapter 4 evaluates an analysis of the kinetic and equilibrium adsorption isotherms of nitrate on four ion exchange resins and justifies the selection of Purolite A520E for a detailed batch and column study. A numerical model based on advection-

dispersion equation and simulating the equilibrium and model parameters to describe the column adsorption data of Purolite A520E also is also described here.

Chapter 5 compares the phosphate removal efficiencies of six adsorbents expected to have high adsorption capacities and justifies the selection of Purolite FerrIX A33E for a detailed batch study.

Chapter 6 compares the phosphate removal efficiencies of three adsorbents in column experiment and selects Purolite FerrIX A33E based on the highest adsorption capacities for detailed study. It also describes the empirical and numerical column modelling of this Purolite.

Chapter 7 describes the suitable methods for recovering phosphorus from water in the form of struvite and hydroxyapatite and also investigates the characteristics of the recovered material.

Chapter 8 compares the fluoride removal percentages of seven adsorbents expected to have high adsorption capacities and justifies the selection of hydrous ferric oxide (HFO) for a detailed study in batch and column study. It also includes batch and column adsorption modelling and a descriptiojn of the regeneration process required for this adsorbent.

Chapter 9 presents conclusions and suggestions for further study.

CHAPTER 2

LITERATURE REVIEW

Chapter 2

Literature Review

2.1. Introduction

Due to water pollution, climate change and the fact that the world's population is increasing, clean water scarcity is becoming a more significant problem for many countries around the world. According to an International Water Management Institute projection, a very significant portion of the world is expected to suffer from both physical (1000 m^3 per person/annum renewable water supply) and economic water scarcity by 2025 (Chartres and Williams, 2006). Reclamation and reuse of treated wastewaters have become important themes in the sustainable management of water because many countries are now experiencing severe water shortages. As the global supplies of clean water diminish and demand for water rises, advanced wastewater treatment is becoming an international focus for the rational use of scarce water resources and as a means of safeguarding aquatic environments from the harm caused by wastewater disposal.

Australia is at the crossroads in terms of its ability to cope with increasing water scarcity in that it has to choose between the more expensive capital and environmental options of more storages and desalination, or minimise these via better water reuse strategies and increased clean water productivity. Nutrients (nitrate and phosphate) and fluoride are important inorganic anions contaminants of water and wastewater which have to be removed by appropriate water treatment process to produce clean water. This chapter reviews the literature on the contamination of nitrate, phosphate and fluoride in water and wastewater and the removal technologies for these contaminants.

2.2. Inorganic anion contaminants in water

2.2.1. Nitrate contamination in water

Nitrate is an essential nutrient for the growth of plants and micro-organisms. Excessive concentration of nitrate in water, however, is one of the most serious environmental and health problems worldwide. The intensive development of agriculture and application of chemicals led to the contamination of many natural water reservoirs and groundwater with nitrates. The reasons behind the rise in nitrate levels are increased usage of nitrogenous fertilisers, changes in land use patterns from pasture to arable crops and increased recycling of domestic wastewater in lowland rivers (Canter, 1997; Su and Puls, 2004; Soares, 2000). High nitrate concentration in water can cause eutrophication which is a serious environmental problem as it can lead to the abundant development of aquatic plants, growth of algae, harm fish and other aquatic life, and disturb the ecological balance of organisms present in water. Some of these outcomes are due to the depletion of the dissolved oxygen level caused by algae decay. Eutrophication is one of the most severe environmental problems in that it promotes excessive plant growth and decay, favouring simple algae and plankton growth over other more complicated plants, and causes a severe reduction in water quality. The water becomes cloudy, typically coloured with a shade of green, yellow, brown, or red. Eutrophication also decreases the value of rivers, lakes, and estuaries for recreation, fishing, hunting, and aesthetic enjoyment.

High nitrate concentrations in drinking water sources can also lead to a potential risk to public health. In humans, increasing nitrate concentrations in drinking water cause several adverse health effects. One effect is phenomenon of “blue-baby syndrome” (methemoglobinemia), especially in infants, and the potential formation of carcinogenic nitrosamines (Majumdar and Gupta, 2000; Tate and Arnold, 1990). One study in recent times (Chiu et al., 2007) has shown that excess nitrate in drinking water may also be

responsible for causing various kinds of cancers in humans. Ward et al. (2005) reviewed the epidemiological evidence for the links between drinking water nitrate and the risk of specific cancers, adverse reproductive and other health outcomes in the context of the current regulatory limit for nitrate in drinking water. Nitrate contaminated water supplies have also been linked to outbreaks of infectious diseases in humans (Lin and Wu, 1996). One literature survey revealed that nitrate ions can cause diabetes (Kostraba et al., 1992) and constitute a precursor of carcinogen.

Owing to the link between health problems and an excessive concentration of nitrate in drinking water, the World Health Organisation (WHO) and regulatory agencies in various countries have stipulated nitrate concentration limits. The nitrate concentration limit recommended by WHO and the European Union is 50 mg NO_3^-/ L (WHO, 2003) while the US Environmental Protection Agency has stipulated 44 mg NO_3^-/ L (EPA, 2000). In Australia, the recommended limit is 50 mg NO_3^-/ L for infants up to 3 months old and 100 mg NO_3^-/ L for adults and children over the age of 3 months (National Health and Medical Research Council, 2011). South Africa stipulates a much lower permissible level of 20 mg NO_3^-/ L (Masukume et al., 2011). Therefore, nitrate is a water pollutant under regulation and it is necessary to reduce its concentration prior to discharge or being used for drinking because there is a clear link between nitrate contaminations and health and environmental problems.

2.2.2. Phosphate contamination in water

Like nitrate, phosphate is a necessary nutrient for plants to live and is the limiting factor for plant growth in many freshwater ecosystems. Yet the addition of phosphate increases algal growth and causes eutrophication as nitrate does to water. Phosphate is

also an important chemical element for many industries and because of its excessive use the wastes produced by these industries can be a major phosphate contaminant in water. Domestic, mining, industrial and agricultural activities and municipal discharges have released phosphate into water bodies in the form of organic and inorganic phosphates (Hussain et al., 2011; Paleka and Deliyanni, 2009; Xu et al., 2010a). The problems of eutrophication were already discussed in section 2.2.1. Like nitrate, the excess phosphate in water should be removed in order to control eutrophication and maintain a sustainable green environment for future generations. To control eutrophication, environmental protection agencies in many countries have recommended that total phosphorus (P) should not exceed 0.005-0.1 mg P/L in natural water bodies (Mueller and Helsel, 1996; European Commission, 2009). The Australian and New Zealand water quality guidelines recommend that the Australian upland rivers, depending on the region of the country, should have a total P concentration < 0.01-0.02 mg P/L, lowland rivers < 0.005-0.01 mg P/L, freshwater lakes and reservoirs < 0.01-0.025 mg P/L, and estuaries < 0.02-0.10 mg P/L (ANZECC, 2000).

Phosphorus is an important resource used in agriculture and many other industries. However, phosphorus resources are limited and there have been some alarming reports that deposits of high-grade phosphate ores are likely to be depleted in the next few decades (Yoshida and Galinada, 2002). Phosphorus has no substitute in food production and in a world of 9 billion people by 2050, securing sufficient phosphorus will be critical for future food security. Yet the world's main source of phosphorus – phosphate rock – is non-renewable and becoming increasingly scarce and expensive. Peak phosphorus was estimated to occur by 2035, after which the demand would outstrip the supply (Cordell et al., 2009). While the exact timeline might be uncertain, there are no alternative sources of phosphorus in the market that could replace the current global production of 20 million

tonnes (Mt) of phosphorus from phosphate rock. While global phosphorus scarcity is likely to be one of the greatest challenges of the 21st century, it is possible to avert a crisis with concerted action. Global P security is directly linked to food security, environmental protection and farmers' livelihoods and can be defined as ensuring that all the world's farmers have access to sufficient phosphorus in the short and long term to grow enough food to feed an expanding world population, while ensuring farmers' livelihoods and minimising damage to the environment and society (Cordell et al., 2011). An enormous quantity of phosphorus is present in wastewater and if this phosphorus is recovered it can be meet part of the phosphorus needs of industries and agriculture, to compensate for the global exhaustion of high-grade phosphate ores.

2.2.3. Fluoride contamination in water

Fluoride contamination of drinking water is one of the most serious health problems worldwide (Fawell et al., 2006). Low concentration of fluoride in drinking water (0.4–1.0 mg/L) has beneficial effects on teeth especially for young children as it promotes calcification of dental enamel and protects teeth against tooth decay. Depending on the concentration and the duration of continuous uptake, the impact of fluoride in drinking water can be beneficial or detrimental to mankind. Fluoride in drinking water has a narrow beneficial concentration range in relation to human health. Small amounts in ingested water are usually considered to have a beneficial effect on the rate of occurrence of dental caries, particularly among children (Loganathan et al., 2013a). However, an excessive intake of fluoride can be harmful. The damage done to health due to prolonged intake of fluoride contaminated water has been reported (Dissanayake, 1991) depending on the fluoride concentration of waters as follows: <0.5 mg/L: dental

carries; 0.5 - 1.5 mg/L: promotes dental health; 1.5 - 4.0 mg/L: dental fluorosis; >4.0 mg/L: dental and skeletal fluorosis; and >10.0 mg/L: crippling fluorosis.

Excessive intake of fluoride can also lead to other diseases such as osteoporosis, arthritis, brittle bones, cancer, infertility, brain damage, alzheimer syndrome and thyroid disorder (Chinoy, 1991; Harrison, 2005; Kumar et al., 2009; Meenakshi, 2006). The mechanism of fluoride toxicity in the human body is described as: while ingested, fluoride initially acts locally on the intestinal mucosa; it can later form hydrofluoric acid in the stomach, which leads to gastro-intestinal irritation or corrosive effects (Islam and Patel, 2011). Following ingestion, the gastro-intestinal tract is the earliest and most commonly affected organ system. Fluoride can also interfere with a number of enzymes disrupting oxidative phosphorylation, glycolysis, coagulation, and neurotransmission (Islam and Patel, 2011). It may also interfere with DNA synthesis (Zhou et al., 2004) and with carbohydrates, lipids, proteins, vitamins and mineral metabolism (Islam and Patel, 2011). Fluoride toxicity also has the ability to interfere with the functions of the brain and pineal gland (Chinoy, 1991; Harrison, 2005). The pineal gland is a major site of fluoride accumulation within the body with higher concentrations of fluoride than either teeth or bone (Chinoy, 1991; Harrison, 2005). Owing to these adverse effects of fluoride, the World Health Organization (WHO) (1996) has recommended a maximum allowable fluoride concentration of 1.5 mg/L in drinking water. However, this fluoride limit depends on climatic conditions, quantity of water intake and other sources of fluoride in the diet. Considering these factors, the US Public Health Service (1962) reported that with increases in the average maximum daily air temperature the upper limit for fluoride concentration in drinking water should fall from 1.7 to 0.8 mg/L.

Groundwater containing large amounts of fluoride has been found in many parts of the world and fluorosis is endemic in at least 25 countries (Tetsuji et al., 1997). The most affected areas are the arid parts of northern China (Inner Mongolia), India, Sri Lanka, African countries like Ghana, Ivory Coast, Senegal, northern Algeria, Kenya, Uganda, Tanzania, Ethiopia, northern Mexico and central Argentina. In India, it was estimated that 56.2 million people were affected by fluorosis and this problem was prevalent in 17–19 out of the 32 States (Nemade et al., 2002; Jagtap et al., 2012) especially in rural and semi-urban areas. Fluoride is widely distributed in the geological environment (Murray, 1986) and generally released into the groundwater by slow dissolution of fluorine-containing rocks (Loganathan et al., 2003). Various minerals, for example fluorite, biotites, topaz, and their corresponding host rocks such as granite, basalt, syenite, and shale, contain fluoride that can be released into the groundwater (Murray, 1986; Loganathan et al., 2003).

Thus, groundwater is a major source of people's intake of fluoride. Besides the natural geological sources for fluoride enrichment in groundwater, various industries are also contributing to fluoride pollution (Vigneswaran et al., 1995; Li et al., 2003). The industries which discharge wastewater containing high fluoride concentrations include glass and ceramic production, semiconductor manufacturing, electroplating, coal fired power stations, beryllium extraction plants, brick and iron works, and aluminium smelters (Liao and Shi, 2005). The effluents of these industries have larger fluoride concentrations than natural waters, ranging from ten to thousands of mg/L (Mishra et al., 2010). It is estimated that more than 200 million people worldwide rely on drinking water with fluoride concentrations that exceed the WHO guideline of 1.5 mg/L (Paulson, 1977).

Table 2.1.

Australin limits for nitrate, phosphate and fluoride contamination.

Parameter	Limit	Reference
Nitrate (NO_3^-)	50 mg NO_3^-/ L (for infants up to 3 months old). 100 mg NO_3^-/ L (for adults and children over the age of 3 months)	National Health and Medical Research Council, 2011).
Phosphate (PO_4^{3-}) Phosphorus (P)	Total P concentration for upland rivers < 0.01-0.02 mg P/L, lowland rivers < 0.005-0.01 mg P/L, freshwater lakes and reservoirs < 0.01-0.025 mg P/L and estuaries < 0.02-0.10 mg P/L.	The Australian and New Zealand water quality guidelines (ANZECC, 2000).
Fluoride (F)	1.5 mg F /L	World Health Organization (WHO) (1996).

2.3. Technology for the removal of inorganic anion contaminants from water

2.3.1. Technologies for the removal of nitrate from water

Several physicochemical and biological processes have been investigated for the removal of dissolved nitrate in water and wastewaters. Due to its high stability and solubility, nitrate has a low tendency for precipitation and adsorption, and therefore it is difficult to remove this ion from water using conventional water treatment technologies

(Islam and Patel, 2010). Several physicochemical and biological methods have been attempted to remove excessive nitrate from water. These include adsorption (Bhatnagar and Sillanpää, 2011a), ion exchange (Öztürk and Bektas, 2004; Zhan et al., 2011), reverse osmosis (Schoeman and Steyn, 2003), electrodialysis (Abou-Shady et al., 2012), denitrification (Soares, 2000), algae growth and disposal of the harvest (Canter, 1997) and a combination of ozonation and sand/activated carbon filtration (Canter, 1997). The World Health Organization (WHO) has suggested biological denitrification and ion exchange as nitrate removal methods, while ion exchange, reverse osmosis and electrodialysis were approved by the US EPA as Best Available Technologies to treat nitrate contaminated water (Canter, 1997; Haugen, 2002). The conventional methods available for nitrate removal have their own strengths and limitations and are found to be expensive, less effective and generate additional by-products. Accordingly, these traditional technologies do not solve the problems related to the excess amount of nitrate in the environment; in turn, they generate nitrate concentrated waste streams that pose a disposal problem due to the high saline content (Soares, 2000; Till, 1998).

Biological denitrification is an efficient process for removing nitrate from wastewater in which heterotrophic bacteria in the absence of oxygen (anaerobic conditions) convert nitrate-N and nitrite-N into nitrogen gas (Prosnansky et al., 2002; van Rijn et al., 2006). This process requires sufficient organic carbon as an electron donor for complete nitrate removal (Cambardella et al., 1999; Greenan et al., 2006; Healy et al., 2006). The availability of the organic carbon for denitrification is an important factor that controls the denitrification process (Tan and Ng, 2008). A wide range of chemical oxygen demand (COD) values have been reported in the literature for complete denitrification (Carucci et al., 1996; Tseng et al., 1998). Again biological denitrification processes are

difficult to apply to inorganic wastewater treatment because additional organic substrates are required to serve as electron donors.

One commonly used treatment method to remove/reduce nitrate is chemical denitrification which employs zero-valent iron (FeO) (Cheng et al., 1997; Huang and Zhang, 2004; Chen et al., 2005; Liou et al., 2005; Ahn et al., 2008) and zero-valent magnesium (Mg0). Chemical reduction (CR) of nitrate can be conducted using various compounds, mainly hydrogen, iron, formic acid and aluminium (Della Rocca et al., 2007). Zero-valent iron (ZVI) has been extensively studied for its ability to reduce different contaminants including nitrate in groundwater (Cheng et al., 1997; Young et al., 1964; Huang et al., 1998; Huang and Zhang, 2002; Alowitz and Scherer, 2002; Westerhoff, 2003). However, this technology has some limitations as discussed by various researchers. For example, Cheng et al. (1997) reported that the main disadvantages of nitrate reduction using ZVI were ammonium production and the pH control requirement (by initial pH reduction or use of buffer). When applying ZVI in an *in situ* remediation technique for nitrate removal, these disadvantages are more critical (Lee, 2007).

The membrane processes electrodialysis reversal (EDR) and reverse osmosis (RO) are widely employed for nitrate reduction. However, these two processes are relatively expensive (Abou-Shady et al., 2012; Schoeman and Steyn, 2003) and moreover, cause process complexity when used in in-situ application for direct decontamination of groundwater.

Advantages and disadvantages of the various methods used for nitrate removal are presented in Figure 2.1.

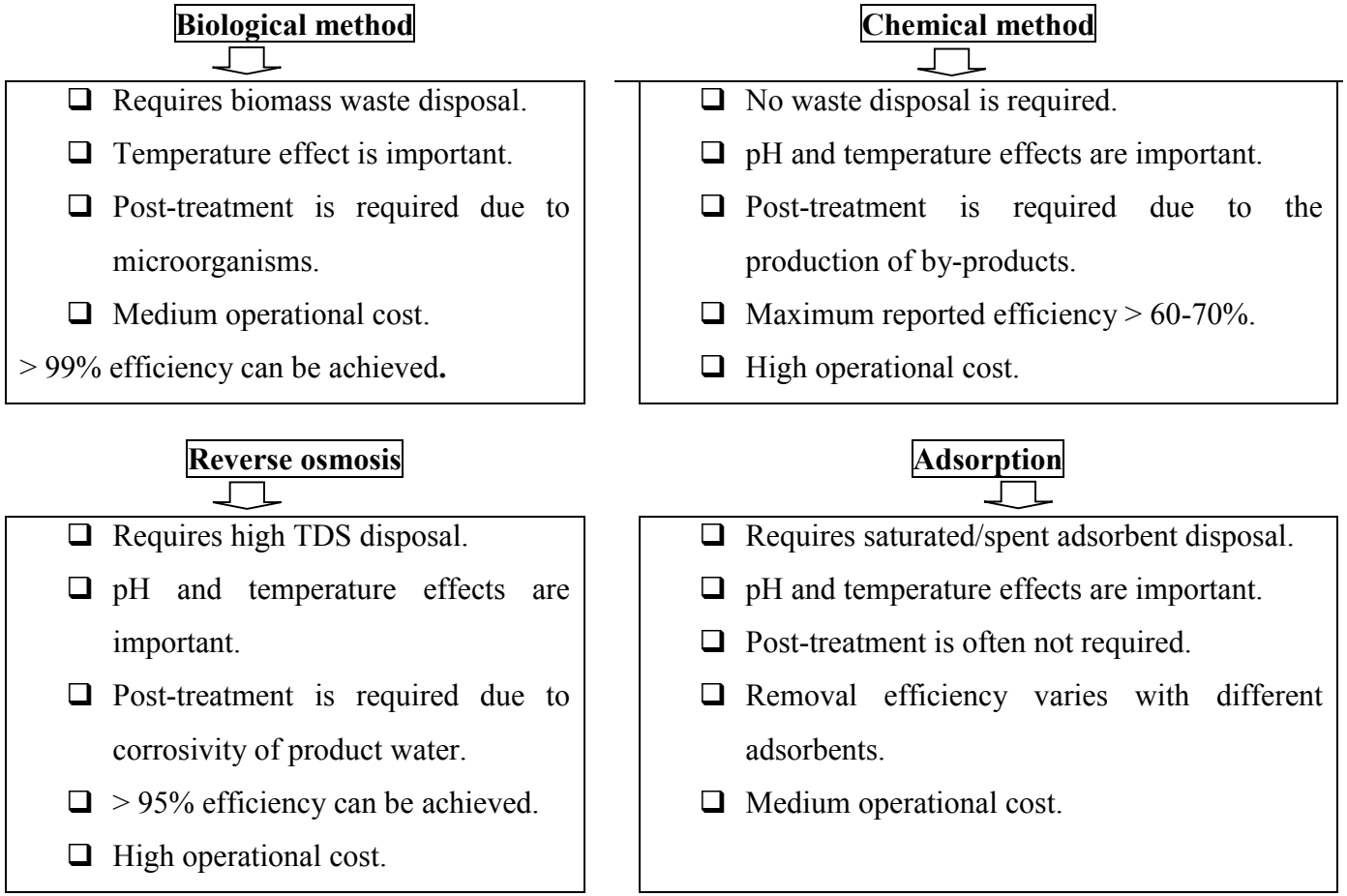

Figure 2.1. Key characteristics of common technologies for nitrate removal from wastewater sources (Redrawn from Bhatnagar and Sillanpaa, 2011a).

Of the various techniques available for removing nitrate, ion exchange/adsorption process is the most suitable for small water supplies contaminated by nitrate (Bhatnagar and Sillanpää, 2011a). This is due to its simplicity, effectiveness and relatively low cost (Bhatnagar and Sillanpää, 2011a). Ion exchange/adsorption methods also have the ability to handle shock loadings and can operate over a wide range of temperatures.

2.3.2. Technologies for the removal of phosphate from water

Development of technologies for phosphate removal started in the 1950s in response to the issue of eutrophication and the need to reduce the levels of phosphate entering surface waters. Several physicochemical and biological processes have been investigated for removing dissolved phosphate in water and wastewaters. The methods available for the removal of phosphate are adsorption (Loganathan et al., 2014; Blaney et al., 2007; Gupta et al., 2012), biological method, constructed wetlands, reverse osmosis, nano filtration and electrodialysis (De-Bashan and Bashan 2004; Le Corre et al., 2009; Morse et al., 1998; Yeoman et al., 1988). Of these, the adsorption process is generally considered to be the best water treatment option due to its convenience, ease of operation, simplicity of design and economics, provided low-cost adsorbents are used (Loganathan et al., 2014; Blaney et al., 2007; Gupta et al., 2012).

In recent decades, however, biological phosphate removal has become firmly established. The development of biological phosphate removal was based on research in the late 1950s, which found that, under certain conditions, activated sludge could take up phosphate in considerable excess to that required for normal bio-mass growth (Greenburg et al., 1955; Levin and Shapiro, 1965; Srinath, 1959). Based on this phenomenon, known as ‘luxury uptake’, a number of applications and processes were developed and the technology is now firmly established, particularly for new or redeveloped works serving

large populations. The technology has the advantage of avoiding the use of chemicals and excess sludge production. However, it requires more complex plant configurations and operating regimes. Biological phosphate removal is achieved in the activated sludge process by introducing an anaerobic and/or anoxic zone ahead of an aerobic stage. In this zone, sufficient readily degradable materials with high chemical oxygen demand (COD) are required and must be available, typically as volatile fatty acids provided by pre-fermenting the sludge using storage or thickeners, or by adding acetic acid or sodium acetate. Recovered phosphorus is in general biologically bound and can be released into solution under anaerobic conditions. Careful sludge management is therefore essential in some processes.

The widespread use of chemical precipitation for phosphate removal in wastewater treatment started in Switzerland during the 1950s. Chemical precipitation is in essence a physicochemical process, comprising the addition of a divalent or trivalent metal salt to wastewater, causing precipitation of an insoluble metal phosphate that is settled out by sedimentation. The most suitable metals are iron and aluminium added as chlorides or sulphates. Lime may also be used to precipitate phosphorus as $Ca_3(PO_4^{3-})_2$. Anionic polymers may be utilised to assist solid separation. Chemical precipitation is a very flexible approach to phosphate removal and can be applied at several stages during wastewater treatment. This approach is not generally favoured because of high chemical costs and the creation of an additional, chemical, tertiary sludge. Chemical precipitation typically produces phosphorus bound as a metal salt within the wasted sludge. It therefore has potential value in agricultural activities, although research on bioavailability is inconclusive (Yeoman et al., 1988). This uncertainty has contributed to the desire to develop alternative technologies that potentially offer a more valuable and consistent product for recycling phosphorus to agriculture and industry.

A summary of the various technologies for phosphate removal is provided in Figure 2.2 (Loganathan et al., 2014).

Chemical precipitation

- Most widely used.
- Low effectiveness, especially at low P concentration.
- Large amounts of chemicals required.
- Costs of chemicals, chemical storage and feeding system.
- Large volumes of waste sludge.
- Acid or alkali neutralisation of effluent required.
- Chemicals used may affect subsequent biological treatment.

Biological methods

- Low effectiveness, especially at low P concentration.
- Low operational cost but infrastructural investment required.
- Low volumes of wastes and no chemicals usage.
- Simultaneous removal of both excess P and N.
- Highly skilled operation (strict anaerobic and aerobic conditions required).
- Uncontrolled microbial growth.

Constructed wetlands

- Low maintenance cost and low-tech process.
- Practical in any location.
- Need land availability.

Electrodialysis

- Excellent removal when P is in ionic form.
- High capital cost.
- No waste production.
- No ion selectively.

Adsorption/Ion Exchange

- Effective even at low P concentration.
- Flexible and Simplicity of design and ease of operation.
- No waste production.
- Can be costly, needs pre-treatment, sorbent regeneration; can use low-cost sorbent (including certain waste materials).
- Low selectivity against competing ions

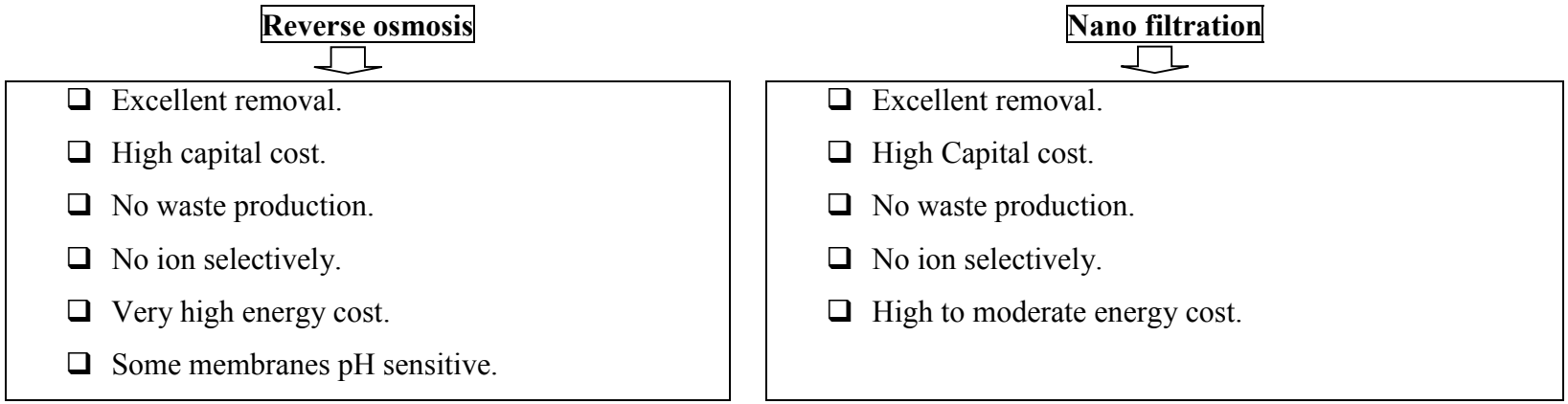

Figure 2.2. Key characteristics of common technologies for phosphate removal from wastewater sources (Redrawn from Loanathan et al., 2014).

Of the various methods of phosphate removal, adsorption/ion exchange are promising because they are simple and economical, result in less sludge production and therefore experience minimal disposal problems (Blaney et al., 2007). Furthermore, these methods seem to be the most suitable for small water supplies contaminated by phosphate because of its simplicity, effectiveness, selective removal in the presence of other ions, easy recovery of phosphate and relatively low cost (Loganathan et al., 2014). These methods can also cope with shock loadings and operate over a wide range of temperatures.

2.3.3. Technologies for the removal of fluoride from water

One method for reducing excessive concentrations of fluoride in water is to blend water that has a high fluoride concentration with water that contains a low fluoride concentration from an alternative source. If such a source is not readily available, defluoridation is the only means remaining to prevent fluorosis (Farwell et al., 2006). For contaminants other than fluoride, water treatment methods are used to remove contaminants to below the maximum level permissible but defluoridation is special in that the treated water should have an optimum fluoride concentration to derive the beneficial effects of fluoride. The main methods of defluoridation are precipitation/coagulation, adsorption, ion exchange, reverse osmosis, and electrodialysis. Of these, precipitation/coagulation and adsorption are convenient methods and are widely used, especially in developing countries' rural areas. The precipitation/coagulation method where lime and Al salts are used to remove fluoride as a CaF_2 precipitate is followed by the removal of left-over fluoride in solution by co-precipitation with adsorption onto the precipitated $Al(OH)_3$. This has been further developed into a technique known as the Nalgonda process in India (Jagtap et al., 2012; Bulusu et al., 1979; Nawlakhe et al., 1975). This process is extensively used in India and Africa (Farwell et al., 2006). However, the

main drawback of this technique is the low effectiveness of fluoride removal and production of toxic AlF complexes in solution (Meenakshi and Maheshwari, 2006).

The scale and treatment site differ between industrialised countries and developing countries. In industrialised countries the treatment of water is generally done at water treatment plants close to the water source but in developing countries it is carried out at the village community or household level (Farwell et al., 2006) using simple inexpensive locally available adsorptive media (Jinadasa et al., 1988; Zevenbergen et al., 1996). Industrialised countries generally use more efficient but more costly adsorption media including synthetic ion exchange resins as well as advanced techniques such as reverse osmosis and electrodialysis. The advantages and shortcomings of the various methods of defluoridation are presented in Figure 2.3.

Of these various fluoride removal methods that of adsorption is generally considered attractive because of its effectiveness, convenience, ease of operation, simplicity of design, and economic and environmental considerations, provided low-cost adsorbents which can effectively remove fluoride around the neutral pH of drinking water are used. This process is discussed in detail in the following sections.

Precipitation/coagulation

- Most widely used.
- Medium cost.
- Low effectiveness; cannot remove fluoride below 5 mg/L because of high solubility product of CaF_2; need secondary treatment.
- Large amounts of chemicals required.
- Precise control of chemicals additions (frequent testing of feed and treated water).
- Costs of chemicals, chemic al storage and feeding system.
- Large volumes of waste sludge; disposal problem.
- Acid neutralisation of treated water required.
- Toxic chemicals left in treated water (Al F complexes, SO4).

Electrodialysis

- Excellent removal and high capital cost.
- High operation al (energy) cost.
- No chemicals required.
- No waste production.
- No ion selectively; beneficial nutrients and other contaminants removed together with fluoride.
- Skilled labour required.
- Polarization problem.

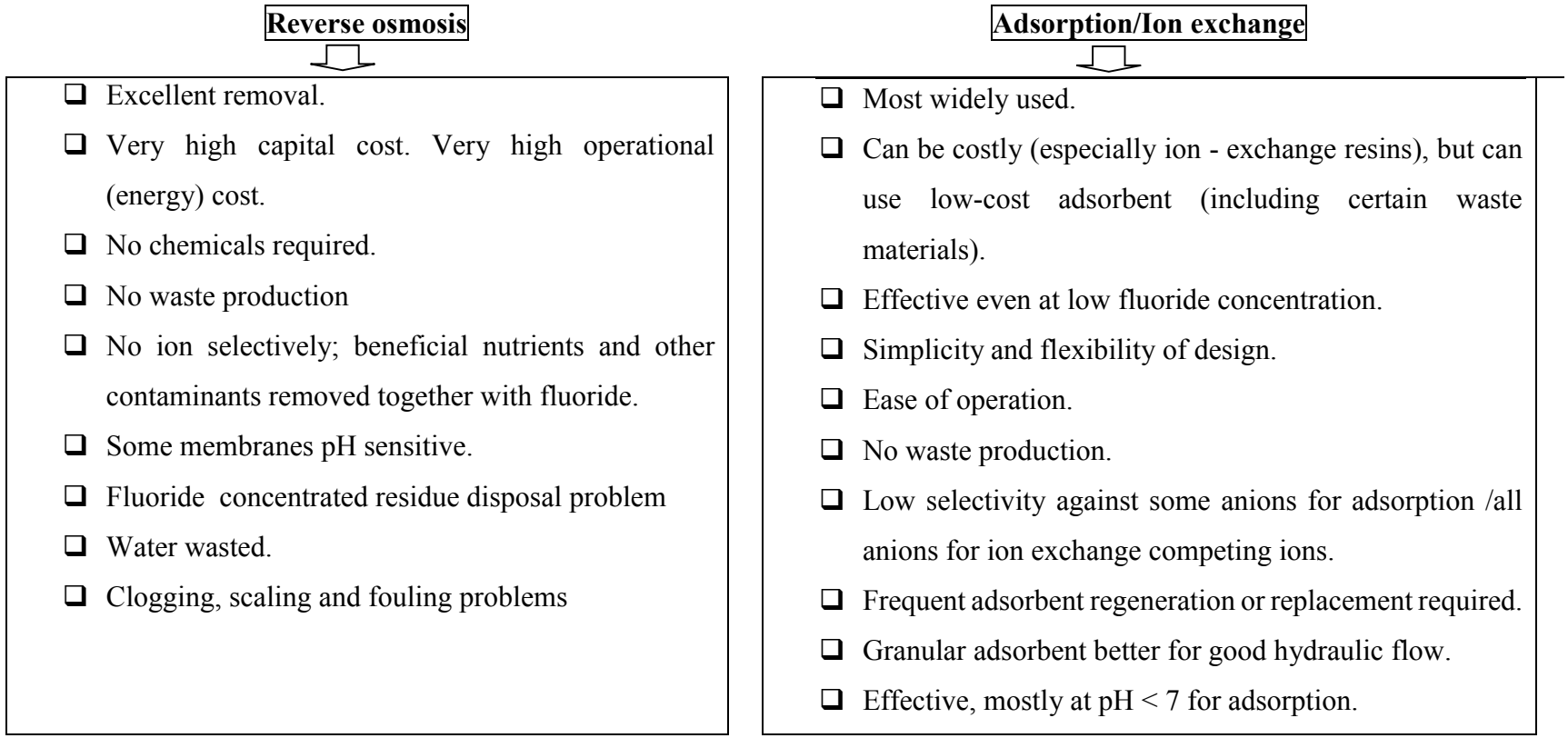

Figure 2.3. Comparison of some fluoride removal technologies (Redrawn from Loganathan et al., 2013a).

2.4. Adsorption process

Adsorption is a complex phenomenon in which a gas, liquid or solid adheres to the surface of a solid or (less frequently) a liquid but does not penetrate it. Adsorption is a mass transfer operation in which substances present in a liquid phase are adsorbed or accumulated on a solid phase and thus removed from the liquid. The constituent that undergoes adsorption is referred to as the adsorbate and the solid onto which the constituent is adsorbed is referred to as the adsorbent. During the adsorption process, dissolved species are transported into the porous solid adsorbent granule by diffusion and are then adsorbed onto the adsorbent's extensive inner surface. The position of the functional groups of the adsorbent determines the type of adsorbent-adsorbate bond and thus the type of adsorption that takes place. Dissolved species are concentrated on the solid surface by chemical reaction (chemisorption) or physical attraction (physical adsorption) to the surface. Physical adsorption is reversible, that is, the adsorbate desorbs in response to a decrease in solution concentration. The physical adsorption occurs at a lower temperature (in the vicinity of room temperature), and it is not site-specific.

On the other hand, chemical adsorption involves an ionic or covalent bond formation between the adsorbate molecules and the atoms of the functional groups of the adsorbent. The chemical adsorption is irreversible and the heat adsorption is typically high. The chemical adsorption is site-specific and it occurs only in certain areas of the adsorbent, mainly on one layer (monolayer). Therefore the amount and position of those functional groups determine the bonds between adsorbent and adsorbate molecules which in turn decide the type of adsorption, physical adsorption or chemisorption (McKay, 1996).

2.4.1. Adsorption Mechanism

In general the adsorption process consists of three steps: (i) external mass transfer of solute molecules from bulk solution to the sorbent particle surface by diffusion or turbulent movement; (ii) diffusion within particle internal structure to transport adsorbate molecules to the available adsorption sites of adsorbents surface; and (iii) rapid uptake (McKay, 1996). When the adsorption process occurs it will continue until it achieves an equilibrium state which depends on physical and chemical characteristics, concentration of adsorbate, temperature and subsequent interaction among adsorbates (McKay, 1996; Chaudhary et al., 2003). While some of the solute adsorbs to the adsorbent, others will be desorbed and these processes repeat continuously in the equilibrium system. This phenomenon is called "seesaw behaviour", an important characteristic of the equilibrium system (Sincero and Sincero, 2003).

In aqueous solution, three interactions compete when considering physical adsorption: (1) adsorbate-water interactions, (2) adsorbate –surface interactions and (3) water-surface interactions. The extent of adsorption is determined by the strength of adsorbate-surface interactions as compared to the adsorbate-water and water-surface interactions. Adsorbate-surface interactions are determined by surface chemistry, while adsorbate-water and water-surface interactions are related to the solubility of the adsorbate. It is important to provide enough surface area for adsorption. The surface area and pore size are important factors that determine the number of adsorption sites and the accessibility of the sites for adsorbates. Generally, there is an inverse relationship between the pore size and surface area: the smaller the pores for a given pore volume, the greater the surface area that is available for adsorption. In addition, the size of the adsorbate that can enter a pore is limited by the pore size of the adsorbent, and is referred to as steric effects.

There are mainly seven mechanisms of adsorption (Faust and Aly, 1987), namely: (1) Van der Waals forces (outer-sphere surface complexation, (2) ion exchange (outer-sphere surface complexation), (3) hydrogen bonding (H-bonding) (inner-sphere surface complexation), (4) ligand exchange (inner-sphere surface complexation), (5) Surface precipitation, (6) diffusion and (7) chemical modification of the adsorbent surface.

The first two mechanisms are governed by weak physical adsorption and are non-specific which is more relevant to nitrate adsorption than phosphate and fluoride. On the other hand, the third and fourth mechanisms are governed by strong chemical adsorption more specific to phosphate and fluoride. The fifth and sixth mechanisms occur for phosphate and fluoride adsorption. The seventh mechanism is governed by both specific and non-specific adsorption and can occur for any anion (Loganathan et al., 2013a; Loganathan et al., 2013b)

2.4.1.1. Van der Waals forces

Physical adsorption is mainly caused by van der Waals and electrostatic bonds between the adsorbate molecules or ions and the atoms or charges of the functional groups. Adsorbates are said to undergo physical adsorption if the forces of attraction include only physical forces such as coulombic attraction of unlike charges that exclude covalent bonding with the surface. In this case, the attraction between an adsorbate and adsorbent increases with increasing polarizability and size, which are directly related to van der Waals forces. In water treatment, there is often interest in the adsorption of organic adsorbates from water (polar solvent) onto a nonpolar solvent (activated carbon). Because activated carbon has cross-linked graphitic crystallite planes that form micropores, the major attractive force between organics and the adsorbent is van der Waals forces that exist between organic compounds and the graphitic carbon basal planes

(Helferich, 1995). This form of adsorption is also known as hydrophobic bonding. Van der Waals forces are weak short range forces acting between two atoms. The larger the adsorbate size the greater the force of attraction. Therefore, adsorbates with high molecular weights such as dissolved organic matter are adsorbed on adsorbents having high surface area through van der Waals forces. This explains the weak adsorption of nitrate, phosphate, fluoride and strong adsorption of dissolved organic matter on activated carbon (Gupta et al., 2009).

2.4.1.2. Ion exchange

In drinking water treatment applications, ion exchange is primarily used for water softening and demineralisation such as removal of Ca^{2+}, Mg^{2+}, Na^{+}, Cl^{-}, SO_4^{2-}, NO_3^{-}. With concerns rising on the health effects of other contaminant ions such as barium, radium, fluoride, nitrate, phosphate, arsenate, the use of ion exchange in water treatment has increased. In water treatment applications, ion exchange involves the exchange of an ion in the aqueous phase for an ion in the solid phase (Figure 2.4). The solid phase or ion exchanger is insoluble and can be of natural resin or synthetic material such as polymeric resin. These exchangers have fixed charged functional groups located on their external or internal surface and associated with these groups are ions of opposite charge called counter ions. These mobile counter ions are associated by electrostatic attraction to each of the charged functional groups to satisfy the criterion that electron neutrality is maintained at all times within the exchange material as well as in the bulk aqueous solution. Depending on the charge of the functional group on the exchanger, the counter ion can either be a cation if the functional group is negative or an anion if the functional group is positive and can exchange with another counter ion in the aqueous phase. The ions are adsorbed physically by fully retaining their inner hydration shell and the

adsorption is due to electrostatic or coulombic attraction. The ion exchange process is rapid and reversible. Ion exchange tends to prefer counter ions of higher valency, higher concentration and ions of smaller hydrated equivalent volume (Helferich, 1995). The order of selectivity for anions by anion exchange resins generally follows the order: citrate > SO_4^{2-}, oxalate > I^- > NO_3^- > PO_4^{3-} > CrO_4^{2-} > Br^- > SCN^- > Cl^- > acetate > F^- (Helferich, 1995).

$$\blacksquare\rightarrow Cl^- + PO_4^{3-}/\ NO_3^-/\ F^- \quad = \quad \blacksquare\rightarrow PO_4^{3-}/\ NO_3^-/\ F^- \quad + \quad Cl^-$$

Figure 2.4. Ion exchange mechanisms of anions (■→adsorbent)

2.4.1.3. Hydrogen bonding

Hydrogen bonding is a special case of dipole-dipole interactions in which the hydrogen atom in a molecule has a partial positive charge and attracts an atom on another molecule, which has a partial negative charge (Helferich, 1995). Often the electronegative end of the molecule is an oxygen or fluoride atom. Hydrogen bonding is one of the strongest types of dipole interaction and is responsible for water forming a liquid at room temperature in spite of its small size. The energy of adsorption in H-bonding is stronger than in van der Waals forces and ion exchange but weaker than in the ligand exchange process discussed in the next paragraph. H-bonding occurs in the adsorption of phosphate and fluoride on ion exchange resins (Meenakshi AND maheshwari, 2006; Solangi et al., 2010) and coal-based adsorbents (Sivasamy et al., 2001). H bonding also occurs in the adsorption of phosphate on metal oxides and organic molecules (Saha et al., 2009).

Examples of the phosphate adsorption process following the hydrogen bonding mechanism used for removing phosphate from water are given in Figure 2.5 (Loganathan et al., 2014).

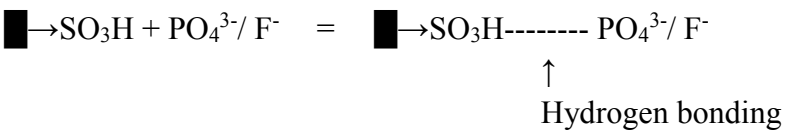

Figure 2.5. Hydrogen bonding mechanisms of anions (→adsorbent)

2.4.1.4. Ligand exchange

A covalent chemical bond forms with the adsorbing anion such as phosphate and fluoride and a metallic cation at the adsorbent surface in ligand exchange, resulting in the release of other potential determining ions such as OH ions previously bonded to the metallic cation (Loganathan et al., 2013a). Thus phosphate and fluoride are said to form an inner sphere complex at the adsorbent surface. Ligand exchangers have the particular advantage of combining high adsorption capacity with high selectivity for the anions. These exchangers can remove large proportions of anions having higher selectivity for adsorption from much diluted solutions of the anions even in the presence of competing anions of lower selectivity. The adsorption creates a negative charge on variable charge surfaces, thereby shifting the zero point of charge to a lower pH.

The development of spectroscopic techniques such as X-ray absorption fine structure (EXAFS) spectroscopy, Fourier transform infrared (FTIR) spectroscopy and X-ray photoelectron (XPS) spectroscopy and their application to the ion adsorption process during the last decade has provided useful information on the structure of the surface

complex at the molecular level (Elzinga and Sparks, 2007; Sparks, 2001). The adsorption of fluoride on several multivalent metal oxides near neutral pH was reported to have increased the pH of solutions as a result of releasing OH^- ions from the adsorbents by ligand exchange of OH^- groups on the adsorbent surface with fluoride in solution (Maliyekkal et al., 2006; Tokunaga et al., 1995). Examples of the phosphate adsorption process following the ligand exchange mechanism for metal oxide adsorbents commonly used for removing phosphate from water are given in Figures 2.6 and 2.7 (Loganathan et al., 2014).

$$\equiv M - OH + H_2PO_4^- \rightarrow \equiv M - H_2PO_4^- + OH^-$$
$$2 \equiv M - OH + H_2PO_4^- \rightarrow (\equiv M)_2HPO_4 + H_2O + OH^-$$

Figure 2.6. Ligand exchange mechanisms phosphate (Loganathan et al., 2014)

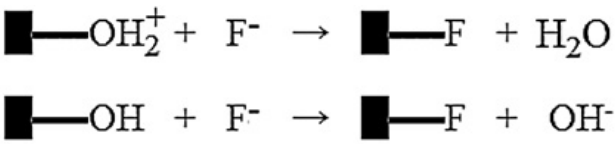

Figure 2.7. Ligand exchange mechanisms fluoride (adsorbent) (Loganathan et al., 2013a).

2.4.1.5. Surface precipitation

Adsorption of phosphate is commonly measured by the decrease in the amount of phosphate in the solution phase after a period of time the solution was in contact with the solid phase. The decrease in phosphate content results not only from adsorption but also from precipitation of phosphate in the solution phase. This is particularly the case if the product of the solution concentrations of the precipitate's constituents exceeds the solubility product of the precipitate. Surface precipitation of metal phosphate can occur even at solution concentrations of phosphate and metals smaller than those expected to form metal precipitates in the solution phase according to the thermodynamic solubility product principle (Sparks, 2001; Loganathan et al., 2014). In such cases, a finite volume adjacent to the mineral surface exists that is oversaturated with respect to precipitate formation (Ford, 2006). X-ray diffraction and scanning electron microscopic data provided evidence for the formation of surface precipitates of phosphate compounds of Ca, Fe, Al, and Zn on adsorbents containing components of these metals (Bowden et al., 2009; Khadhraoui et al., 2002; Koilraj and Kannan, 2010; Oguz, 2005; Roques et al., 1991). Using scanning electron microscopy, Nagamine et al. (2003) demonstrated that when a phosphate solution was mixed with an equal volume of a $CaCl_2$ solution having the same concentration as phosphate with pH adjusted to 8.8 to 9.0 and passed through a macroporous TiO_2, calcium hydroxyl phosphate was crystallised inside the pores. The phosphate adsorbed to TiO_2 in the pores was deemed able to provide nuclei for this crystallisation process.

$$Zn\ Al\ Zr - LDH + H_2PO_4^- \longrightarrow$$

$$ZnAl\ Zr - LDH - Zn_3(PO_4)_2 . 4H_2O$$

(LDH - layered double hydroxide)

Ca based sorbent (bentonite, calcium hydroxide, coal)

+ $H_2PO_4^-$ ⟶hydroxyapatite on sorbent surface

Figure 2.8. Surface precipitation mechanisms phosphate (Loganathan et al., 2014).

2.4.1.6. Diffusion

Adsorption of phosphate on many microporous sorbents (e.g. hydrous metal oxides, especially those having an amorphous structure) is recognised as a two-step process: firstly, an initial rapid adsorption (within an hour) that reaches a pseudo-equilibrium at the solid-solution interface; and secondly, a much slower process (days to months) where the phosphate ions move by intra-particle diffusion into the interior pores and channels of the sorbent (Trivedi and Axe, 2006). For example, studies on removal of phosphate from aqueous solutions by date palm fibres showed that phosphate moved into the internal cells of the fibres by diffusion (Riahi et al., 2009). Evidence for this process was provided by scanning and transmission electron microscopy and energy dispersive spectroscopy.

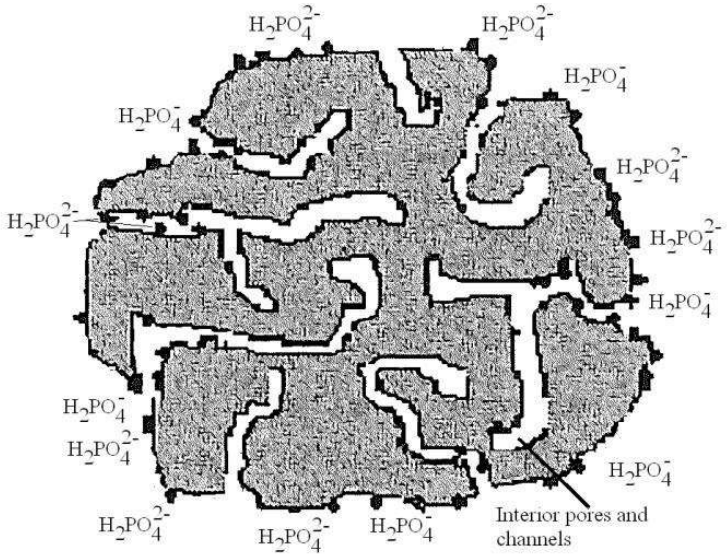

Figure 2.9. Diffusion mechanisms phosphate (Loganathan et al., 2014).

2.4.1.7. Chemical modification

The adsorption capacity of nitrate and fluoride on adsorbents can be increased by chemical modification of adsorbent surfaces (Loganathan et al., 2013a; Loganathan et al., 2013b). This is particularly of advantage in the case of adsorbents possessing negative surface charges which tend to repel the similarly charged nitrate and fluoride ions. In such adsorbents, positively charged multivalent cations such as Al^{3+}, La^{4+}, Zr^{4+}, Fe^{3+}, and Ce^{3+} are impregnated onto the adsorbent to create positive charges on the adsorbent surface for attracting nitrate and fluoride by coulombic forces as well as producing adsorption sites capable of chemical interaction with nitrate and fluoride (Liao and Shi, 2005; Samatya et al., 2007; Luo and Inoue, 2004; Onyango et al., 2004; Onyango et al., 2006; Zhou et al., 2004). These metallic cations act as a bridge in adsorbing fluoride onto the adsorbent.

2.4.2. Factors affecting the adsorption process

The important factors that affect the adsorption process are: (a) the characteristics of the adsorbent: surface charge, surface area, particle size, pore structure; (b) the characteristics of the adsorbate: solubility, molecular structure, ionic or neutral nature; (c) the characteristics of the solution: pH, ionic strength, temperature, presence of other anions; and (d) duration of adsorption. The maximum amount of adsorption is proportional to the amount of surface area on the surface and within the pores of the adsorbents that is accessible to the adsorbate.

2.4.2.1. Factors affecting nitrate adsorption

2.4.2.1.1. pH

Nitrate adsorption is affected by pH changes of the solution on many adsorbents. Generally an increase in pH leads to a decrease in nitrate adsorption. Öztürk and Bekta (2004) reported that the most effective pH value for nitrate removal was 2 for powdered activated carbon adsorbent and above this pH, nitrate adsorption decreased. They also found that for other adsorbents, nitrate adsorption did not change with pH. Ohe et al. (2003) reported that the maximum removal of nitrate by the prepared activated carbon (AC) such as coconut shells and charcoal (CB) occurred at equilibrium pH 2 – 4. The reason for the highest removal of nitrate at the lower pHs is that the positive charges on the adsorbent surface is highest at low pHs. A positively charged surface site on the adsorbent favours the adsorption of the nitrate anions due to electrostatic attraction (Öztürk and Bekta, 2004).

The percentage removal of nitrate by layered double hydroxides (LDHs) was also found to decrease gradually when pH increased and the optimum pH level proved to be 6 (Islam and Patel, 2010). Chatterjee and Woo (2009) reported that nitrate adsorption by

chitosan beads containing an amine group rose when the solution's pH decreased. This was explained by the fact that a decrease in the pH of the solution resulted in more protons being available to protonate the chitosan amine group. This resulted in improved nitrate adsorption by the chitosan beads due to increased electrostatic interactions between the negatively charged nitrate group and the positively charged amine group. Desorption of nitrate from the loaded beads was accomplished by increasing the pH of the solution to the alkaline range, and desorption of 87% was achieved around pH 12.0. The nitrate adsorption capacity of industrial waste like activated red mud was reported to decrease once the pH level rose above 7 (Cengeloglu et al., 2006).

2.4.2.1.2. Co-existing anions

In real systems several other ions are present which can compete with nitrate, so the effects of the presence of sulphate, phosphate and ammonium ions on nitrate adsorption need to be studied. The effect of competing anions reduced the nitrate adsorption by layered double hydroxides (LDHs) and hydroxyapatite (HAP) and it was in the order of $CO_3^{2-} > PO_4^{3-} > Cl^- > SO_4^{2-}$ for Zn-Al-Cl and Mg-Al-Cl LDH and in the order $Cl^- > CO_3^{2-} > SO_4^{2-} > PO_4^{3-}$ for HAP (Islam and Patel, 2009; Islam et al., 2010). The nitrate adsorption of some agricultural wastes such as wheat straw was also affected by other anions. In the presence of a mixed ion solution, the preferential adsorption of the anions for wheat straw was in the following order, $SO_4^{2-} > H_2PO_4^- > NO_3^- > NO_2^-$ and the capacity of nitrate adsorption was reduced by 50% at a concentration gradient of 10, 20, 30, 40 and 50 mg/L for the anions (Wang et al., 2007). Namasivayam and Holl (2005) reported that the presence of SO_4^{2-}, F, PO_4^{3-} and ClO_4^- considerably reduced the uptake of nitrate by other adsorbents like cross-linked and quaternised Chinese reed.

2.4.2.1.3. Temperature

Temperature is a significant factor that impacts on adsorption. Daifullah (2004) reported that the adsorption capacity of carbon is an endothermic process and it was better at higher temperature due to acceleration of slow adsorption steps or the creation of new active adsorption sites. Temperature had no consistent effect on nitrate adsorption of many adsorbents. The adsorption of nitrate by calcined hydrotalcite-type (H7550) compounds was affected by temperature. Socias-Viciana et al. (2008) reported that adsorption capacities of the calcined adsorbent hydrotalcite-type (H7550) increased from 25ºC to 40ºC. They also reported that the removal efficiency ranged from 70.5% for HT550 at 25ºC to 99.5% for HT850 at 40ºC (Socias-Viciana et al., 2008). Nitrate adsorption by activated carbon was also affected by temperature and it was reported by Demiral and Gunduzo˘glu (2010) that the maximum nitrate adsorption capacity of activated carbon increased from 9.14 to 27.55 mg/g as the temperature increased from 25 to 45°C.

2.4.2.2. Factors affecting phosphate adsorption

2.4.2.2.1. pH

Of the many factors influencing phosphate adsorption, pH is generally considered to be the most important one. Genz et al. (2004) reported that the maximum phosphate adsorption of granulated ferric hydroxide and activated aluminium oxide occurred within the range pH 5.5 to 8.2. For high phosphate concentrations (> 4 mg P/L), there was a steep increase in phosphate adsorption from pH 5.5 to 8.2 on both adsorbents (Genz et al., 2004). A steep rise in phosphate adsorption in the presence of high Ca concentration from pH 4 to 8 was also reported by Bastin et al. (1999) in their study on adsorption of phosphate by a formulation called OX, which contained a mixture of iron oxide

(ferrihydrite) and gypsum. The increased phosphate adsorption was attributed to calcium phosphate precipitation. It could also be due to an increase in positive surface charge caused by Ca^{2+} adsorption (Bolan et al., 1993).

In contrast to the above findings, phosphate adsorption declined when the pH increased such as for aluminium oxide coated media (AOCM), and an increase of pH from 5 to 9 consistently decreased phosphate adsorption with a maximum adsorption of 2.5-3.0 mg P/g at pH 5. This was reported by Sansalone and Ma (2009). Chitrakar et al. (2006a and b) also showed that phosphate adsorption from sodium phosphate solution decreased progressively from pH 2 to 9. The decrease in phosphate adsorption as pH increased is probably due to an increase in negative charges on the adsorbents as pH increases, which represents negatively charged phosphate ions. In contrast, phosphate sorption from sea water increased from pH 2 to 6 and then decreased progressively to 9. The reason behind this behaviour was that in the pH range 2-4, sulphate in sea water greatly affected phosphate sorption because the sorbent preferred divalent sulphate to monovalent $H_2PO_4^-$.

The ion exchange materials' phosphate adsorption capacity was not affected by the change in pH. For example, Awual et al. (2011) produced a novel fibrous anion exchanger named FVA and found that this resin had a high adsorption capacity and selectivity for phosphate at pH 2.0-8.3 and adsorption capacity did not change within the pH range.

2.4.2.2.2. Co-existing ions

Several anions co-exist with phosphate in wastewater, and they can compete for adsorption. For oxides and hydroxides of metals, phosphate has higher affinity than most other anions. For example, Chitrakar et al. (2006a) showed that the tendency for

adsorption of anions on metal oxides such as goethite at pH 8 followed the selectivity order, Cl^-, NO_3^-, SO_4^{2-} << CO_3^{2-}, HPO_4^{2-} and on akaganeite the order was Cl^-, CO_3^{2-} < NO_3^- < SO_4^{2-} < HPO_4^{2-}. Similarly, Genz et al. (2004) reported that the adsorption sequence for removing anions from membrane bioreactor (MBR) filtrates was Cl^- < NO_3^- < SO_4^{2-} < HCO_3^- < PO_4^{3-} for granulated ferric hydroxide sorbent and Cl^- ~ NO_3^- < SO_4^{2-} ~ HCO_3^- < PO_4^{3-} for activated aluminium oxide sorbent. The selectivity order for the adsorption of phosphate from sodium phosphate solution, sea water and waste water on a synthetic amorphous zirconium hydroxide, was found to be Na^+, K^+, Ca^{2+} < Cl^- < SO_4^{2-} << PO_4^{3-} (Chitrakar et al., 2006b).

In contrast to metal oxides and hydroxides, some ion exchange resins have shown lower selectivity for phosphate than `other anions such as nitrate. For example, Samatya et al. (2006a) and Johir et al. (2011) indicated that Purolite A520E had higher affinity for nitrate than phosphate and sulfate.

2.4.2.2.3. Temperature

The effects of temperature on phosphate removal could be explained by physical or chemical influences. Physically, water temperature may have an influence on particle transport processes or particle collision rates, mainly through the effect on viscosity, and thus on the mixing energy dissipated in water. With decreasing temperature, the viscosity increases and the poor rapid-mixing conditions caused by low water temperature might lead to inhomogeneous distribution of species in the water, which can lead to poor phosphate removal. In a phosphate adsorption study on metal oxide and hydroxides such as goethite conducted at temperatures of 25, 45 and 65^{o}C by Paleka and Deliyanni (2009) the maximum adsorption capacity occurred at a temperature of 25^{o}C. Higher temperature

caused the adsorption capacity to decline, indicating that adsorption is an exothermic process.

2.4.2.3. Factors affecting fluoride adsorption

2.4.2.3.1. pH

Similar to phosphate, pH is generally considered to be an important factor for fluoride adsorption. Generally, fluoride adsorption is small at both very low and very high pH. The main reason for a reduction in fluoride adsorption below pH 4 is that fluoride forms weakly ionised HF at these pH values (Liao and Shi, 2005; Ghorai and Pant, 2005; Sujana et al., 1998; Raichur and Basu, 2001). At a pH above 7–8 the removal of fluoride decreases not only because the adsorbent surface becomes negatively charged but also because the concentrations of hydroxyl, bicarbonate and silicates ions increase so that they compete with fluoride for adsorption. In addition to the larger number of positive surface charges at low pH values increasing fluoride adsorption, surface protonation at a pH less than the pH of PZC provides more H atoms at the adsorbent surface leading to elevated H-bonding between the H atoms and fluoride in solution; this results in increased fluoride adsorption (Tang et al., 2009). Adsorption by a ligand exchange mechanism is also favoured at low pH because of a stronger attractive force between fluoride and the adsorbent surface and the presence of more hydroxylated sites for exchange with fluoride than at a high pH (Cengelo˘glu, 2002; Teng et al., 2009; Li et al., 2003).

One of the most important properties of the adsorbent influencing the extent of fluoride adsorption is the pH at the point of zero charge (PZC). At pH values above the PZC the adsorbents' surface is negatively charged, and therefore the negatively charged fluoride ions are not attracted to the adsorbent surface. At pH values less than the PZC the surface is positively charged, therefore fluoride ions are adsorbed. In some situations,

at low pH values, fluoride exists as positively charged AlF complexes and this can reduce fluoride adsorption (Loganathan et al., 2013a; Ku and Chiou, 2002; Lai and Liu, 1996).

It is apparent from a literature review that fluoride adsorption is generally lowest at extremely low and high pH values. The adsorption is highest around the neutral pH that is commonly found in natural water. Therefore prior pH adjustment is not normally required for the effective removal of fluoride in treatment plants (Loganathan et al., 2013a).

2.4.2.3.2. Co-existing anions

With reference to fluoride adsorption, the extent of the competition of other anions depends on the relative concentrations of the ions and their affinity to the adsorbent. Meenakshi and Viswanathan (2007) reported that the order of adsorption of anions by the chelating resin was reported to be $F^- > Cl^- > NO_3^- > SO_4^{2-}$. They also found that increased concentrations of Cl^-, SO_4^{2-}, Br^-, NO_3^- and HCO_3^- decreased fluoride adsorption by an anion exchange resin which adsorbs anions by an ion exchange mechanism, whereas these anions had no effect on fluoride adsorption by a chelating resin which adsorbed fluoride selectively by a H-bonding mechanism. Solangi et al. (2010) studied the adsorption of fluoride by a thio-urea amended amberlite resin in the presence of PO_4^{3-}, Cl^-, SO_4^{2-}, Br^-, NO_3^-, NO_2^-, HCO_3^- and CO_3^{2-} at five times the molar concentration of fluoride. They observed that Br^-, NO_2^-, and PO_4^{3-} had little interference with fluoride adsorption; the other ions had no interference. This was explained as being due to the strong H-bonding of fluoride with the groups in the resin.

In their literature review, Loganathan et al. (2013a) concluded that the non-specifically adsorbing anions (e.g. nitrate, chloride) do not compete with fluoride for adsorption on adsorbents that adsorb fluoride using specific adsorption. Only anions that

are adsorbed by specific adsorption (e.g. phosphate, selenate, arsenate) compete with fluoride for adsorption. When fluoride is adsorbed by non-specific adsorption the non-specifically adsorbing anions can compete with fluoride.

2.4.2.3.3. Temperature

Although temperature had no consistent effect on fluoride adsorption, the adsorption capacity of many fluoride adsorbents increased with temperature showing an endothermic nature of adsorption such as granular ferric hydroxide (Kumar et al., 2009), fly ash (Chaturvedi et al., 1990), calcined Mg/Al/CO_3 LDH (Lv et al., 2006), LDH/chitosan (Viswanathan and Meenakshi, 2010) and spent catalyst (Lai and Liu, 1996). On the other hand, adsorption capacity of some other adsorbents decreased with temperature showing an exothermic nature of adsorption such as chelating resin (Meenakshi and Viswanathan, 2007), alum sludge (Sujana et al., 1998), calcined Zn/Al LDH (Das et al., 2003), modified activated carbon (Daifullah et al., 2007), LDH/chitin (Sundaram et al., 2008) and geo-materials (Sujana et al., 2009).

The contrary behaviours of fluoride adsorbents concerning the effect of temperature were not clearly stated in previous studies. The reasons can be the temperature range studied, the nature of the adsorbent, and the conditions used in the studies. For example, at extremely low temperatures (5, 10^{o}C), the rate of adsorption was reported to be low because the rate of movement of fluoride to the adsorption sites is low. Lai and Liu (1996) reported that fluoride adsorption on spent catalyst increased significantly when the temperature increased from 5^{o}C to 25^{o}C but very little further increase in adsorption was observed when the temperature rose to 50^{o}C. Sujana et al. (1998) also stated that the exothermic nature of adsorption of fluoride on alum sludge was because the rising temperature increased the tendency for fluoride to escape from the

adsorbent. Another reason behind this behaviour was an increase in thermal energy of adsorbed fluoride at higher temperatures, causing increased desorption.

2.4.3. Adsorption process application

The practical application of the adsorption process for removing contaminants from water is accomplished by mixing the adsorbent with adsorbate either in a batch-type contact unit operation or a continuous flow packed column bed system. Adsorption processes are characterised by adsorption equilibrium, adsorption kinetics and fixed bed adsorption.

2.4.3.1. Batch study

In batch contact unit systems, a predetermined amount of adsorbent is mixed with the water for a given contact period and subsequently is separated by sedimentation or filtration. The flexibility of this process makes it adaptable for many applications particularly in drinking water treatment plants. The adsorption process is characterised by mainly two phenomena: (i) adsorption equilibrium, and (ii) adsorption kinetics.

2.4.3.1.1. Adsorption equilibrium

Adsorption equilibrium is described by an equation relating the amount of adsorbate adsorbed onto the adsorbent and the equilibrium concentration of the adsorbate in solution at a given constant temperature (Sincero and Sincero, 2003; Chaudhary et al., 2003). The analytical forms of adsorption isotherms are complex due to the solid surfaces' structural and energetic heterogeneity. As the adsorption processes proceeds, the adsorbed adsorbate tends to desorb into the solution until the rates of adsorption and desorption attain an equilibrium state which is called adsorption equilibrium. At

equilibrium, no change can be observed in the concentration of the adsorbate on the solid surface or in the bulk solution. The position of equilibrium is characteristic of the entire system, the adsorbate, adsorbent, solvent, temperature, pH, and so on. Adsorbed quantities at equilibrium usually increase with an increase in the adsorbate concentration. The presentation of the amount of adsorbate adsorbed per unit mass of adsorbent as a function of the equilibrium concentration in bulk solution, at constant temperature, is termed the adsorption isotherm.

Equilibrium adsorption is the most informative and important test for estimating the adsorption capacity of an adsorbent for an adsorbate in a given condition (concentration and temperature) and the competition among absorbates in the case of multi-component adsorption (Suzuki, 1990). For a given adsorbate-adsorbent system, the adsorption equilibrium can be expressed as follows:

$$q = \int(C, T) \tag{2.1}$$

where, q= amount adsorbed per unit mass of adsorbent, commonly expressed as moles of adsorbate per gram of adsorbent or equivalent quantities

C= concentration of the adsorbate in the solution

T= temperature

At constant temperature, the amount of adsorption may be considered as

$$q = \int(C) \tag{2.2}$$

T = constant

Description of adsorption equilibrium by an appropriate isotherm equation is the first step in the design of an adsorption system since it reflects the capacity or affinity of

an adsorbent for a particular adsorbate. At the end of the equilibrium period the aqueous-phase concentration of the adsorbate is measured and the adsorption equilibrium capacity is calculated for each experiment using the mass balance expression,

$$q_e = \frac{(C_0 - C_e)V}{M} \tag{2.3}$$

where, q_e= equilibrium adsorbent-phase concentration of adsorbate, mg adsorbate/g adsorbent; C_0 = initial aqueous-phase concentration of adsorbate, mg/L; C_e = equilibrium aqueous-phase concentration of adsorbate, mg/L; V = volume of the solution (L) and M = mass of adsorbent (g). Removal efficiency is calculated using Equation 2.4.

$$\text{Removal efficiency (\%)} = \frac{(C_0 - C_e)}{C_0} \text{ x } 100 \tag{2.4}$$

2.4.3.1.2. Adsorption kinetics

The adsorption kinetics is the measure of rate of adsorption, and it describes the adsorbate transport mechanism from bulk solution to the adsorption site on adsorbent surface. There are basically four steps an adsorbate passes through to get adsorbed onto the porous adsorbent. First, the adsorbate must be transported from bulk solution to the boundary layer (bulk solution transport) of the wastewater surrounding the adsorbent. The transportation occurs by diffusion if the adsorbent is in a quiescent state. In the turbulent mixing batch reactors, transporting the bulk solution occurs by turbulent mixing. The second step is characterised by the adsorbate being transported by molecular diffusion

through the boundary layer (film diffusion transport) surrounding the adsorbent particles. The third step occurs after passing through the boundary layer, when the adsorbate must be moved through the pores of the adsorbent to the available adsorption sites (pore transport). The intraparticle transport may occur by molecular diffusion through the wastewater solution in the pores (pore diffusion) of by diffusion along the surface of the adsorbent (surface diffusion).

Finally, when the adsorbate reaches the adsorption site, the adsorption bond is formed between the adsorbate and the adsorbent. This step is very rapid for physical adsorption (Tien, 1994). Thus, it is either the bulk solution transport, film diffusion transport, film diffusion transport or pore transport that controls the rate of organic material removed from the wastewater. In turbulent mixing as it happens in batch reactor, it is most likely that a combination of film diffusion and pore diffusion controls the rate of adsorption (Tien, 1994). At the initial stage, the film diffusion may control the adsorption rate but after the accumulation of adsorbates within the pore of the adsorbent, it is possible that the adsorption rate is controlled by the pore transport.

The procedure of kinetic tests is identical to that of equilibrium tests. The aqueous samples are taken at pre-set time intervals during the adsorption process and the concentrations of adsorbates are measured. The amount of adsorption at time t, q_t (mg/g), is calculated as shown in Equation 2.5.

$$q_t = \frac{(C_0 - C_t)V}{M} \tag{2.5}$$

where, C_0 = initial concentration of adsorbate (mg/L); C_t = concentration of adsorbate at time t (mg/L); V = volume of the solution (L), and M = mass of dry adsorbent (g). Removal efficiency is calculated using Equation 2.6.

$$\text{Removal efficiency}\,(\%) = \frac{(C_0 - C_t)}{C_0} \text{ x } 100 \tag{2.6}$$

2.4.3.2. Column study

In large-scale application of the adsorption process, a solution containing the pollutant flows continuously through a column of adsorbent or a packed bed where dynamic adsorption of the solute occurs. The columnar operation allows more efficient utilisation of the adsorptive capacity than the batch process. The adsorbent at the inlet end of the column is contacted continuously by the solution at the initial solute concentration. As the change in concentration at each subsequent layer is small, the adsorbent in the column acts like a series of layers, with each layer in contact with a fresh solution of constant solute concentration. This procedure results in maximum loading of the adsorbent (high x/M on the adsorption isotherm) at a constant solute concentration and this contrast to the continuously declining solute concentration in the batch process. Applying the adsorption system in practice is usually carried out in the fixed bed adsorption mode. The adsorbent is packed in a column and the target pollutants are passed through either end to be adsorbed by the adsorbent. In the course of adsorption, a saturated zone is formed near the inlet of the column and a zone with increasing concentration is observed at the frontal part.

The main feature of the dynamic behaviour of a fixed bed adsorption is the change in effluent concentration with time. These concentration-time curves are commonly referred to as the breakthrough curves, and the time at which the effluent concentration reaches the threshold value is called the breakthrough time. The rational design of an adsorption system is therefore based on the accurate predictions of breakthrough curves for specified conditions. There are different empirical and analytical methods for predicting the breakthrough curve of the fixed bed adsorption system. The scale-up procedure is based on the experimentally determined breakthrough curve (Vermeulen et al., 1973), Collin's length of unused bed (LUB) method (Collins, 1967), and the methods based on adsorption equilibrium and mass transfer are used to predict the breakthrough curve of a fixed bed adsorption system. Finite difference and orthogonal collocation methods are the most commonly used methods to solve the ordinary and partial differential equations that described the fixed bed adsorption dynamics. The actual adsorption process is complex and unsteady, and the external mass transfer, intraparticle diffusion, and equilibrium relationship need to be considered in the model at the same time. Therefore, the numerical solution is the preferred method for solving the dynamic equations. When an index parameter is used to represent the overall adsorbate concentration, the computational difficulties are further reduced by the use of linear driving force models (Rutheven, 1984; Vigneswaran and Moon, 1999; Lee, 1995).

2.4.4. Adsorption Batch Modelling

2.4.4.1. Equilibrium Modelling

A number of isotherm models have been proposed by previous researchers that describe the adsorption process, for example Langmuir, Freundlich, Tempkin, Sips, BET, Henry's Law, etc. which have been developed relating q and C_e. Most of them, however,

are not suitable for adsorption in water due to a few but important drawbacks. The most used adsorption isotherm models for water are the Langmuir and Freundlich models for the reason that they are simple and fit better to the experimental data.

2.4.4.1. 1. Langmuir Modelling

The equilibrium between a solute and an adsorbent's surfaces are commonly represented by single-component adsorption isotherms, which basically consider the following surface complexion reaction,

$$R + X \leftrightarrow RX \tag{2.7}$$

where, R represents the adsorbent in its initial form, X is the aqueous phase species, and RX is the species X on the adsorbent phase.

The Langmuir isotherm model is employed to evaluate the homogeneous adsorption in water. This was originally proposed by Langmuir (1918) for the homogeneous adsorption of gases but it is now extensively used for adsorption of ions from solution (Faust and Aly, 1987). The basic assumptions underlying Langmuir's model, which is also called the ideal localised monolayer model, are:

- The molecules are adsorbed on definite sites on the surface of the adsorbent.
- Each site can accommodate only one molecule (monolayer).
- The area of each site is a fixed quantity determined solely by the geometry of the surface.
- The adsorption energy is the same at all sites.
- The adsorbed molecules cannot migrate across the surface or interact with neighbouring molecules.

The Langmuir equation was originally derived from kinetic considerations and has been widely used as an empirical equation for qualitative purposes in both single component and multicomponent systems (Manes, 1980). Later, it was developed on the basis of statistical mechanics, thermodynamics, the law of mass action, theory of absolute reaction rates, and the Maxwell-Boltzmann distribution law (Young and Crowell, 1962).

The Langmuir model is semi-empirical and derives from Equation 2.7 assuming a monolayer adsorption phenomenon on a homogeneous surface (Crittenden et al., 1985; Matsui et al., 1998). Considering Equation 2.7 at equilibrium, the Langmuir parameter K_L (L/mg) representing the equilibrium constant can be expressed as,

$$K_L = [RX]/[R]\,[X] \tag{2.8}$$

At equilibrium, the Langmuir equation arises from Equation 2.8, considering $[X] = C_e$; $[RX] = q_e$; and $[R] = q_0 - q_e$, where q_0 (mg/g) represents the maximum capacity of the adsorbent.

Equation 2.8 then becomes,

$$K_L = q_e / (q_0 - q_e)\, C_e \tag{2.9}$$

And a simple modification leads to Equation 2.8 which is the equation for the Langmuir adsorption isotherm model,

$$q_e = \frac{q_{max} K_L C_e}{1 + K_L C_e} \tag{2.10}$$

where, C_e = equilibrium concentration of the adsorbate (mg/L), q_e = amount of the adsorbate adsorbed per unit mass of the adsorbent (mg/g), q_{max} = maximum amount of the adsorbate adsorbed per unit weight of the adsorbent (mg/g); K_L = Langmuir constant related to the energy of adsorption (L/mg).

The Langmuir isotherm model advocates that uptake occurs on a homogeneous surface by monolayer adsorption without adsorbed molecules interacting. The model assumes uniform energies of adsorption onto the surface and no transmigration of adsorbate in the plane of the surface (Hameed et al., 2007).

This model can be linearised as follows:

$$\frac{C_e}{q_e} = \frac{1}{q_{max} K_L} + \frac{C_e}{q_{max}} \tag{2.11}$$

The parameters K_L and q_{max} are deduced from nonlinear regression of C_e / q_e vs Ce. The Langmuir equation can also be expressed in terms of a dimensionless separation factor, R_L, which is defined as (Weber et al., 1974):

$$R_L = \frac{1}{1 + (K_L C_0)} \tag{2.12}$$

where, C_0 = the highest initial adsorbate concentration, K_L = the Langmuir's adsorption constant (L/mg). The value of R_L is interpreted as follows: R_L= 0 for the irreversible case, 0 <R_L< 1 for favourable equilibrium, R_L= 1 for the linear case, and R_L> 1 for unfavourable equilibrium.

2.4.4.1.2. Freundlich Modelling

Unlike the Langmuir isotherm, the Freundlich isotherm is an empirical model which does not imply a maximum adsorption capacity of the adsorbent (Amuda and Ibrahim, 2006). In the Freundlich equation the adsorbed amount increases infinitely with the increase in concentration, which is unrealistic. The Freundlich adsorption equation is perhaps the most widely used mathematical description of adsorption in aqueous systems. The Freundlich equation is expressed as follows (Freundlich, 1926):

$$q_e = K_F C_e^{1/n} \tag{2.13}$$

This model can be linearised as follows:

$$\ln q_e = \ln K_F + \frac{1}{n} \ln C_e \tag{2.14}$$

where, C_e = equilibrium concentration of adsorbate (mg/L), q_e = amount of adsorbate adsorbed per unit mass of adsorbent (mg/g), K_F and n = Freundlich constants (mg/g). K_F (mg /g) $(L/mg)^{1/n}$ and n (dimensionless) are the Freundlich constants determined from the linear regression analysis. The value of the parameter n is representative of both the adsorption intensity and the surface heterogeneity. Despite the fact that parameter n lacks physical meaning, it is generally admitted that $0 < 1/n < 1$ indicates favourable adsorption, while $1/n = 1$ characterises a linear adsorption phenomenon (Fytianos et al., 2000). The K_F constant may be considered as a rough indication of the adsorption capacity expressed or as an adsorption affinity parameter.

The Freundlich isotherm's drawback is that it does not converge with Henry's law at low surface coverage. Therefore it fails to describe equilibria as $q \rightarrow 0$ and is thermodynamically inconsistent (McKay, 1996). However, this problem has been overcome by extrapolation of data to zero concentration (Fritz and Schlunder, 1981) and its ability to fit a broad set of experimental data still makes it a popular model for studying adsorption and ion exchange phenomena.

2.4.4.1.3. Tempkin Modelling

The Tempkin model is another empirical model that is used to describe adsorption data and it is depicted using the following equation (Aharoni and Ungarish, 1977):

$$q_e = \frac{RT}{b} \ln (A_T C_e) \tag{2.15}$$

$$q_e = \frac{RT}{b} \ln (A_T) + \frac{RT}{b} \ln (C_e)$$

$$\frac{RT}{b} = B$$

This model can be linearised as follows:

$$q_e = B \ln (A_T) + B \ln (C_e) \tag{2.16}$$

where, C_e = equilibrium concentration of adsorbate (mg/L); A_T =Tempkin isotherm equilibrium binding constant (L/g); b = Tempkin isotherm constant; R=

universal gas constant (8.314 J/mol/K); T= Temperature at 298K; B = Constant related to heat of adsorption (J/mol).

2.4.4.2. Kinetic Modelling

Researchers have proposed a number of kinetic models that describe the adsorption kinetic process. These are known as the pseudo-first-order, pseudo-second-order, homogeneous surface diffusion model (HSDM), Elovich and intraparticle diffusion models.

2.4.4.2.1. Pseudo-first-order modelling

A simple kinetic model that describes the process of adsorption is the pseudo-first-order equation (Ho and McKay, 1998). Lagergren (1898) introduced this model for the adsorption in solid/liquid systems based on the chemical kinetic first-order equation

$$\frac{dq_t}{dt} = k_1\left(q_e - q_t\right) \tag{2.17}$$

where, q_e = amount of adsorbate adsorbed at equilibrium (mg/g); q_t = amount of adsorbate adsorbed at time, t (min) (mg/g) and k_1 = equilibrium rate constant of pseudo-first-order adsorption (1/min). After integration with the initial condition $q_t = 0$ and $t = 0$; we obtain the linearised form of this equation:

$$\ln\left(q_e - q_t\right) = \ln q_e - k_1 t \tag{2.18}$$

where, values of k_1 can be calculated from the plot of log(qe - qt) vs. t .

2.4.4.2.2. Pseudo-second-order modelling

The pseudo-second order kinetic equation was proposed by Blanchard et al. (1984) and is expressed as:

$$\frac{dq_t}{dt} = k_2\left(q_e - q_t\right)^2 \tag{2.19}$$

where, q_e= amount of adsorbate adsorbed at equilibrium (mg/g); q_t = amount of adsorbate adsorbed at time, t (min) (mg/g) and k_2 = equilibrium rate constant of pseudo-second-order (1/min).

Separating the variables in Eq. (2.19) gives:

$$\frac{dqt}{(qe-qt)2} = k_2\, dt \tag{2.20}$$

Integrating and applying boundary conditions, t = 0 and q_t = 0 to t = t and q_e = qt, gives

$$q_t = \frac{qe^2 k_2\, t}{1+q_e\, k_2 t} \tag{2.21}$$

Equation (2.21) can be rearranged to obtain

$$q_t = \frac{qe^2 k_2\, t}{1/qe^2 k_2 + t/qe} \tag{2.22}$$

and the linear form of

$$\frac{t}{q_t} = \frac{1}{k_2 q_e^2} + \frac{t}{q_e} \quad (2.23)$$

where, k_2 and q_e are calculated from the intercept and slope of the plots of t/q_t vs. t. If the data fit well to the pseudo-second-order process, the calculated q_e values will agree very well with the experimental q_e value. The good agreement of the data with the pseudo-second-order kinetics model would suggest that chemisorption may serve as the adsorption mechanism (Tovar-Gómez et al., 2013; Yan et al., 2010; Tor et al., 2009).

2.4.4.2.3. Elovich model

When the adsorption process involves chemisorption in a solid surface, and the adsorption velocity decreases over time due to covering of the superficial layer, the Elovich model, Equation 2.25, is mostly used for this purpose (Wu et al., 2009). Sparks (1989) and Zhang and Stanforth (2005) reported that when the adsorbate ions and the surface sites interact chemically through a second order mechanism, the application of the Elovich equation expressed in Equation 2.24 is more appropriate:

$$\frac{dqt}{dt} = \alpha \exp(-\beta qt) \quad (2.24)$$

where, α is the initial adsorption rate (mg/g min) and β is a desorption constant (g/mg). These coefficients are computed from the plots of q_t vs. ln (t) according to the Equation 2.25:

$$q_t = (1/\beta) \ln (\alpha\beta) + =(1/\beta) \ln (t) \quad (2.25)$$

2.4.4.2.4. Intraparticle diffusion model

Adsorption is a multi-step process involving transport of the solute molecules from the aqueous phase to the surface of the solid particulate, followed by diffusion of the solute molecules into the pore interiors (Weber and Morris, 1963; Allen et al., 1989). Weber and Morris (1963) reported that in the diffusion phase the amount of solute adsorbed is proportional to the half-power of time.

The most widely applied intraparticle diffusion equation for an adsorption system was developed by Weber and Morris (1963) as follows:

$$q_t = k_i (t^{1/2}) + C \quad (2.26)$$

where, k_i is intraparticle diffusion rate constant (mg/g $min^{1/2}$). The k_i is the slope of straight line portions of the plot of q_t vs. $t^{1/2}$. When intra-particle diffusion plays a significant role in controlling the kinetics of the adsorption process, the plots of q_t vs. $t^{1/2}$ yield straight lines passing through the origin and the slope gives the rate constant k_i.

The deviation of the straight lines from the origin may be due to the difference in the rate of mass transfer in the initial and final stages of adsorption (Panday et al., 1986; Mall et al., 2006). The values of slopes indicate that the pores are micropores and the intraparticle diffusional resistance is due to micropores only (Goswami and Gosh, 2005). The diffusion rate parameters indicate that the intraparticle diffusion controls the adsorption rate, which is the slowest part of the adsorption process. Sometimes the plots obtained are related by two straight lines; the first straight portion depicting the macropore diffusion and the second representing the micropore diffusion (Allen et al., 1989).

2.4.4.2.5. Homogeneous surface diffusion model (HSDM)

The adsorption process can be complex and considerable use is made of mathematical models to describe possible rate controlling mechanisms as well as computers to perform accurate and quick computations (Tien, 1994; Do, 1998). The homogeneous surface diffusion model (HSDM) consists of a three-step process: (i) the adsorbate diffuses through a stagnant liquid film layer surrounding the adsorbent particle; (ii) the adsorbate adsorbs from the liquid phase onto the outer surface of the adsorbent particle; and (iii) the adsorbate diffuses along the inner surface of the adsorbent particles until it reaches its adsorption site (Tien, 1994; Najm, 1996). Several methods are available in the literature for solving the homogeneous diffusion equation but the search for accuracy, simplicity and reducing the number of limiting assumptions continues. One common method using a single constant surface diffusivity to generate theoretical concentration decay curves for three adsorption systems is described here (Beverloo et al., 1984; Hutchinson and Robinson, 1990; Miyahara and Okazaki, 1993). The model is simple and easy to use and provides accurate solutions for a wide range of adsorbents over a wide range of experimental conditions.

Equations 2.27 – 2.30 are used in the model.

$$\frac{\partial q}{\partial t} = D_s\left(\frac{\partial^2 q}{\partial r^2} + \frac{2}{r}\frac{\partial q}{\partial r}\right) \tag{2.27}$$

Initial and boundary conditions are:

$$t = 0 \;;\; q = 0 \tag{2.28}$$

$$r = 0 \;;\; \frac{\partial q}{\partial r} = 0 \tag{2.29}$$

$$r = r_p \;;\; D_s \rho_p \frac{\partial q}{\partial r} = k_f (C - C_s) \tag{2.30}$$

where q is surface concentration at any radial distance (r) from the centre of the particle during adsorption, mg/g; D_s, the surface diffusion coefficient (the rate of diffusion of the adsorbate along the surface of the adsorbent), m^2/s; k_f, the external mass transfer coefficient, m/s; ρ_p, the apparent density of the adsorbent, kg/m^3; C, the bulk phase concentration of adsorbate, mg /L; C_s is the concentration of the adsorbate on the external surface, mg /L. Freundlich equation is used as the boundary condition in HSDM calculations. Using the isotherm parameters and equations (2.27) - (2.30), k_f and D_s can then be calculated.

2.4.5. Adsorption Column Modelling

2.4.5.1. Bohart-Adams Model

The Bohart-Adams model (1920) established the fundamental equations describing the relationship between C_t/C_o and t in a continuous flow system. This model was established based on the surface reaction theory and it assumed that equilibrium is not instantaneous. The model expression is shown below:

$$\ln C_t/C_o = k_{AB}C_o t - k_{AB}N_o Z/F \tag{2.31}$$

where, C_o and C_t (mg/L) are the inlet and effluent adsorbate concentration, respectively, k_{AB} (L/mg.min) is the kinetic constant, F (cm/min) is the linear velocity calculated by dividing the filtration velocity by the column section area, Z (cm) is the bed depth of column and N_o (mg/L) is the adsorbate saturation concentration. The values for

k_{AB} and N_o are determined from the intercept and slope of the linear plot of $\ln(C_t/C_o)$ against time (t). The Bohart-Adams adsorption model is commonly applied to experimental data to describe the initial part of the breakthrough curve.

2.4.5.2. The Thomas model

The Thomas model (1944) assumes plug flow behaviour in the bed, and uses the Langmuir isotherm for equilibrium and second order reversible reaction for kinetics. This model is suitable for adsorption processes where the external and internal diffusion limitations are absent. The linearised form of the Thomas model can be expressed as follows:

$$\ln (C_o/C_t - 1) = k_{Th}q_oM/Q - k_{Th}C_ot \quad (2.32)$$

where, k_{Th} (mL/min.mg) is the Thomas rate constant; q_o (mg P/g) is the equilibrium phosphate uptake per g of the Purolite resin; C_o (mg/L) is the inlet phosphate concentration; C_t (mg P/L) is the outlet phosphate concentration at time t; M (g) is the mass of adsorbent, Q (mL/min) is the filtration velocity and t (min) stands for filtration time.

A linear plot of $\ln[(C_o/C_t)-1]$ against time (t) is employed to determine values of k_{Th} and q_o from the intercept and slope of the plot. The Thomas model is based on the assumption that the process follows Langmuir kinetics of adsorption-desorption with no axial dispersion. It describes the rate driving force as obeying the second order reversible reaction kinetics (Aksu and Gonen, 2004). The good fit of the experimental data with the Thomas model would indicate that external and internal diffusion will not constitute the limiting step (Aksu and Gonen, 2004; Padmesh et al., 2005).

2.4.5.3. The Yoon–Nelson model

Yoon and Nelson (1984) developed a model based on the assumption that the rate of decrease in the probability of adsorption of the adsorbate molecule is proportional to the probability of the adsorbate adsorption and the adsorbate breakthrough on the adsorbent. This model was also derived based on the assumption that the rate of decrease in the probability of adsorption for each adsorbate molecule is proportional to the probability of adsorbate adsorption and the probability of adsorbate breakthrough on the adsorbent (Yoon and Nelson, 1984). The linearised form of the Yoon–Nelson model for a single component system is expressed as:

$$\ln [C_t/(C_o - C_t)] = k_{YN}t - \tau k_{YN} \quad (2.33)$$

where, k_{YN} (1/min) is the rate velocity constant, τ (min) is the time required for 50% phosphate breakthrough. A linear plot of $\ln [C_t/(C_o - C_t)]$ against sampling time (t) is used to determine values of k_{YN} and τ from the intercept and slope of the plot.

2.4.5.4. The ANN Model

Tovar-Gómez et al. (2013) introduced the ANN approach in an effort to improve the capability of the Thomas model. They demonstrated that the hybrid ANN-Thomas model predicted the fluoride breakthrough in columns containing bone char better than the Thomas model, especially for unsymmetrical breakthrough curves. The software, Neurosolutions, supplied by NeuroDimension, Inc (USA) was used for the modelling. Previous studies have used these input variables for the modelling of breakthrough curves using black-box ANN models (Oguz and Ersoy, 2010; Faur et al., 2008; Cavas et al.,

2011) because they have a statistical influence on how well the dynamic adsorption process performs. Additionally, this set of input variables is uncorrelated, which agrees with the principle component analysis approach. The architecture of the hybrid ANN model was determined based on preliminary calculations using a trial and error procedure where the combination of input variables, the number of hidden layers and neurons were changed until a proper ANN architecture was found.

2.4.5.5. Fixed bed numerical modelling

In order to formulate the dynamic model for the fixed bed absorber, the following assumptions are used: 1) The system is under isothermal conditions; 2) The flow pattern is an axially dispersed plug flow and the radial concentration gradient is insignificant; 3) The shape of the adsorbent is spherical and its pore structure is uniform; 4) The liquid film mass transfer resistance at the outer surface of the solid particles can be described by a driving force; 5) Intraparticle diffusion can be characterised by the homogeneous surface diffusion model; and 6) Adsorption equilibrium isotherm can be represented by the Langmuir equation.

The mass balance equations and the boundary conditions of the fixed bed system are given by the following equations, which were devised by Tien (1994), Ruthven (1984) and Yang (1986):

$$\frac{\partial C}{\partial t} = D_L \frac{\partial^2 C}{\partial z^2} - V\frac{\partial C}{\partial z} - \frac{1-\varepsilon_b}{\varepsilon_b}\frac{3k_f}{R}\left(C - C_s\right) \tag{2.34}$$

where, C (mg/L) is the adsorbate concentration in the adsorber at any given time and position, C_s (mg/L) is the adsorbate concentration at the particle-liquid film interface,

t (min) is the time, z (m) is the axial coordinate, D_L (m^2/s) is the axial dispersion coefficient, V (m/s) is the interstitial velocity, ϵ_b is the bed voidage, R (m) is the particle radius of adsorbent and k_f (m/s) is the film mass transfer coefficient.

The above Equation 2.34 can be solved by using the initial and boundary conditions, C = 0 and z = 0,

$$D_L \left.\frac{\partial C}{\partial z}\right|_{z=0} = -v\left(C|_{z=0^-} - C|_{z=0^+}\right) \tag{2.35}$$

and at z=L,

$$\left.\frac{\partial C}{\partial z}\right|_{z=L} = 0 \tag{2.36}$$

The homogeneous surface diffusion equation can be expressed as:

$$\frac{\partial q}{\partial t} = D_s\left(\frac{\partial^2 q}{\partial r^2} + \frac{2}{r}\frac{\partial q}{\partial r}\right) \tag{2.37}$$

Initial and boundary conditions are:

$$t = 0 \;;\; q = 0 \tag{2.38}$$

$$r = 0 \;;\; \frac{\partial q}{\partial r} = 0 \tag{2.39}$$

$$r = r_p \;;\; D_s \rho_p \frac{\partial q}{\partial r} = k_f\left(C - C_s\right) \tag{2.40}$$

where q is surface concentration at any radial distance (r) from the centre of the particle during adsorption, mg /g; D_s, the surface diffusion coefficient (the rate of diffusion of the nitrate along the surface of the adsorbent), m^2/s; k_f, the external mass transfer coefficient, m/s; ρ_p, the apparent density of the adsorbent, kg/m^3; C, the bulk

phase concentration, mg/L; C_s, the concentration on the external surface, mg/L. The Langmuir isotherm describes the adsorption equilibrium relationship between liquid and solid phase concentrations.

Axial dispersion coefficient, D_L, can be estimated from the following empirical correlation introduced by Delgado (2006) and Jourak et al. (2011):

$$\frac{1}{Pe_L} = \frac{Pe_m}{5}\left(1-p^2\right)+\frac{Pe_m^2}{25}p(1-p)^3\left\{\exp\left[-\frac{5}{p(1-p)Pe_m}\right]-1\right\}+\frac{1}{\tau Pe_m} \tag{2.41}$$

$$p = \frac{0.48}{Sc^{0.15}}+\left(\frac{1}{2}-\frac{0.48}{Sc^{0.15}}\right)\exp\left(-\frac{75Sc}{Pe_m}\right) \tag{2.42}$$

where, Pe_L, Pe_m, Sc and τ□ are the Peclet number for axial dispersion, Peclet number for particle, Schmidt number and the tortuosity, respectively. The external mass transfer coefficient, k_f, is estimated from the following empirical correlation equation depicted by Chu et al. (1953):

$$k_f = 5.7V_s Re^{-0.75}Sc^{-0.67} \tag{2.43}$$

where, Re, Sc and V_s are Reynolds number, Schmidt number and superficial velocity, respectively. The molecular diffusion coefficient, D_m, can be calculated using the following Wilke-Chang equation (1955):

$$D_m = 7.4\times10^{-8}\frac{(\phi M_b)^{1/2}T}{\mu V_a^{0.6}} \tag{2.44}$$

where, Φ , M_b , T, μ , and V_a are an association factor of solvent, molecular weight of solvent, temperature, viscosity of solvent and solute molar volume at its normal boiling temperature, respectively. In order to simulate the experimental breakthrough curves, one needs to solve the dynamic equations described above. The orthogonal collocation method (OCM) and the variable coefficient ordinary differential equation solver (VODE) are used for that purpose (Villadsen and Michelsen, 1978; Brown et al., 1989; Abdul et al., 2010; Shim et al., 2012).

2.5. Adsorbents

The pore size is an important factor of the adsorbent which influences the adsorption capacity. Most of the solid adsorbents possess a complex porous structure that consists of pores of different sizes and shapes. In terms of the experience of adsorption science, the total porosity is usually classified into three groups of micropores (smaller than 2 nm), mesopores (in the range of 2 to 50 nm) and macropores (larger than 50 nm) (IUPAC, 1985). Adsorption in micropores is essentially a pore filling process because the micropores' sizes are comparable to those of adsorbate molecules. All atoms or molecules of the adsorbent can interact with the adsorbate species. That is the fundamental difference between adsorption in micropores and larger pores like mesopores and macropores. Consequently the size of the micropores determines the accessibility of adsorbate molecules to the internal adsorption surface, and the pore size distribution of micropores is an important property for characterising the absorptivity of adsorbents.

In the case of mesopores whose walls are formed by many adsorbent atoms or molecules, the boundary of interphases (adsorbent surface area) has a distinct physical meaning. The action of adsorption forces occurs at a close distance from the mesopores'

walls. Therefore, the mono and multilayer adsorption takes place successively on the surface of mesopores, and their filling proceeds according to the mechanism of capillary adsorbate condensation (Oscik, 1982). The basic parameters characterising mesopores are: specific surface area, pore volume and pore-size or pore-volume distribution (Mc Kay, 1996). Mesopores, like macropores, also play an essential role in the transport of adsorbate molecules inside the micropore volume. The mechanism of adsorption on the surface of macropores does not differ from that for flat surfaces. The specific surface area of macroporous solids is very small, which explains why adsorption on this surface is usually neglected. The capillary adsorbate condensation does not occur in macropores. The interactions of the adsorbate with the adsorbent surface and the various mechanisms of adsorption were discussed in Section 2.4.1.3.

2.5.1. Nitrate adsorbents

Several adsorbents such as ion exchange resins, carbon-based, naturally occurring, agricultural wastes, zeolites, industrial wastes, biosorbents and other synthetic organic and inorganic compounds have been used by previous researchers to remove nitrate from water (Canter, 1997; Kapoor and Viraraghavan, 1997; Bhatnagar and Sillanpää, 2011a; Loganathan et al., 2013b). Of these particular studies, Bhatnagar and Sillanpää (2011a) and Loganathan et al. (2013b) reviewed most of the nitrate adsorbents and their characteristics properly and came to the following conclusions.

Of all the nitrate adsorbents, carbon-based, naturally occurring, agricultural wastes, industrial wastes, biosorbents, ion exchange resins, and other synthetic organic and inorganic compounds and chemically modified adsorbents show the most promise for removing nitrate from water and wastewater. Generally, ion exchange resins, double

layered hydroxides/hydrotalcite-type compounds and modified adsorbents have indicated higher nitrate adsorption capacity compared to other conventional adsorbents. Besides these advantages, ion exchange resins are also cost-effective because they can be regenerated. Modified adsorbents are now very effective for nitrate adsorption and their only disadvantage is the cost of modification. On the other hand while cheaper adsorbents such as industrial and agricultural wastes have not shown higher adsorption capacity they can be employed in large quantities to improve nitrate removal efficiency. Modified adsorbents have been shown to increase the nitrate adsorption capacity by 4 – 11 times the unmodified adsorbents and therefore they can potentially be utilised in waters that have extremely high concentrations of nitrate and where ultra-pure waters are required (Loganathan et al., 2013b).

Various adsorbents' efficiency in removing nitrate, the methods used and the adsorption capacities have been evaluated in recent studies (Bhatnagar and Sillanpää, 2011a; Loganathan et al., 2013b). These reviewers have shown that most of the nitrate adsorption experiments were done in batch method and most of the adsorbents were satisfactorily described using the Langmuir equilibrium model. The maximum Langmuir capacities were 1.7 - 92.1 mg/g for unmodified and 125 - 363 mg/g for modified adsorbents in most studies. Again the pseudo-second-order kinetic model was found to fit well with the data.

2.5.2. Phosphate adsorbents

The adsorbents tested for phosphate removal can be classified as ion exchange resins, multivalent metal oxides and hydroxides, silicates, Ca and Mg carbonates, layer double hydroxides (LDHs), natural and synthetic organic compounds, industrial by-

products, and organic wastes (Loganathan et al., 2014). Very recently, Loganathan et al. (2014) reviewed the adsorption characteristics of these adsorbents extensively and came to the following conclusions.

Of all the phosphate adsorbents, metal oxides and hydroxides of Fe, Al, and Zr, LDHs, and highly porous metal oxide/polymer composites generally had the highest phosphate adsorption capacities (3.3-113 mg/g). The adsorption capacities of some adsorbents (e.g., LDHs, Fe and Al oxides and hydroxides, red mud) were increased by modification of adsorbents and acid treatments. Another process of enhancing adsorption capacities was surface modification of adsorbents which required grafting metals and their organic functions although this is not a wise choice considering the cost of modifications. Despite their high costs these adsorbents are promising if extremely low phosphate concentrations are required in the treated water. Many industrial by-products and organic wastes were also used as phosphate adsorbents in spite of having low adsorption capacities. These adsorbents are attractive because they require only low production and disposal costs and furthermore their low adsorption capacities can be overcome by using large volumes of adsorbents.

The ability of various adsorbents to remove phosphate efficiently, the methods used and adsorption capacities were extensively discussed by Loganathan et al. (2014). They reported that equilibrium adsorption data generally fitted well to the Langmuir or Freundlich adsorption isotherm models or both. Much of the kinetic data fitted to the pseudo-second-order model.

2.5.3. Fluoride adsorbents

A wide range of adsorbents have been used so far to remove fluoride from water and wastewater. They consist of multivalent metal oxides and hydroxides, layer double hydroxides (LDHs), ion exchange resins, zeolites, carbon materials, natural industrial by-products, and organic wastes (Loganathan et al., 2013a). Loganathan et al. (2013a) reviewed the adsorption characteristics of a large list of fluoride adsorbents extensively and came to the following conclusions.

Of all the adsorbents, multivalent metal oxides and hydroxides and layered double hydroxides are the most promising because of their high fluoride adsorption capacities (1.08 - 28.0 mg/g). On the other hand, ion exchange resins and fibres, zeolites, and carbon materials have low adsorption capacities. However, the adsorption capacities of these adsorbents could be increased by modifying them in different ways. The adsorbents' surfaces are modified by incorporating organic functional groups or multivalent metallic cations. Other processes of modification of these adsorbents (e.g. layered double hydroxides, alumina) are calcining at high temperatures to increase the adsorption capacity. In spite of having low adsorption capacities, natural and industrial by-products could be used for removing fluoride in rural areas, especially in developing countries because they are inexpensive.

The effectiveness of various adsorbents' ability to adsorb fluoride from drinking water, the methods used for the assessment, and the kinetics and equilibrium models that best explain the adsorption process were presented by Loganathan et al. (2013a). They stated that the pH and type and concentration of other ions present in water are dominant factors influencing fluoride adsorption.

2.6. Desorption of adsorbates and regeneration of adsorbents

Regeneration of adsorbent is one of the most important factors contributing to the overall efficiency of the adsorption process. A suitable adsorbent should not only have high adsorption capacity and cost-effectiveness but should also: firstly, be amenable to easy desorption of the adsorbed materials; and secondly, be able to efficiently regenerate the adsorbent and reuse it for a long time. In a real water treatment plant the adsorption process is conducted in a fixed bed resin with the water passing through the adsorbent until a certain treatment objective is reached. The adsorbent is then taken offline and regenerated while another column is used to supply continuous treatment. There are two methods for regenerating an adsorbent: concurrent and counter current. In the concurrent process the regenerant passes through the adsorbent in the same flow direction as the contaminated water, while in the counter current, it is in the opposite direction as the solution being treated.

2.6.1. Nitrate desorption and adsorbent regeneration

Desorption of nitrate is done by leaching of adsorbed nitrate using acids, bases and salts. Simple low-cost salts such as NaCl, KCl, Na_2SO_4 have been used in desorbing nitrate (Johir et al., 2011). Generally, different concentrations of these salts are used for efficient desorption (1M, 2M, 3M). With reference to the reagents, NaCl is the most effective salt when it comes to desorbing nitrate. 1M NaCl is able to deadsorb 95-97% of adsorbed nitrate (Johir et al., 2011).

2.6.2. Phosphate desorption and adsorbent regeneration

After adsorption the phosphate in the adsorbents was desorbed by using acids, bases and salts. Phosphate in adsorbents with weak adsorption strength and where the adsorption mechanism was non-specific (ion exchange or outer sphere complexation) (Johir et al., 2011; Xu et al., 2010a; Xu et al., 2010b; Xu et al., 2011) were desorbed by simple low-cost salts such as NaCl and KCl. These salts, however, were found to be ineffective in desorbing phosphate from adsorbents that strongly adsorb phosphate by specific adsorption mechanisms, i.e. ligand exchange or inner sphere complexation (Cheng et al., 2009; Zeng et al., 2004).

On the other hand, acids and bases have been successfully used to remove both specific and non-specific adsorbed phosphate. This is because phosphate adsorption decreases at pH below 3-4 and above 8-10 (Urano et al., 1992). High concentrations of acids and bases are not suitable for certain adsorbents (oxides of Si, Fe, and Al; LDH; carbonates of Ca and Mg) because they can dissolve or corrode parts of the adsorbents or cause structural changes, leading to problems in regeneration and reuse of the sorbents (Cheng et al., 2009; Chitrakar et al., 2006a; Delaney et al., 2011).

2.6.2.1. Phosphate recovery

The recovery of desorbed phosphorus is very important to minimise the future global scarcity of this substance, making it one of the greatest challenges of the twenty-first century. Phosphorus rock, the main source of phosphorus at present, is non-renewable and becoming increasingly scarce and expensive. It has been estimated that peak phosphorus use will occur by 2035, after which demand will outstrip supply (Cordell

et al., 2009). Phosphorus is essential for food production as it is a key ingredient in fertilisers to sustain high crop fields for all life forms (e.g. plants, animals and bacteria). Phosphates recovered from wastewater plants might be a viable industrial raw material for the manufacture of phosphate fertilisers. For this reason, it is very important to develop a recovery process for phosphorus from phosphorus-containing wastewater as an alternative source in order to ameliorate the approaching global exhaustion of high-grade phosphate ores.

The main technologies for recovering phosphorus from wastewater are chemical phosphate precipitation strategies that require the addition of lime, aluminium or iron salts and struvite crystallisation. Metal salt precipitation produces inorganic sludge when converted into Ca, Mg and NH_4 phosphates by treating wastewaters with appropriate salts (De-Bashan and Bashan, 2004; Morse et al., 1998). Phosphate recovery from municipal wastewater without metal salt precipitation is also possible, using existing technologies (Stratful et al., 1999; Driver et al., 1999; Durrant et al., 1999; Strickland, 1999; Woods et al., 1999). Phosphate precipitation with Fe and Al salts is a process widely employed in wastewater treatment, but it produces insoluble precipitates that cannot be used in agriculture as fertilisers (De-Bashan and Bashan, 2004). On the other hand, struvite precipitation (magnesium ammonium phosphate, $MgNH_4PO_4.6H_20$) represents an interesting way to recover phosphorus from wastewater, especially at high phosphate concentrations. Precipitation through $CaCl_2$ yielded 75% of phosphorus in the sludge without requiring pH adjustment. This can potentially be a simple recovery process for usable phosphorus from wastewater material (Kuroda et al., 2002).

2.6.2.1.1. Struvite

The most promising compound produced by the recovery of phosphorus from wastewater plants is magnesium ammonium phosphate ($MgNH_4PO_4.6H_20$), commonly known as struvite, which precipitates spontaneously in some wastewater processes (Booker et al., 1999; Stratful et al., 2001; Williams, 1999). Struvite certainly has potential in the fertiliser market if its formation and collection are controlled and cost-effective. Small quantities of recovered struvite are currently being tested as fertiliser, mainly in Japan (Ueno and Fiji, 2001). Struvite is a white crystalline substance consisting of magnesium, ammonium and phosphate in equal molar concentrations of 1:1:1. Struvite forms according to the general reaction shown below although this Equation 2.45 is a simplification of the chemistry involved in struvite precipitation:

$$Mg^{2+} + NH_4^+ + PO_4^{3-} + 6H_20 \rightarrow MgNH_4PO_4.6H_20 \qquad (2.45)$$

Struvite is most likely to form in areas of increased turbulence, as its solubility decreases with pH and its formation is often associated with anaerobic and post-digestion processes. Struvite in wastewater treatment plants was identified as early as 1937 in a multiple-stage sludge digestion system (Rawn et al., 1937). The extent of struvite precipitation and the characteristics of the precipitating solid depend on the solution pH, supersaturation, temperature and presence of foreign ions (Lee et al., 2003; Chimenos et al., 2003; Munch and Barr, 2001; Nelson et al., 2003; van Rensburg et al., 2003). Physicochemical characteristics of the wastewater, such as temperature, ions concentrations and pH, are determining factors in the struvite crystallisation process.

Precipitation occurs when magnesium, ammonium and phosphate concentrations exceed the solubility product of struvite (Doyle and Parsons, 2002).

2.6.2.1.2. Hydroxyapatite

Another common phosphorus recovery method is calcium–phosphorus precipitation which has the advantage of low cost and ease of handling. Phosphorus recovery is achieved by direct precipitation of calcium phosphate (hydroxyapatite, $Ca_5(PO_4)_3$ OH) (Yi and Lo, 2003), using calcite as the seeding material (Donnert and Salecker, 1999a; Donnert and Salecker, 1999b). The hydroxyapatite crystallises at pH 8.0–8.5 without inducing the precipitation of calcium carbonates which usually complicates the process. Phosphorus removal efficiencies in this process ranged from 75% to 85% (Moriyama et al., 2001).

The low solubility of hydroxyapatite may have important implications for its possible use in the production of fertiliser by direct formation (Johansson and Gustafsson, 2000). Seed crystal material made of calcium silicate hydrate (tobermorite crystals), applied to the removal of phosphorus by crystallisation, and yielded precipitated hydroxyapatite. This material can be incorporated into soil and has the characteristics of a good plant fertiliser (Moriyama et al., 2001).

2.6.3. Fluoride desorption and adsorbent regeneration

Desorption of fluoride is carried out by leaching of adsorbed fluoride by acids, bases and salts. The selection of a desorbing agent largely depends on the influence of pH on fluoride adsorption and the strength of adsorption (Loganathan, 2013a). Adsorption on most of the adsorbents decreases at high pH levels, and therefore bases having these

high levels are commonly used for desorption of fluoride from such adsorbents. In materials where fluoride adsorption increases with pH, acids have been found to be more effective as desorbing agents. For example, in a hydrous manganese oxide coated alumina (Teng et al., 2009) and a thio-urea modified amberlite resin (Solangi et al., 2010), fluoride adsorption decreased at lower pH values. Consistent with this adsorption pattern, the percentage of fluoride desorption was found to be higher at low pH values. Adsorption of fluoride by most adsorbents is strong and not easily reversible, partly due to the chemical nature of the adsorption process. For efficient fluoride desorption stronger acids and bases are required; they also need more time in their interaction with the adsorbent (Maliyekkal et al., 2006; Onyango et al., 2006; Raichur and Basu, 2001; Das et al., 2003).

2.7. Conclusion

The extensive literature review in this chapter has shown that elevated concentrations of some inorganic anions in water such as nitrate, phosphate and fluoride can cause damage to the environment and people's health. High concentrations of nitrate and phosphate in water can cause eutrophication which is a serious environmental problem, and furthermore high nitrate and fluoride concentrations in drinking water sources can endanger public health. Of the various methods used to remove nitrate, phosphate and fluoride, adsorption/ion exchange strategies are the most promising because they are simple and economical, result in less sludge production and therefore experience minimal disposal problem. Several materials have been investigated as adsorbents for the removal of nitrate, phosphate and fluoride. However, the selectivity of these anions' adsorption on these adsorbents needs to be employed in order for these

anions to be removed effectively. What is required is the presence of other ions commonly found in water and wastewater.

pH is a very important factor influencing the surface charge on the adsorbent as well as adsorption process. On the other hand, natural water contains several other anions such as Cl^-, SO_4^2 which can equally compete in the adsorption process of nitrate, phosphate and fluoride. It is therefore important to study the effect of pH and competing ions during adsorption.

Most studies on nitrate, phosphate and fluoride removal by adsorbents have been done using batch experiments and only a few have been reported in fixed bed column systems which are more relevant to real operating systems on natural waters. Moreover, many previous studies on the adsorptive removal of these inorganic anions have not considered desorption after the adsorbent is saturated with anions. Easy desorption is important for multiple reuse of the adsorbent as this reduces operational costs. Future research needs to explore highly efficient, low cost adsorbents that can be easily regenerated for reuse over several operational cycles without significant loss of adsorptive capacity and have good hydraulic conductivity to prevent filters clogging during a fixed bed treatment process.

Recovery of phosphorus from phosphorus-containing wastewater is essential for developing an alternative source to overcome the global scarcity of phosphorous. The emerging technology that is using struvite crystallisation (magnesium-ammonium phosphate) and hydroxyapatite (calcium phosphate), to remove phosphorus may serve as a catalyst for making it a recyclable product. However, struvite and hydroxyapatite are not widely applied as a fertiliser because of its limited availability and issues concerning cost-effectiveness. Only a few studies have recovered phosphorus as struvite and apatite following the adsorption of phosphate.

CHAPTER 3

University of Technology Sydney

COMPARISON OF NITRATE AND PHOSPHATE ADSORPTION ON TWO ION EXCHANGE RESINS

Chapter 3

Comparison of nitrate and phosphate adsorption on two ion exchange resins*

3.1. Introduction

As discussed in Chapter 2, water pollution is caused by the excessive presence of nitrate and phosphate which contribute to serious environmental problems worldwide. Nitrate and phosphate are implicated in the eutrophication of receiving surface waters. In addition to these impacts, elevated nitrate concentration in drinking water can be toxic to infants (Jorgensen and Williams, 2001). To alleviate the environmental impact of nitrate and phosphate, novel technologies have been developed to reduce effluent nitrate and phosphate concentrations of both industrial and domestic wastewaters. The nitrate and phosphate that are removed from the wastewater can be recovered and used as fertiliser.

Several physicochemical and biological processes have been investigated for the removal of dissolved nutrients (nitrate and phosphate) in water and wastewater and these processes were described in Chapter 2. The methods available for the removal of nitrate and phosphate are ion exchange (Bae et al., 2002; Boumediene and Achour et al., 2004; Lohumi et al., 2004), biological denitrification (Mori et al., 1996; Wasik et al., 2001), catalytic reduction (Lüdtke et al., 1998; Gavagnin et al., 2002), reverse osmosis (Schoeman and Steyn, 2003) and electrodialysis (Hell et al., 1998; El Midaoui et al., 2002). However, the application of these processes is limited as they are relatively

*** Much of this chapter was published in T. Nur, M.A.H. Johir, P. Loganathan, S. Vigneswaran, and J. Kandasamy, "Effectiveness of purolite A500PS and A520E ion exchange resins on the removal of nitrate and phosphate from synthetic water", Desalination and Water Treatment 47 (2012): 50-58.**

expensive and it merely transfers the nitrate and phosphate into concentrated waste brine that may pose a disposal problem (Wasik et al., 2001). The advantage of a catalytic reduction process is the rapid removal of nitrate from water (Gavagnin et al., 2002; Peel et al., 2003). Yet this process has the disadvantage in that it incurs a high capital cost. Phosphorus can be removed by biological processes. Although these processes are environmentally friendly, one cannot remove phosphorus below a particular concentration if there is a lack of easily biodegradable organic carbon present in the wastewater.

Of the various methods of nutrient removal, adsorption/ion exchange methods are very promising, because they require a simple and cost-effective operation, resulting in less sludge production and therefore minimal disposal problems. These methods seem to be the most suitable for small water supplies contaminated by nutrients because of their simplicity, effectiveness, selectivity, recovery and relatively low cost (Bae et al., 2002; Boumediene and Achour et al., 2004). Furthermore these methods also have the ability to: firstly, handle shock loadings; and secondly, operate over a wide range of temperatures. Several materials such as fly ash, cement, surfactant-modified zeolite, alunite, polymeric ion exchangers, and agricultural residues have been investigated as adsorbents for removing phosphate and/or nitrate anions (Zhao and Sengupta, 1998; Li and Bowman, 2001; Agyei et al., 2002; Orlando et al., 2002; Ozacar, 2003). Of these materials, ion exchange resins are considered able to remove both nitrate and phosphate (Johir et al. 2011; Samatya et al., 2006b; Bulgariu et al., 2010; Primo et al., 2009; Pintar et al., 2001; Liang et al., 1999). However, ion exchangers which selectively remove nitrate and phosphate need to be employed so that they remove these nutrients effecitvely.

Nitrate-specific resins have an affinity for the following ions in decreasing order; NO_3^-> SO_4^{2-}> Cl^-> HCO_3^- (Burge and Halden, 1999). Several ion exchange resins were used for removing nitrate from drinking water. The characteristics of adsorption behaviour of resins are generally inferred in terms of both adsorption kinetics and equilibrium isotherms. Samatya et al. (2006a and 2006b) used the ion exchange resin Purolite A520E to remove nitrate from water and found that this resin gave promising results for column-mode removal of nitrate from ground water. By fitting their data to Langmuir adsorption isotherm, they reported the maximum adsorption value of 18.5 mg N/g dry resin. Bulgariu et al. (2010) reported an uptake capacity of nitrate on Purolite A100 resin of 4.37 mg N/g which was less compared with that found by Samatya et al. (2006a) concerning Purolite A520E which was 18.5 mg N/g. Removal of nitrate from aqueous solutions was studied using two nitrate selective anion exchangers - Purolite A520E and Purolite A300 - under a fixed bed configuration by Primo et al. (2009). Their results showed that Purolite A300 proved to be more efficient than Purolite A520E in removing nitrate.

The methods currently available for the removal of nitrate and phosphate by ion exchangers are specific only for one of these nutrients. Purolite as an adsorbent has been studied to remove nitrate and not phosphate except in a recent study by Johir et al. (2011) where the removal of nitrate and phosphate from wastewater was tested using Purolite A520E and Purolite A500PS in ion exchange columns. They found that 40% and 80% of phosphates were removed by Purolite A520E and Purolite A500PS, respectively, whereas a higher percentage (80-95%) of nitrate was removed by both the resins at 1950 bed volumes with 12 cm bed height and 2.5 m/h filtration velocity. No previous study has considered the effect of Purolite in simultaneously removing both nitrate and phosphate.

The effects of different concentrations and ratios of nitrate and phosphate on their removal by Purolite have not been investigated in previous studies either.

In this chapter the effectiveness of the ion exchange resins, Purolite A520E and Purolite A500PS, to remove both nitrate and phosphate simultaneously from wastewater was studied. Purolite A500PS and Purolite A520E resins were selected for this study because a previous study (Johir et al. 2011) documented their high efficiency of removal of nitrate and phosphate respectively. This study had several objectives in mind: (i) investigation of the competitive adsorption of nitrate and phosphate when they are present at different concentration ratios in synthetic water; (ii) study of kinetic and equilibrium adsorption isotherms of nitrate and phosphate adsorption on these ion exchange resins; (iii) study of column adsorption of nitrate and phosphate on these ion exchange resins; (iv) modelling of batch equilibrium and kinetic data, (v) modelling of column adsorption data; and (vi) regeneration of the ion exchange resins.

3.2. Material and Methods

3.2.1. Ion exchange resins

Two ion exchange resins, namely Purolite A520E and Purolite A500PS were used as adsorbents. Purolite A520E is a macroporous strong base anion exchange resin consisting of macroporous polystyrene cross-linked divinylbenzene with a triethylamine functional group and specially designed to remove nitrates from water for potable purposes (Gu et al., 2004; Purolite 2013). Purolite A500PS is also a macroporous strong base anion exchanger but consists of styrene–divinylbenzene with a trimethylamine functional group. It has been designed for use as an organic scavenger, for example the

removal of tannins, fulvic and humic acids, from domestic effluents (Ahmad et al., 2012; Purolite 2013). However, Johir et al. (2011) noted that has a good phosphate and nitrate ion exchange capacity. The macroporous matrix and special ion-exchange group functionality impart ideal selectivity to adsorb nitrate and phosphate. The characteristics of these ion exchange resins are presented in Table 3.1.

Table 3.1.

Typical chemical and physical characteristics of the two Purolites used (www.purolite.com).

Parameters	Purolite A520E	Purolite A500PS
Polymer Matrix Structure	Macroporous styrene-divinylbenzene	Macroporous polystyrene crosslinked divinylbenzene
Physical Form and Appearance	Opaque cream spherical beads	Spherical beads
Functional Groups	Quaternary Ammonium	$R\text{-}(Me)_3N^+$
Ionic Form (as shipped)	Cl^-	Cl^-
Screen Size Range (U.S. Standard Screen)	16-40 mesh, wet	16-50 mesh, wet
Particle Size Range (microns)	+1200 <5%, -300 <1%	+1200 <2 %, -420 <2%
Moisture Retention, Cl^- form	50-56%	63-70%
Reversible Swelling $Cl^{-®}$ OH (SO_4/NO_3)	Negligible	20% max (-)
Specific Gravity (Cl^- form)	-	1.04
Total Exchange Capacity, Cl^- form wet, volumetric dry, weight	0.9 eq/l min 2.8 meq/g min	0.8 eq/l min
pH Range (Stability), Cl^- Form	0-14	0-14
Operating Temperature, (Cl^- form)	100°C	100°C

3.2.2. Feed solution

The feed solution consisted of distilled water spiked with nitrate and phosphate to produce solutions with different concentrations of nitrate (10-50 mg N/L) and phosphate (2-20 mg P/L). Nitrate and phosphate were added in the form of Analar grade KNO_3 and KH_2PO_4, respectively.

3.2.3. Chemical analysis

Analyses of nitrate and phosphate ions were carried out using Metrohm ion chromatograph (Model 790 Personal IC) equipped with an auto sampler and conductivity cell detector. The separation was achieved using an A SUPP column 3 (150 mm x 4 mm). Na_2CO_3 (3.2 mmol/L) and $NaHCO_3$ (1.0 mmol/L) were used as mobile phase with a flow rate of 0.9 mL/min.

3.2.4. Batch adsorption studies

3.2.4.1. Equilibrium adsorption isotherm

Equilibrium adsorption experiments were conducted in a set of glass flasks with 100 mL solutions spiked with nitrate and phosphate (20-50 mg N/L and 10-30 mg P/L) and different ion exchange resin concentrations of 0.1-10 g/L at room temperature (24 ± 1^{o}C). The suspensions were agitated in a flat shaker at a shaking speed of 120 rpm for 72 h to ensure that the adsorption equilibrium is reached. The experiments were duplicated and the average values were recorded. The difference between duplicate values was

within ± 2%. The amount of nitrate and phosphate adsorption at equilibrium, q_e (mg N/g), was calculated using Equation 3.1,

$$q_e = \frac{(C_0 - C_e)V}{M} \quad (3.1)$$

where C_0 = initial concentration of adsorbate (mg/L); C_e = equilibrium concentration of adsorbate (mg/L); V = volume of the solution (L) and M = mass of adsorbent (g).

Removal efficiency was calculated using Equation 3.2,

$$\text{Removal efficiency (\%)} = \frac{(C_0 - C_e)}{C_0} \times 100 \quad (3.2)$$

The experimental results were treated with both Langmuir and Freundlich isotherm models. The equations for Langmuir and Freundlich isotherms as discussed in Chapter 2 are presented again in Table 3.2. Previous studies have widely used these adsorption models to describe nitrate and phosphate adsorption on ion exchange resins (Samatya et al., 2006a; Bulgariu et al., 2010; Loganathan et al., 2014). Furthermore, a recent review paper cited 20 studies on nitrate removal employing Langmuir and Freundlich adsorption isotherms (Bhatnagar and Sillanpää, 2011a).

3.2.4.2. Adsorption kinetics

Batch adsorption kinetic experiments were conducted with different concentrations of ion exchange resins and various adsorbate concentrations (nitrate and phosphate) in a glass flask containing 100 mL of adsorbate solution and agitated in a flat shaker at a shaking speed of 120 rpm for 6 h at room temperature (24 ± 1°C). Aqueous

samples were taken at different time intervals and the concentrations of nitrate and phosphate were measured. The amount of nitrate and phosphate adsorption at time t, q_t (mg/g), was calculated using Equation 3.3,

$$q_t = \frac{(C_0 - C_t)V}{M} \tag{3.3}$$

where C_0 = initial concentration of adsorbate (mg/L); C_t = concentration of adsorbate at time t (mg/L); V = volume of the solution (L), and M = mass of dry adsorbent (g).

The adsorption kinetic data were analysed using pseudo-first-order and pseudo-second-order kinetic models which are presented in Table 3.3.

3.2.5. Column mode experiments

The fixed-bed column was made-up of a pyrex glass tube with an inner diameter of 2.0 cm. The column was packed with the Purolite to yield the desired bed height of 12 cm. The total volume of ion exchange resin was about 9.4 x 10^{-6} to 5.97 x 10^{-5} m^3. An up-flow mode of filtration was applied at filtration velocities of 2.5 and 5.0 m/h controlled by a peristaltic pump. At the bottom of the filtration column (underneath the ion exchange resin), glass beads with a height of 2 cm were placed in order to provide a uniform flow of the solution through the column. The concentrations of nitrate and phosphate in synthetic feed solution were 20 mg N/L and 30 mg P/L, respectively. The effluent samples were collected at regular time intervals and subjected to nitrate and phosphate analysis using ion-chromatograph.

The time for breakthrough appearance and the shape of the breakthrough curve are very important characteristics for determining the operation and dynamic response of an adsorption fixed-bed column. The breakthrough curves show the loading behaviour of nitrate and phosphate to be removed from solution in a fixed-bed column and are usually expressed in terms of adsorbed nitrate-N / phosphate-P concentration (C_{ad}), inlet nitrate-N / phosphate-P concentration (C_o), outlet nitrate-N / phosphate-P concentration (C_t) or normalised concentration defined as the ratio of outlet nitrate / phosphate concentration to inlet nitrate / phosphate concentration (C_t/C_o) as a function of time. The maximum column capacity, q_{total} (mg N/P), for a given feed concentration and filtration velocity is equal to the area under the plot of the adsorbed nitrate-N / phosphate-P concentration, C_{ad} ($C_{ad}=C_o-C_t$) (mg/L) versus effluent time (t, min). It can be calculated using Equation 3.4:

$$q_{total} = \frac{Q}{1000}\int_{t=0}^{t=total} C_{ad}\,dt \tag{3.4}$$

Equilibrium uptake q_{eq} (mg N/g or mg P/g) or maximum capacity of the column is defined by Equation 3.5 as the total amount of adsorbed phosphate-P concentration (q_{total}) per g of adsorbent (M) at the end of the total flow time:

$$q_{eq} = \frac{q_{total}}{M} \tag{3.5}$$

The detention times of Purolite during fluidization are calculated using Equation 3.6:

$$t = H/v \tag{3.6}$$

where, t is the detention time (h), H is the column bed height (m) and v is the upflow velocity.

Three empirical models, namely Bohart-Adams model (Bohart, 1920), Thomas model (Thomas, 1944) and Yoon-Nelson model (Yoon and Nelson, 1984) were used to analyse the data which were discussed in Chapter 2. The methods of calculating the model parameters are presented in Table 3.4.

Table 3.2.

The models and equations used for describing batch equilibrium adsorption.

Model	Equation	Graphical method used to calculate model constants
Langmuir Isotherm	$q_e = \frac{q_{max} K_L C_e}{1 + K_L C_e}$	$\frac{C_e}{q_e} = \frac{1}{q_{max} K_L} + \frac{C_e}{q_{max}}$
	C_e = equilibrium concentration of adsorbate (mg/L), q_e = amount of nitrate and phosphate adsorbed per unit mass of Purolite (mg/g), q_{max} = maximum amount of nitrate and phosphate adsorbed per unit mass of Purolite (mg/g); K_L = Langmuir constant related to the energy of adsorption (L/mg)	
Freundlich Isotherm	$q_e = K_F C_e^{1/n}$	$\ln q_e = \ln K_F + \frac{1}{n} \ln C_e$
	C_e = equilibrium concentration of adsorbate (mg/L), q_e = amount of nitrate and phosphate adsorbed per unit mass of Purolite (mg/g), K_F and n = Freundlich constants (mg/g) (K_F is related to the nitrate and phosphate adsorption capacity of Purolite).	

Table 3.3.

The models and equations used for the description of batch kinetic adsorption.

Model	Equation	Graphical method used to calculate model constants
Pseudo-first-order kinetic	$\frac{dq_t}{dt} = k_1(q_e - q_t)$	$\ln(q_e - q_t) = \ln q_e - k_1 t$
	q_e = amount of nutrients adsorbed at equilibrium (mg/g); q_t = amount of nutrients adsorbed at time, t (min) (mg/g) and k_1 = equilibrium rate constant of pseudo-first-order sorption (1/min).	
Pseudo-second-order kinetic	$\frac{dq_t}{dt} = k_2(q_e - q_t)^2$	$\frac{t}{q_t} = \frac{1}{k_2 q_e^2} + \frac{t}{q_e}$
	q_e = amount of nutrients adsorbed at equilibrium (mg/g); q_t = amount of nutrients adsorbed at time, t (min) (mg/g) and k_2 = equilibrium rate constant of pseudo-second-order (1/min).	

Table 3.4.

The models and equations used for describing column adsorption.

Model	Equation	Graphical method used to calculate model constants
Bohart-Adams model	$\ln C_t/C_o = k_{AB}C_o t - k_{AB}N_o Z/F$	The values for k_{AB} and N_o determined from the intercept and slope of the linear plot of ln (C_t/C_o) against time (t).
	C_0 = inlet adsorbate concentration (mg/L), C_t = effluent adsorbate concentration (mg/L), k_{AB} = kinetic constant, (L/mg.min), F = linear velocity calculated by dividing the filtration velocity by the column section area (cm/min), Z = bed depth of column (cm), N_o = saturation adsorbate concentration (mg/L) and t = filtration time (min).	
Thomas model	$\ln(C_o/C_t - 1) = k_{Th}q_oM/Q - k_{Th}C_o t$	A linear plot of ln [(C_o/C_t) −1] against time (t) was employed to determine values of k_{Th} and q_o from the intercept and slope of the plot.
	k_{Th} = Thomas rate constant (mL/min.mg), q_o= equilibrium adsorbate uptake per g of Purolite (mg/g), C_o = inlet adsorbate concentration (mg/L), C_t = outlet adsorbate concentration at time t (mg/L), M = mass of Purolite (g), Q = filtration velocity (mL/min) and t = filtration time (min).	
Yoon–Nelson model	$\ln[C_t/(C_o - C_t)] = k_{YN}t - \tau k_{YN}$	A linear plot of ln [$C_t/(C_o - C_t)$] against sampling time (t) was used to determine values of k_{YN} and τ from the intercept and slope of the plot.
	k_{YN} = rate velocity constant (1/min), τ = the time required for 50% nitrate and phosphate breakthrough (min),C_o = inlet adsorbate concentration (mg/L), C_t = outlet adsorbate concentration at time t (mg /L) t = filtration time (min).	

3.2.6. Regeneration of ion exchange resins

Regenerating the ion exchange resins (Purolite A520E and Purolite A500PS) adsorbed with nitrate and phosphate was also undertaken in batch and column experiments. The saturated resins were washed with 0.1-1.0 M NaCl and Na_2SO_4 solutions in the batch method. After each experiment the saturated resins were placed in a small container containing the regenerating solution of 20 ml and were shaken using a flat shaker at a shaking speed of 150 rpm. The desorbed solutions were collected at different time intervals for 30 min and analysed for nitrate and phosphate concentrations. The column regeneration studies were carried out using 1 M NaCl and the regeneration was done by leaching the resin containing the adsorbed nitrate and phosphate with the leaching solution at a filtration velocity 10 m/h for 30 min.

3.3. Results and discussion

3.3.1 Comparison between the two Purolites in removing nitrate and phosphate

The batch kinetics experimental results showed that both Purolite ion exchange resins can remove nitrate and phosphate. However, more nitrate was removed (almost 80%) by Purolite A520E than by Purolite A500PS (65%) at a resin dose of 1.5 g/L with nitrate concentration of 20 mg N/L (Figure 3.1a). This could be due to the fact that Purolite A520E is reported to be a nitrate selective resin that can remove larger amounts of nitrate than Purolite A500PS which is usually recommended for organic removal (www.purolite.com). Purolite A520E has higher selectivity towards nitrate removal. The explanation may be that this resin is more hydrophobic than Purolite A500PS and therefore selective in adsorbing nitrate which has less hydration energy than phosphate

(Gu et al., 2004; Awual et al., 2011). In contrast to nitrate removal, Purolite A500PS was more efficient in removing phosphate (almost 65%) than Purolite A520E (48%) at a resin dose of 1.5 g/L with phosphate concentration of 10 mg P/L (Figure 3.1b). The greater removal of phosphate by Purolite A500PS may be due to the higher number of negative charges on the phosphate anion at the neutral pH of the solution than nitrate, subsequently resulting in the higher adsorption of phosphate onto the positively charged resin.

Similar findings were also observed by Johir et al. (2011) in their column adsorption experiments on nitrate and phosphate from MBR effluents containing phosphate$^-$-P and nitrate-N concentrations of 3.1 and 11 mg/L, respectively for Purolite A520E and Purolite A500PS (previously known as Purolite A500P). They found that almost 94% of nitrate was removed by Purolite A520E whereas the removal of phosphate was only 25-45% at 1950 bed volumes with 12 cm bed height and 2.5 m/h filtration velocity for both Purolites. The removal efficiency of phosphate was observed to be better for Purolite A500P than Purolite A520E. However, the the two resins' removal efficiency of nitrate was virtually the same. The results in Figure 3.1 and those noted by Johir et al. (2011) show that Purolite A520E has a strong selectivity for nitrate than phosphate but Purolite A500PS appears to have nearly the same affinity for phosphate as nitrate when the influent N: P concentration ratio was 2:1.

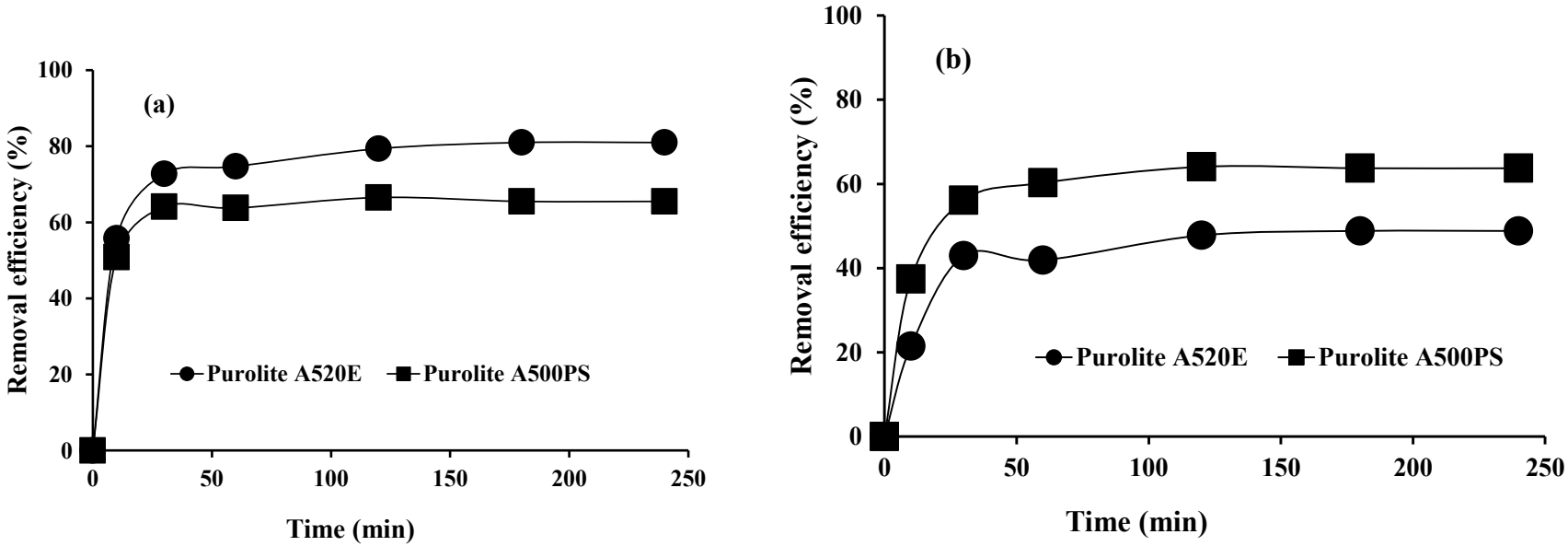

Figure 3.1. Comparison between the two Purolite ion exchange resins in removing (a) nitrate and (b) phosphate (initial concentration of nitrate and phosphate were 20 mg N/L and 10 mg P/L respectively, dose of ion exchange resin = 1.5 g/L).

3.3.2. Effect of other ions

A second set of experiments were conducted to study the effect of the presence of phosphate on the removal of nitrate by the two Purolites (Figure 3.2) and the effect of the presence of nitrate on the removal of phosphate by the two Purolites (Figure 3.3) at two concentrations of phosphate and nitrate. Figure 3.2(a) shows that the removal of nitrate by Purolite A520E was not affected by the presence of phosphate. However, the removal efficiency of phosphate by Purolite A520E in the presence of nitrate decreased by almost 50% (Figure 3.3a). This may be due to the lower affinity of Purolite A520E to the phosphate ion than the nitrate ion during ion exchange processes as Purolite A520E is a highly nitrate selective resin. These results show that in the presence of nitrate and phosphate in water, nitrate can effectively compete with phosphate for adsorption on Purolite A520E.

The removal efficiency of nitrate and phosphate by Purolite A500PS is similar to Purolite A520E. The removal efficiency of phosphate by Purolite A500PS declined from 80-86% to less than 60% in the presence of a low concentration of nitrate and in the case of a high concentration it fell from 82% to 34% at a resin dose of 1.5 g/L (Figure 3.3b). It also emerged that the removal efficiency of nitrate by Purolite A500PS was not very much affected by the presence of phosphate and in the case of a high concentration of phosphate it slightly decreased (Figure 3.2b). This shows that nitrate is effectively competing with phosphate in Purolite A500PS as well. Although Purolite A500PS can remove both nitrate and phosphate effectively it is also a nitrate selective resin.

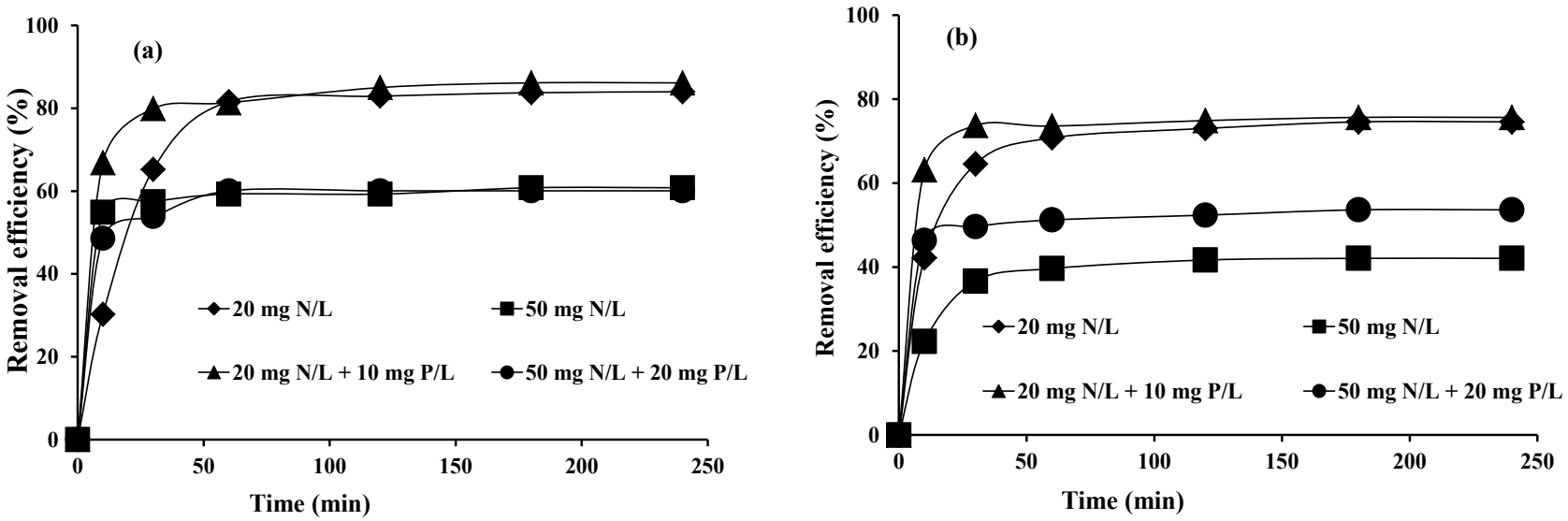

Figure 3.2. Effect of the presence of phosphate on the removal of nitrate by (a) Purolite A520E and (b) Purolite A500PS at the dose of ion exchange resin = 1.5 g/L).

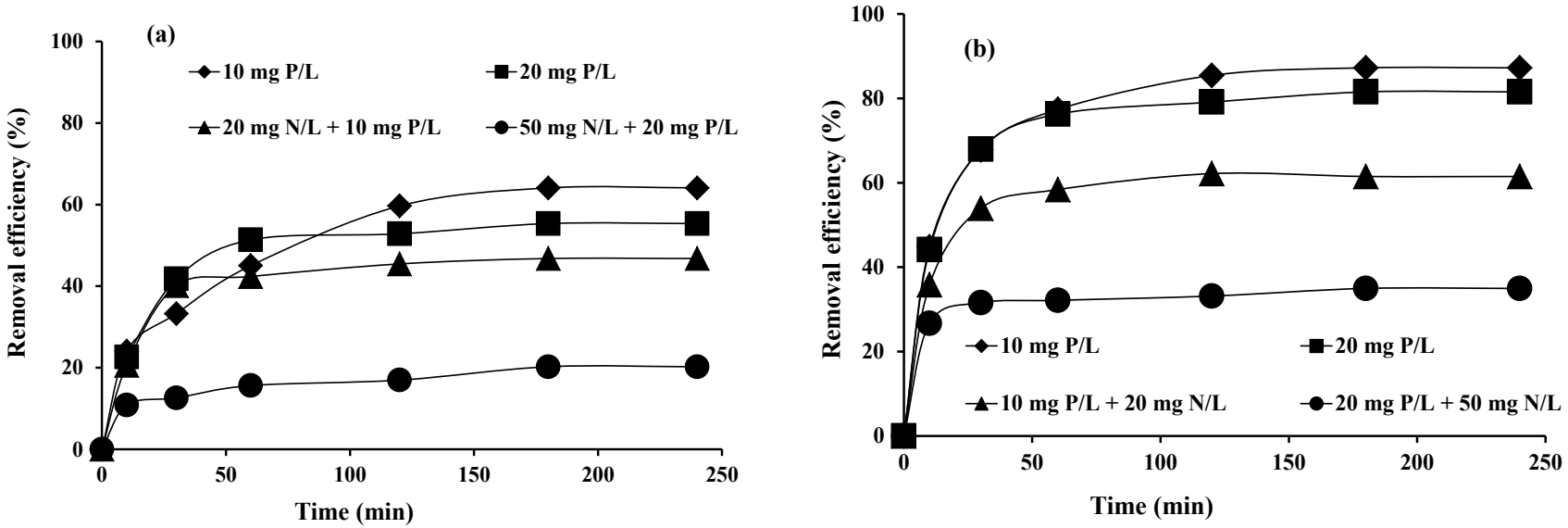

Figure 3.3. Effect of the presence of nitrate on the removal of phosphate by (a) Purolite A520E and (b) Purolite A500PS at the dose of ion exchange resin = 1.5 g/L).

3.3.3. Selectivity of ion exchange resins

The above experiments were conducted at two ratios and two concentrations of nitrate and phosphate. To evaluate further the influence of the competitive effects of nitrate and phosphate on their removals by these two Purolite ion exchange resins and to determine the selectivity of the resins for nitrate and phosphate, further experiments were conducted at more than two concentrations and two ratios of nitrate and phosphate. The results are presented in Figure 3.4. At different ratios of N to P (1:1 to 1:5) (concentration of nitrate increased), the ratios of the amounts of N to P adsorbed was higher than the ratio of the initial solution concentrations of N to P for both Purolites (Figure 3.4a). This shows that both Purolites are nitrate selective. At all N to P ratios in solution, the ratio of N to P adsorbed was higher for Purolite A520E than for Purolite A500PS, suggesting that the nitrate selectivity for adsorption was higher for Purolite A520E than for Purolite A500PS.

The selectivity of Purolite A520E for nitrate increased at a faster rate than Purolite A500PS with increase in N: P ratio. When the P: N ratio in solution was increased at a constant concentration of nitrate (N=50 mg/L) (Figure 3.4b), the P: N ratio of adsorbed nitrate and phosphate rose as expected but this ratio in the resin was less than in solution. This indicated that both resins are nitrate selective as observed in Figure 3.4(a). However, the P: N ratio in the resin was higher for Purolite A500PS than for Purolite A520E, demonstrating that the nitrate selectivity for adsorption is less for Purolite A500PS as again observed in Figure 3.4(a).

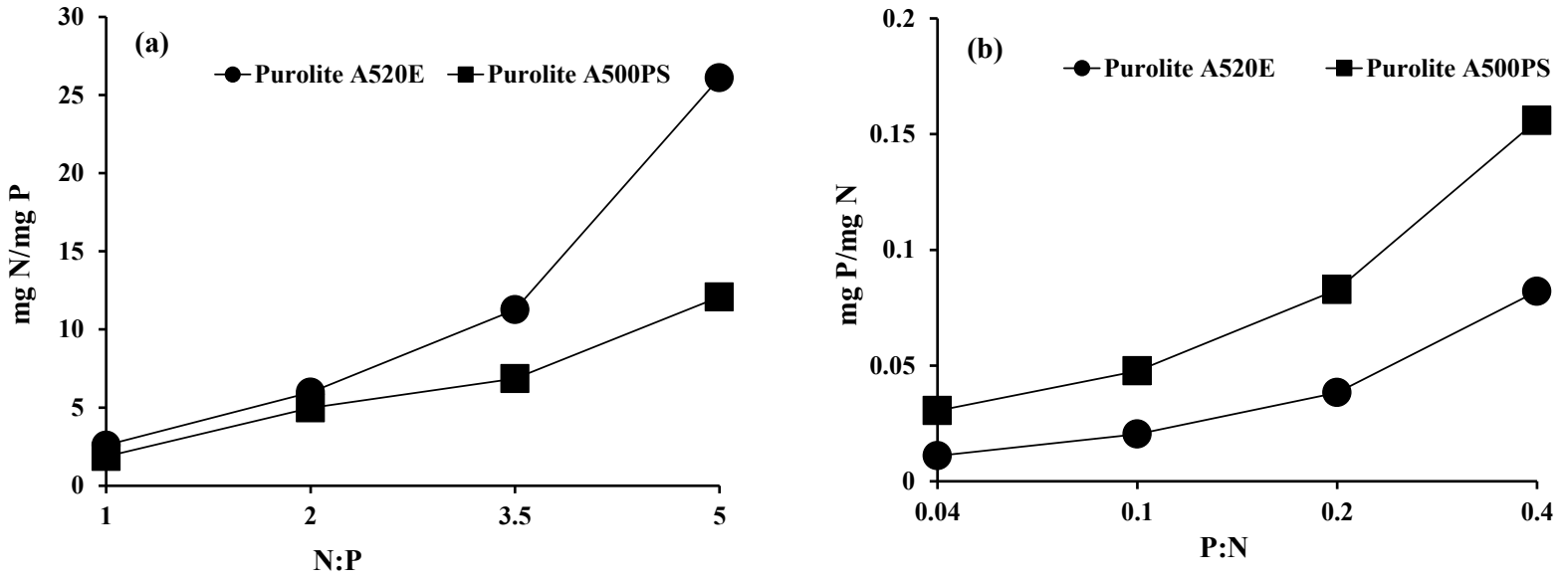

Figure 3.4. Effect of solution (a) nitrate to phosphate ratio at the concentration of 10 mg P/L and (b) phosphate to nitrate ratio at the concentration of 50 mg N/L on the N/P and P/N removal by Purolite resins, respectively.

3.3.4. Comparison between the two Purolites in column method for removing nitrate

In the first column experiment, the two adsorbents Purolite A520E and Purolite A500PS were evaluated for removing nitrate from aqueous solution at different conditions such as two varying initial filtration velocities (v = 2.5 m/h and 5.0 m/h) at a constant adsorbent bed height of 12 cm and inlet concentration of 20 mg N/L. The breakthrough curves obtained for the different adsorbents exhibited different shapes (Figure 3.5). The two adsorbents showed almost a similar curve for the two filtration velocities. The breakthrough generally occurred faster and the breakthrough curve was steeper with the higher filtration velocity of 5.0 m/h. (Figure 3.5). The time to reach the plateau of C_t/C_0 decreased significantly with an increase in the filtration velocity, which is similar to a previous study on nitrate adsorption by amine cross-linked wheat straw (Xing et al., 2011). The plateau of C_t/C_0 occurred at 35 h and 29 h for the inlet filtration velocity of 5.0 m/h with the values of C_t/C_0 of 0.94 and 0.92 for Purolite A520E and Purolite A500PS, respectively. The faster breakthrough exhibited by the higher flow rate is due to rapid movement of the adsorbent zone along the bed, reducing the contact time between nitrate and the ion exchange resin. The gradual breakthrough at the slower flow rate suggested longer residence time of nitrate in the column. Similar trends have been reported for nitrate removal by another ion exchange resin (Hekmatzadeh et al., 2012) and an amine-cross-linked wheat straw (Xu et al., 2010b). The reason behind the increase of breakthrough time with falling filtration velocity is due to an increase in empty bed contact time. The lower the bed contact time, the less effective the diffusion process becomes, resulting in less column sorption capacity for nitrate (Suksabye et al., 2008; Mondal, 2009). Faster breakthrough of adsorbates and steeper breakthrough at higher

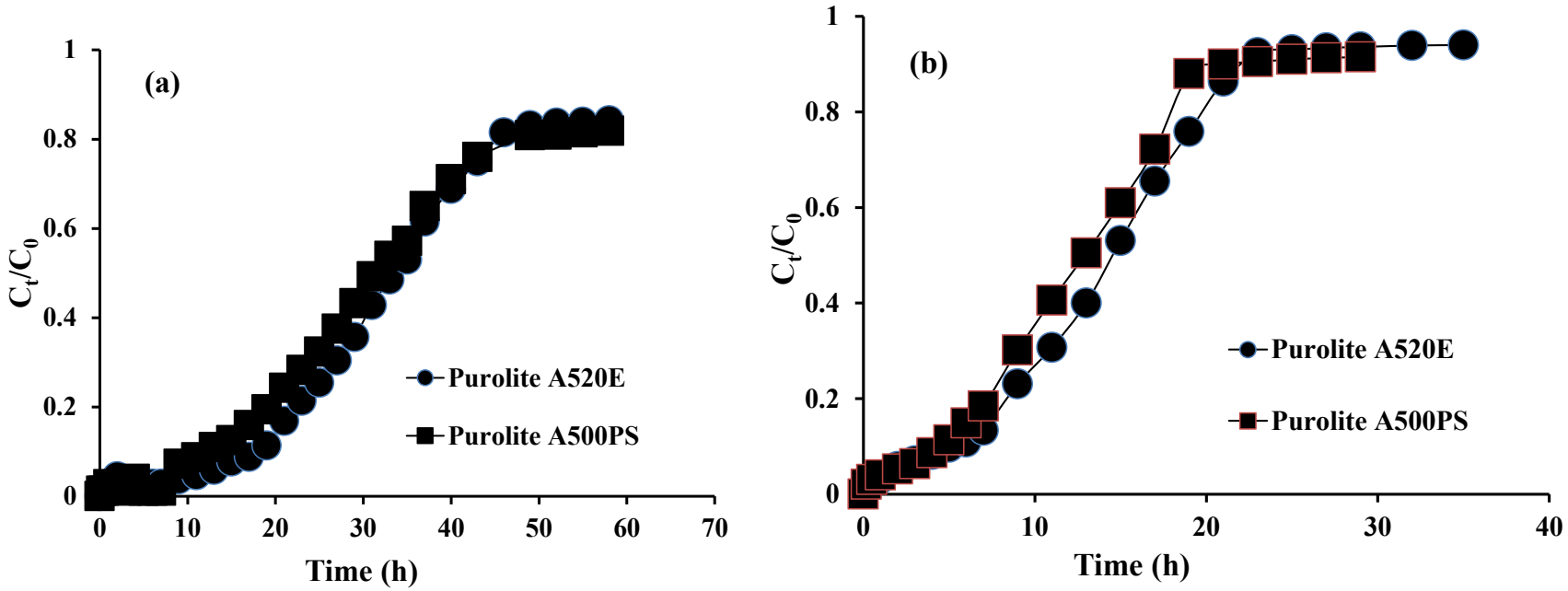

Figure 3.5. Breakthrough curves of nitrate adsorption for the two Purolites at filtration velocity of (a) 2.5 m/h and (b) 5.0 m/h (initial concentration = 20 mg N/L and bed height = 12 cm).

filtration velocities have also been reported elsewhere for adsorption onto other adsorbents (Yahaya et al., 2011, Srivastava et al., 2008).

3.3.5. Comparison between the two Purolites in column method for removing phosphate

In the next column experiment, the two adsorbents Purolite A520E and Purolite A500PS were evaluated for removing phosphate from aqueous solution at different conditions such as two varying initial filtration velocities (v = 2.5 m/h and 5.0 m/h) at a constant adsorbent bed height of 12 cm and an inlet concentration of 30 mg P/L. The breakthrough curves obtained for the different Purolites exhibited different shapes (Figure 3.6). The plateau of C_t/C_0 occurred at 21 h and 27 h for the inlet filtration velocity of 2.5 m/h with the values of C_t/C_0 of 0.70 and 0.72 for Purolite A520E and Purolite A500PS, respectively. The breakthrough generally occurred faster and the breakthrough curve was steeper with a higher filtration velocity at 5.0 m/h as observed for nitrate (Figure 3.6). The plateau of C_t/C_0 occurred at 17 h and 15 h for the inlet filtration velocity of 5.0 m/h with the values of C_t/C_0 of 0.92 and 0.90 for phosphate adsorption on Purolite A520E and Purolite A500PS, respectively. Faster breakthrough of adsorbates and steeper breakthrough at higher filtration velocities have been reported elsewhere for phosphate adsorption onto other adsorbents (Srivastava et al., 2008; Yahaya et al., 2011).

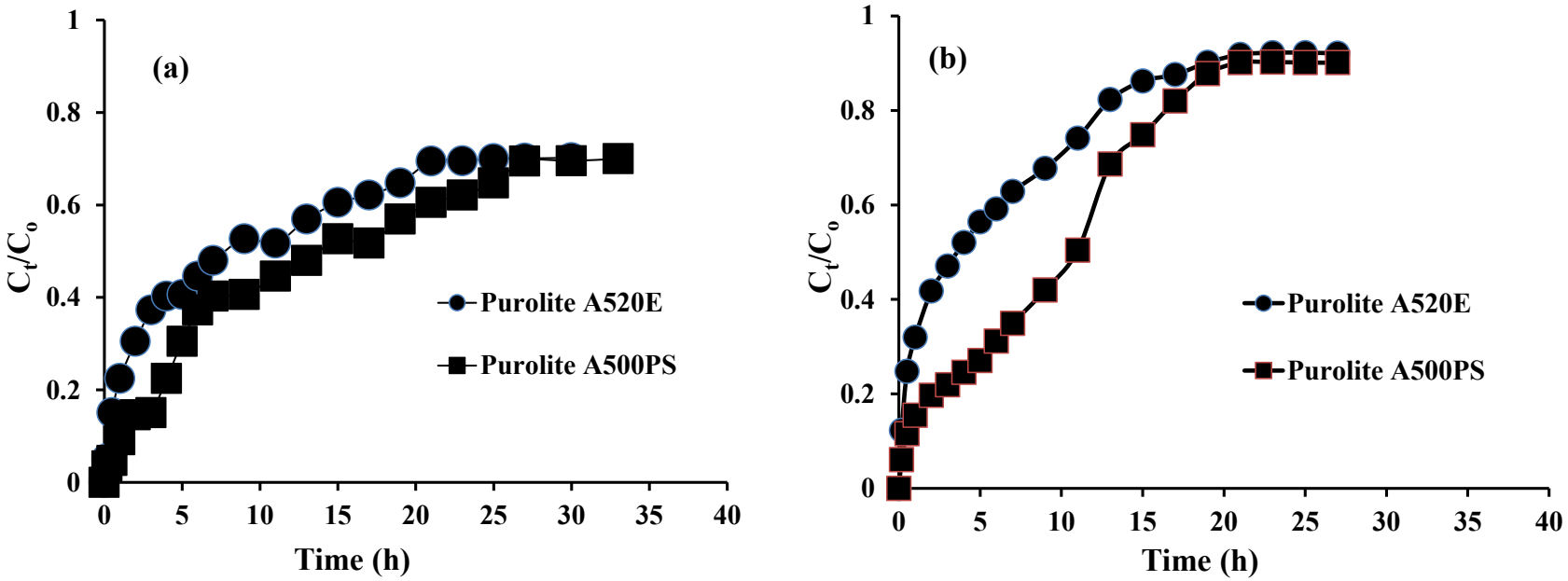

Figure 3.6. Breakthrough curves of phosphate adsorption for the two Purolites at filtration velocity of (a) 2.5 m/h and (b) 5.0 m/h (initial concentration = 20 mg N/L and bed height = 12 cm).

3.3.6. Modelling of batch equilibrium adsorption

In general, the results of the equilibrium adsorption isotherm experiments indicated an increase in removal efficiency of nitrate and phosphate, coupled with an increase in ion exchange resin concentrations. This could be due to the following: (i) increase in the number of adsorption sites; (ii) maximum adsorption capacity of the resins has not been reached; and (iii) solution concentration of adsorbate has been very much reduced. The equilibrium adsorption data were fitted to Langmuir and Freundlich isotherm models (Table 3.5). Both models fitted well for the adsorption of nitrate on Purolite A520E (R^2 = 0.96-0.97) (Figure 3.7). However, the adsorption of nitrate on Purolite A500PS can be explained satisfactorily only by reference to the Freundlich model (Figure 3.8), which showed good correlation (R^2 = 0.98). The data fit to the Langmuir model was very poor (R^2 = 0.04).

On the other hand, the data for the adsorption of phosphate on both resins did not fit well to the Langmuir model (Table 3.5). However, the adsorption of phosphate on the resins fitted well to the Freundlich model, which showed a high coefficient of determination (R^2 = 0.92) for Purolite A500PS as well as for Purolite A520E (Figure 3.9 and 3.10). The model parameters (K_L, q_{max}, K_F and n) obtained from the simulations are presented in Table 3.5.

The maximum value of nitrate adsorption on Purolite A520E was 33 mg N/g using the Langmuir equation and the Freundlich parameter K_F was 4.29 mg N/g. Samatya et al. (2006a) reported that the maximum adsorption capacity of nitrate on Purolite A520E was 18.51 mg N/g from Langmuir fit and the Freundlich parameter K_F was 3.33 mg N/g in a

batch experiment. Primo et al. (2009) reported that the maximum adsorption capacity of nitrate on Purolite from a column experiment was 18.81 mg N/g.

According to the manufacturer's information, Purolite A520E resin has quaternary ammonium as a functional group, with a total ion exchange capacity of 2.8 mEq/g of dry resin (39.2 mg N/g) (Table 3.5). The Langmuir maximum adsorption capacity obtained in the current study (33 mg N/g) agrees fairly well with the manufacturer's value. The maximum phosphate adsorption capacity on Purolite A500PS was 94.34 mg P/g from the Langmuir equation, but the R^2 value was poor ($R^2 = 0.51$). Therefore the above phosphate adsorption capacity cannot be considered to be a true value. The Freundlich model fitted well to both nitrate and phosphate adsorption in the two Purolites ($R^2 = 0.92$) (Table 3.5). The Freundlich constant K_F which is related to the adsorption capacity was higher for Purolite A520E in the case of nitrate adsorption whereas the opposite was true for phosphate adsorption. This agrees with the conclusions made in sections 3.3.1-3.3.3.

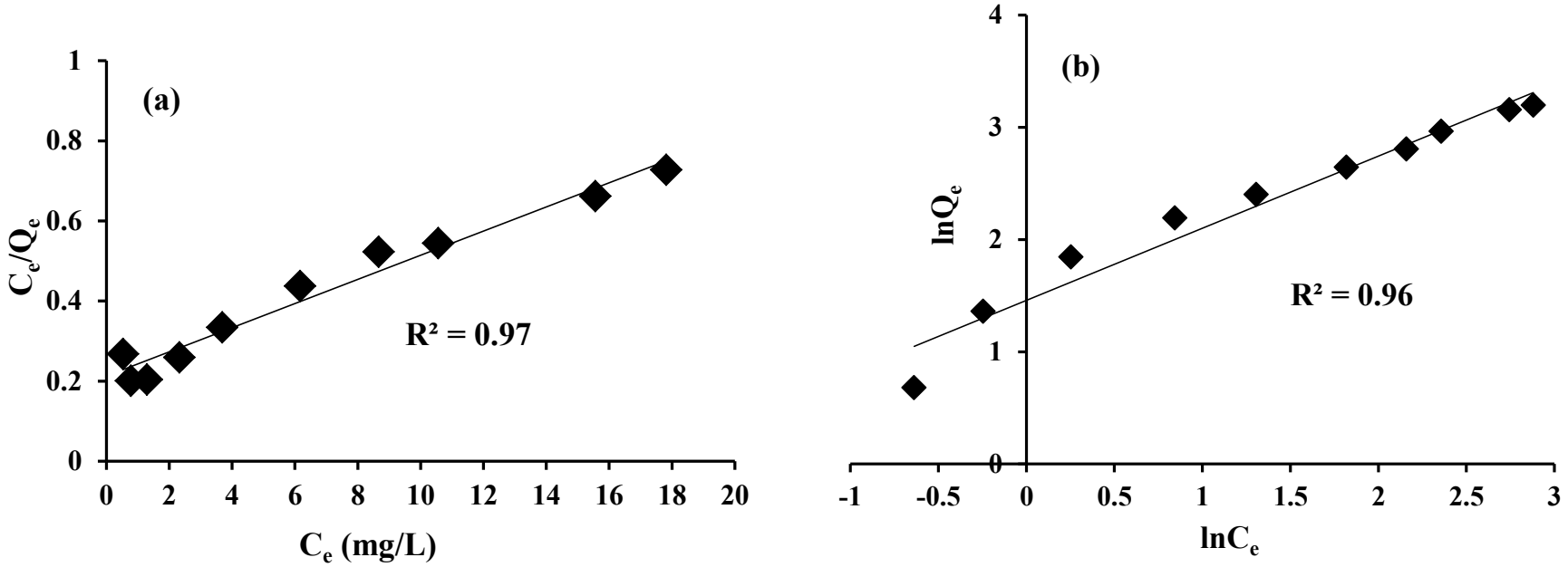

Figure 3.7. Isotherm modelling of nitrate adsorption on Purolite A520E (a) Langmuir (b) Freundlich

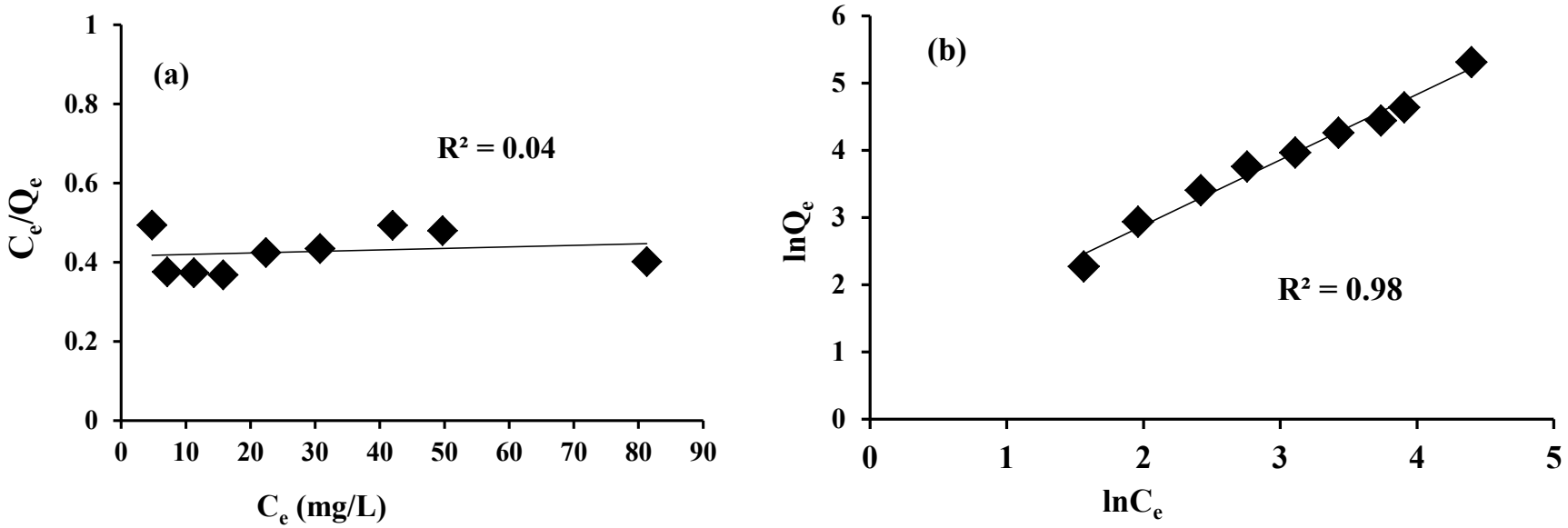

Figure 3.8. Isotherm modelling of nitrate adsorption on Purolite A500PS (a) Langmuir (b) Freundlich

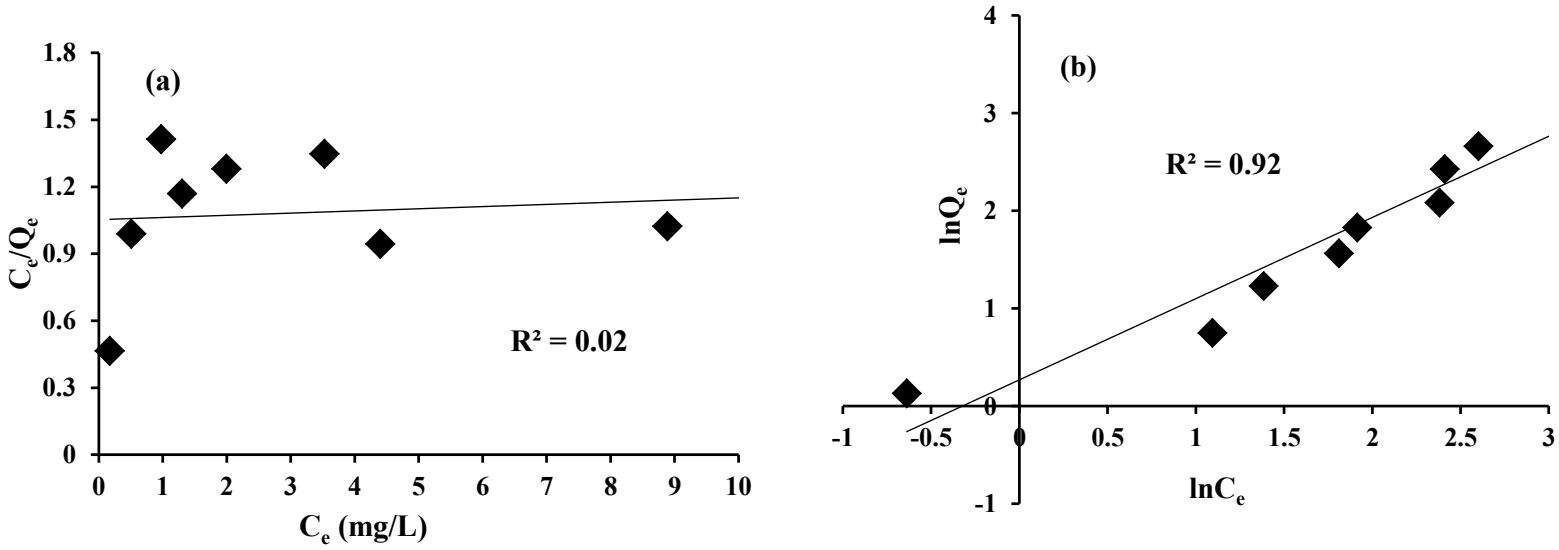

Figure 3.9. Isotherm modelling of phosphate adsorption on Purolite A520E (a) Langmuir (b) Freundlich.

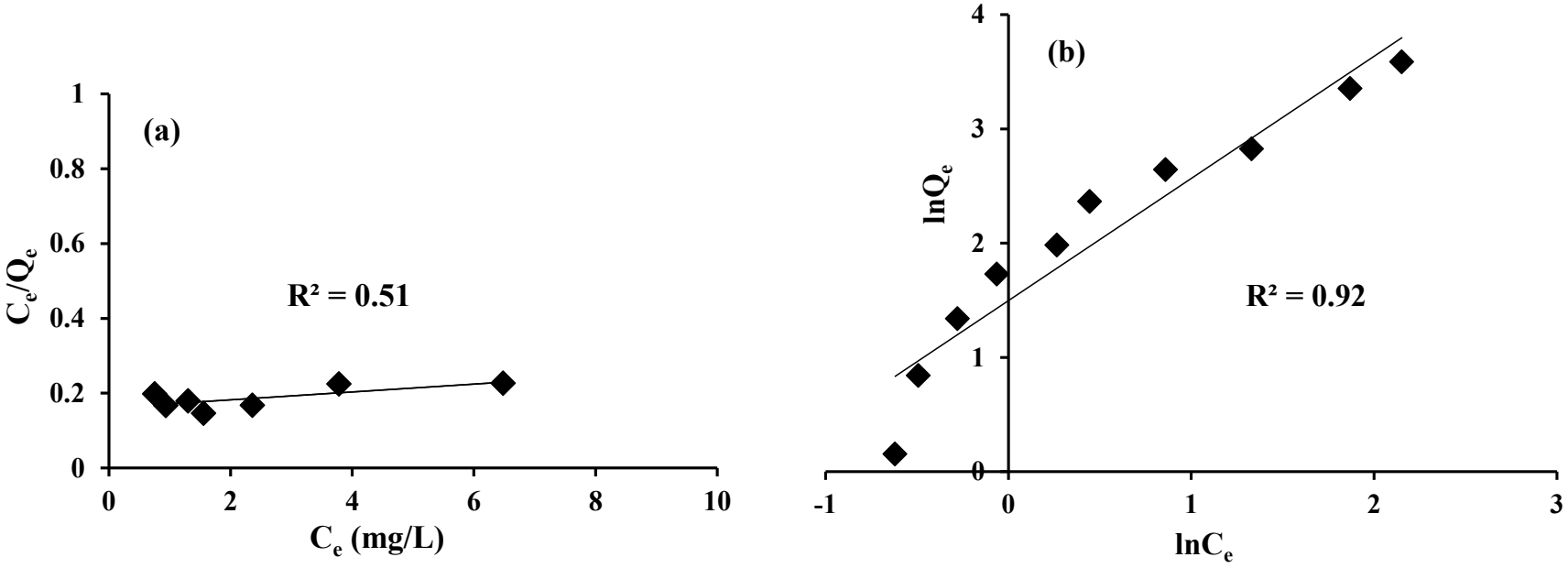

Figure 3.10. Isotherm modelling of phosphate adsorption on Purolite A500PS (a) Langmuir (b) Freundlich

Table 3.5.

Adsorption isotherm parameters of the Langmuir and Freundlich models for nitrate and phosphate adsorption on Purolite A520E and Purolite A500PS.

Model Parameters	Adsorption of nitrate onto		Adsorption of phosphate onto	
	Purolite A520E	Purolite A500PS	Purolite A520E	Purolite A500PS
Langmuir Isotherm Model				
q_{max} (mg N,P/g)	33	1000	-250	94.34
K_L (L/mg N,P)	0.141	0.003	-0.012	0.089
R^2	0.97	0.04	0.02	0.51
Freundlich Isotherm Model				
K_F (mg N,P/g)	4.29	2.45	3.40	4.49
n	1.54	1.03	1.12	0.909
R^2	0.96	0.98	0.92	0.92

3.3.7. Modelling of adsorption kinetics

In adsorption kinetics, mass transfer and diffusion of adsorbate particles from bulk liquid phase to adsorbent surface determine the rate of adsorption. The adsorption data showed that generally the pseudo-first-order kinetic model fitted poorly to the data for adsorption of nitrate and phosphate on both Purolites (Tables 3.6 and 3.7) (Figures 3.11-3.18). Only for the lower resin dosage of 1.5 g/L did the data fit satisfactorily to the pseudo-first-order kinetic model for both nitrate and phosphate adsorption on both resins.

In contrast to the pseudo-first-order kinetic model, the adsorption of phosphate and nitrate onto both ion exchange resins was much better evaluated using the pseudo-second-order kinetic model with R^2 of 0.99 and above (Tables 3.6 and 3.7; (Figures 3.11-3.18). Previous studies of nitrate adsorption on Purolite also revealed that the kinetics adsorption data were better described when using the pseudo-second order kinetic model (Bulgariu et al., 2010).

Furthermore, the values of q_e calculated from the pseudo-first-order kinetic model were less than the experimental value of q_e while the experimental values of q_e were very similar to the q_e values calculated from the pseudo-second-order kinetic model (Tables 3.4 and 3.5). These findings also demonstrated that the adsorption reaction can be satisfactorily described by the pseudo-second-order kinetic model. The satisfactory fits of the data to the second-order-kinetic model implies that the ion exchange process rates are limited only by the nitrate and phosphate ions and functional groups from the resin surface that are available to interact (Bulgariu et al., 2010).

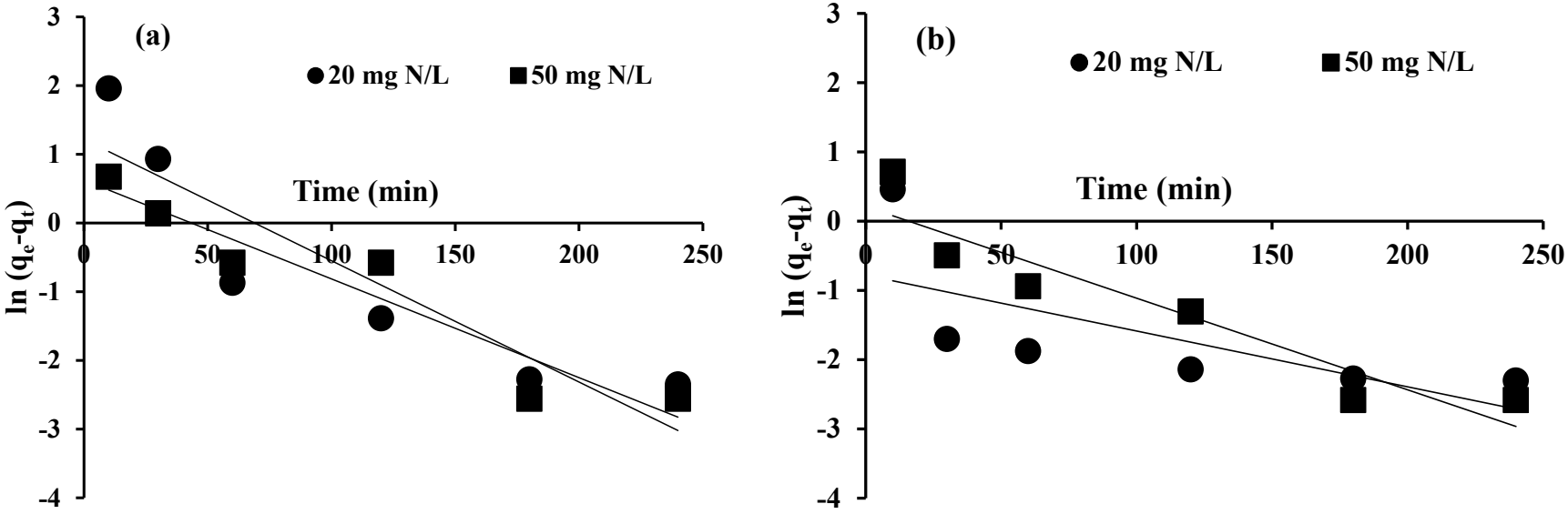

Figure 3.11. Pseudo-first-order order kinetic modelling of nitrate adsorption on Purolite A520E (a) 1.5 g resin/L (b) 3.0 g resin/L

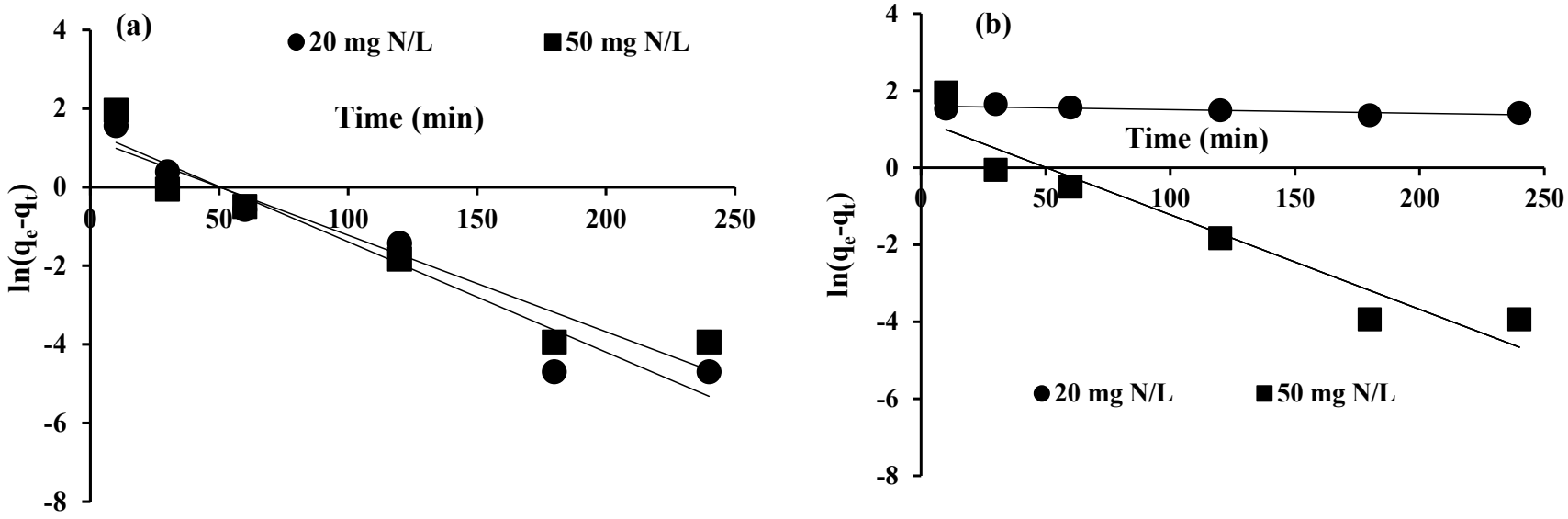

Figure 3.12. Pseudo-first-order kinetic modelling of nitrate adsorption on Purolite A500PS (a) 1.5 g resin/L (b) 3.0 g resin/L

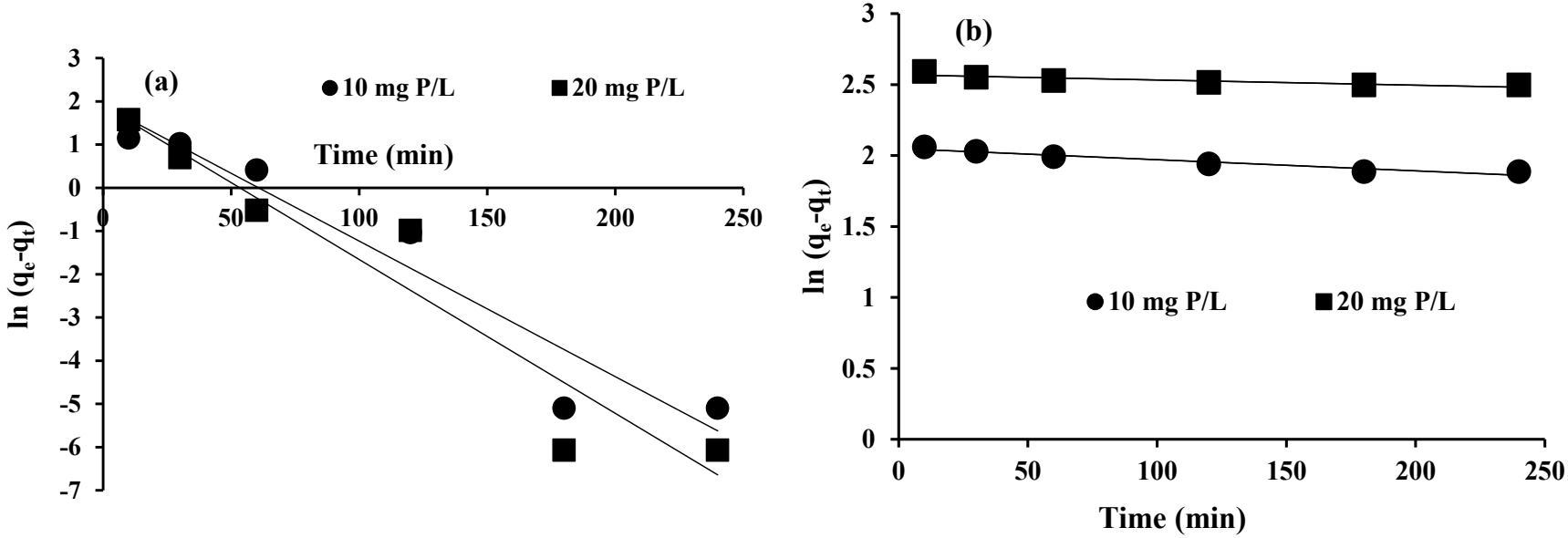

Figure 3.13. Pseudo-first-order kinetic modelling of phosphate adsorption on Purolite A520E (a) 1.5 g resin/L (b) 3.0 g resin/L

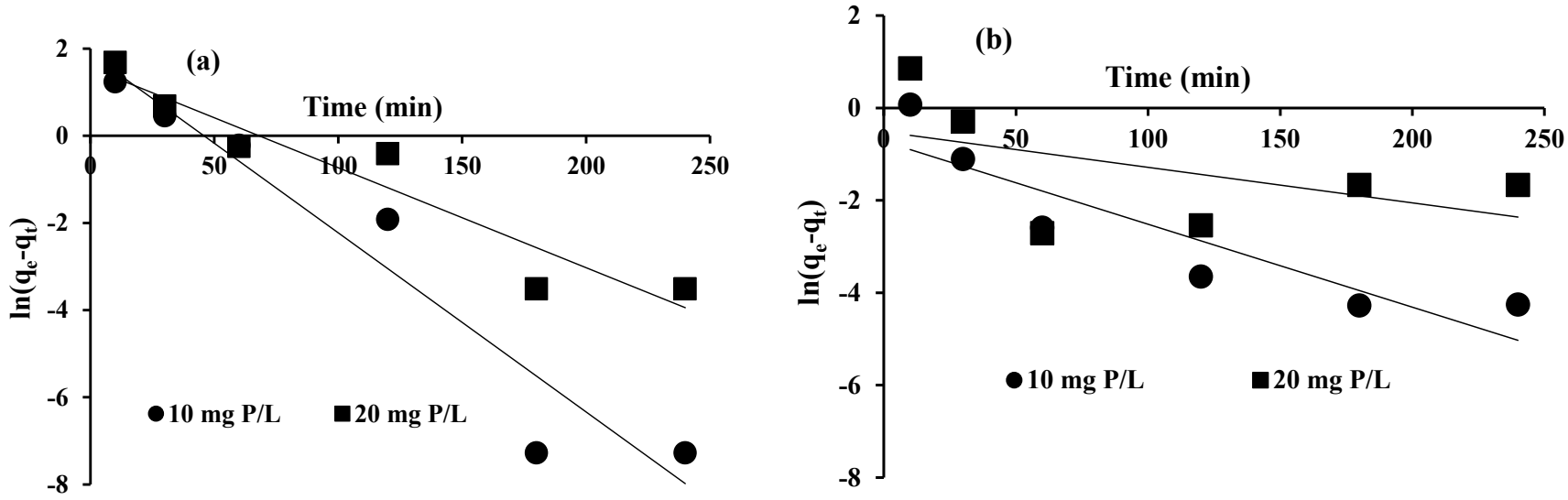

Figure 3.14. Pseudo-first-order kinetic modelling of phosphate adsorption on Purolite A500PS (a) 1.5 g resin/L (b) 3.0 g resin/L

.

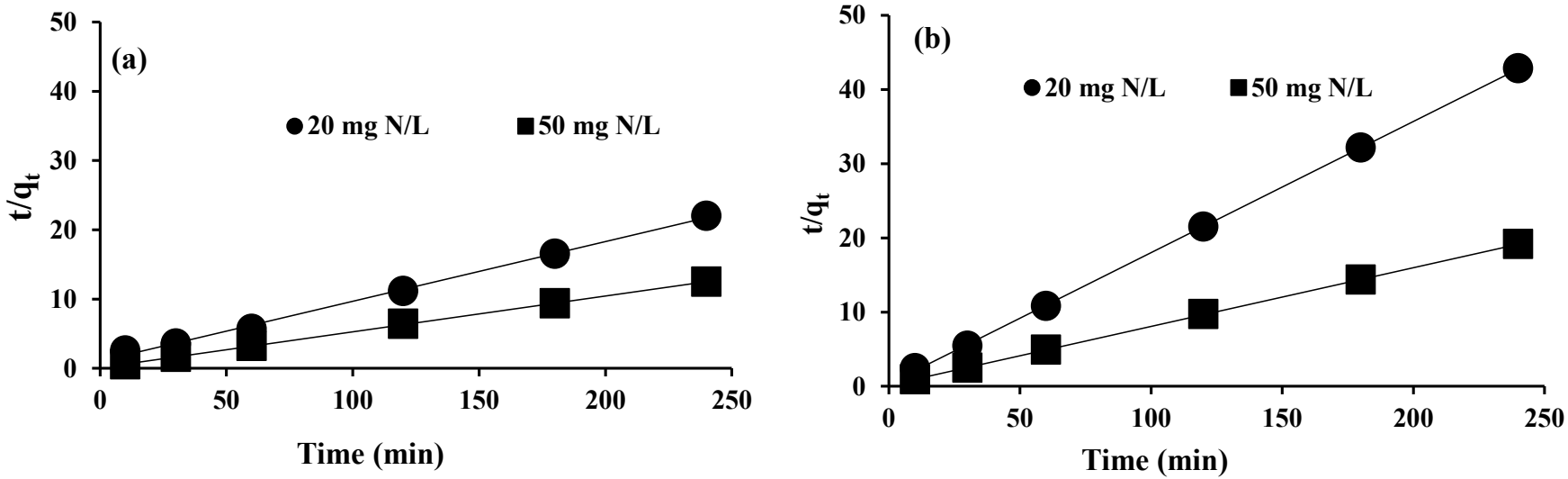

Figure 3.15. Pseudo-second-order kinetic modelling of nitrate adsorption on Purolite A520E (a) 1.5 g resin/L (b) 3.0 g resin/L

.

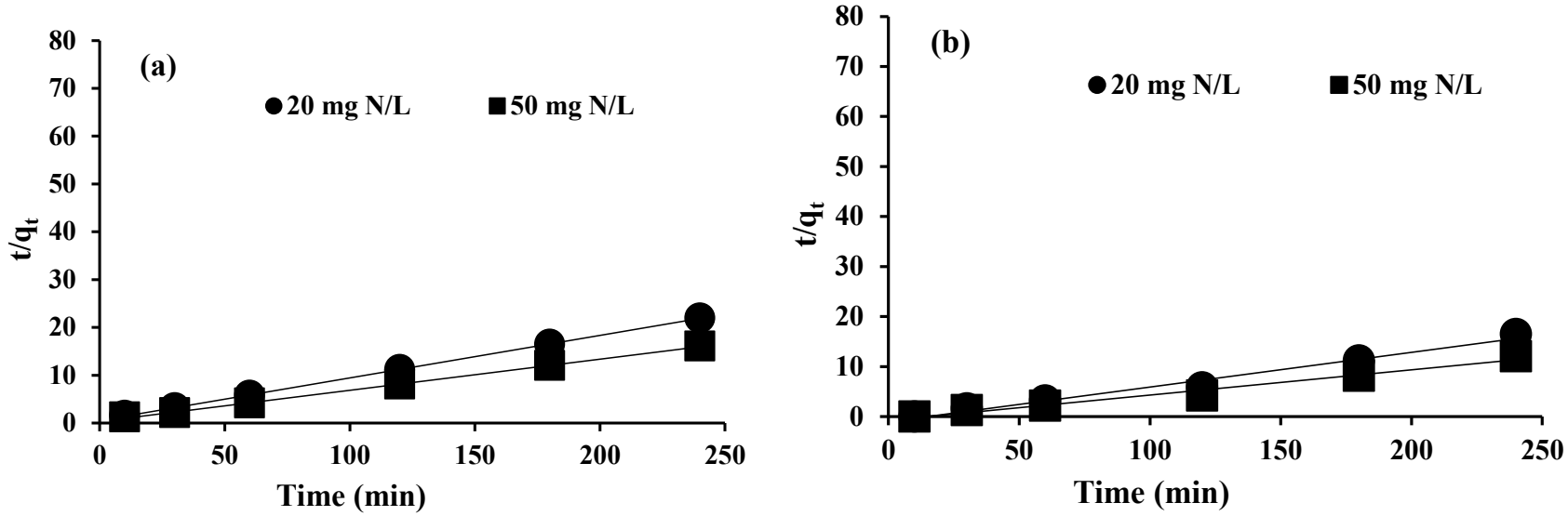

Figure 3.16. Pseudo-second-order kinetic modelling of nitrate adsorption on Purolite A500PS (a) 1.5 g resin/L (b) 3.0 g resin/L

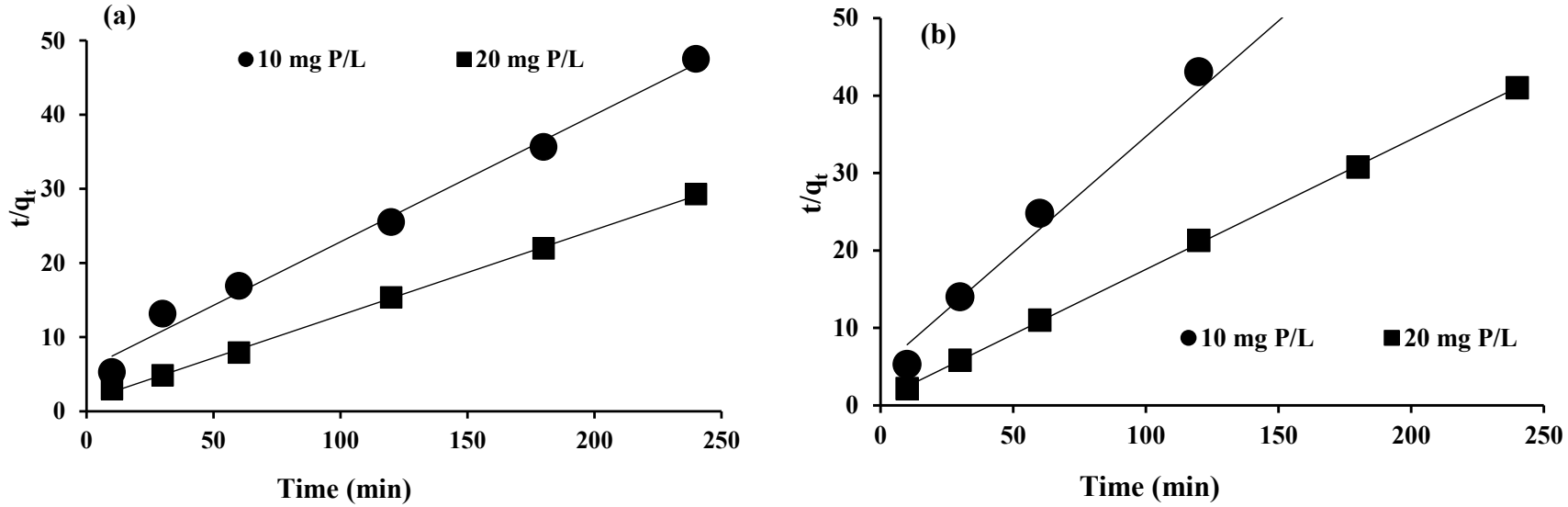

Figure 3.17. Pseudo-second-order kinetic modelling of phosphate adsorption on Purolite A520E (a) 1.5 g resin/L (b) 3.0 g resin/L

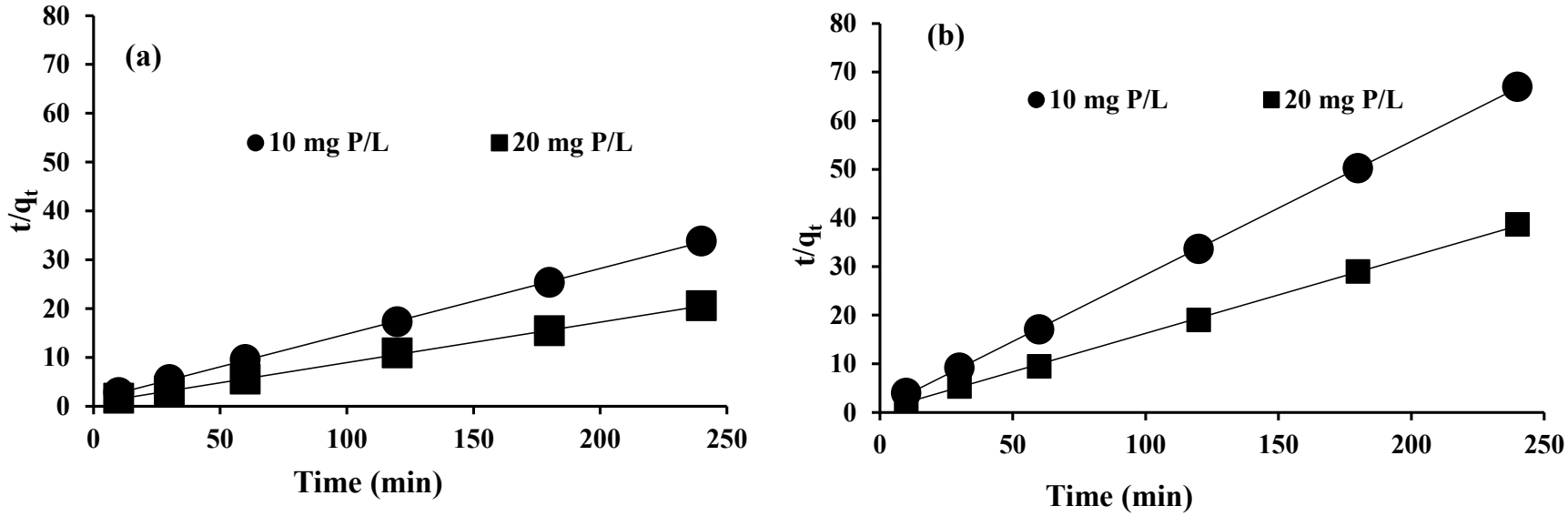

Figure 3.18. Pseudo-second-order kinetic modelling of phosphate adsorption on Purolite A500PS (a) 1.5 g resin/L (b) 3.0 g resin/L

Table 3.6.

Adsorption kinetic parameters of pseudo-first-order and second-order kinetics models for the adsorption of nitrate onto Purolite A520E and Purolite A500PS.

				Pseudo-first-order model			Pseudo-second-order model		
Purolite	Concentration of Purolite (g/L)	Concentration of raw water (mg N/L)	q_e experimental (mg N/g)	q_e (mg N/g)	$k_1 \times 10^{-2}$ (min^{-1})	R^2	q_e (mg N/g)	$k_2 \times 10^{-2}$ (g/mg N. min)	R^2
A520E	1.5	20	11.00	3.38	1.76	0.82	11.60	0.71	0.99
		50	19.30	1.86	14.41	0.91	19.34	2.62	0.99
	3.0	20	5.70	0.46	0.81	0.48	5.66	9.31	0.99
		50	12.60	1.23	1.32	0.88	12.62	4.00	1.00
A500PS	1.5	20	10.97	3.19	2.08	0.94	11.36	1.37	0.99
		50	14.95	3.93	2.82	0.91	15.63	0.85	0.99
	3.0	20	4.91	0.42	0.76	0.39	4.97	9.86	0.99
		50	9.25	1.17	1.26	0.85	8.35	2.47	0.99

Table 3.7.

Adsorption kinetic parameters of pseudo-first-order and second-order kinetics models for the adsorption of phosphate onto Purolite A520E and Purolite A500PS

				Pseudo-first-order			Pseudo-second-order		
Purolite	Concentration of Purolite (g/L)	Concentration of raw water (mg P/L)	q_e experimental (mg P/g)	q_e (mg P/g)	$k_1 x10^2$ (min^{-1})	R^2	q_e (mg P/g)	$k_2 x10^{-2}$ (g/mg P.min)	R^2
A520E	1.5	10	5.06	6.69	3.11	0.93	5.85	0.51	0.99
		20	8.20	6.68	3.53	0.91	8.70	0.92	0.99
	3.0	10	1.95	0.38	1.85	0.84	2.25	4.34	0.99
		20	2.87	0.56	0.86	0.33	3.94	3.52	0.99
A500PS	1.5	10	7.10	6.58	4.11	0.93	7.45	1.32	0.99
		20	11.70	4.76	2.29	0.91	12.08	1.02	0.99
	3.0	10	3.60	0.49	1.79	0.82	3.65	8.51	0.99
		20	6.40	0.60	0.77	0.25	6.33	5.69	0.99

3.3.8. Modelling of column adsorption

The column adsorption data was fitted to three empirical models, specifically the Bohart-Adam's, Thomas and Yoon-Nelson models for the adsorption of nitrate and phosphate on both the Purolites at two filtration velocities (v = 2.5 m/h and 5.0 m/h) (Tables 3.8 and 3.9). For the low filtration velocity of 2.5 m/h, the data fitted almost satisfactorily to all three models for both nitrate and phosphate adsorption on both resins with good R^2 values (0.81-0.96). The exceptions were: firstly, nitrate adsorption onto Purolite A500PS for the Bohart-Adam's model (R^2 = 0.63); and secondly, phosphate adsorption on Purolite A520E for the Thomas and Yoon-Nelson model (R^2 = 0.71). In contrast to the low filtration velocity, the adsorption of phosphate and nitrate onto both ion exchange resins was better described by the three models with good R^2 values (0.82-0.98) at the higher filtration velocity (v = 5.0 m/h) (Tables 3.8 and 3.9). Purolite A520E using the Thomas model adsorption capacity (21.3 mg/g) absorbed more nitrate compared to the Purolite A500PS (18.1 mg/g). On the other hand, Purolite A500PS using the Thomas model phosphate adsorption capacity (34.6 mg/g) was superior to Purolite A520E (23.2 mg/g). Adsorption capacities calculated from the breakthrough curves also provided the same information (Tables 3.8 and 3.9). Differences in the adsorption capacities of the two Purolites observed in column study are similar to those obtained in the batch study reported earlier in this chapter.

Considering the values of R^2 for the models' fit to the data and breakthrough curves, it can be concluded that all three models can reasonably well describe the behaviour of the adsorption of nitrate and phosphate on the Purolite resins in a fixed-bed column. The exception is perhaps the Bohart-Adams model for nitrate adsorption on Purolite A500PS, where the models' fit to the data was poor.

Table 3.8.

Model parameters for the adsorption of nitrate and phosphate by the two Purolites (initial concentration = 20 mg N/L and 30 mg P/L, bed height = 12 cm and filtration velocity = 2.5 m/h).

	Adsorption of nitrate onto		Adsorption of phosphate onto	
	Purolite A520E	Purolite A500PS	Purolite A520E	Purolite A500PS
Bohart-Adams Model				
k_{AB}(L/mg N,P. min) x 10^{-5}	0.0001	0.0001	0.0008	0.0004
N_o (mg N,P/L) x 10^3	15.4	11.8	1.3	3.1
R^2	0.82	0.63	0.87	0.94
Thomas Model				
k_{Th} (mL/min.mg N,P) x 10^{-2}	0.095	0.093	0.041	0.056
q_o (mg N,P/g)	21.3	18.1	23.2	34.6
R^2	0.96	0.93	0.71	0.81
Yoon-Nelson Model				
k_{YN} (1/min) x 10^{-3}	0.003	0.003	0.004	0.002
τ (min) x 10^3	1712	1462	450	1146
R^2	0.95	0.91	0.71	0.81
Breakthrough adsorption capacity (mg N,P/g)	14.2	13.1	8.9	11.1

Table 3.9.

Model parameters for the adsorption of nitrate and phosphate by the two Purolites (initial concentration = 20 mg N/L and 30 mg P/L, bed height = 12 cm and filtration velocity = 2.5 m/h).

	Adsorption of nitrate onto		Adsorption of phosphate onto	
	Purolite A520E	Purolite A500PS	Purolite A520E	Purolite A500PS
Bohart-Adams Model				
k_{AB}(L/mg N,P. min) x 10^{-5}	0.0002	0.0003	0.0006	0.0003
N_o (mg N,P/L) x 10^3	12.6	9.6	2.7	3.5
R^2	0.94	0.89	0.86	0.89
Thomas Model				
k_{Th} (mL/min.mg N,P) x 10^{-2}	0.161	0.196	0.073	0.089
q_o (mg N,P/g)	16.4	15.2	13.0	19.7
R^2	0.95	0.97	0.91	0.98
Yoon-Nelson Model				
$K_{F\ (mg\text{-}N,P/g)}$	0.004	0.006	0.006	0.003
n	882	673	237	699
R^2	0.98	0.96	0.82	0.89
Breakthrough adsorption capacity (mg N,P/g)	12.9	11.6	8.6	12.9

3.3.9. Regeneration of ion exchange resins

The adsorbed nitrate and phosphate were desorbed from the ion exchange resins by regenerating the two resins using different concentrations (0.1, 0.5 and 1.0 M) of NaCl and Na_2SO_4. Nitrate desorption was conducted on Purolite A520E and phosphate desorption was conducted on Purolite A500PS because these resins were selective for the respective nutrients (section 3.3.3). The regeneration was done by shaking the resin with the regeneration solutions. From the experimental investigation it was found that NaCl solution was 50% more effective than Na_2SO_4 in regenerating the ion exchange resin and recovering nitrate and phosphate (Figure 3.19). A NaCl solution of 1.0 M can recover almost 91-95% of adsorbed nitrate and phosphate from the resins. In contrast Na_2SO_4 with a similar concentration can recover only 30-40% of adsorbed nitrate and phosphate within the 5 min shaking period. Other researchers also reported good regeneration efficiency by NaCl which showed a desorption efficiency of ~95% (Primo et al., 2009).

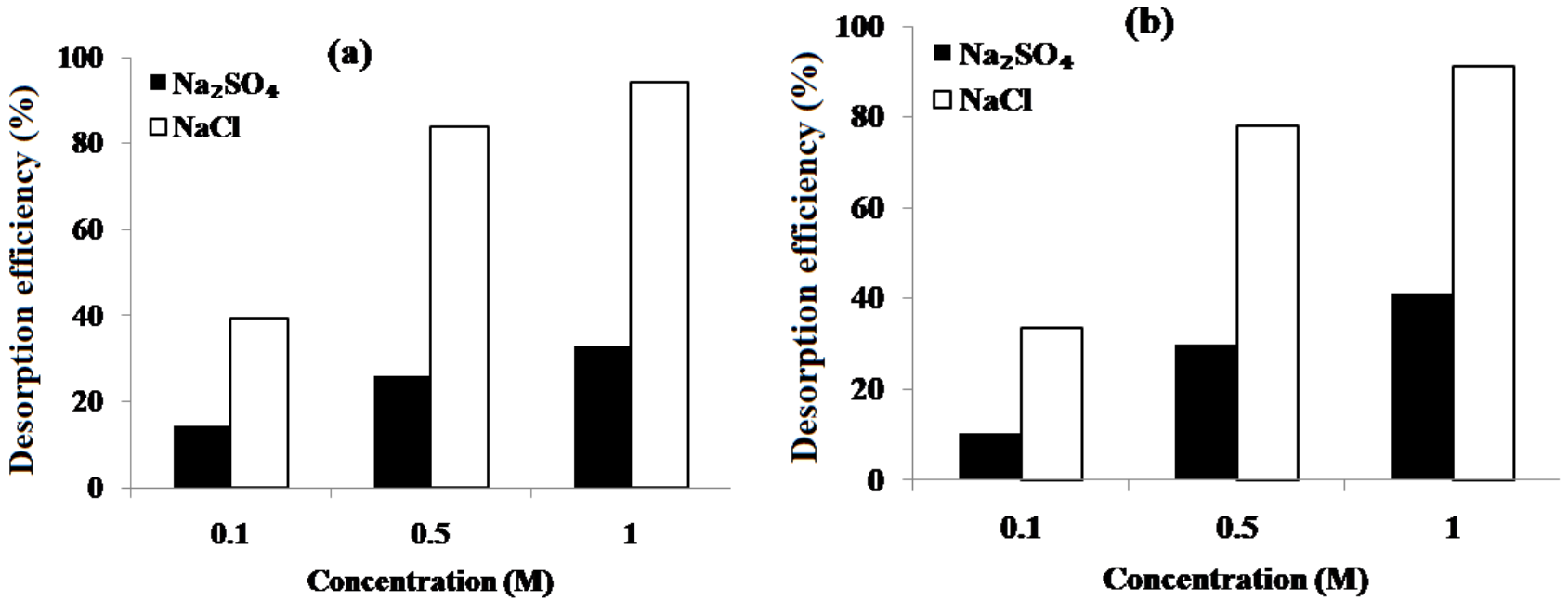

Figure 3.19. Effect of regenerating solution (NaCl and Na_2SO_4) using different concentrations (0.1, 0.5 and 1.0 M) on the recovery of (a) nitrate from Purolite A520E and (b) phosphate from Purolite A500PS.

Since 1.0 M NaCl proved to be better than Na_2SO_4 for desorbing nitrate and phosphate from the two resins in batch experiments, this reagent was used for regenerating both Purolites in the column experiment. For both Purolites, 90-95% of the nitrate and phosphate was desorbed by 1.0 M NaCl in 30 min (42 bed volumes). Approximately 70% of nitrate and phosphate was desorbed within 10 min (14 bed volumes). Previous studies have shown that nitrate selectivity for adsorption was higher for Purolite A520E than Purolite A500PS. Furthermore Purolite A500PS is more efficient than Purolite A520E when removing phosphate. For this reason the regenerated Purolite A520E and Purolite A500PS adsorbents were tested for reuse after every adsorption-desorption cycle. This was done utilising fresh 1M NaCl for each desorption cycle for nitrate and phosphate respectively (Figure 3.20).

The results showed that the efficiency of nitrate/phosphate adsorption-desorption was nearly the same for two cycles and only declined by a fraction in the third cycle. The decline in efficiency of adsorption/desorption was not more than 10%, indicating that the Purolite resins can potentially adsorb nitrate/phosphate and can be reused at least three times. Further studies need to be conducted for more adsorption/desorption cycles so that the number of such cycles that can be used without significantly reducing the adsorption capacity, can be determined.

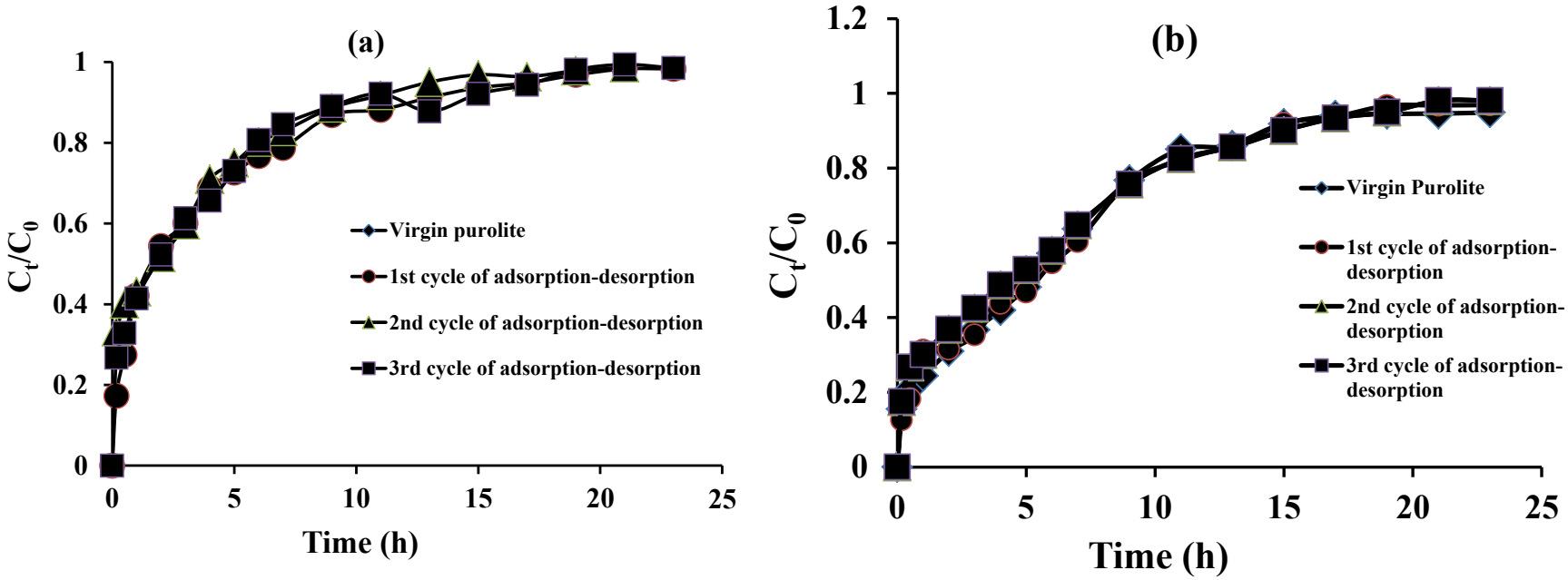

Figure 3.20. Breakthrough curves for (a) nitrate adsorption on Purolite A520E and (b) phosphate adsorption on Purolite A500PS after desorption by 1 M NaCl in the column adsorption experiment for three adsorption-desorption cycles.

3.4. Conclusions

Two ion-exchange resins, Purolite A520E and Purolite A500PS, can be used to effectively remove nitrate and phosphate from water. Both Purolites were better at removing nitrate than phosphate from solutions containing these two ions at various concentration ratios. They were consequently considered to be nitrate selective. The nitrate selectivity for adsorption was higher for Purolite A520E than Purolite A500PS. However, Purolite A500PS was more efficient than Purolite A520E when removing phosphate. Based on the competitive study, it emerged that nitrate competes effectively with phosphate for adsorption on Purolite A520E whereas the removal efficiency of nitrate by Purolite A500PS was not very much affected by the presence of phosphate. In the case of a high concentration of phosphate, removal efficiency only slightly decreased.

The adsorption of phosphate and nitrate on both Purolites was better described using the pseudo-second-order kinetic model than the pseudo-first-order kinetic model. The Freundlich model provided a better fit for the adsorption data of nitrate and phosphate than the Langmuir model for both Purolites. The Langmuir adsorption capacity was 33 mg N/g for Purolite A520E, whereas the highest column adsorption capacity was 21.3 mg N/g at the inlet concentration of 20 mg N/L, 12 cm bed height and 2.5 m/h filtration velocity. Conversely, the highest column adsorption capacity for removing phosphate was 23.2 mg P/g at the inlet concentration of 30 mg P/L, 12 cm bed height and 2.5 m/h filtration velocity for Purolite A500PS. Breakthrough column adsorption data fitted well to the Bohart-Adams, Thomas and Yoon-Nelson models for nitrate and phosphate adsorption on both Purolites.

Both Purolites can be regenerated by 1M NaCl and reused for nitrate and phosphate adsorption at least three times without significantly reducing the adsorption capacity.

CHAPTER 4

University of Technology Sydney

NITRATE REMOVAL USING PUROLITE A520E: pH AND CO-IONS' EFFECTS AND ADSORPTION MODELLING

Chapter 4

Nitrate removal using Purolite A520E: pH and co-ions' effects and adsorption modelling*

4.1. Introduction

In Chapter 3 two ion-exchange resins, Purolite A520E and Purolite A500PS were used to remove nitrate and phosphate from water in batch and column experiments. The nitrate selectivity for adsorption was higher for Purolite A520E than Purolite A500PS which was similar to previous analyses of Purolite A520E (Samatya et al., 2006a and 2006b). Johir et al. (2011) also obtained similar results for these two Purolites using column adsorption experiments on MBR effluents from natural wastewater. For these reasons, Purolite A520E was selected for further experiments on removing nitrate from water and the results are discussed in this chapter. Special attention is given to other anions' competition of adsorption on this resin, effect of solution pH and column adsorption modelling.

The characteristics of adsorption behaviour on resins are generally inferred in terms of both adsorption kinetics and equilibrium isotherms. Samatya et al. (2006a, 2006b) used Purolite A520E to remove nitrate from water and found that this resin elicited promising results for batch and column-mode removal of nitrate from ground water. By fitting their batch adsorption data to the Langmuir adsorption isotherm, they reported a maximum adsorption value of 18.5 mg N/g dry resin. However, the effectiveness of

*** Much of this chapter was published in T. Nur, W.G. Shim, P. Loganathan, S. Vigneswaran, and J. Kandasamy, "Nitrate removal using Purolite A520E ion exchange resin: Batch and fixed-bed column adsorption modelling", International Journal of Environmental Science and Technology, doi 10.1007/s13762-014-0510-6.**

Purolite A520E in removing nitrate from water was not compared to other ion exchange resins. In this chapter nitrate removal by four ion exchange resins including Purolite A520E is compared and discussed.

pH is a very important factor influencing the surface charge of the ion exchange media as well as nitrate adsorption. At low pH, the nitrate adsorption capacity is expected to increase due to the strong electrostatic interactions between the positively charged adsorption sites and negatively charged nitrate. On the other hand, OH^- ion concentration in the solution increases as pH increases. Therefore at high pHs, OH^- ions compete with nitrate ions causing a decrease in adsorption capacity.

In reality, the nitrate contaminated water contains several other anions such as Cl^-, SO_4^{2-}, F^- and PO_4^{3-} which can equally compete in the adsorption process, so it is important to study the effect of these ions during adsorption. However, the selectivity of adsorption of nitrate by these resins in the presence of other anions varied depending on the length of carbon chain in the resin. The higher the carbon chain length of the functional group in the resin, higher the selectivity of nitrate adsorption. This is explained as due to the longer carbon chain making the resin more hydrophobic, and thus, the resin becomes more selective in adsorbing anions such as nitrate with less hydration energies (Valincius et al., 2004). Kapoor and Viraraghavan (1997) also reported that the nitrate to SO_4^{2-} selectivity increased from a factor of 100 to1,000 when the ammonium nitrogen in the resin was surrounded by ethyl groups in place of methyl groups.

Most studies on ion exchange resins removing nitrate have been done using batch experiments and only a few have been reported in fixed-bed systems (Hoek et al., 1988; Hekmatzadeh et al., 2012). Although batch experiments are useful in comparing adsorption capacities among adsorbents within a short period of time and obtaining

information on the effects of many solution variables on adsorption, they have a disadvantage in that they do not provide information about the hydrodynamic parameters of fixed-bed columns such as the dispersion coefficient (Loganathan et al., 2014). Another drawback is their discontinuity and the need to perform complicated phase separation operations (Zagorodni, 2007). Fixed-bed column experiments, on the other hand, do not have the above drawbacks and the results of such experiments can be directly applied to: firstly, obtaining reliable solutions to design optimisation; and secondly, predicting the breakthrough curves of fixed-bed columns in real water treatment processes.

The numerical solution of nitrate removal models in a fixed-bed column packed with ion exchange resins has gained very little attention and very few numerical models are available (Hekmatzadeh et al., 2012). A suitable numerical solution can help to reduce the number of experiments associated with new operating conditions and a novel and well-researched model can be used as a reliable solution to design, optimise and predict the breakthrough curves of fixed-bed columns in real water treatment processes. In this chapter, a numerical model is used to describe the column adsorption of nitrate on Purolite A520E.

The objectives of the study presented in this chapter are as follows: (i) analysis of the kinetic and equilibrium adsorption isotherms of nitrate on four ion exchange resins and justify the selection of Purolite A520E for a detailed study; (ii) investigate the effects of pH and the presence of other ions on nitrate adsorption of Purolite A520E; (iii) model batch adsorption equilibrium data using the Langmuir and Freundlich Isotherm models; (iv) model batch adsorption kinetic data by pseudo-first-order, pseudo-second-order, and homogeneous surface diffusion models; (v) examine the breakthrough curves for the adsorption of nitrate using the Thomas model; and (vi) develop a numerical model based

on advection-dispersion equation and simulating the equilibrium and model parameters to describe the column adsorption data.

4.2. Material and Methods

4.2.1. Ion exchange resins

Four ion exchange resins, namely Purolite A520E, Purolite A500PS, Purolite FerrIX A33E and Dowex 21k were used as adsorbents. The characteristics of Purolite A520E and Purolite A500PS were described in Chapter 3 in Table 3.1. Purolite FerrIX A33E resin, previously called ArsenXnp, is a hybrid strong base anion exchange resin with quaternary ammonium functional groups blended with hydrous iron oxide nanoparticles that have a very high attraction for arsenic (Zagorodni, 2007). Dowex 21K XLT is another strong base anion exchange resin composed of Styrene-DVB with trimethylamine functional groups (Sigma-Aldrich, 2013). This resin has been used to effectively remove uranium from groundwater at low nitrate concentration but not at high nitrate concentration (Phillips et al., 2008). This may be due to the resin having high affinity towards nitrate, but no study has been conducted on the nitrate removal effectiveness of this resin. All four resins had Cl^- as the exchangeable anion in the as-received form.

The methods of preparing the feed solution and chemical analysis are the same as those described in Chapter 3.

4.2.2. Batch adsorption studies

Equilibrium adsorption isotherm and adsorption kinetics experimental methods are also the same as those described in Chapter 3.

4.2.3. Adsorption modelling

4.2.3.1. Batch adsorption equilibrium modelling

The data for batch adsorption at different adsorbent doses were treated with Langmuir and Freundlich isotherm models, the details of which were discussed in Chapter 2. The equations of the models and the graphical methods used to calculate the model parameters are explained in Table 3.2.

4.2.3.2. Batch adsorption kinetic modelling

The batch adsorption kinetic data are analysed by pseudo-first-order and pseudo-second-order kinetics models which were also discussed earlier in Chapter 2**.** The equations for the pseudo-first-order and pseudo-second-order kinetic models and the methods of calculating the model parameters were presented in Table 3.3. The adsorption data are also analysed by HSDM adsorption kinetics model which is described below.

4.2.3.2.1. HSDM adsorption kinetics model

The HSDM used to study the Purolite A520E adsorption kinetics is presented in Equations 4.1 – 4.4. HSDM consists of a three-step process: (i) the adsorbate diffuses through a stagnant liquid film layer surrounding the adsorbent particle; (ii) the adsorbate adsorbs from the liquid phase onto the outer surface of the adsorbent particle; and (iii) the adsorbate diffuses along the inner surface of the adsorbent particles until it reaches its adsorption site (Najm, 1996).

The equations are expressed as:

$$\frac{\partial q}{\partial t} = D_s\left(\frac{\partial^2 q}{\partial r^2} + \frac{2}{r}\frac{\partial q}{\partial r}\right) \tag{4.1}$$

Initial and boundary conditions are:

$$t = 0 \;;\; q = 0 \tag{4.2}$$

$$r = 0 \;;\; \frac{\partial q}{\partial r} = 0 \tag{4.3}$$

$$r = r_p \;;\; D_s \rho_p \frac{\partial q}{\partial r} = k_f\left(C - C_s\right) \tag{4.4}$$

where q is surface concentration at any radial distance (r) from the centre of the particle during adsorption, mg N/g; D_s, the surface diffusion coefficient (the rate of diffusion of the nitrate along the surface of the adsorbent), m^2/s; k_f, the external mass transfer coefficient, m/s; ρ_p, the apparent density of the adsorbent, kg/m^3; C, the bulk phase concentration, mg N/L; C_s is the concentration on the external surface, mg N/L.

In this work the Freundlich equation was used as the boundary condition in HSDM calculations. The fit of the equilibrium data to the Freundlich adsorption isotherm and the

isotherm parameters obtained were used. Using the isotherm parameters and Equations 4.1-4.4, k_f and D_s were calculated.

These equations were solved using an orthogonal collocation method (OCM) and the variable coefficient ordinary differential equation solver (VODE). The partial differential equations of the batch system were first transformed into ordinary differential equations. The resulting equations were then integrated numerically in the time domain. Nelder-Mead simplex method (Guo et al., 2005) which is based on minimising the differences between the experimental and predicted results was used to obtain the best fit values for the parameters, D_s and K_f. The minimisation of the differences was performed using the following object function:

$$\text{Minimum} = \sum_{j} \left(C_{exp,j} - C_{cal,j} \right)^2 \tag{4.5}$$

where, $C_{exp,j}$ is the experimental nitrate concentration data $C_{cal,j}$ is the calculated nitrate concentration. A detailed explanation to this method is given elsewhere (Villadsen and Stewart, 1967; Brown et al., 1989; Guo et al., 2005).

4.2.4. Effect of pH

The effect of pH on nitrate adsorption was studied by agitating 1g of Purolite A520E at pHs from 4 to 10 with 100 mL of nitrate solution containing 20 mg N/L in a set of glass flasks. The suspensions were agitated in a flat shaker at a shaking speed of 120 rpm for 24 h at room temperature (24 ± 1°C). Aqueous samples were taken at different time intervals and the concentrations of nitrate were measured.

4.2.5. Effect of co-ions

The effect of complementary anions (Cl^-, SO_4^{2-}, F^- and PO_4^{3-}) on nitrate adsorption by Purolite A520E was studied at a constant initial nitrate concentration of 20 mg N/L, adsorbent dose of 1 g/L and pH 7 by varying anion concentrations from 25 to 200 mg/L using NaCl, Na_2SO_4, NaF and KH_2PO_4. The suspensions were agitated in a flat shaker at a shaking speed of 120 rpm for 24 h at room temperature (24 ± 1°C). Aqueous samples were taken at different time intervals and the concentrations of nitrate in the supernatant were measured.

4.2.6. Fixed-bed column studies

The description of the fixed-bed column studies is similar to that presented in Chapter 3.

4.2.7. Fixed-bed column modelling

The Thomas model (Thomas, 1944) is used to analyse the column adsorption data. The methods of calculation of the model parameters were presented in Table 3.4**.** A numerical model is also used to describe nitrate column adsorption data. As this is the first time this model is used in the thesis, it is discussed in the next section.

4.2.7.1. Numerical model

The mass balance equations and the boundary conditions of the fixed-bed system are given by the following equations, which were previously described (Ruthven, 1984; Guo et al., 2005; Ahmad et al., 2012):

$$-D_L \frac{\partial^2 C}{\partial z^2} + v\frac{\partial C}{\partial z} + \frac{\partial C}{\partial t} + \frac{1-\varepsilon_B}{\varepsilon_B}\rho_s \frac{\partial q}{\partial t} = 0 \quad (4.6)$$

where, D_L= axial dispersion coefficient (m^2/s), C = concentration in bulk solution, mg/L, v = velocity of the fluid, (m/s), z = bed depth, (m), ε_b= bed porosity.

The above equation can be solved by using the initial and boundary conditions, C = 0 at t = 0 and z = 0,

$$D_L \left.\frac{\partial C}{\partial z}\right|_{z=0} = -v\left(C|_{z=0^-} - C|_{z=0^+}\right) \quad (4.7)$$

and at z=L,

$$\left.\frac{\partial C}{\partial z}\right|_{z=L} = 0 \quad (4.8)$$

The D_s values depend only on the influent nitrate concentration. Therefore the D_s values derived from the batch kinetic experiments were used in the fixed-bed simulation. On the other hand, in batch mode adsorption experiments, k_f depends on the agitation speed, but in fixed-bed system it is a function of Reynolds (R_e) and Schmidt (S_c) numbers. Hence, k_f will not be the same as that derived from batch kinetics data. Therefore, k_f was determined by matching the fixed-bed experimental data with values derived from the

theoretical equations. Axial dispersion coefficient, D_L, was also determined by this procedure.

4.3. Results and discussion

4.3.1. Batch equilibrium adsorption

The results of batch equilibrium experiment for the four resins showed that the removal efficiency of nitrate improved with increased resin dose due to A larger surface area being available for adsorption (Figure 4.1a). Of the four resins, Purolite A520E and Dowex 21k had very high (around 75% and 70%, respectively) removal efficiency at a low resin dose of 1.0 g/L. These results imply that a very low dose of these two ion exchange resins can easily remove high amounts of nitrate from wastewater.

4.3.2. Batch kinetic adsorption

The kinetics of nitrate adsorption at an initial nitrate concentration of 20 mg N/L and adsorbent dosage of 1.5 g/L showed that the adsorption capacity increased with contact time up to approximately 2h and became steady afterwards (Figure 4.1b). Of the four adsorbents, Purolite A520E proved to be the most efficient at removing nitrate (84%) followed by Dowex 21k (81%), and Purolite A500PS (75%) within 120 min. The lowest removal efficiency was found for Purolite FerrIX A33E (48%).

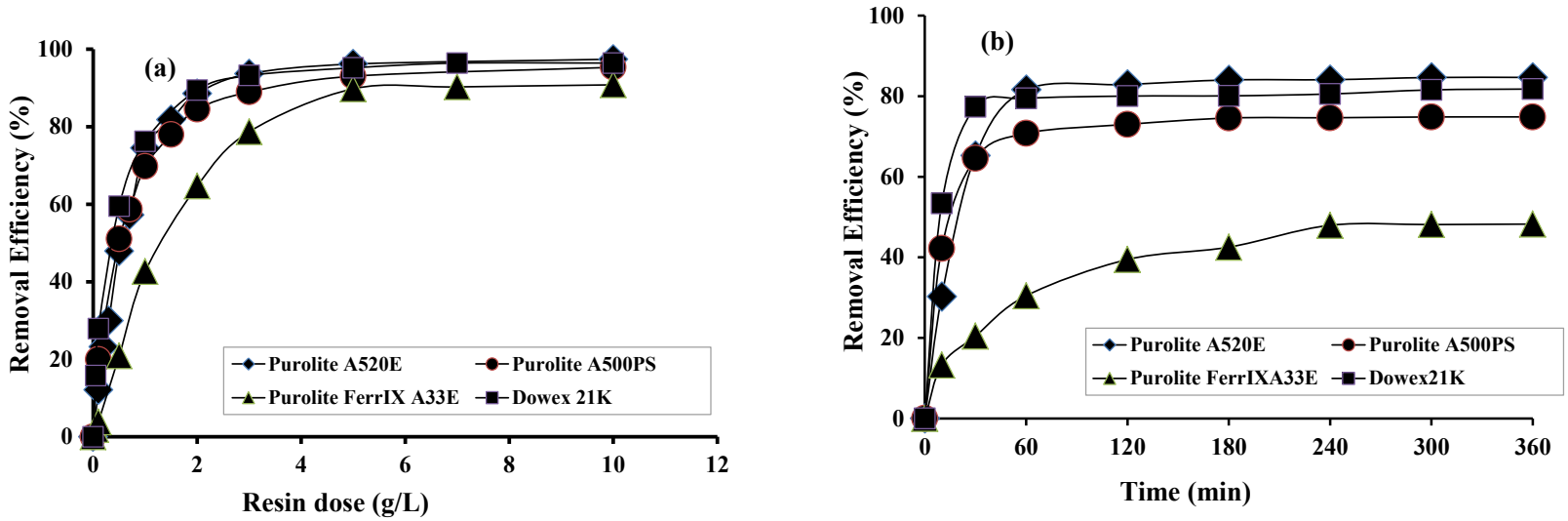

Figure 4.1. Effect of (a) resin dose and (b) contact time on the removal of nitrate of four adsorbents (initial nitrate concentration 20 mg N/L and resin dose 1.5 g/L).

4.3.3. Batch adsorption equilibrium modelling

The adsorption data of all four adsorbents were fitted to the two mostly used equilibrium models, i.e. the Langmuir and Freundlich models. The estimated isotherms parameters are summarised in Table 4.1.

4.3.3.1. Langmuir Model

Of the four resins, the data for only Purolite A520E and Purolite FerrIX A33E satisfactorily fitted to the Langmuir Isotherm equation with the maximum adsorption capacity of 32.2 mg N/g and 8.77 mg N/g and good R^2 values (0.98 and 0.97, respectively) (Figure 4.2 and Table 4.1). The main mechanism of adsorption of nitrate on Purolite A520E is electrostatic or coulombic interaction between the positively charged quaternary ammonium functional group in the resin and the negatively charged NO_3^- in solution (Helfferich, 1995; Gu et al., 2004). During adsorption, NO_3^- exchanged with Cl^-, which was already adsorbed onto the resin by an ion exchange process (Primo et al., 2009).

4.3.3.2. Freundlich Model

Isotherm data of all four adsorbents fitted satisfactorily to the Freundlich Isotherm model with very good R^2 value (0.91-0.98) (Figure 4.2 and Table 4.1). Again Purolite A520E had the highest value for the Freundlich parameter K_f which was related to the adsorption capacity. The values of K_f ranges from 2.02 to 3.97 (mg N/g) $(L/mg)^{1/n}$ and n value varied from 1.01 to 2.16, i.e. 1/n values varies from 0.46 to 0.99 for all adsorbents

which are below 1 indicating that it is a favorable adsorption. The value of the exponent 1/n gives an indication of the adequacy and capacity of the adsorbent/adsorbate system (Bilgili, 2006). Commonly, an exponent between 1 and 10 shows beneficial adsorption.

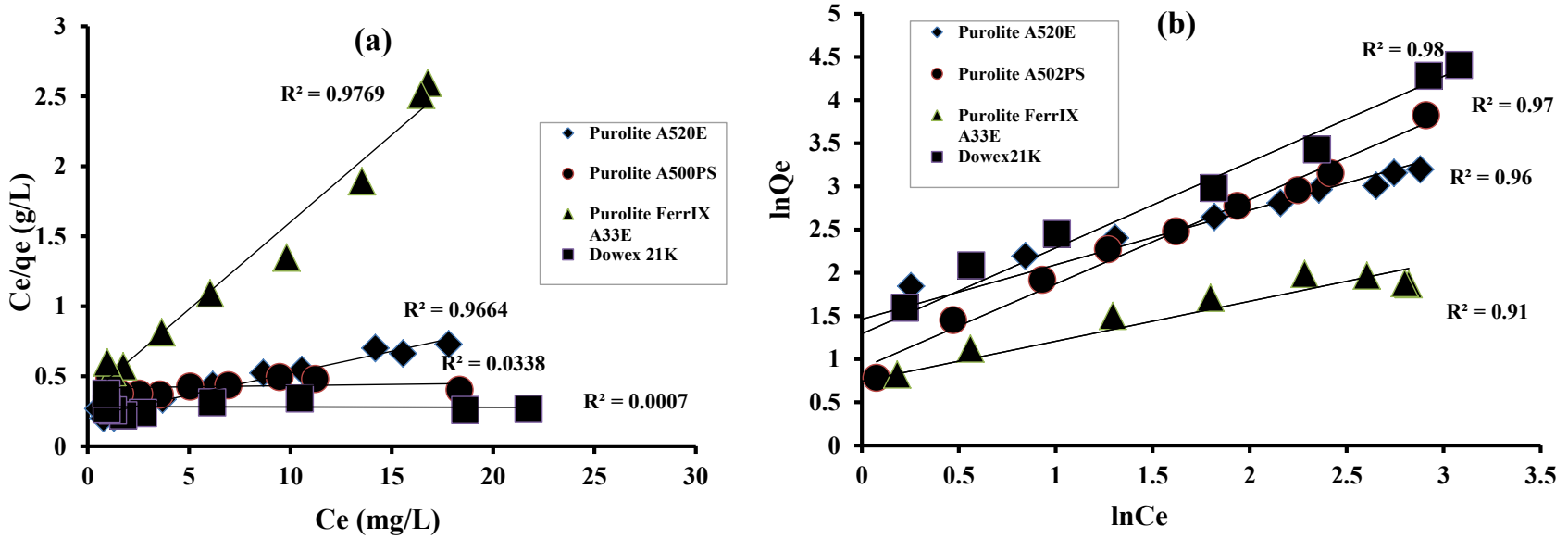

Figure 4.2. (a) Langmuir and (b) Freundlich isotherm models fit for nitrate adsorption on four adsorbents.

Table 4.1.

Adsorption isotherm parameters of the Langmuir and Freundlich models for nitrate adsorption on all four adsorbents.

Isotherm models	Adsorbents			
	Purolite A520E	Purolite FerrIX A33E	Purolite A502PS	Dowex21K
Langmuir Isotherm Model				
q_{max} (mg N/g)	32.20	8.77		
K_L (L/mg N)	0.15	0.35	Negative values	
R^2	0.97	0.95		
Freundlich Isotherm Model				
K_F (mg N/g)(L/mg N)$^{1/n}$	3.97	2.02	2.43	3.51
n	1.59	2.16	1.03	1.01
R^2	0.98	0.91	0.96	0.97

4.3.4. Batch adsorption kinetics modelling

Both the batch equilibrium (Figure 4.1a) and kinetic studies (Figure 4.1b) showed that Purolite A520E had the highest removal efficiency of nitrate among the four resins. This resin also had the highest value for Freundlich constant that is related to the adsorption capacity (Table 4.1). Therefore, Purolite A520E was chosen for further testing and modelling.

Figure 4.3 shows the kinetics of nitrate adsorption on Purolite A520E at two resin concentrations using HSDM, pseudo-first-order and second-order models. All three models predicted the experimental data very well as seen from the very high R^2 values (Table 4.2). Furthermore, the values of q_e calculated from pseudo-first-order and pseudo-second-order kinetic models were almost similar to the experimental value of q_e (Table 4.2). The results show that any of the three models can be used when a design is being considered.

The HSDM results show that the surface diffusion D_s was higher at lower resin concentration, which indicates that the surface diffusion D_s is a function of the equilibrium concentration C_e. This agreed with the findings of Ahmad et al. (2012) where an increase in equilibrium concentration, C_e increased the value of D_s for organic matter adsorption on Purolite A500PS.

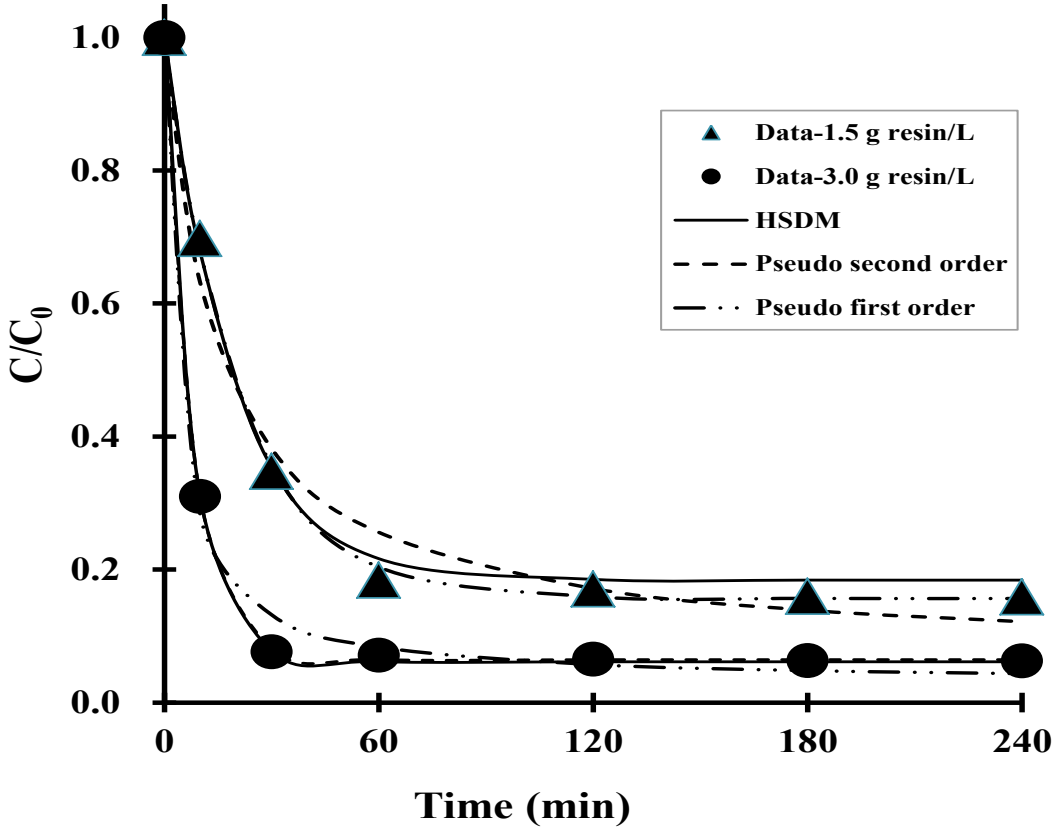

Figure 4.3. HSDM, pseudo first order and pseudo-second-order kinetic model predictions of the experimental data for the adsorption of nitrate onto Purolite A520E (initial nitrate concentration 20 mg N/L and resin doses 1.5 g/L and 3.0 g/L) (Experimental values are shown by data points, and model predictions are represented by lines).

Table 4.2.

HSDM, pseudo-first-order (PFO) and pseudo-second-order (PSO) kinetics model parameters for the adsorption of nitrate onto Purolite A520E.

		q_e (mg/g)	K_1 (1/min)	K_2 (1/min)	K_f (m/s)	Ds (m^2/s)	R^2
1.5 g resin / L	Experimental	11.0					
	PFO	10.9	$4.81x10^{-2}$				0.99
	PSO	12.1		$5.37x10^{-3}$			0.99
	HSDM				$1.40x10^{-5}$	9.37×10^{-9}	0.99
3.0 g resin / L	Experimental	5.7					
	PFO	5.6	$13.0x10^{-2}$				0.99
	PSO	5.8		$4.86x10^{-2}$			0.99
	HSDM				$9.08x10^{-6}$	2.26×10^{-9}	0.99

4.3.5. Effect of pH on nitrate adsorption

During nitrate adsorption, the pH of the suspension did not significantly change much and the final pH was almost the same as the initial pH. Nitrate adsorption capacity was almost the same at pH 5 to 8 (Figure 4.4), but it fell at pH < 5 and pH > 8. At low pH, the nitrate adsorption capacity probably decreased due to competition between Cl^- and nitrate which added to the falling pH and nitrate anions for active sites. On the other hand, OH^- ion concentration in the solution rose when the pH increased for the addition of NaOH and OH^- ions compete with nitrate ions causing a decrease in adsorption capacity. This property of the resin is very useful for a field operation where there could be variations in the pH of inlet water. Furthermore different locations the pH in the water may vary and since the activity of resin is independent of the pH within the 5-8 range, this makes a variety of applications possible.

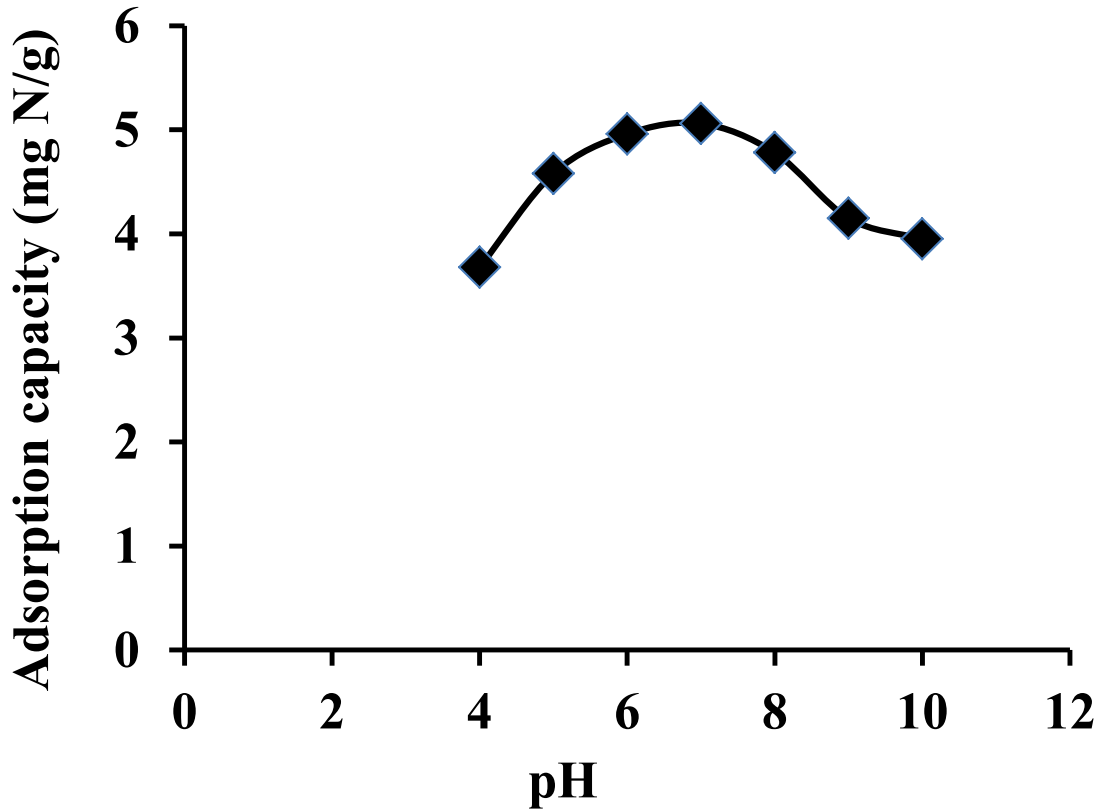

Figure 4.4. Influence of final pH of Purolite A520E suspension on nitrate adsorption (initial nitrate concentration 20 mg N/L and resin dose 1.0 g/L).

4.3.6. Effect of complementary ions

Effects of SO_4^{2-}, F^- , Cl^- and PO_4^{3-} on nitrate adsorption showed that the presence of these anions at concentrations ranging from 25 to 200 mg/L at pH 7.0 reduced the adsorption of nitrate from a solution containing 20 mg N/L appreciably with the increase in initial concentration of these anions (Figure 4.5). The order of nitrate adsorption capacity reduction by these anions was $Cl^- > SO_4^{2-} > PO_4^{3-} > F^-$ which was similar to previous studies' results for Purolite A520E (Samatya et al., 2006a). The main mechanism of adsorption of nitrate on Purolite A520E is electrostatic interaction or coulombic forces between the positively charged quaternary ammonium functional group in the resin and the negatively charged nitrate in solution (Helfferich, 1995; Gu et al., 2004). During adsorption, nitrate exchanged with Cl^-, which was already adsorbed onto the resin by an ion exchange process (Primo et al., 2009). The ethylamine-based quaternary ammonium functional group in Purolite A520E is more hydrophobic than the methylamine-based quaternary ammonium functional group in some of the other ion exchange resins, and therefore, it selectively adsorbs anions having less hydration energies (Gu et al., 2004). Because nitrate has lerss hydration energy than SO_4^{2-}, it is expected to be preferentially adsorbed in the presence of SO_4^{2-} on Purolite A520E, despite the latter anion having more charges (Kapoor and Viraraghavan, 1997; Gu et al., 2004; Samatya et al., 2006a).

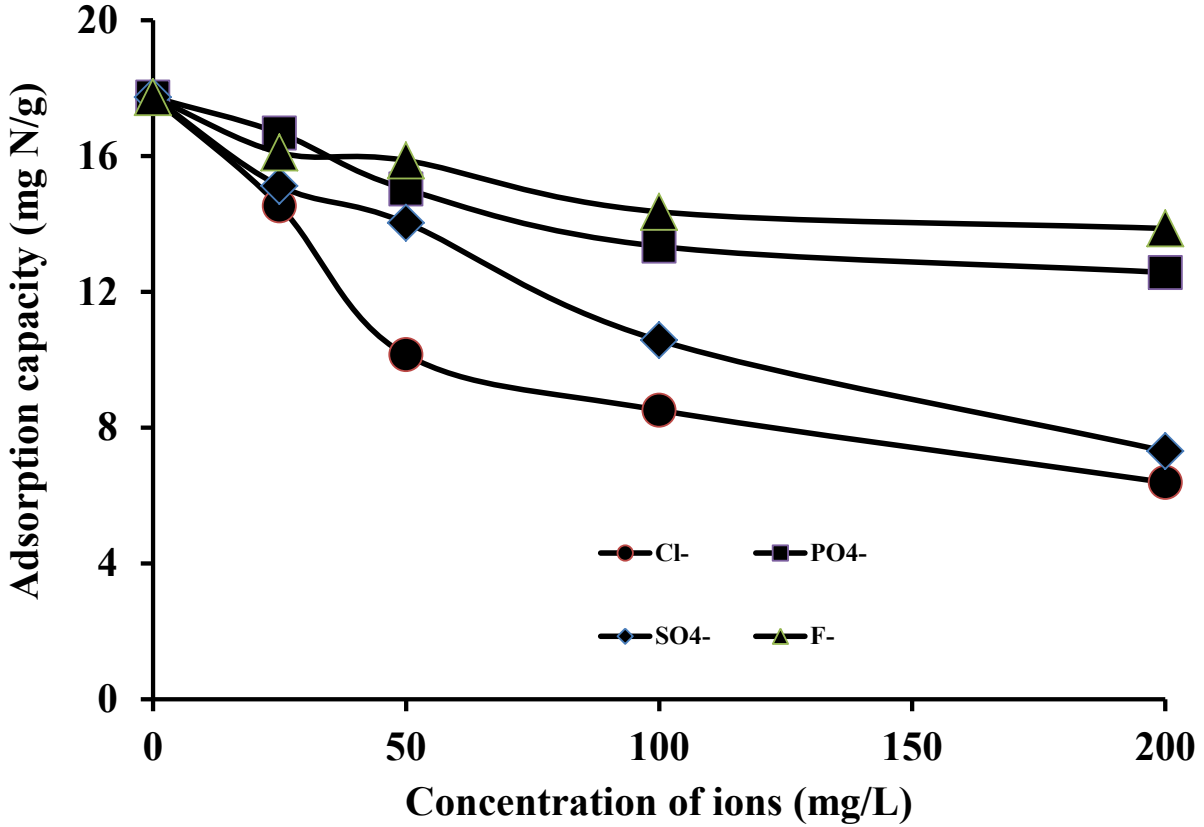

Figure 4.5. Influence of background ions on the adsorption of nitrate by Purolite A520E (initial nitrate concentration 20 mg N/L and adsorbent dose 1g/L).

4.3.7. Fixed-bed column studies

As expected, the breakthrough of nitrate in the column generally occurred faster with a higher filtration rate (Figure 4.7). When the inlet filtration rate was 5.0 m/h, the plateau of C_t/C_0 occurred within 23 h of operation (958 BV) and the value of C_t/C_0 was 0.92. The time to reach the plateau of C_t/C_0 increased significantly with a decrease in the filtration rate. The saturation time rose to 52 h (1083 BV) for the inlet flow rate of 2.5 m/h and the value of C_t/C_0 was 0.82. The faster breakthrough exhibited by the higher flow rate is due to the adsorption zone moving faster along the bed, reducing the contact time between nitrate and the ion exchange resin. The gradual breakthrough at the slower flow rate suggested longer residence time of nitrate in the column. Similar trends have been reported for nitrate removal by another ion exchange resin (Hekmatzadeh et al., 2012) and an amine-cross-linked wheat straw (Xu et al., 2010b) and Cr(VI) removal by a fungal biomass (Verma et al., 2014). However, Hekmatzadeh et al. (2012) reported that filtration velocity had no effect on the adsorption of nitrate on an ion exchange resin. The differences in the effects of filtration velocity may be due to the type of adsorbent and adsorbate, and experimental conditions such as filtration velocities, bed heights and influent concentrations used in the different studies.

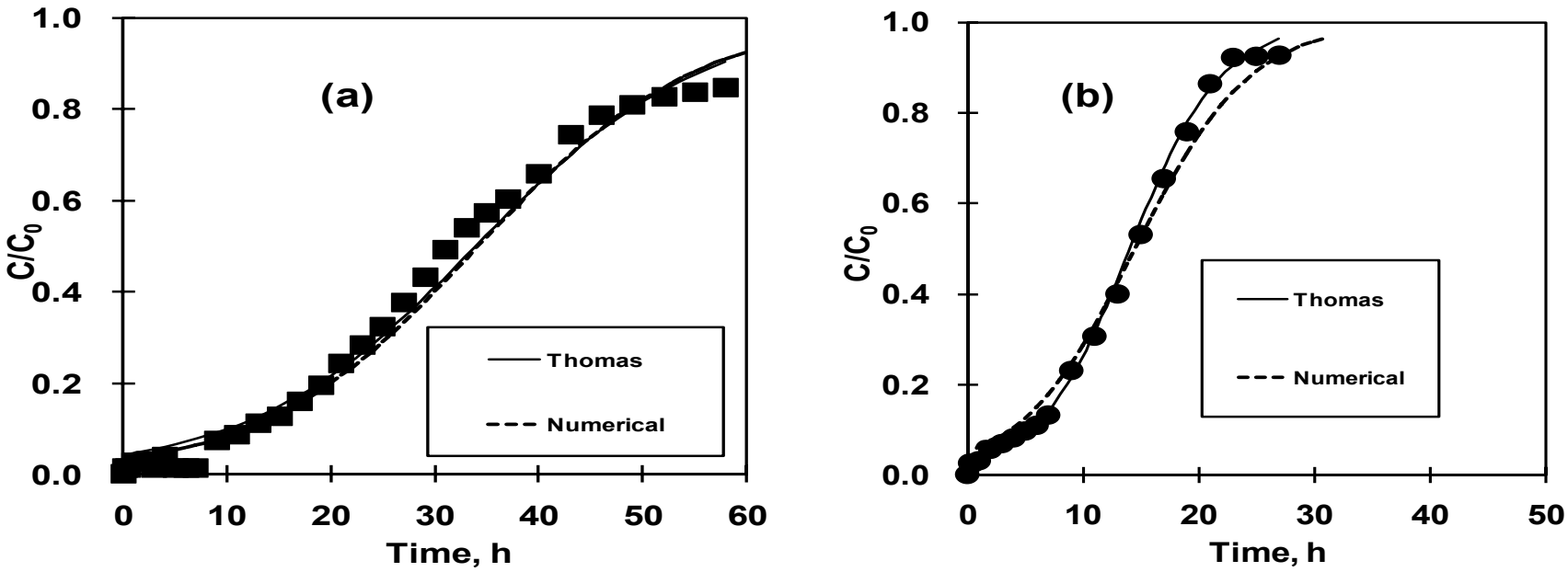

Figure 4.6. Experimental breakthrough curves for the filtration velocities (a) 2.5 m/h and (b) 5.0 m/h and model simulation curves for Purolite A520E (bed height = 12 cm and initial nitrate concentration = 20 mg N/L) (Experimental values are shown by data points, and model predictions are represented by lines).

4.3.8. Fixed-bed column modeling

Both the Thomas model's and numerical model's fits to the experimental data were very good as seen from the very high R^2 values ($R^2 \geq 0.96$) (Table 4.3, Figure 4.7).

4.3.8.1. Thomas model

The k_T and q_o values obtained from the Thomas model are presented in Table 4.3. Increase of flow rate decreased the adsorption capacity (q_o) which has also been reported elsewhere for other adsorbents (Ahmad and Hameed, 2010; Aksu and Gonen, 2004). The values obtained for nitrate adsorption capacity of 9.69 and 8.22 mg N/g for the lower and higher flow rates, respectively, are approximately the same as those determined by manual calculation (Equations 3.4 and 3.5) from the breakthrough curves (13.5 and 12.0 mg N/g for the lower and higher flow rates, respectively). However, these values are less than the Langmuir adsorption capacity of 32.2 mg N/g obtained in the batch study. The primary reason for less adsorption capacity values in the column experiment compared to the Langmuir adsorption value is that the flow through adsorption column is not in equilibrium unlike in the batch experiments. Another reason is that column adsorption was determined using a smaller solution nitrate concentration compared to the nitrate concentration at which Langmuir adsorption maximum was determined.

4.3.8.2. Numerical model

The effect of filtration velocity on the breakthrough curves for the adsorption of nitrate on PuroliteA520E is depicted in Figure 4.7 and the values of kinetic parameters

(D_L, k_f and D_S) for different conditions are presented in Table 4.3. The breakthrough time of nitrate was higher at slower filtration velocity. However, the faster the filtration velocity, the smaller is the external mass transfer resistance, which leads to narrower mass transfer zone and sharper breakthrough curves. The model predicts reasonably well the experimental results as shown in Figure 4.7 and by the very high R^2 values (R^2 = 0.98, 0.99; Table 4.3). Macroscopically, when the filtration velocity increases, the residence time in the bed decreases and this leads to less bed utilisation. Therefore, the breakthrough time and the bed capacity will decrease with increasing filtration velocity.

Microscopically, it is expected that the change of filtration velocity will affect the film diffusion, but not the intraparticle diffusion. The higher the filtration velocity, the smaller the film resistance and a larger k_f results (Danny et al., 2001). The intraparticle diffusion coefficient (D_s) values for the two filtration velocities were approximately the same (Table 4.3), showing that the change in filtration velocity does not affect the rate of intraparticle diffusion (D_s) which is similar to the results reported by Danny et al. (2001) for copper and cadmium adsorption on bone char. In contrast to the intraparticle diffusion coefficient (D_s), the axial dispersion coefficient, D_L increased with filtration velocity which was also noted by Hekmatzadeh et al. (2012) for nitrate adsorption on an ion exchange resin. Hekmatzadeh et al. (2012) explained the increase in D_L with filtration velocity as being caused by the increase in interstitial flow velocity.

Table 4.3.

Column study model parameters and statistical estimations for two filtration rates (bed height = 12 cm and initial concentration = 20 mg N/L).

Model	Parameter	V = 2.5 m/h	V = 5.0 m/h
Thomas	k_T (L/mg . min)	0.098	0.193
	q_0 (mg/g)	9.69	8.22
	R^2	0.96	0.99
Numerical modeling	D_s (m^2/sec)	6.50×10^{-8}	6.60×10^{-8}
	k_f (m/s)	9.25×10^{-7}	1.85×10^{-6}
	D_L (m^2/sec)	1.00×10^{-6}	5.50×10^{-6}
	R^2	0.98	0.99

4.3.9. Conclusions

Of the four anion exchange resins tested in the batch study, Purolite A520E had the capacity to remove the largest amount of nitrate. The kinetics of nitrate adsorption by Purolite A520E in the batch study was satisfactorily described by pseudo-first-order, pseudo-second-order and HSDM models. The empirical Thomas model and a numerical model based on advection-dispersion equation adequately described nitrate adsorption behaviour in a fixed-bed column containing Purolite A520E at two filtration velocities. The breakthrough curve was steeper and breakthrough occurred more rapidly for the higher filtration rate. The experimental and Thomas model predicted breakthrough adsorption capacities (12.0-13.5 mg N/g and 8.2-9.7 mg N/g, respectively) and agreed fairly well. However, the Langmuir adsorption maximum calculated from the batch study (32.2 mg N/g) was much higher than the column values. In Chapter 3, it was shown that Purolite A520E can be regenerated and used at least three times without significantly reducing adsorption capacity. It can therefore be concluded that Purolite A520E is a potential nitrate adsorbent with high adsorption capacity which can be used in a cost-effective manner to remove nitrate from water. However, the presence of co-ions such as Cl^- and SO_4^{2-} at high concentrations may reduce the effectiveness of this resin's ability to adsorb nitrate. Finally, solution pH had little effect on nitrate adsorption in the pH range 5-8.

CHAPTER 5

BATCH STUDIES ON PHOSPHATE ADSORPTION BY AN IRON OXIDE-IMPREGNATED STRONG BASE ANION EXCHANGE

Chapter 5

Batch studies on phosphate adsorption by an iron oxide-impregnated strong base anion exchange resin*

5.1. Introduction

In Chapter 3 two ion exchange resins were used to remove nitrate and phosphate. The results showed that the two resins were more selective in the adsorption of nitrate than phosphate. This is not very surprising because the ion exchange resin adsorb anions through non-specific adsorption; although depending on the length of organic carbon chain the resin becomes more selective in adsorbing certain anions. On the other hand, phosphate has been shown to adsorb specifically on many metal oxides which have high phosphate adsorption capacity (Loganathan et al., 2014). This aspect has been considered when designing adsorbents for removing phosphate from water. For example, Gupta et al. (2012) reported that Purolite 500A anion exchange resin had a Langmuir adsorption capacity of 64 mg N/g for nitrate adsorption whereas it had only 7 mg P/g for phosphate adsorption. Therefore, they used two columns in series, one with Purolite for removing nitrate followed by the other with hydrous ferric oxide for the removal of phosphate from water containing both these anions. Others have used polymeric anion exchanger bound with ferric oxide nanoparticles to successfully remove phosphate (Blaney et al., 2007; Martin et al., 2009). These studies noted that adsorbents containing ferric oxide are required for effectively remove phosphate.

Purolite FerrIX A33E media is a nanoparticle derived resin designed to selectively remove arsenic (arsenate and arsenite) from water supply (www.purolite.com). This resin

***A small part of this chapter was published in T. Nur, M.A.H. Johir, P. Loganathan, T. Nguyen, S. Vigneswaran, and J. Kandasamy, "Phosphate removal from water using an iron oxide impregnated strong base anion exchange resin", Journal of Industrial and Engineering Chemistry (2014): 1301–1307.**

unites a unique blend of hydrous iron oxide nanoparticles that have a very high attraction for arsenic with a durable, non-friable, spherical polymer substrate. As this resin was found to be effective in removing arsenic anions, it is expected to have a strong affinity for phosphate anions as well, because phosphate-like arsenic is specifically adsorbed onto iron oxides (Loganathan et al., 2014). However, no detailed study has been conducted on phosphate adsorption using this ion exchange resin.

The aim of the present research is to study and model the removal of phosphate from synthetic wastewater employing six adsorbents in a batch experiment. The objectives of this study were to: (i) compare the phosphate removal efficiencies of six adsorbents expected to have high adsorption capacities and justify the selection of Purolite FerrIX A33E for a detailed study; (ii) model equilibrium batch isotherm data of phosphate adsorption; (iii) model batch kinetic data of phosphate adsorption; (iv) determine the effect of pH and complementary anions on phosphate adsorption; and (v) develop a suitable method to regenerate the adsorbent for reuse.

5.2. Material and methods

5.2.1. Adsorbents

Four ion exchange resins, Purolite A520E, Purolite A500PS, Purolite FerrIX A33E and Dowex 21k XLT and two multivalent metal oxide adsorbents, HFO (iron (iii) oxide $HFeO_2$) and Zirconium (IV) hydroxide (H_4O_4Zr) were used to compare their removal efficiencies of phosphate from water. The basis for selecting these adsorbents is that a recent review on phosphate adsorption reported that multivalent metal oxides and some ion exchange resins have high phosphate adsorption capacities (Loganathan et al.,

2014). The characteristics of Purolite A520E, Purolite A500PS and Dowex 21k XLT were described in Chapters 3 and 4.

Purolite FerrIX A33E is a blend of hydrous iron oxide nanoparticles and highly porous polystyrene cross-linked with divinylbenzene polymer, which has an arsenic operating capacity of 0.5-4 g As/L and available in the form of spherical beads (0.3-1.2 mm diameter). The physical and chemical properties of Purolite FerrIX A33E are discussed in Table 5.1**.** The highly porous nature of the resin bead allows for maximum utilisation of the impregnated iron oxide. The polymer component of the adsorbent had positively charged quaternary ammonium functional groups with chloride as counter ion (www.aquascotland.com).

Table 5.1.

Typical chemical and physical characteristics of the Purolite FerrIX A33E (www.purolite.com-FerrIX A33E)

Parameters	Purolite FerrIX A33E
Polymer Matrix Structure	Polystyrene cross-linked with divinylbenzene
Physical Form and Appearance	Brown spherical beads
Moisture Retention, Cl^- form	35-65%
Operating Temperature,(Cl^- form)	40^oC
Fe content	13%

5.2.2. Feed solutions

The feed solutions were prepared using KH_2PO_4 with distilled water spiked with different concentrations of phosphate (5-30 mg P/L). The pH of the solutions ranged from 7.2 to 7.6. The methods used in the chemical analysis are the same as those described in Chapter 3.

5.2.3. Batch adsorption studies

Equilibrium adsorption isotherm and adsorption kinetics experimental methods were also the same as those described in Chapter 3.

5.2.3.1. Effect of pH

Of the six adsorbent (Purolite A520E, Purolite A500PS, Purolite FerrIX A33E and Dowex 21k XLT, HFO (iron (iii) oxide $HFeO_2$) and Zirconium (IV) hydroxide (H_4O_4Zr)), Purolite FerrIX A33E had the highest phosphate adsorption capacity (see later section). Therefore, the effect of pH of the medium and the influence of initial phosphate concentration were investigated with reference to Purolite FerrIX A33E only. The effect of pH was studied using 1g of Purolite FerrIX A33E at the pH ranges from 4 to 10 at a phosphate concentration of 10 mg P/L in a set of glass flasks containing 100 mL of phosphate solution. The suspensions were agitated in a flat shaker at a shaking speed of 120 rpm for 6h at room temperature (24 ± 1^{o}C). Aqueous samples were taken at different time intervals and the concentrations of nitrate were measured**.**

5.2.3.2. Effect of co-ions

Natural water and wastewater may contain many anions at different concentrations which can compete with phosphate for adsorption. The extent of the competition depends on the relative concentrations of the ions and their affinity for the adsorbent. Therefore, the effect of complementary anions (Cl^-, SO_4^{2-}, F and NO_3^-) on phosphate adsorption by Purolite FerrIX A33E was studied at a constant initial phosphate concentration of 10 mg P/L, adsorbent dose of 1 g/L, and pH 7 by varying anion concentrations from 25 to 200 mg/L using NaCl, Na_2SO_4, NaF and KNO_3. The suspensions were agitated in a flat shaker at a shaking speed of 120 rpm for 72 h at room temperature (24 ± 1°C). The aqueous samples were taken at different time intervals and the concentrations of phosphate were measured.

5.2.4. Adsorption Modelling

5.2.4.1. Batch Adsorption Equilibrium Modelling

The data for batch adsorption at different adsorbent doses were treated with the Langmuir, Freundlich and Tempkin isotherm models, the details of which were discussed in Chapter 2. Equations and graphical methods of the Langmuir and Freundlich models used to calculate the model parameters were explained in Chapter 3. The Tempkin model is used for the first time in this chapter, so the equations and the graphical methods used to calculate this particular model's parameters are explained in Table 5.2.

5.2.4.2. Batch adsorption kinetic modelling

The batch adsorption kinetic data are analysed by pseudo-first-order, pseudo-second-order, Elovich and intraparticle diffusion kinetic models. Pseudo-first-order and pseudo-second-order kinetics models were discussed earlier in Chapter 2. The equations for the pseudo-first-order and pseudo-second-order kinetic models and the methods of calculating the model parameters were presented in Chapter 3. Elovich and intraparticle diffusion kinetic models are used for the first time in this chapter, so the equations for these kinetic models and the methods of calculating the model parameters are presented in Table 5.3.

Table 5.2.

Tempkin model and equations used for tdescribing batch equilibrium adsorption

Model	Equation	Graphical method used to calculate model constants
Tempkin Isotherm	$q_e = \frac{RT}{b} \ln (A_T C_e)$	$q_e = B \ln (A_T) + B \ln (C_e)$
	C_e = equilibrium concentration of adsorbate (mg/L); A_T =Temkin isotherm equilibrium binding constant (L/g); b = Temkin isotherm constant; R= universal gas constant (8.314J/mol/K); T= Temperature at 298K; B = Constant related to heat of adsorption (J/mol).	

Table 5.3.

Elovich and an intraparticle diffusion models and equations used for describing batch kinetic adsorption.

Model	Equation	Graphical method used to calculate model constants
Elovich	$\frac{dqt}{dt} = \alpha \exp(-\beta qt)$	$q_t = (1/\beta) \ln(\alpha\beta) + =(1/\beta) \ln(t)$
	q_t = amount of adsorbent adsorbed at time, t (min) (mg/g), α = the initial adsorption rate (mg/g min) and β = desorption constant (g/mg).	
Intraparticle diffusion	$q_t = k_i (t^{1/2})$	$\ln q_t = \ln k_i + ½ \ln t$
	q_t = amount of adsorbent a adsorbed at time, t (min) (mg/g); k_i is intraparticle diffusion rate constant (mg/g $min^{1/2}$).	

5.2.5. Regeneration of adsorbent

The regeneration of the phosphate saturated Purolite FerrIX A33E adsorbed with phosphate was conducted in a batch experiment. The saturated resin was washed with 0.1-1.0 M NaCl, Na_2SO_4, NaOH and MQ solutions in batch method. In this method the phosphate saturated resin was collected and placed in a small container containing the regenerating solution of 20 ml and was shaken in a flat shaker at a shaking speed of 150 rpm. The desorbed solutions were collected at different time intervals from 30 min and analysed for phosphate concentrations.

5.3. Results and discussion

5.3.1. Batch equilibrium adsorption

Initially, batch equilibrium experiments were conducted with six adsorbents, consisting of four ion exchange resins, namely Purolite A500PS, Purolite A520E, Purolite FerrIX A33E and Dowex 21K and two multivalent metal oxides, these being HFO and Zirconium (IV) hydroxide. The batch adsorption experiments showed that the removal efficiency of phosphate improved as expected with increased adsorbent dosage due to the availability of more adsorption sites which was similar to phosphate absorption on other adsorbents. Of the six adsorbents tested (Figure 5.1a), Purolite FerrIX A33E produced the highest removal efficiency at all dosages of adsorbents for an initial phosphate concentration 10 mg/L from a solution volume of 100 mL. The removal efficiency was 96-99% for Purolite FerrIX A33E dosages of 3-10 g/L. Next to Purolite FerrIX A33E, the highest removal efficiency of phosphate was shown by HFO (95%) and Zirconium (IV) hydroxide (94%) at an adsorbent dose of 10 g/L. Purolite A500PS and Dowex 21K showed the same removal efficiency (93%).

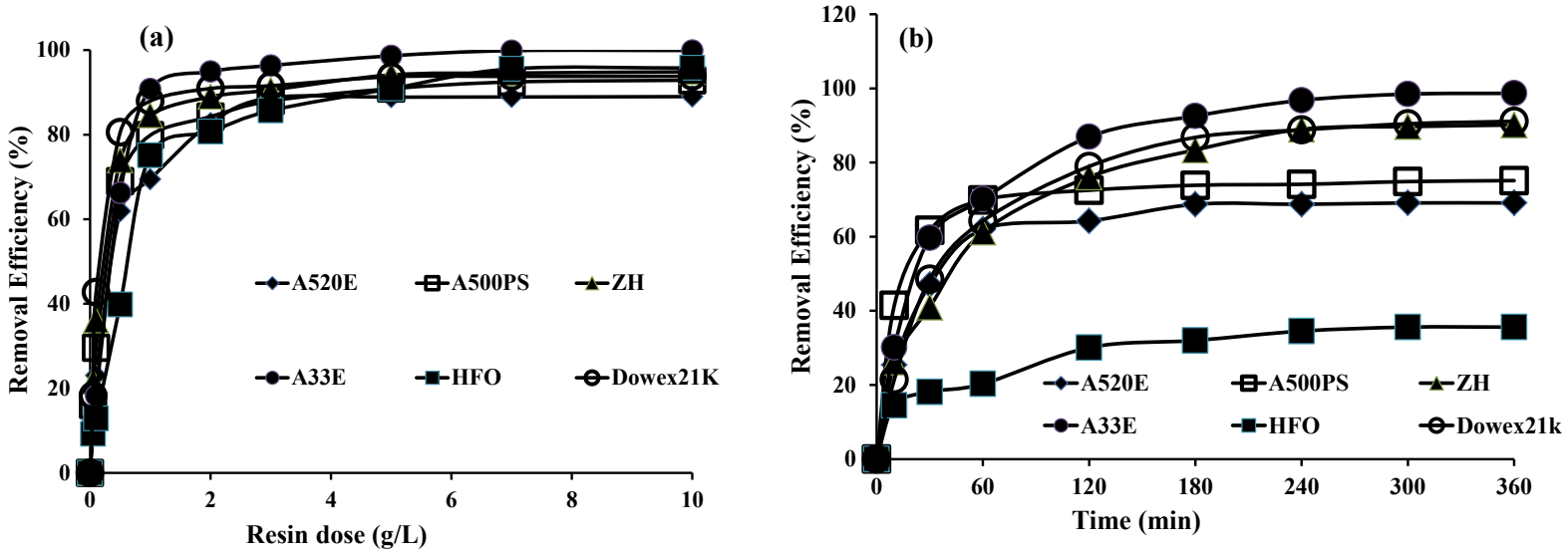

Figure 5.1. Effect of (a) resin dose and (b) contact time on the removal of phosphate by six adsorbents (initial phosphate concentration 10 mg P/L and adsorbent dose 1g/L).

5.3.2. Batch kinetic adsorption

The kinetics of phosphate adsorption at an initial phosphate concentration of 10 mg/L and adsorbent dosage dosage of 1 g/L showed that adsorption capacity increased with contact time up to approximately 2h and became steady afterwards (Figure 5.1b). Of the six adsorbents, Purolite FerrIX A33E had the highest phosphate removal efficiency (98%) followed by Dowex 21k (91%), Zirconium (IV) hydroxide (89%), Purolite A500PS (75%) and Purolite A520E (69%) within 240 min. HFO was found to have the least removal efficiency (36%).

5.3.3. Batch adsorption equilibrium modelling

The adsorption data of all six adsorbents was fitted to three mostly used equilibrium models such as the Langmuir, Freundlich and Tempkin models. The estimated adsorption parameters are summarised in Table 5.4.

5.3.3.1. Langmuir Model

The Langmuir isotherm model is a well-known and widely used model which assumes monolayer adsorption onto surfaces that takes place at a finite number of identical sites. The Langmuir adsorption isotherm plot (Q_e vs. C_e) indicates the applicability of this particular isotherm. The adsorption equilibrium data of six adsorbents satisfactorily fitted to the Langmuir adsorption model (R^2 = 0.83-0.95) (Figures 5.2 - 5.4) and the maximum adsorption capacity for the six adsorbents varied from 1.58 to 48 mg P/g (Table 5.4). These results are similar to previous studies on phosphate adsorption on other adsorbents where the Langmuir model proved to adequately describe the adsorption

process in most studies (Loganathan et al., 2014; Table 5.5). The Langmuir adsorption capacity obtained for Purolite Ferrix A33E was the highest of the six adsorbents which was 48 mg P/g. This adsorption capacity is among the highest values reported for most adsorbents in the literature (Loganathan et al., 2014; Table 5.5). The high adsorption capacity for this adsorbent is probably due to the presence of nano-sized iron oxide particles in the adsorbent which can have an adsorption capacity in the order of 145 mg P/g Fe (1.1 mole P/mole Fe_3O_4) (Cloutier et al., 1985). Based on this adsorption capacity the contribution of the iron oxide to the total adsorption capacity of the Purolite resin is estimated to be 19 mg P/g resin (13% Fe in resin x 145 mg P/g).

5.3.3.2. Freundlich Model

The Freundlich model is another widely used isotherm model applicable to adsorbents with surface heterogeneity. All equilibrium adsorption data of the six adsorbents fitted satisfactorily well to this model with very good R^2 values (0.93-0.99) (Figures 5.2 - 5.4) similar to previous studies on phosphate adsorption (Loganathan et al., 2014). Purolite Ferrix A33E had the highest value for the Freundlich parameter K_f which is related to the adsorption capacity. The values of K_f ranged from 7.47 to 15.5 (mg P/g) $(L/mg)^{1/n}$ and n values varied from 1.00 to 1.53 (Table 5.4). Because the value of n lies between one and ten, the adsorption process is considered to be a favourable one.

5.3.3.3. Tempkin Model

This isotherm model contains a factor that explicitly takes into account adsorbent–adsorbate interactions. By ignoring the extremely low and high values of adsorbate concentrations, the model assumes that heat from the adsorption (function of temperature) of all adsorbate molecules would decrease linearly rather than logarithmically with increased coverage. Of the six adsorbents, only Purolite Ferrix A33E and Purolite A520E fitted well to the Tempkin model with good R^2 values (0.89 and 0.90) (Table 5.4) (Figures 5.2 – 5.4). For all adsorbents, phosphate adsorption was better described by the Langmuir and Freundlich models than the Tempkin version. Similar results have been reported for the adsorption of phosphate by low cost Aleppo pine adsorbent (Benyoucef and Amrani, 2011) and oven-dried sludge and cement kiln dust (Mortul et al., 2007).

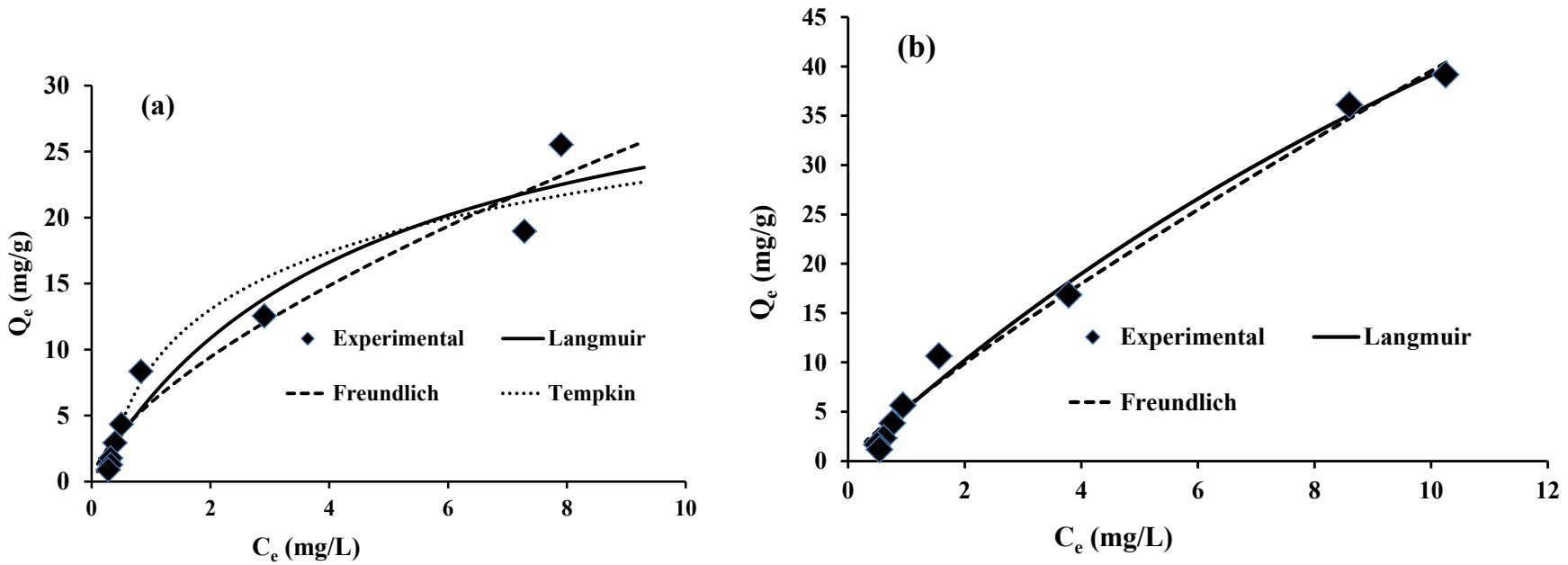

Figure 5.2. Langmuir, Freundlich and Tempkin isotherm models' fit for phosphate removal by (a) Purolite FerrIX A33E and (b) Purolite A500PS.

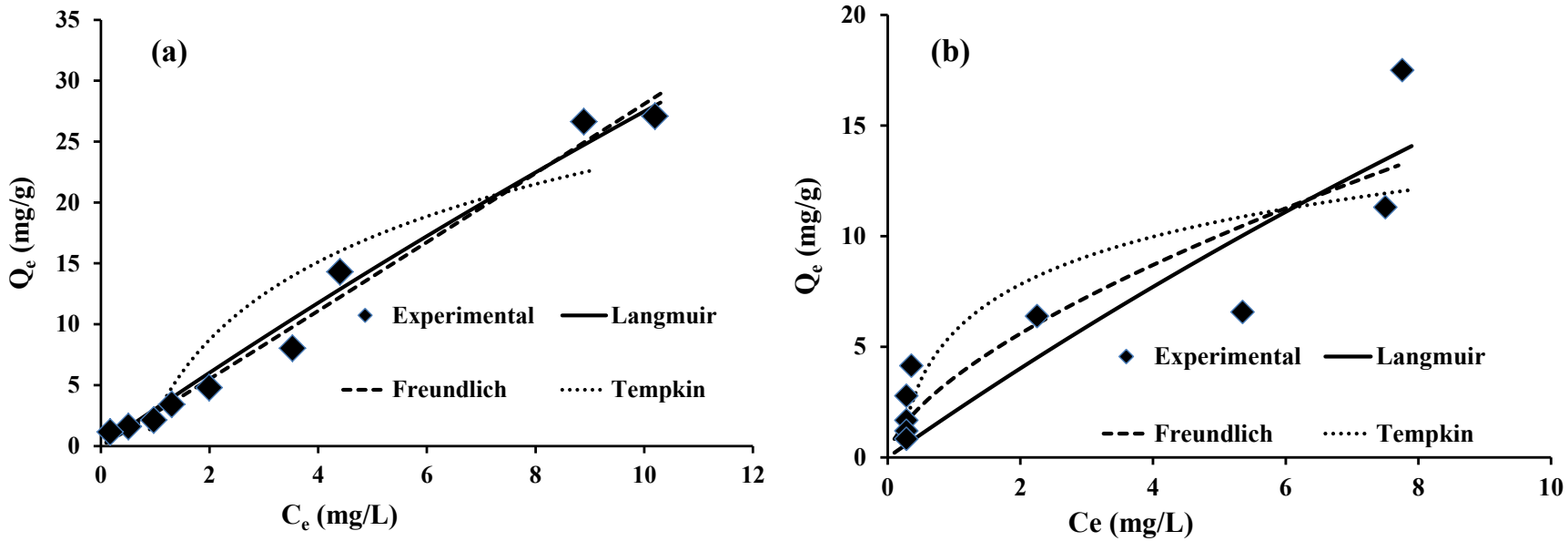

Figure 5.3. Langmuir, Freundlich and Tempkin Isotherm model fit for phosphate removal by (a) Purolite A520E and (b) HFO.

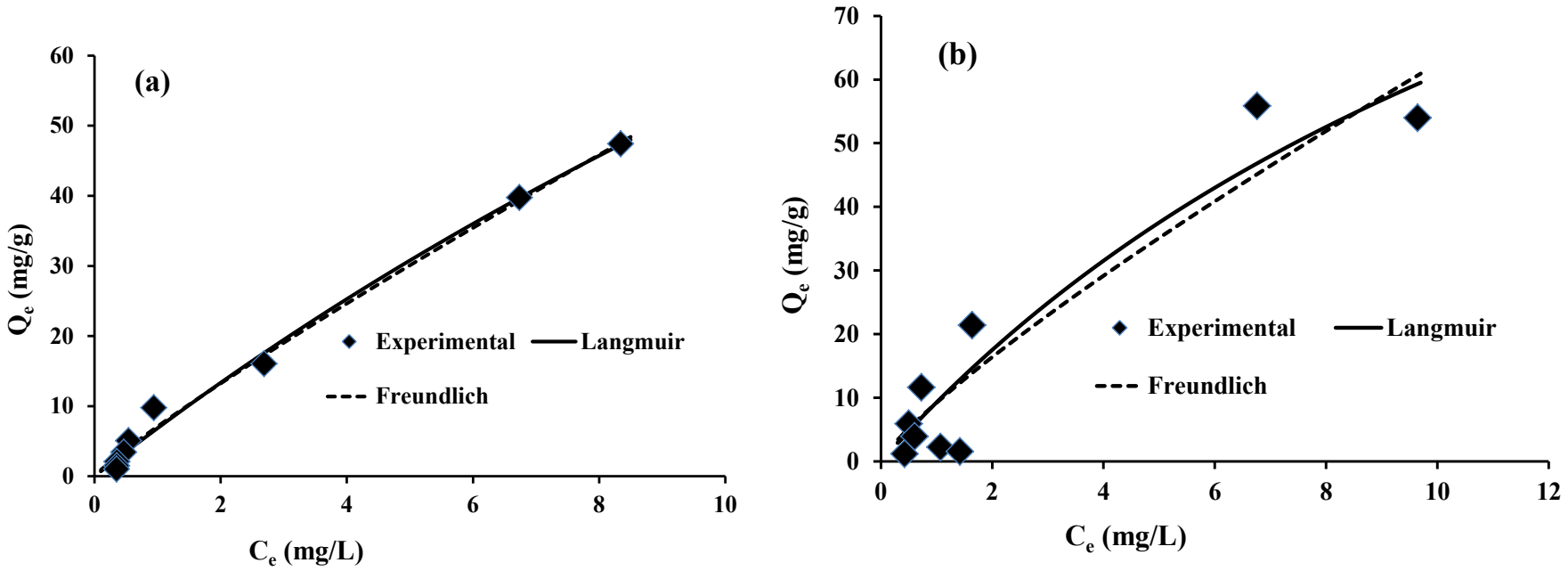

Figure 5.4. Langmuir, Freundlich and Tempkin isotherm models' fit for phosphate removal by (a) Zirconium Hydroxide (ZH) and (b) Dowex 21K XLT.

Table 5.4.

Adsorption isotherm parameters of Langmuir, Freundlich and Tempkin models for phosphate adsorption on all adsorbents.

Model parameters	Adsorbents					
	Purolite FerrIX A33E	Purolite A500PS	Purolite A520E	HFO	ZH	Dowex21K
Langmuir Isotherm Model						
$q_{max\ (mg\ P/g)}$	48	25.2	13.3	9.2	2.39	1.58
$K_{L\ (L/mg)}$	0.22	0.012	0.042	0.023	0.030	0.062
R^2	0.95	0.92	0.90	0.89	0.87	0.83
Freundlich Isotherm Model						
K_F (mg P/g)$(L/mg)^{1/n}$	15.5	14.4	9.89	8.93	8.22	7.47
n	1.53	1.16	1.00	1.47	1.12	1.20
R^2	0.99	0.94	0.95	0.95	0.93	0.95
Tempkin Isotherm Model						
A_T (L/mg)	9.22		6.29			
b_T	1920	N/A	622	N/A		
B(J/mol)	6.16		1.29			
R^2	0.90		0.89			

Table 5.5.

Comparison of Langmuir adsorption capacity for phosphate on Purolite FerrIX A33E with that of various other adsorbents in synthetic solutions as reported in the literature

Adsorbent	Experimental conditions (Equilibrium concentration (mg P/L); I, initial concentration (mg P/L))	Adsorption capacity (mg P/g)	Reference
Akagenite	25°C, pH 7, E 1-250	60	Deliyanni et al. (2007)
Akagenite granulated	20°C, pH 5.5, E 0-4	17-23	Genz et al. (2004)
Activated alumina	20°C, pH 5.5, E 0-4	12-14	Genz et al. (2004)
Activated alumina	E 0-2	3.3	Wang et al. (2004)
Iron/zirconium binary oxide	25°C, pH 4, E 0-80	13.7	Long et al. (2011)
MgAlLDH (granular)	25°C, pH 6.9, E 0-150	47.3	Kuzawa et al. (2006)
Zeolite	20°C, E 0-40	0.13	Ma et al. (2011)
Activated carbon	E 0-28	3.2	Mahmudov and Huang (2011)
Activated carbon (granular)	20°C, E 0-25	1.2	Ma et al. (2011)

Table 5.5 (continued)

Adsorbent	Experimental conditions (Equilibrium concentration (mg P/L); I, initial concentration (mg P/L))	Adsorption capacity (mg P/g)	Reference
Anion exchange resin from soybean hulls	25°C, pH 7, 10 g resin, I 0-620	20	Marshall and Wartelle (2004)
Bauxsol	pH 5.2-6.2, E 0-43	14-15	Akhurst et al. (2006)
Blast furnace slag	25°C, E 0-600	44.2	Sakadevan and Bavor (1998)
Activated red mud	30°C, pH 5.2, E 0-62	22.5	Pradhan et al. (1998)
Activated red mud	25°C, E 0-800	54, 113	Li et al. (2006)
Raw red mud	25°C, E 0-800	38	Li et al. (2006)
Blast furnace slag	30°C, E 0-11	29	Gong et al. (2009)
Basic oxygen furnace slag	20°C, E 0-120	11-20	Xue et al. (2009)
Fly ash	E 0-900	20-26	Li et al. (2006)
Iron oxide tailings	20-21°C, pH 6.6-6.8, E 0-130	5-8	Zeng et al. (2004)
Purolite A500P anion exchange resin	Resin dose 0.5-10 g/L, I 15	7	Martin et al. (2009)

Of the six adsorbents, Purolite Ferrix A33E fitted very well to all three isotherm models with the highest R^2 values (0.90 - 0.99). It had the maximum Langmuir adsorption capacity of 48 mg P/g and this also applied to all model parameters related to adsorption capacity.

5.3.4. Batch adsorption kinetic modelling

In adsorption kinetics, mass transfer and diffusion of adsorbate particles from bulk liquid phase to adsorbent surface determine the rate of adsorption. The adsorption kinetic data for all six adsorbents was fitted to four mostly used kinetic models such as pseudo-first and second-order, Elovich and intraparticle diffusion models (Figure 5.3). The estimated kinetic parameters values are summarised in Table 5.4.

5.3.4.1. Pseudo-first-order kinetic model

The adsorption data of all adsorbents showed that generally pseudo-first-order kinetic model had very poor fit (R^2 = 0.38-0.91) (Table 5.6; Figures 5.5 -5.7). Only the data for Purolite FerrIX A33E fitted satisfactorily to the pseudo-first-order kinetic model with good R^2 value (0.91). Again the experimental value of qe differed greatly from the q_e values calculated from the pseudo-first-order kinetic model (Table 5.6).

5.3.4.2. Pseudo-second-order kinetic model

Of all the available kinetic models, the pseudo-second-order model described best the experimental kinetic data for the entire adsorption period for most of the systems. In

contrast to the pseudo-first-order kinetic model, the adsorption of phosphate onto all adsorbents except zirconium hydroxides was much better evaluated by the pseudo-second-order kinetic model with R^2 of 0.88-0.99 (Table 5.4; Figure 5.3). The better fit of data to the pseudo-second-order model suggests that the chemisorption process could be the rate-limiting step in the adsorption (Tovar-Gómez et al., 2013). Previous studies of phosphate adsorption on Purolite also demonstrated that the kinetics adsorption data were better described by the pseudo-second-order kinetic model (Loganathan et al., 2014).

Furthermore, the experimental value of qe was almost similar to the q_e values calculated from the pseudo-second-order kinetic model (Table 5.4). These findings also demonstrated that the adsorption reaction can be satisfactorily described by the pseudo-second-order kinetic model. The satisfactory fits of the data to the pseudo-second-order-kinetic model imply that the iron exchange process rates are limited only by the phosphate ions and functional groups from the resin surface that are available to interact (Yan et al., 2010).

5.3.4.3. Elovich kinetic model

Although the Elovich equation is also used successfully to describe second-order kinetics assuming that the actual solid surfaces are energetically heterogeneous, the equation does not propose any definite mechanism for adsorbate–adsorbent (Sparks, 1989). It has been widely accepted that the chemisorption process can be described using this semi-empirical equation (Zhang and Stanforth, 2005). The applicability of the simple Elovich equation for the present kinetic data generally agrees with the results of other researchers, enabling the Elovich equation to describe properly the kinetics of phosphate adsorption on soil and soil minerals (Chien and Clayton, 1980). Table 5.4 lists the kinetic

constants obtained from the Elovich equation. Of the six adsorbents, except zirconium hydroxide and Dowex 21K, all fitted well with the Elovich model (0.92-0.97) (Table 5.6; Figures 5.5 – 5.7). The value of initial adsorption rate (α) varies from 0.76 to 6.81 (mg P/g min) and the highest values is for Purolite A520E. The desorption constant (β) varies from 0.61 to 1.85 (g/mg P). The lowest value of desorption constant (β) is for Purolite FerrIX A33E which means that it has the highest adsorption capacity because it is the inverse of adsorption capacity.

5.3.4.4. Intraparticle diffusion model

Adsorption is a multi-step process involving transport of the solute ions from the aqueous phase to the surface of the solid particulates and then, diffusion of the solute ions into the interior of the pores which is likely to be a slow process and is therefore rate determining. The pseudo-second-order and Elovich kinetic models cannot identify the diffusion mechanism and therefore kinetic results were then analysed employing an intra-particle diffusion model. All adsorption kinetic data except zirconium hydroxide fitted well to the intra particle diffusion model (Weber and Morris, 1963) with good R^2 values (0.90-0.93) (Table 5.4; Figure 5.3). The values of the intra particle diffusion constant (K_i) varied from 0.037 to 0.57 (mg P/g $min^{1/2}$) and the highest value is for Purolite FerrIX A33E. According to this model, if these lines pass through the origin then intra-particle diffusion is the rate-controlling step (Weber and Morris, 1963; Arami et al., 2008).

If the plots do not pass through the origin this indicates some degree of boundary layer control and furthermore shows that the intra-particle diffusion is not the only rate-limiting step. It is possible that other kinetic models may control the rate of adsorption,

all of which may be operating simultaneously. From Figure 5.3, it can be seen that only the data for Purolite FerrIX A33E passed through the origin.

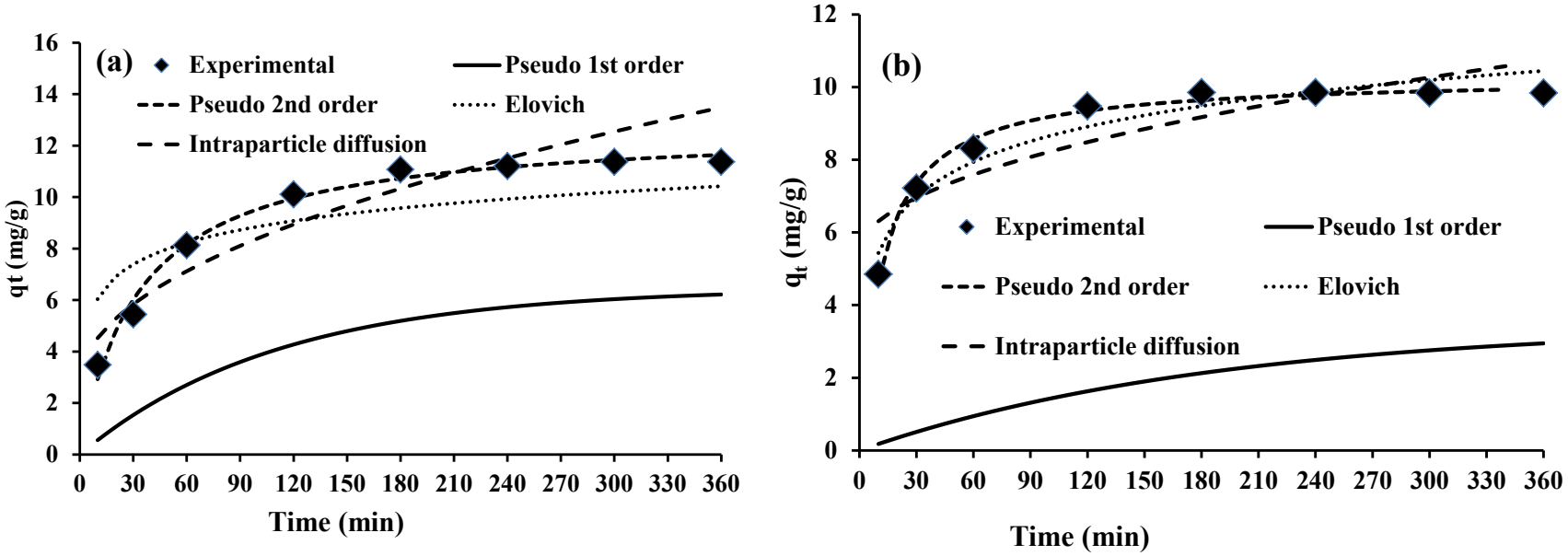

Figure 5.5. Pseudo- first- and second-order, Elovich and intraparticle diffusion kinetic models fit for phosphate removal by by (a) Purolite FerrIX A33E and (b) Purolite A500PS.

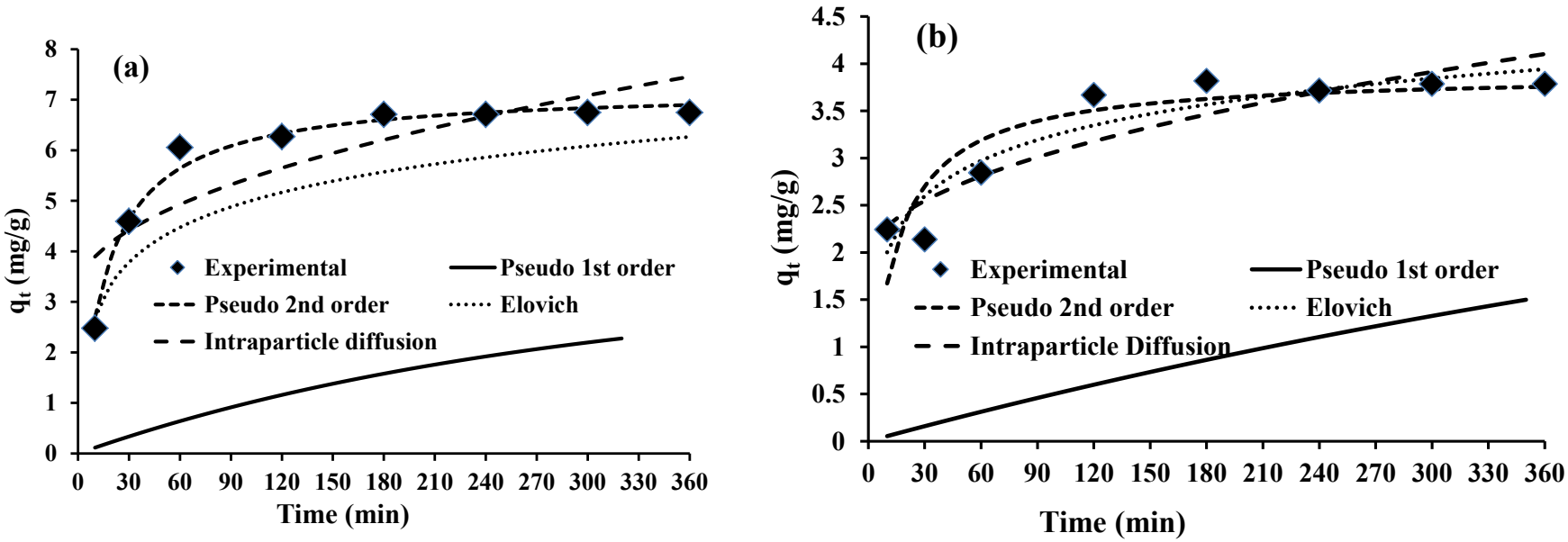

Figure 5.6. Pseudo first- and second-order, Elovich and intraparticle diffusion kinetic models fit for phosphate removal by (a) Purolite A520E and (b) HFO..

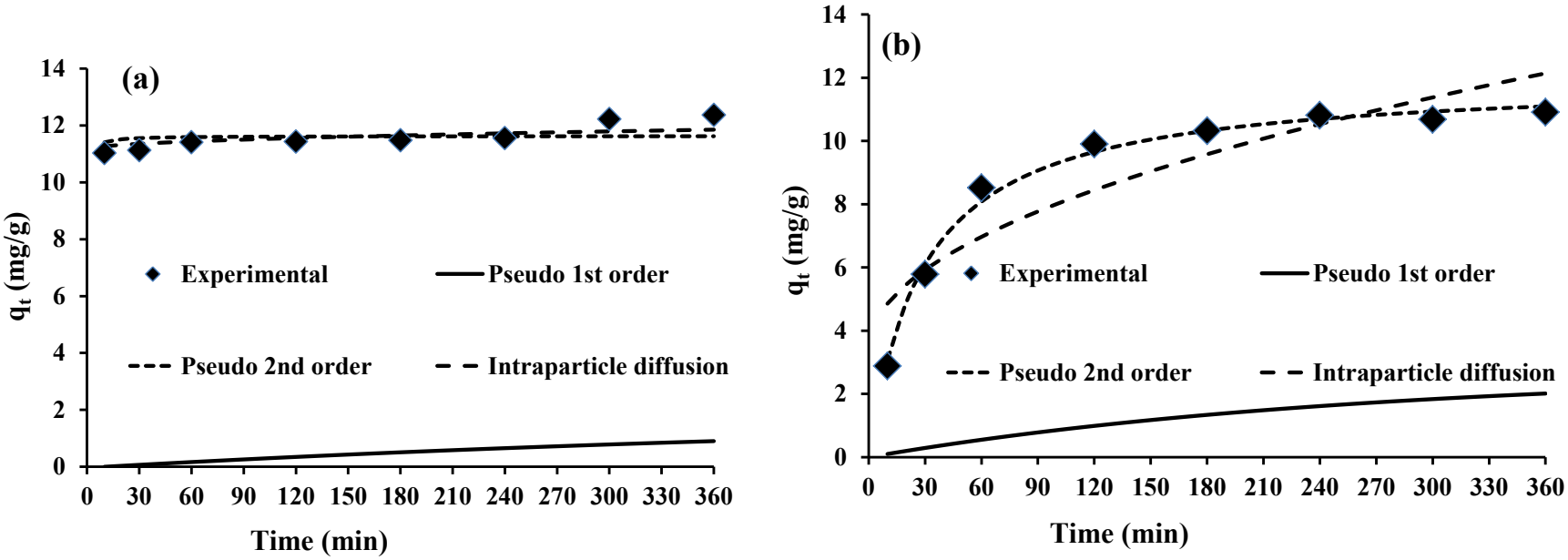

Figure 5.7. Pseudo-first- and second-order, Elovich and intraparticle diffusion kinetic models fit for phosphate removal by (a) Zirconium Hydroxide (ZH) and (b) Dowex 21K XLT.

Table 5.6.

Batch adsorption kinetic parameters for the adsorption of phosphate on six adsorbents.

Model Parameter	Purolite FerrIX A33E	Purolite A500PS	Purolite A520E	HFO	ZH	Dowex21K
q_e experimental (mg P/g)	11.37	9.86	6.75	3.78	12.21	10.91
Pseudo-first-order kinetic model						
q_e (mg P/g)	6.47	3.46	3.38	3.87	1.93	2.7
K_1 (1/min)* 10^{-3}	9.11	5.31	3.54	1.41	1.83	3.84
R^2	0.91	0.75	0.69	0.71	0.38	0.42
Pseudo–second-order kinetic model						
q_e (mg P/g)	12.72	10.3	7.22	3.89	11.6	12.0
K_2 (g/mg P. min)	61.5	90.9	22.4	4.44	8110	59.4
R^2	0.99	0.99	0.99	0.88	0.15	0.99

Table 5.6 (continued)

Model Parameter	Purolite FerrIX A33E	Purolite A500PS	Purolite A520E	HFO	ZH	Dowex21K
Elovich model						
α (mg/g P min)	0.76	6.81	1.78	2.18	N/A	
β (g/mg P)	0.61	0.72	0.87	1.85		
R^2	0.98	0.97	0.95	0.93		
Intraparticle diffusion model						
K_i (mg P/g $min^{1/2}$)	0.57	0.28	0.23	0.11	0.037	0.46
C	2.73	5.43	3.18	1.92	11.2	3.4
R^2	0.95	0.88	0.85	0.91	0.44	0.90

It was evident in all the batch experiments that Purolite FerrIX A33E had the best removal efficiency in both equilibrium and kinetic experiments with maximum adsorption capacity. For these reasons, Purolite FerrIX A33E was selected for investigating the influence of pH and complementary anions on phosphate adsorption.

5.3.5. Effect of pH on phosphate adsorption

During adsorption the pH of the suspension was not changed and the final pH was almost the same as the initial pH. Phosphate adsorption capacity was also same at the pH range of 4 to 10 (Figure 5.8) though slightly higher at pH 7.0. Previous studies of phosphate adsorption on ion exchange resins agreed with these results that the favourable pH for phosphate adsorption lies between 4-10 and for most of the adsorbents it was 7.0 (Marshell and Wartelle, 2004; Awual et al., 2011).

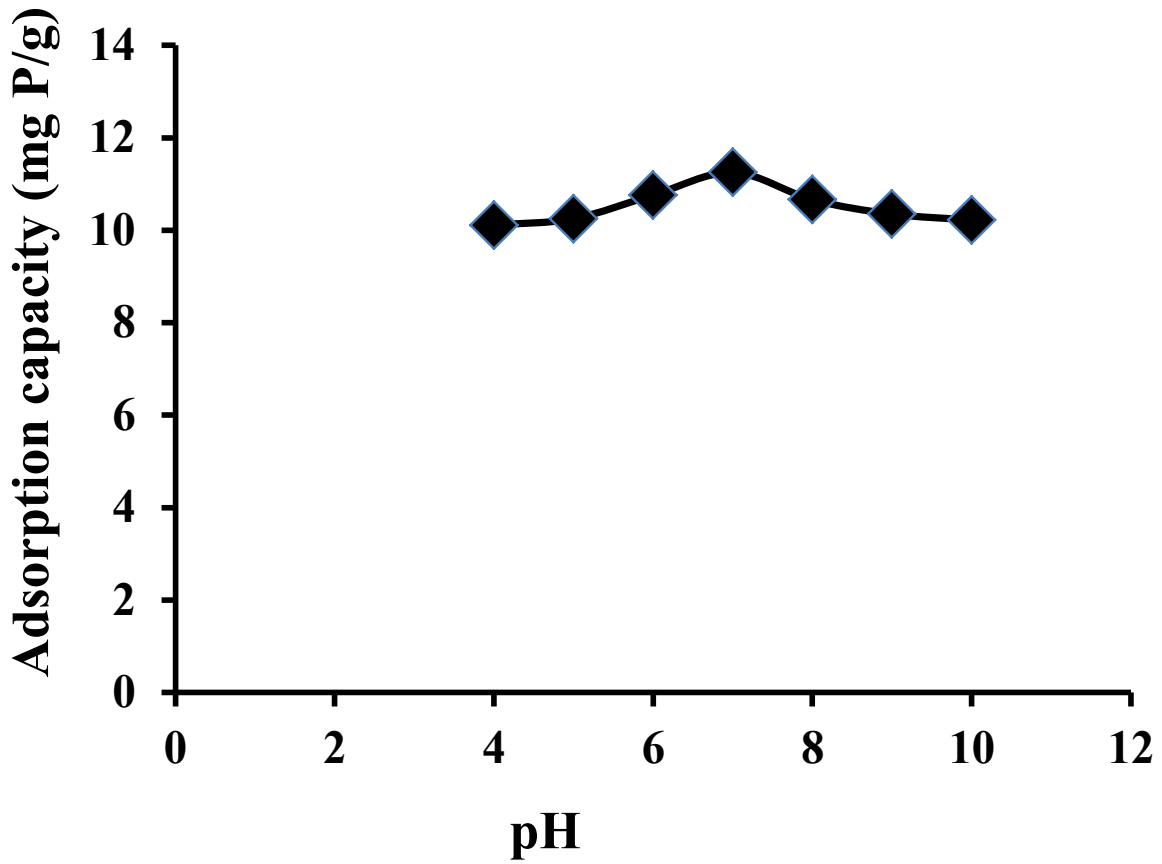

Figure 5.8. Influence of final pH of Purolite FerrIX A33E suspension on phosphate adsorption

5.3.6. Effect of complementary ions

Many anions co-exist with phosphate in wastewater. The ratios of the anions' concentrations in natural water and wastewater are very different and therefore such ratios need to be considered in assessing the extent of competition. Effects of SO_4^{2-}, F^- , Cl^- and NO_3^- on phosphate adsorption showed that the presence of these anions at concentrations ranging from 25 to 200 mg/L at pH 7.0 reduced the phosphate adsorption appreciably when the initial concentration of these anions increased (Figure 5.9). The order of phosphate adsorption reduction by these anions was $SO_4^{2-} > Cl^- > NO_3^- > F^-$.

This outcome can be explained based on the adsorption mechanisms of these anions. In general, nitrate and chloride do not interfere with phosphate adsorption at a similar concentration in water because they are non-specifically adsorbed, whereas phosphate is specifically adsorbed in many sorbents. Sulphate, carbonate, and bicarbonate are specifically adsorbed in certain sorbents, and therefore they can compete with phosphate for adsorption depending on their relative concentrations. Sulphate can be adsorbed specifically and non-specifically and therefore it competed with phosphate better than Cl^- and NO_3^- on Purolite FerrIX A33E. This is because phosphate and sulphate are known to be specifically (inner-sphere complexation) and non-specifically (outer-sphere complexation) adsorbed. The specific adsorption is on the iron oxide in Purolite FerrIX A33E and the non-specific adsorption is on the organic portion of the adsorbent. Cl^- and NO_3^- are non-specifically adsorbed (outer-sphere complexation) and therefore unable to compete well with phosphate at equal concentrations. The decreased order of competition observed in this study ($SO_4^{2-} > Cl^- > NO_3^- > F^-$) is consistent with the findings in other studies of phosphate adsorption (Loganathan et al., 2014).

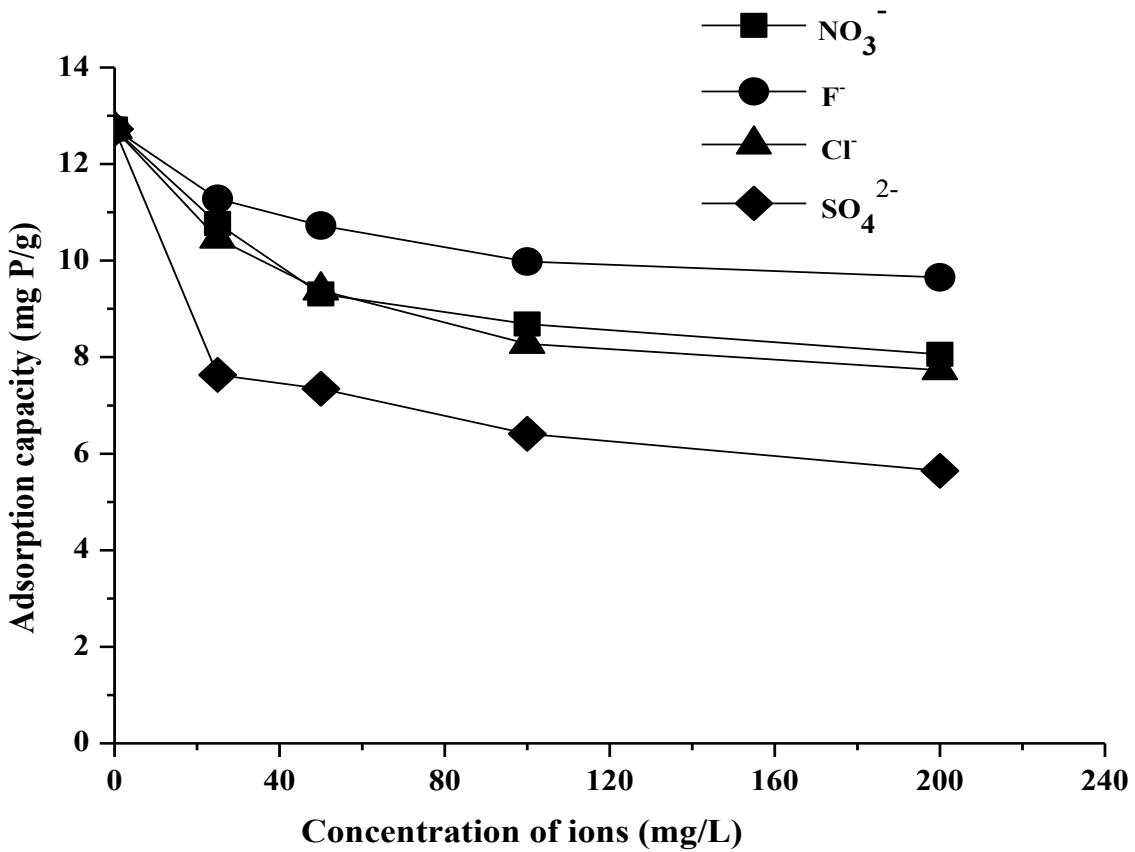

Figure 5.9. Effect of complementary anions on the adsorption of phosphate using FerrIX A33E (initial phosphate concentration 10 mg P/L and adsorbent dose 1g/L).

5.3.7. Regeneration of adsorbent

Following the adorption of phosphate on Purolite FerrIX A33E the adsorbent was regenerated using different reagents in batch experiments. Concerning the reagents used for the regeneration of the Purolite resin, NaOH was found to be effective in desorbing the phosphate. No detectable phosphate was desorbed using 1 M NaCl, Na_2SO_4 and water. Only 60-70% of the adsorbed phosphate was desorbed by 0.5 M NaOH whereas 90-95% of the phosphate was desorbed by 1M NaOH and 0.1M NaOH could desorb only 20-30% of the phosphate within 30 minutes (Figure 5.10).

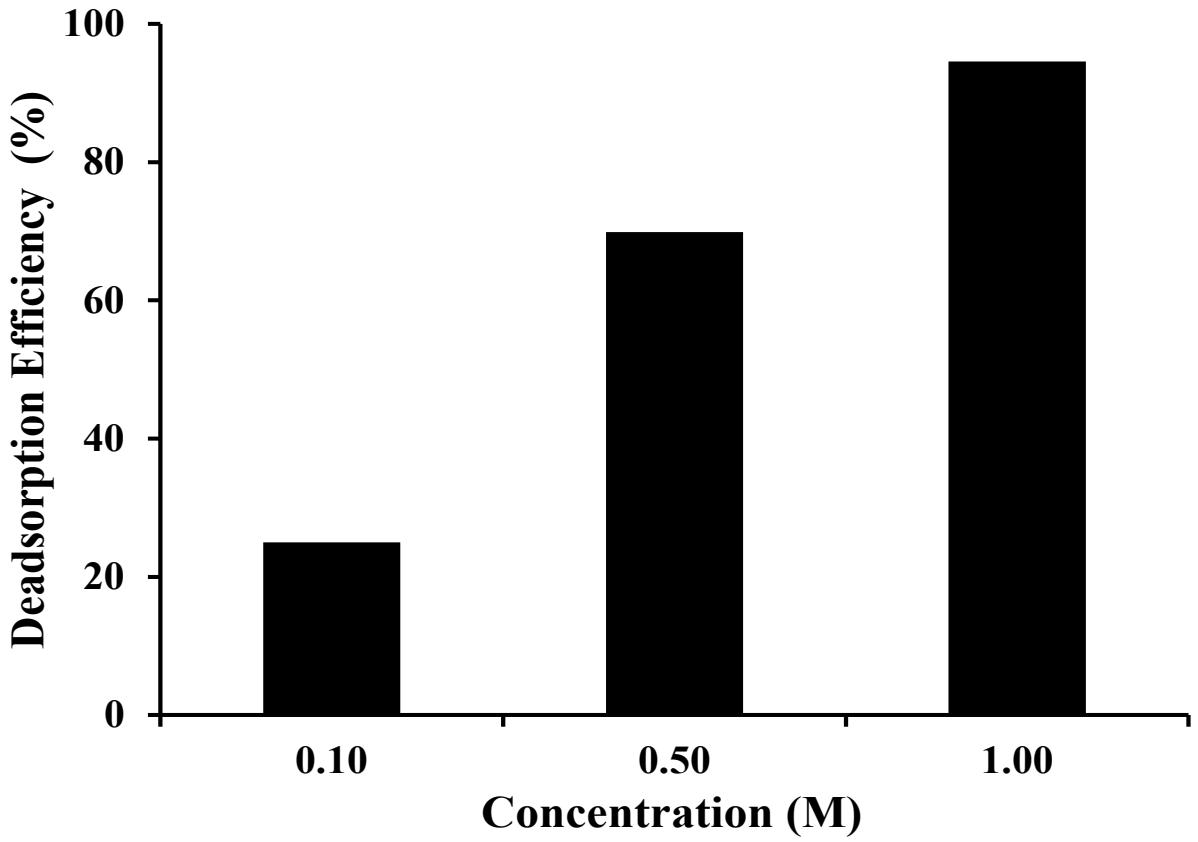

Figure 5.10. Batch regeneration study with NaOH at three different concentrations.

5.4. Conclusions

Of the six adsorbents tested in the batch study (Purolite A520E, Purolite A502PS, Purolite FerrIX A33E, Dowex 21k XLT , HFO (iron (iii) oxide $HFeO_2$) and Zirconium (IV) hydroxide (H_4O_4Zr)), Purolite FerrIX A33E had the highest phosphate removal capacity. The batch adsorption isotherm data for Purolite FerrIX A33E was satisfactorily explained using the Langmuir, Freundlich and Tempkin isotherm models while the kinetic adsorption data fitted reasonably well to the pseudo-second-order, Elovich and intraparticle diffusion models. Freundlich adsorption constant related to adsorption capacity was higher for Purolite FerrIX A33E. The Langmuir adsorption capacity of Purolite FerrIX A33E was 48 mg P/g which constituted one of the highest phosphorus adsorption capacities reported in the literature for adsorbents. Therefore Purolite FerrIX A33E is a potential adsorbent for removing phosphate from aqueous solutions. pH had little effect on phosphate adsorption of Purolite FerrIX in the pH range 4 – 10. Furthermore, Cl^-, NO_3^- and F^- did not have much effect on phosphate adsorption but SO_4^{2-} reduced phosphate adsorption at equal concentrations of the anions. When the co-ions were at a high concentration, the decreasing order of competition of the anions was as follows: $SO_4^{2-} > Cl^- > NO_3^- > F^-$. Column experiments with Purolite FerrIX A33E will be discussed in Chapter 6.

CHAPTER 6

University of Technology Sydney

COLUMN STUDIES ON PHOSPHATE ADSORPTION BY AN IRON OXIDE IMPREGNATED STRONG BASE ANION EXCHANGE RESIN

Chapter 6

Column studies on phosphate adsorption by an iron oxide impregnated strong base anion exchange resin*

6.1. Introduction

As discussed in literature review, fixed-bed sorption processes are ideal for the reduction of dissolved phosphate to near-zero level provided the adsorbent is phosphate selective, cost-effective and amenable to efficient regeneration and reuse for several cycles of operation. But majority of the studies reported in literature on adsorptive removal of phosphate from water were conducted in batch type of adsorption experiments (Loganathan et al., 2014). The results from these studies cannot be directly applied to real system of water treatment, where fluid flows continuously through a column of adsorbent or a packed bed involving dynamic adsorption of the solute. The columnar operation allows more efficient utilization of the adsorptive capacity than the batch process. The adsorbent at the inlet end is contacted continuously by the solution at the initial solute concentration and the change in concentration at each subsequent layer is small. Therefore, the adsorbent in the column acts like a series of layers, with each layer in contact with a fresh solution of constant solute concentration. This procedure results in

***Major parts of this chapter was published in "T. Nur, M.A.H. Johir, P. Loganathan, T. Nguyen, S. Vigneswaran, and J. Kandasamy, "Phosphate removal from water using an iron oxide impregnated strong base anion exchange resin", Journal of Industrial and Engineering Chemistry (2014): 1301–1307" and in "T. Nur , W.G. Shim , M.A.H. Johir , S. Vigneswaran & J. Kandasamy , Modelling of phosphorus removal by ion-exchange resin (Purolite FerrIX A33E) in fixed-bed column experiments, Desalination and Water Treatment 52 (2013) 784-790".**

maximum loading of the adsorbent at constant solute concentration, and is in contrast to the continuously declining solute concentration in batch process.

In Chapter 5, it was found from batch experiments of phosphate adsorption that among six adsorbents, three anion exchange resins, Purolite FerrIX A33E, Purolite A500PS and Purolite A520E had the three best Langmuir adsorption capacities which were quite good compared with other phosphate adsorbents reported in literature (Loganathan et al., 2014). The equilibrium adsorption data of these three adsorbents fitted satisfactorily with Langmuir and Freundlich Isotherm model with good R^2 values (0.90-0.99). Of the six adsorbents, the values of Freundlich parameter K_F for all three adsorbents were also highest**.** For this reason, these three ion exchange resins were chosen for the fixed bed column experiments on phosphate removal and subsequently select the best phosphate adsorbent among them.

Numerical solution of adsorption data obtained in fixed bed columns packed with ion exchange resins has gained very little attention and very few numerical models are available in literature (Hekmatzadeh et al., 2012). A suitable numerical solution can help to reduce the number of experiments associated with new operating conditions and a well-researched model can be used as a reliable solution to design, optimize and predict the breakthrough curves of fixed bed columns in real water treatment processes. In this chapter, a numerical model will be used to describe the column phosphate adsorption on Purolite FerrIX A33E.

The aims of the present research are: (i) compare the phosphate removal efficiencies of Purolite FerrIX A33E, Purolite A500PS and Purolite A520E adsorbents in column study and justify the selection of Purolite FerrIX A33E for a detailed study; (ii) study the effects of bed height, initial phosphate concentration and filtration velocity on

phosphate adsorption on Purolite FerrIX A33E; (iii) model column adsorption data by the empirical models of Bohart-Adams, Thomas and Yoon-Nelson; (iv) develop a numerical model based on advection-dispersion equation and simulate the model parameters to describe the column adsorption data; (v) develop a suitable method to regenerate the adsorbent for reuse, as well as recovery of the desorbed phosphate for beneficial use.

6.2. Material and methods

6.2.1. Adsorbents

Three ion exchange resins namely Purolite A520E, Purolite A500PS and Purolite FerrIX A33E were used as adsorbents. The physical and chemical properties of these resins were described in Chapters 3 and 5.

The method of preparing feed solution and chemical analysis are same as described in Chapter 3.

6.2.2. Column mode experiments

The methods used for the fixed bed column studies are same as those described earlier in Chapter 3.

Three empirical models, Bohart-Adams model (1920), Thomas model (1944), Yoon and Nelson (1984) and a numerical model were used to analyse the data. These models and the methods of calculation of the model parameters were described in Chapters 2 and 3. The numerical model was also described earlier in Chapter 4.

6.2.3. Regeneration of adsorbent and phosphate recovery

The column regeneration studies were carried out using different desorbing agents such as 1 M NaCl, 1 M Na_2SO_4, 1 M NaOH, and MQ water. The regeneration was performed by leaching the resin containing the adsorbed phosphate with the leaching solution at a filtration velocity of 10 m/h for 30 min. Since phosphate was enriched through the adsorption process, the enriched phosphate was desorbed by the regeneration solutions and recovered as calcium phosphate by adding different concentrations of $CaCl_2$ to the leachate.

6.3. Results and Discussion

6.3.1. Comparison between three Purolites in column method of phosphate removal

In the first experiment, three adsorbents Purolite A520E, Purolite A500PS and Purolite Ferrix A33E were evaluated for the removal of phosphate from aqueous solution at different conditions such as two initial phosphorus concentrations (20 mg P/L and 30 mg P/L) and two filtration velocities (v = 5 m/h and 10 m/h). The breakthrough curves obtained for the different adsorbents exhibited different shapes (Figure 6.1 and 6.2). The three adsorbents showed almost similar curve in the case of the two concentrations. Among the three Purolites, Purolite A520E and Purolite A500PS gave sharp curves where an increase of effluent concentration of phosphate from 40 and 60% C_0 occurred after 17 h - 21 h, respectively, and Purolite Ferrix A33E demonstrated slightly flattened curves but reached almost 85% saturation at 30h when the initial phosphate concentration was 20 mg P/L (filtration velocity = 2.5 m/h and bed height = 12 cm) (Figure 6.1). This trend

can be attributed to the adsorption kinetics, which is related to the pore size distribution of the adsorbents.

When the initial phosphorus concentration was 30 mg P/L (Figure 6.1), the saturation time for three Purolites was same and it was 21 h. But the values of C_t/C_0 for Purolite A520E, Purolite A500PS and Purolite Ferrix A33E were 0.70, 0.49 and 0.90, respectively. From this experiment, we can say that the percentage of exhaustion was more in the case of Purolite Ferrix A33E compared to Purolite A520E and Purolite A500PS within the same service time.

Another experiment was conducted at two filtration velocities (v = 5 m/h and 10 m/h) but at a constant initial concentration of 20 mg P/L (Figure 6.2). For the higher filtration velocity, the time to reach the plateau oand exhaustion rate were almost the same for the three Purolites. The time to reach the plateau was 21h and exhaustion rates were 0.92, 0.90 and 0.87 for Purolite A520E, Purolite A500PS and Purolite Ferrix A33E, respectively when the flow rate was 5 m/h and 0.98, 0.98 and 0.96 when the flow rate was 10 m/h.

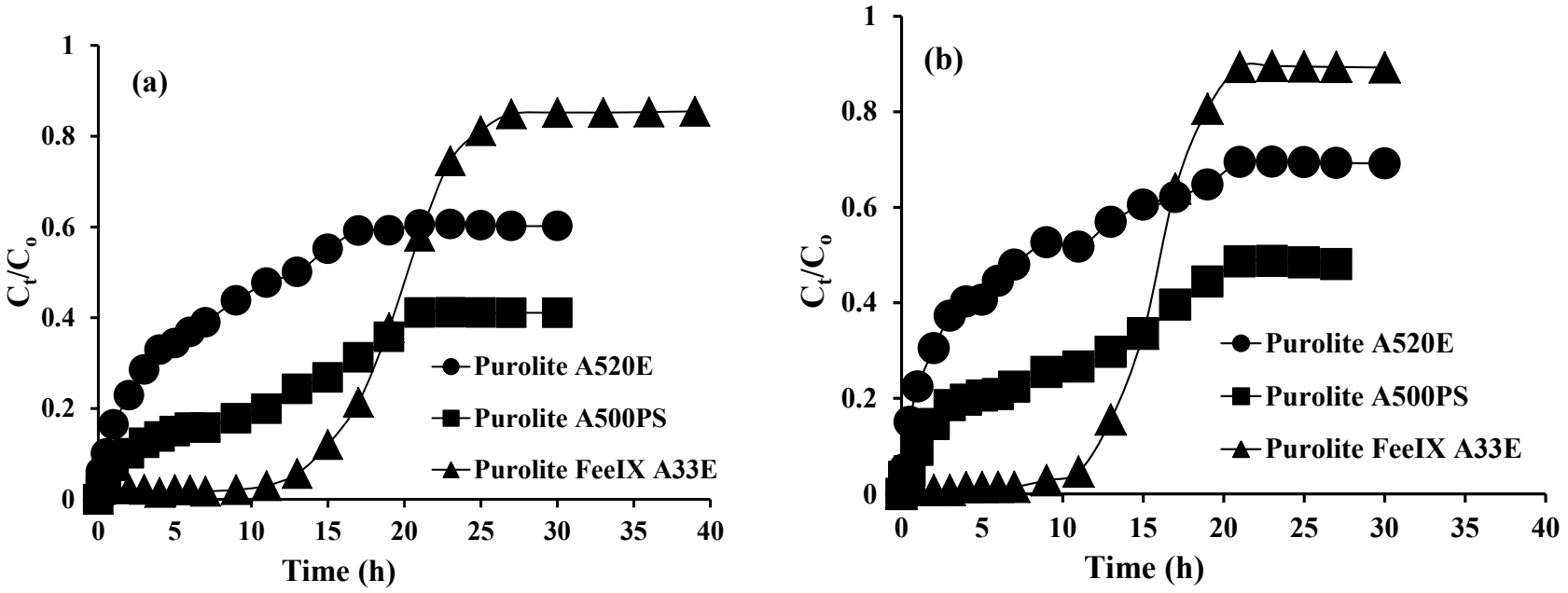

Figure 6.1. Breakthrough curves for three Purolites at different inlet initial concentration (a) 20 mg P/L and (b) 30 mg P/L (filtration velocity = 2.5 m/h and bed height=12 cm).

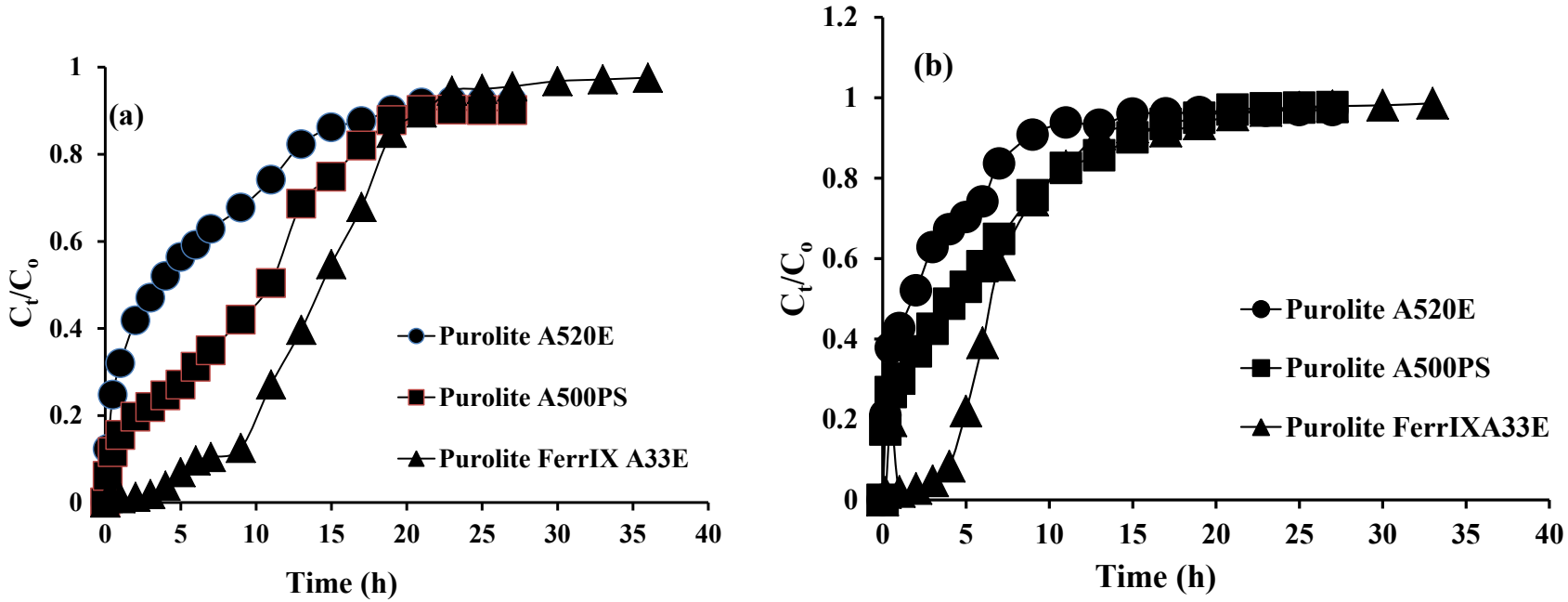

Figure 6.2. Breakthrough curves for three Purolites at different filtration velocity (a) 5 m/h and (b) 10 m/h (initial concentration = 20 mg P/L and bed height = 12 cm).

6.3.2. Comparison between the three Purolites in column adsorption model fits

The column adsorption data was fitted to three empirical models Bohart-Adam's, Thomas and Yoon-Nelson model for the adsorption of phosphate on three Purolites at two initial concentrations (20 mg P/L and 30 mg P/L) and at two filtration velocities (5.0 m/h and 10.0 m/h) (Table 6.1 and 6.2). The results showed that all three models fitted better to the column data of Purolite FerrIX A33E (R^2 = 0.90 - 0.99) than the other two Purolites (R^2 = 0.72 - 0.99). Furthermore, the adsorption capacity values of Purolite FerrIX A33E calculated by Thomas model for all different conditions were highest among all three Purolites. Moreover, the phosphate adsorption capacities of the column for three Purolites calculated from the breakthrough curves for the two inlet initial concentrations and filtration velocities were highest for Purolite FerrIX A33E. These results were consistent with those of the batch adsorption data presented in Chapter 5 that Purolite FerrIX A33E was the best adsorbent of the three resins. Threfore, Purolite FerrIX A33E was selected for further experimentation.

Table 6.1.

The model parameters for three Purolites (initial concentration = 20 mg N/L and 30 mg P/L, bed height = 12 cm and filtration velocity = 2.5 m/h).

	Initial concentration = 20 mg P/L			Initial concentration = 30 mg P/L		
	Purolite A520E	Purolite A500PS	Purolite FerrIX A33E	Purolite A520E	Purolite A500PS	Purolite FerrIX A33E
Bohart-Adams Model						
k_{AB}(L/mg. min) x 10^{-5}	38.01	34.20	11.21	82.81	21.82	9.23
N_o (mg/L) x 10^3	2.38	3.57	15.31	5.13	4.99	20.01
R^2	0.86	0.80	0.92	0.85	0.85	0.90
Thomas Model						
k_{Th} (mL/min.mg) x 10^{-2}	6.31	8.91	17.72	0.056	4.72	16.11
q_o (mg/g)	9.29	10.11	11.31	10.11	11.99	12.81
R^2	0.72	0.80	0.91	0.81	0.80	0.94
Yoon-Nelson Model						
k_{YN} (1/min) x 10^{-3}	3.11	1.61	3.31	1.11	1.51	4.11
τ (min) x 10^3	0.61	1.61	1.40	2.29	1.43	1.31
R^2	0.76	0.80	0.93	0.81	0.79	0.95
Breakthrough adsorption capacity	5.61	8.92	11.43	7.52	10.55	13.24

Table 6.2.

The model parameters for the three Purolites (filtration velocity = 5.0 m/h and 10.0 m/h, initial concentration = 30 mg P/L and bed height = 12 cm).

	Filtration velocity = 5.0 m/h			Filtration velocity = 10.0 m/h		
	Purolite A520E	Purolite A500PS	Purolite FerrIX A33E	Purolite A520E	Purolite A500PS	Purolite FerrIX A33E
Bohart-Adams Model						
k_{AB}(L/mg. min) x 10^{-5}	29.60	28.69	19.11	38.37	30.01	33.21
N_o (mg/L) x 10^3	4.48	6.36	16.41	5.68	8.19	17.72
R^2	0.86	0.79	0.92	0.79	0.82	0.98
Thomas Model						
k_{Th} (mL/min.mg) x 10^{-2}	7.31	9.16	13.61	9.23	9.52	13.92
q_o (mg/g)	3.73	16.07	19.24	8.51	17.74	22.71
R^2	0.79	0.89	0.94	0.91	0.90	0.96
Yoon-Nelson Model						
k_{YN} (1/min) x 10^{-3}	5.51	3.51	9.11	1.11	1.51	14.11
τ (min) x 10^3	0.24	0.59	0.61	0.13	0.26	0.31
R^2	0.82	0.87	0.97	0.81	0.89	0.99
Breakthrough adsorption capacity	8.31	12.95	15.93	9.14	14.92	16.37

6.3.3. Experiments with Purolite Ferrix A33E at different conditions

Effects of bed height, initial concentration and filtration velocity on the adsorption of phosphate by Purolite FerrIX A33E were presented in the form of breakthrough curves (Figures 6.3-6.5). The breakthrough curves became less sharp when the mass transfer rates were decreased (Cloutier et al., 1985). Since mass transfer rates were finite, the breakthroughs were diffused and exhibited an S-shape pattern.

6.3.3.1. Effect of adsorbent bed height

Figure 6.3 shows the breakthrough curves obtained for phosphate adsorption on Purolite FerrIX A33E resin at bed heights of 3, 6, 12, 14, 16, 17 and 19 cm (12, 28, 56, 66, 76, 80 and 86 g of resin), at a constant filtration velocity 2.5 m/h and inlet concentration 20 mg P/L. Based on Figure 6.3 it is evident that at low bed heights, the breakthrough occurred faster than that at high bed heights. This pattern of breakthrough at different bed heights is similar to the findings in other column studies reported on different adsorbents and adsorbates (Ahmad et al., 2012, Yahaya et al., 2011). The starting time of saturation occurred after 3, 9, 13, 19, 23, 25 and 28 h when the bed height was 3, 6, 12, 14, 16, 17 and 19 cm, respectively, and 50% saturation was achieved within the interval of 5, 13, 21, 25, 31, 34 and 39 h, respectively. As the bed height increased, phosphate had more time to contact with the Purolite ion exchange resin as shown by the higher detention time (Table 6.3), resulting in more efficient removal of phosphate. Thus, the higher bed height resulted in a greater decrease in phosphate concentration in the effluent.

The uptake of phosphorus increased with the increase in the bed height from 3 to 19 cm. This was reflected from the breakthrough with a bed height of 3 cm; the adsorbent gets saturated early compared to other bed heights. Accumulation of adsorbents in the fixed-bed column is largely dependent on the quantity of sorbent inside the column. Both bed capacity and exhaustion time increased with increasing bed height, as more binding sites available for sorption, also resulted in a broadened mass transfer zone. The increase in adsorption with that in bed depth was due to the increase in adsorbent doses in larger beds which provide greater service area (or adsorption sites). High adsorption capacity was observed at the highest bed height due to an increase in the surface area of adsorbent, which provided more binding sites for the adsorption (Ahmad et al., 2012; Yahaya et al., 2011)

The slope of the breakthrough curve decreased with increase in bed height as a result of broadened influent movement zone (Yahaya et al., 2011). However, it is found that the complete pattern of adsorption breakthrough curve was formed at all bed heights. The adsorption of phosphate increased when bed height rose from 3 to 19 cm, because of the increased amount of adsorption sites available at higher bed heights.

6.3.3.2. Effect of initial phosphate concentration

The effect of increase in the influent phosphate concentration from 5 to 30 mg P/L on breakthrough curves is shown in Figure 6.4. The starting time of saturation occurred at 30, 23, 17, 15 and 13 h and 50% saturation was achieved after an operation period of 45, 28, 21, 19 and 15 h for the influent concentrations of 5, 10, 15, 20 and 30 mg P/L, respectively. The breakthrough time occurred faster and the breakthrough curves were sharper with increasing influent phosphate concentration. These results are consistent

with nitrate adsorption on an ion exchange resin (Hekmatzadeh et al., 2012). These results demonstrate that the change of concentration gradient affects the saturation rate and breakthrough time, or in other words, the diffusion process is concentration dependent. As the influent concentration increases, phosphate loading rate increases, so does the driving force for mass transfer, and decreases in the adsorption zone length (Goel et al., 2005). The extended breakthrough curve at low influent concentration indicates that a higher volume of solution can be treated.

6.3.3.3. Effect of filtration velocity

The effect of filtration velocity on the adsorption of phosphate on Purolite FerrIX A33E resin was investigated by varying the filtration velocity (2.5, 5.0 and 10.0 m/h) at a constant adsorbent bed height of 12 cm and the inlet concentration of 30 mg P/L. The breakthrough generally occurred faster and the breakthrough curve was steeper with higher filtration velocity (Figure 6.5). The time to reach the plateau of C_t/C_0 increased significantly with a decrease in the filtration velocity. The plateau of C_t/C_0 occurred at 9, 15, and 23 h for the inlet filtration velocity of 10, 5.0, and 2.5 m/h with the values of C_t/C_0 of 0.90, 0.85, and 0.83, respectively. Faster breakthrough of adsorbates and steeper breakthrough at higher filtration velocities have also been reported elsewhere for adsorption onto other adsorbents (Yahaya et al., 2011, Srivastava et al., 2008).

At a lower filtration velocity, phosphate had more time to contact with Purolite resin as indicated by the higher detention time (Table 6.5), which allowed the diffusion of the phosphate ions into the pores of the adsorbent, resulting in a higher proportion of the removal of the influent phosphate ions in the column (lower C_t/C_o). However, the quantity of phosphate ions removed was lower at lower filtration rate (Table 6.5), due to

the lower amounts of phosphate ions (lower bed volumes) passing through the column per unit time. Mixed results have been reported in the literature on the effect of filtration velocity on adsorption capacity. Increase of filtration velocity was found to decrease the adsorption of Cu on activated carbon (Yahaya et al., 2011), whereas increase of filtration velocity increased adsorption of Pb on oil palm fibre (Nwabanne and Igbokwe, 2012). However, Hekmatzadeh et al. (2012) reported that filtration velocity had no effect on the adsorption of nitrate on an ion exchange resin. The differences in the effects of filtration velocity may be due to the type of adsorbent and adsorbate, and experimental conditions such as filtration velocities, bed heights and influent concentrations used in the different studies.

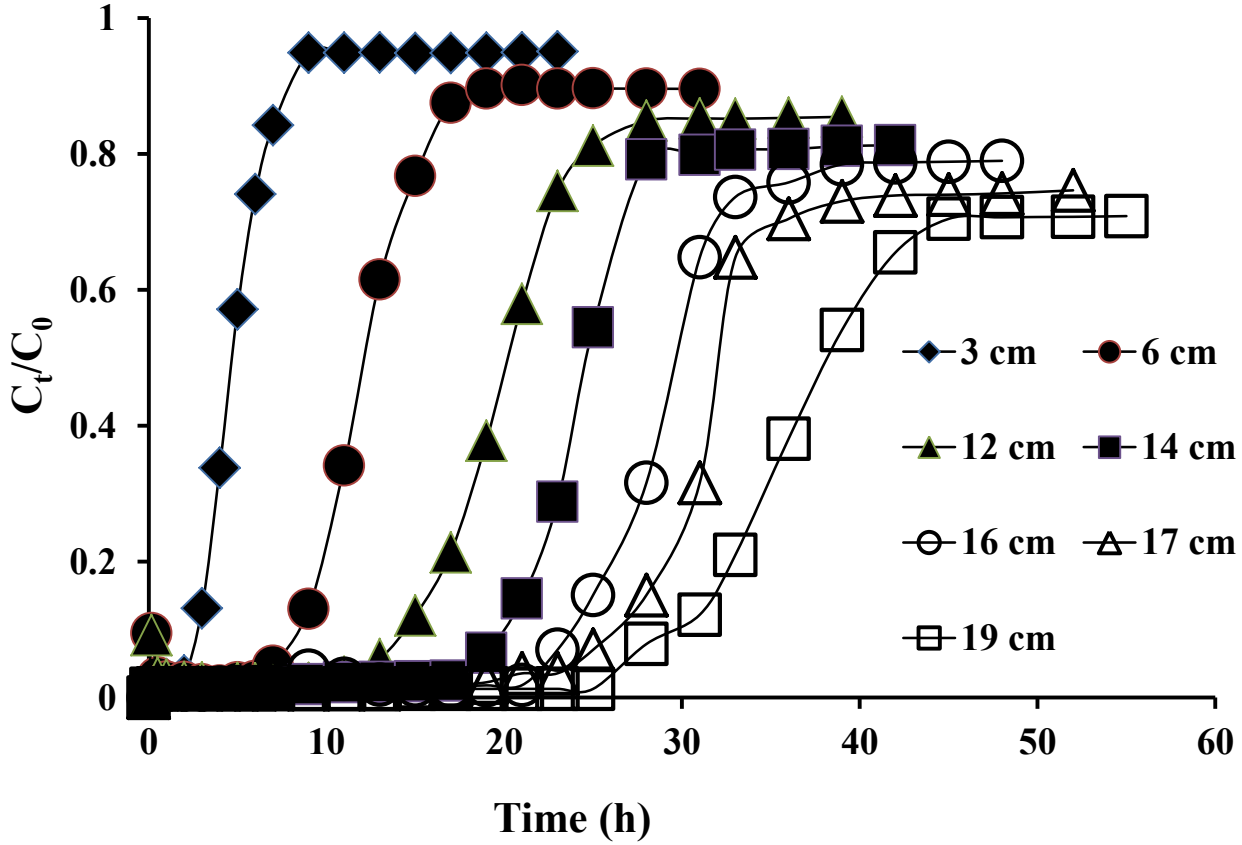

Figure 6.3. Breakthrough curves for different bed heights of Purolite FerrIX A33E (initial phosphate concentration = 20 mg P/L and filtration velocity = 2.5 m/h).

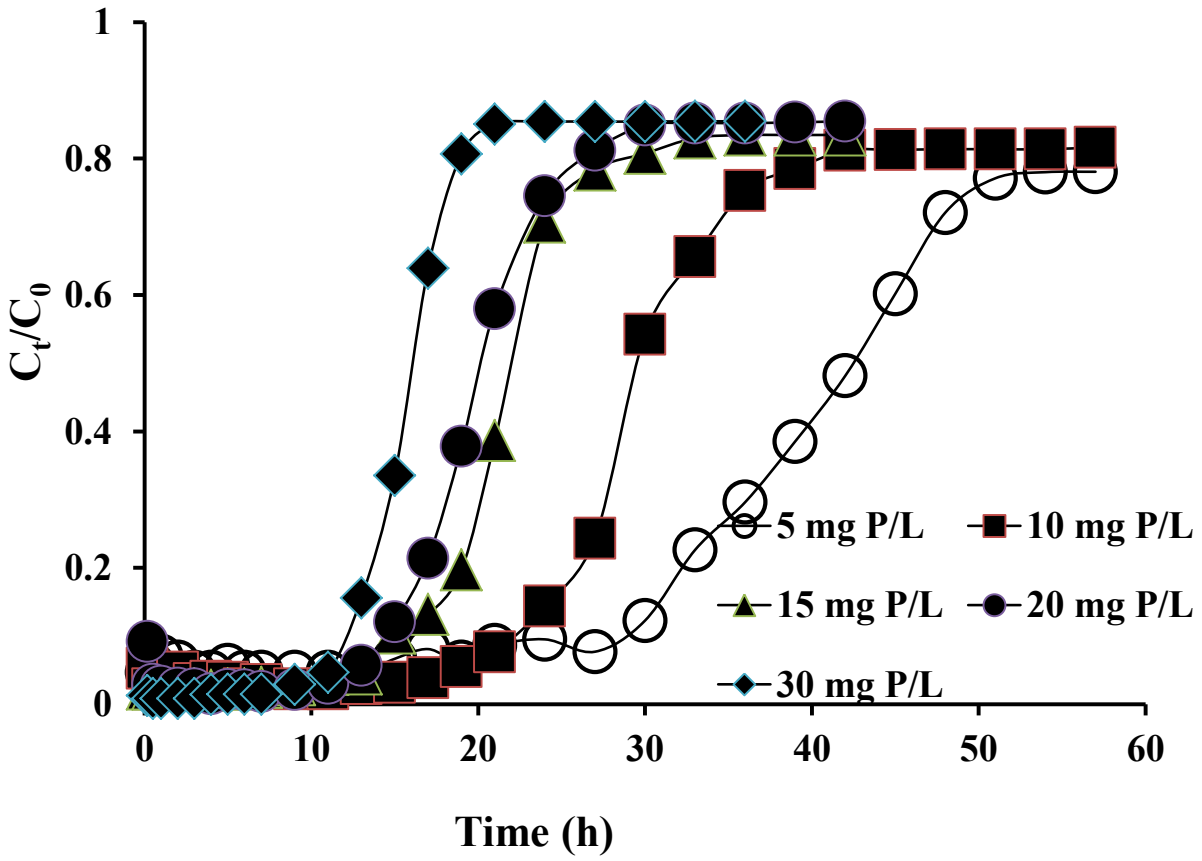

Figure 6.4. Breakthrough curves for different inlet P concentrations passing through Purolite FerrIX A33E columns (bed height = 12 cm and filtration velocity = 2.5 m/h).

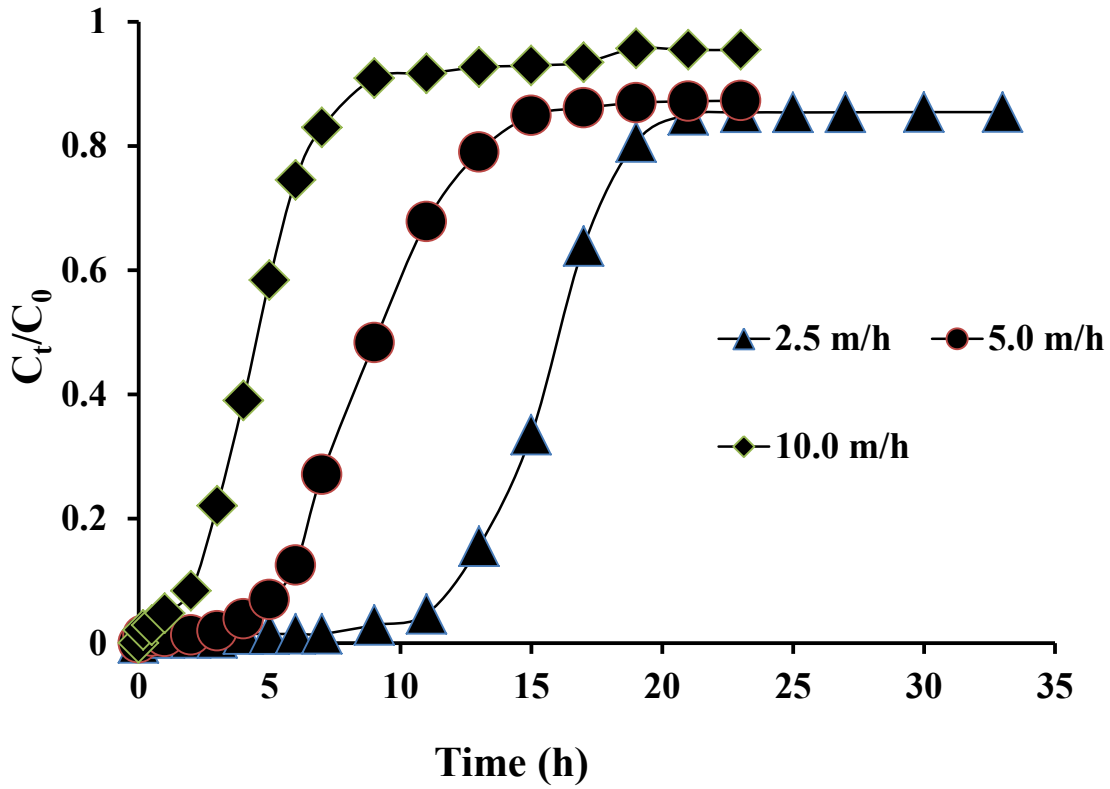

Figure 6.5. Breakthrough curves for different filtration velocities through Purolite FerrIX A33E columns (bed height =12 cm and initial phosphate concentration = 30 mg P/L).

6.3.4. Column Adsorption Modelling for Purolite FerrIX A33E

6.3.4.1. Bohart-Adams model

The model's fit to the experimental data was good for all the inlet phosphate concentrations ($R^2 \geq 0.72$, Table 6.4) and filtration velocities ($R^2 \geq 0.80$, Table 6.5), but only for the low bed heights (3-14 cm, $R^2 \geq 0.80$, Table 6.3). The values of k_{AB} calculated from the model decreased when inlet phosphate-P concentration and bed height increased, but it increased when the filtration velocity increased. The value of N_o increased with the increasing inlet concentration and bed height but decreased with increasing filtration velocity. The increase in k_{AB} with filtration velocity shows that the overall system kinetics was dominated by external mass transfer in the initial part of adsorption in the column (Aksu and Gonen, 2004).

6.3.4.2. Thomas model

The high R^2 values (0.80-0.98) obtained for the model fit to experimental data indicate that Thomas model described the column data very well (Tables 6.3, 6.4, 6.5). The model prediction of the column adsorption capacity (q_o) increased with bed height (Table 6.3), inlet phosphate concentration (Table 6.4), and filtration velocity (Table 6.5) consistence with the observations made earlier based on the breakthrough curves. The values obtained for q_o from the model are approximately equal to those calculated from the breakthrough curves.

6.3.4.3. Yoon–Nelson model

The experimental data fitted satisfactorily to Yoon-Nelson model for all phosphate concentrations and filtration velocities (R^2 = 0.76-0.99, Table 6.4 and 6.5) but, similar to Bohart-Adams model, the fit was good only at low bed heights (3-14 cm, $R^2 \geq 0.83$, Table 6.3). The rate constant k_{YN} increased and the 50% breakthrough time (τ) decreased when both filtration velocity and inlet concentration increased (Tables 6.4 and 6.5), but the opposite trend occurred with increasing bed height (Table 6.3). With the increase of bed height, τ rose while k_{YN} fell, which was also observed for Cu adsorption on rice husk-based activated carbon (Yahaya et al., 2011).

Considering the values of R^2 for the models fits to the data and breakthrough curves, it can be concluded that all three models can be used to reasonably describe the behaviour of the adsorption of phosphate on the Purolite resin in a fixed-bed column. The exception is perhaps the use of the Bohart-Adams and Yoon-Nelson models at high bed heights, where the models' fits to the data were poor.

Table 6.3.

The parameters of three models for different bed heights of Purolite FerrIX A33E (initial concentration = 20 mg P/L and filtration velocity = 2.5 m/h).

Bed Height	Bohart-Adams Model			Thomas Model			Yoon-Nelson Model			Breakthrough adsorption capacity	Detention time
(cm)	k_{AB}(L/mg.min) x 10^{-5}	N_o (mg/L) x10^3	R^2	k_{Th} (mL/min.mg) x 10^{-2}	q_o (mg/g)	R^2	k_{YN} (1/min)x 10^{-3}	τ (min) x 10^3	R^2	q_{eq} (mg/g)	t (h)
3	50.3	11.8	0.88	65.8	11.4	0.98	15.3	0.3	0.96	11.4	0.012
6	17.8	16.5	0.86	22.8	12.6	0.96	5.3	0.9	0.90	13.5	0.024
12	8.6	17.0	0.91	13.2	12.7	0.94	3.5	1.5	0.93	11.1	0.048
14	7.0	20.7	0.80	12.0	13.4	0.91	3.2	1.8	0.83	11.7	0.056
16	5.6	21.8	0.63	10.9	13.6	0.86	1.6	3.1	0.63	12.2	0.064
17	5.0	23.2	0.72	9.6	13.7	0.90	1.6	3.2	0.75	12.0	0.068
19	4.4	25.0	0.42	8.7	14.5	0.84	1.5	3.4	0.61	12.5	0.076

Table 6.4.

The parameters of three models for different inlet P concentrations through Purolite FerrIX A33E column (bed height = 12 cm and filtration velocity = 2.5 m/h).

Influent concentration	Bohart-Adams Model			Thomas Model			Yoon-Nelson Model			Breakthrough adsorption capacity	Detention time
(mg P/L)	k_{AB}(L/mg. min) x 10^{-5}	N_o(mg/L) x10^3	R^2	k_{Th} (mL/min.mg) x 10^{-2}	q_o (mg/g)	R^2	k_{YN} (1/min) x 10^{-3}	τ (min) x10^3	R^2	q_{eq} (mg/g)	t (h)
5	14.1	8.4	0.83	24.8	4.7	0.88	0.9	3.3	0.81	4.1	0.048
10	13.5	11.1	0.72	19.8	7.4	0.89	2.1	2.2	0.76	6.9	0.048
15	11.7	12.8	0.93	18.6	7.6	0.89	2.8	1.5	0.76	7.0	0.048
20	11.2	15.3	0.84	17.7	11.3	0.91	3.3	1.4	0.82	11.4	0.048
30	9.2	20.0	0.90	16.1	12.8	0.94	4.1	1.3	0.85	13.2	0.048

Table 6.5.

The parameters of three models for different filtration velocities through Purolite FerrIX A33E column (bed height = 12 cm and initial concentration = 30 mg P/L).

Filtration velocity	Bohart-Adams Model			Thomas Model			Yoon-Nelson Model			Breakthrough adsorption capacity	Detention time
(m/h)	k_{AB}(L/mg.min) x 10^{-5}	N_o (mg/L) x 10^3	R^2	k_{Th} (mL/min.mg) x 10^{-2}	q_o (mg/g)	R^2	k_{YN} (1/min) x 10^{-3}	τ (min) x 10^3	R^2	q_{eq} (mg/g)	t (h)
2.5	5.8	29.7	0.80	11.5	16.4	0.91	4.0	1.3	0.85	12.9	0.048
5.0	19.1	17.7	0.92	13.6	19.2	0.84	9.0	0.6	0.97	15.9	0.024
10.0	33.2	16.4	0.98	13.9	22.7	0.80	14.0	0.3	0.99	16.3	0.012

6.3.4.4. Numerical modelling

In order to simulate the experimental breakthrough curves, one need to solve the dynamic equations described in Chapter 4 (Equations 4.6 – 4.8), which consist of bulk and solid phase concentrations simultaneously. In this work, the orthogonal collocation method (OCM) and the variable coefficient ordinary differential equation solver (VODE) were used for that purpose (Villadsen and Michelsen, 1978; Brown et al., 1989; Abdul et al., 2010; Shim et al., 2012). The values of kinetic parameters (D_L, k_f and D_S) for different conditions are given in Table 6.6.

6.3.4.4.1. Effect of bed height

The effect of bed length (height) on adsorption breakthrough curves at inlet concentrations of 22 - 24 mg/L and constant inlet velocity (2.5 m/h) are shown in Figure 6.6 with model simulation results. The adsorption breakthrough curves appeared earlier and their shapes also become slightly sharper (or steeper) when the bed length is shorter. However, the shapes of the concentration curve S were stable and completely formed, which indicates that the constant pattern behaviours were established for all testing conditions. Fixed bed model predictions with different empirical coefficients gave reasonable fits to the experimental data although some deviations were observed.

6.3.4.4.2. Effect of concentration

Figure 6.7 shows the effect of influent concentration on adsorption breakthrough curves at constant bed length (12 cm) and inlet velocity (2.5 m/h). As expected, the adsorption breakthrough time of phosphate is highly dependent on the inlet concentration.

The higher the influent concentration, the earlier was the breakthrough time. As influent concentration increased, sharper breakthrough curves were obtained. This can be explained by the fact that a lower concentration gradient caused a slower transport due to a decrease in the diffusivity or mass transfer rate. The larger the inlet concentration, the steeper is the slope of breakthrough curve and earlier is the breakthrough time. These results demonstrate that the change of concentration gradient affects the saturation rate and breakthrough time, or in other words, the diffusion process is concentration dependent.

This result can also be explained in terms of the velocity of the wave front and the mean retention time, which is derived from the equilibrium theory and can be written as follows (Ruthven, 1984; Yang, 1986; Noll et al., 1992):

$$V_c = \left(\frac{\partial z}{\partial t}\right)_c = \frac{V}{1+\left(\frac{1-\varepsilon}{\varepsilon}\right)\left(\frac{dq^*}{dc}\right)} \tag{6.1}$$

$$\bar{t} = \frac{L}{V}\left[1+\left(\frac{1-\varepsilon}{\varepsilon}\right)\left(\frac{dq^*}{dc}\right)\right] \tag{6.2}$$

where, V_c is the propagation velocity of concentration front, V is the interstitial gas velocity, ϵ is the voidage (porosity) of adsorbent bed, $dq^*/dc$is the slope of the adsorption equilibrium isotherm, $\bar{t}$ is the mean retention time, L is the adsorbent bed length, respectively.

As described above, V_c and $\bar{t}$ are greatly dependent on the slope of adsorption equilibrium isotherm derived. In this work, the favourable type of isotherm, Langmuir, was obtained from the column equilibrium results. Thus faster V_c and shorter $\bar{t}$ are obtained when the inlet concentration increased. In addition, the breakthrough curves became gradually broader (or steeper) as the influent concentration decreased (or increased). This trend is closely related with the rate of mass transfer driving force. In other words, higher the inlet concentration, the greater are the diffusion flux (or intraparticle diffusivity) and the narrower mass transfer zone, leading thus to sharper breakthrough curve (Table 6.6). The model fit the experimental data reasonably well although some deviations were observed (Figure 6.7).

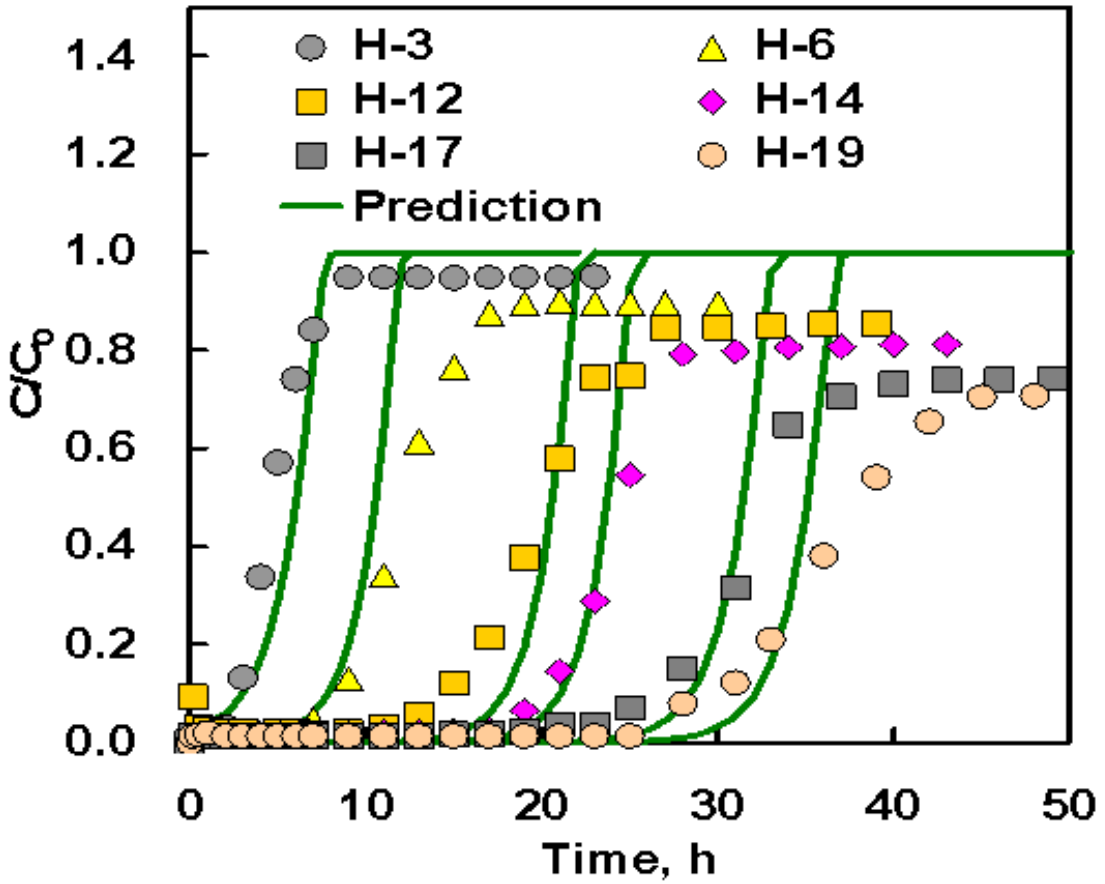

Figure 6.6. Effect of bed length on the adsorption breakthrough curves for Purolite FerrIX A33E (H - 3, H - 6, H - 12, H - 14, H - 17, H – 19 represent bed heights of 3, 6, 12, 14, 17 and 19 cm, respectively).

Table 6.6.

Experimental conditions and kinetic parameters for phosphate adsorption on Purolite FerrIXA33E.

Run no.	Length cm	Velocity l/min	Feed concentration mg P/L	$D_L^* \times 10^6$ m^2/s	$k_f^{**} \times 10^6$ m/s	$D_S^{***} \times 10^{10}$ m^2/s	R^2
C-1			6.1			1.067	0.97
C-2	12	2.5	9.8	4.574	4.280	1.090	0.98
C-3			13.6			1.114	0.97
V-1		2.5	34.8	1.297	3.598	1.259	0.99
V-2	12	5	36.7	4.574	4.279	1.273	0.98
V-3		10	36.1	16.96	5.089	1.269	0.98
L-1	3		21.6			1.167	0.97
L-2	6		24.0			1.183	0.96
L-3	12		24.0			1.183	0.99
L-4	14	2.5	24.3	1.297	3.598	1.185	0.97
L-5	17		22.0			1.170	0.98
L-6	19		22.0			1.170	0.98

*axial dispersion coefficient calculated from Eq (2.43) described in Chapter 2.

**external mass transfer coefficient calculated from Eq (2.45)) described in Chapter 2. ***homogeneous surface diffusivity calculated from batch kinetics (Ahmad et al., 2012)

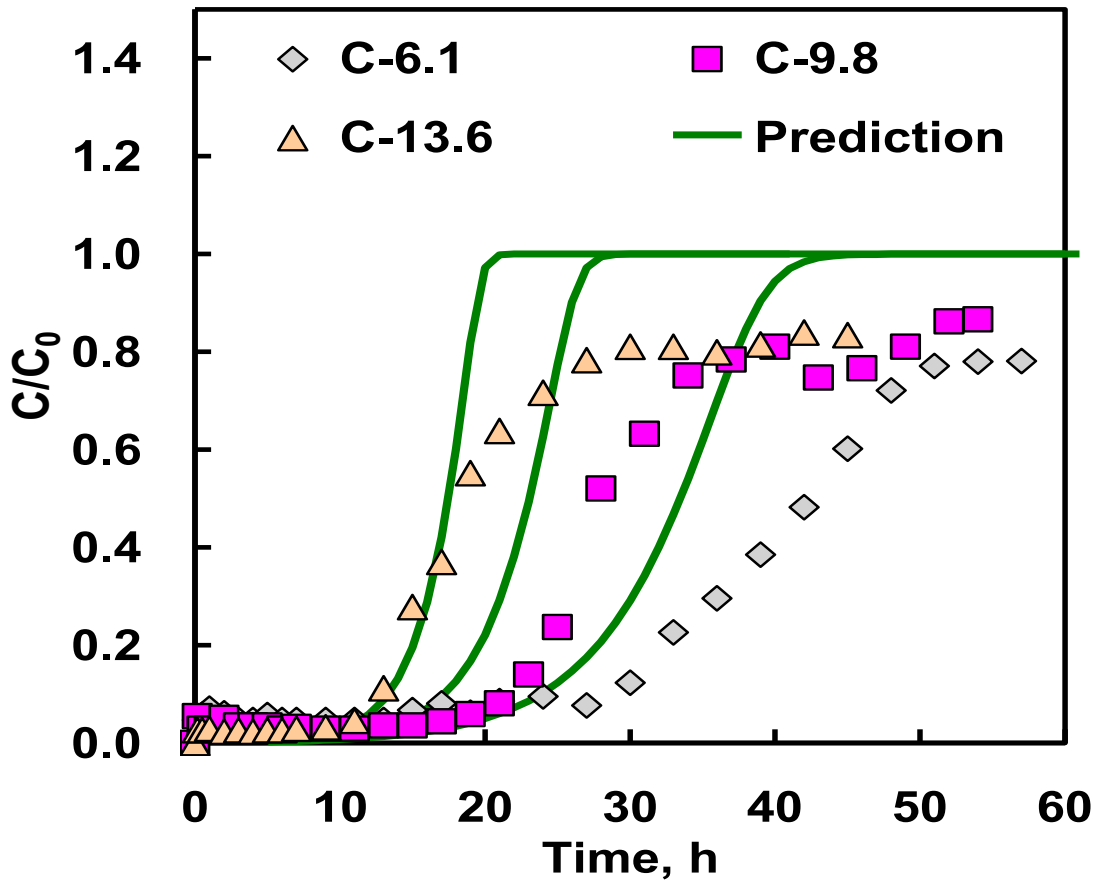

Figure 6.7. Effect of inlet P concentration on the adsorption breakthrough curves for Purolite FerrIX A33E (C - 6.1, C – 9.8, C – 13.6 represent P concentrations of 6.1, 9.8 and 13.6 mg P/L, respectively).

6.3.4.4.3. Effect of filtration velocity

Figure 6.8 shows the effect of filtration velocity (or flow rate) on adsorption breakthrough curves at the constant bed length (12 cm) and similar inlet concentration ranges (35 - 37 mg/l). The shapes of adsorption breakthrough curves were gradually steeper (or sharper) as the filtration velocity increased. The breakthrough time of phosphate also increased with decreasing the filtration velocity. This result can also be explained from the mean retention time given in Eq. (6.5) and the external mass transfer resistance. The slower breakthrough curves of phosphate are evident from Eq. (6.4) when the inlet velocity decreased. However, the higher the inlet velocity, the smaller is the external mass transfer resistance, which lead to the narrower mass transfer zone and the sharper breakthrough curves. The model predicts reasonably well the experimental results as shown in Figure 6.8.

6.3.4.4.4. Sensitive analysis

Sensitivity analysis has been carried out to examine the influence of the core parameters, D_L, k_f and D_s, on the adsorption behaviour. In this work, the reference breakthrough curve was taken from the fixed bed results with an influent concentration of 34.8 mg/l, a bed length of 12 cm, and an influent velocity of 2.5 m/h, respectively. To systematically investigate the pattern of adsorption breakthrough curve, each parameter values were changed between 5 times lower and 5 times greater than that of the reference one. It is clear from Figure 6.9 that the shapes of breakthrough curves for phosphate were highly sensitive to changes in the external mass transfer, k_f. However, the breakthrough curves were slightly sensitive or insensitive to variations in both the axial dispersion, D_L and the intra-particle diffusivity, D_S. These results apparently reveal that the dynamic

adsorption behaviours of phosphate in FerrIX A33E are mainly controlled by the external mass transfer rather than the axial dispersion and the intra-particle diffusion.

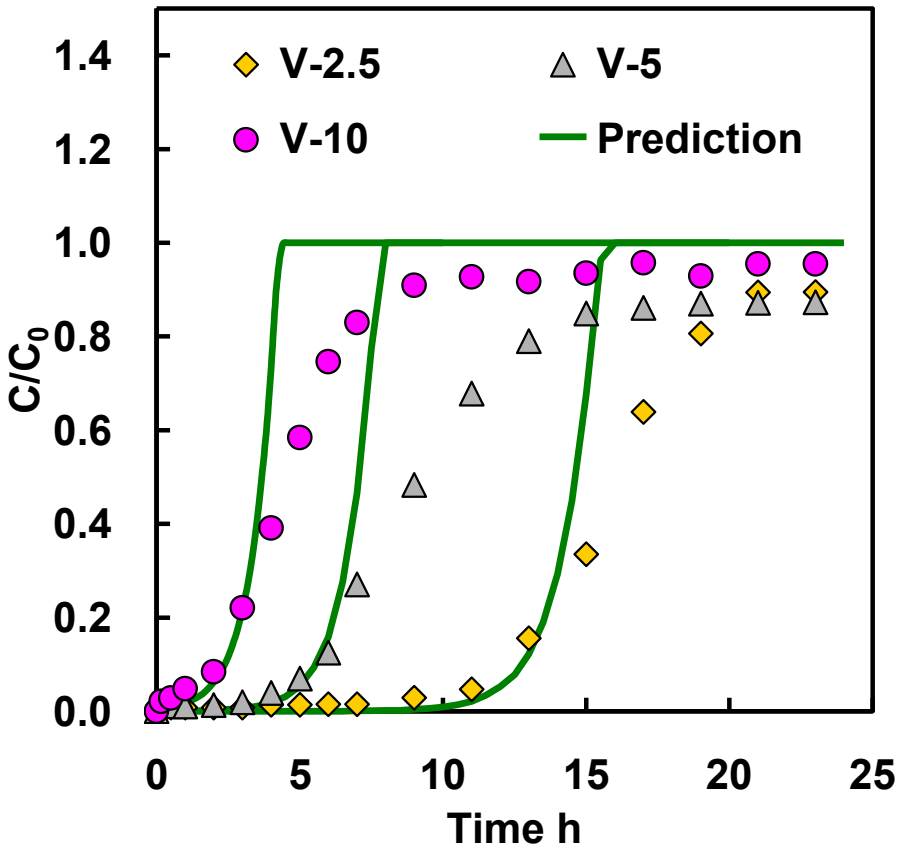

Figure 6.8. Effect of velocity on the adsorption breakthrough curves of Purolite FerrIX A33E (V - 2.5, V - 5.0, V - 10 represent flow velocities of 2.5, 5.0 and 10.0 m/h, respectively).

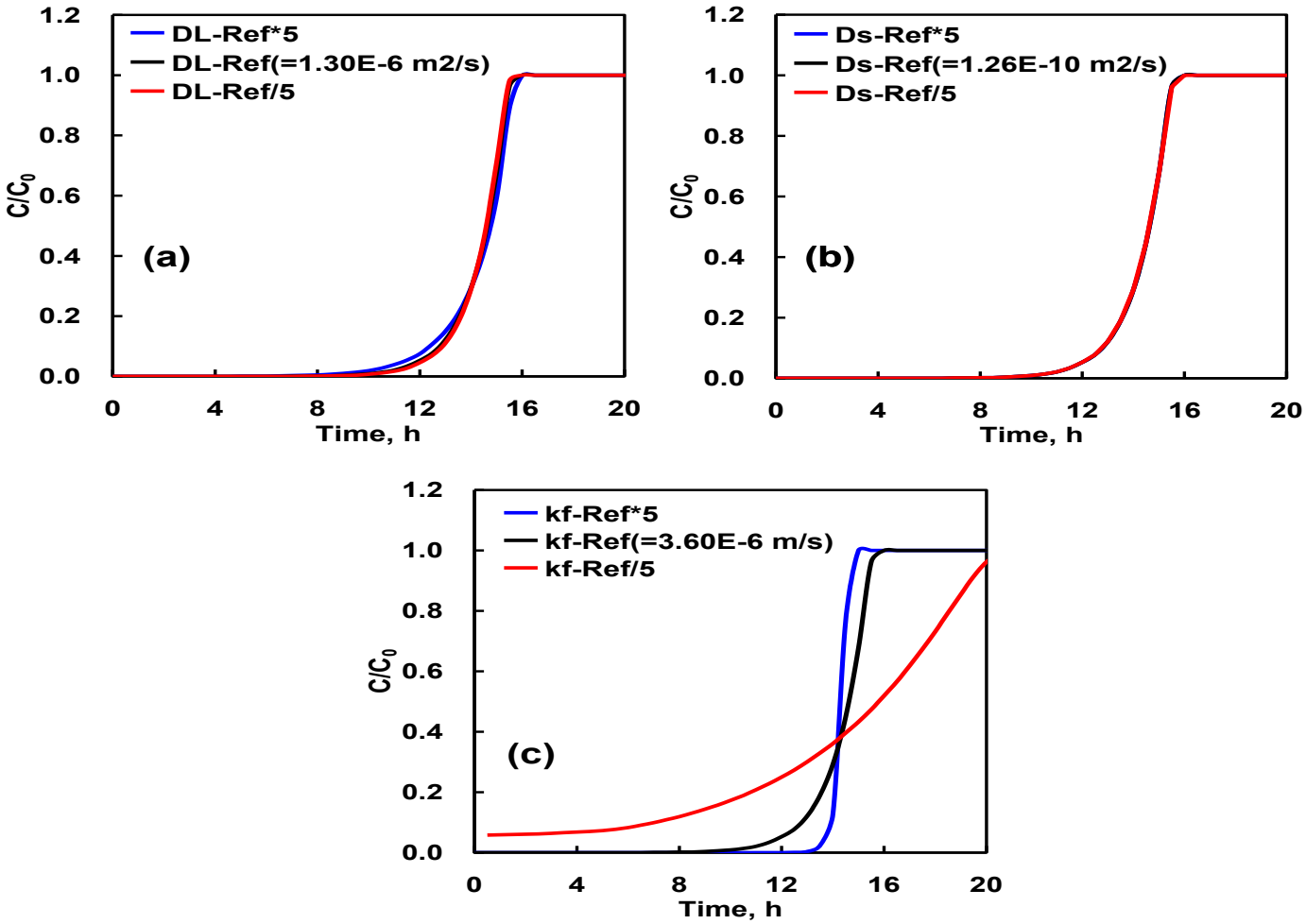

Figure 6.9. Effect of model parameters on the adsorption breakthrough curves of Purolite FerrIX A33E: (a) Axial dispersion, (b) External mass transfer, (c) Homogeneous surface diffusivity.

6.3.5. Regeneration of Purolite FerrIX A33E resin

Among the reagents used for the regeneration of Purolite FerrIX A33E, NaOH was found to be effective in desorbing the phosphate from the column. No detectable phosphate was desorbed using 1 M NaCl, Na_2SO_4 and water. The inability of the high concentrations of Cl^- and SO_4^{2-} in the Na salts in desorbing the phosphate ions from the adsorbent suggests that phosphate ions were specifically adsorbed by inner sphere complexation probably on the Fe oxide component of the adsorbent (Loganathan et al., 2014; , Deliyanni et al., 2007; Genz et al., 2004). This is consistent with the adsorption capacity of the iron oxide in the Purolite resin estimated in Chapter 5 (19/48 mg P/g), which is more than the amount of phosphate adsorbed in the column, suggesting that all the phosphate in the column may have adsorbed to the iron oxide component of the resin.

Only 60-70% of the adsorbed phosphate was desorbed by 0.5 M NaOH whereas 90-95% of the phosphate was desorbed by 1.0 M NaOH in 30 min (42 bed volumes). Approximately 70% phosphate was desorbed within 10 min (14 bed volumes). The regenerated adsorbent was tested for reuse after every adsorption-desorption cycle using fresh 1M NaOH for each desorption cycle (Figure 6.10). The results showed that the efficiency of phosphate adsorption-desorption was nearly the same for two cycles and dropped a little in the third and fourth cycle. The decline in efficiency of adsorption/desorption was within 56%, indicating that the Purolite resin has good potential to adsorb phosphate and is reusable for at least three times and for the fourth cycle it was about 38%. From this result, it could be concluded that the Purolite FerrIX A33E can be used at least four times because the adsorption capacity after four cycles was quite good comparing other phosphate adsorbents (Table 5.3, Chapter 5). Further studies need to be conducted for higher number of adsorption/ desorption cycles to

determine the number of such cycles that can be performed without significantly reducing the adsorption capacity.

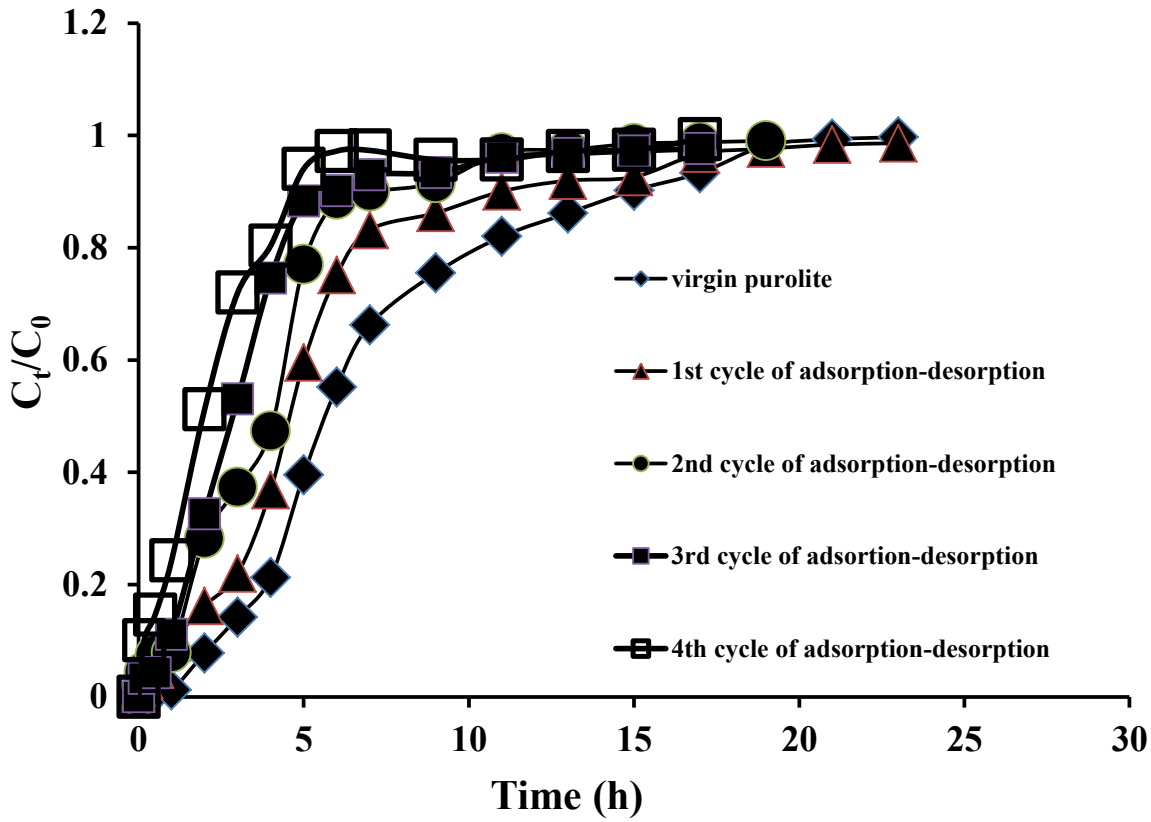

Figure 6.10. Breakthrough curves for phosphate desorption by 1 M NaOH in the column adsorption experiment (bed height 12 cm, initial concentration 30 mg P/L, filtration velocity 10 m/h) for fourth adsorption-desorption cycles of Purolite FerrIX A33E.

6.3.6. Recovery of desorbed phosphate

The effect of different concentrations of $CaCl_2$ added to the solution containing the desorbed phosphate on the reduction in solution concentration of phosphate is shown in Figure 6.11. The results showed that increase in $CaCl_2$ concentration decreased solution phosphate concentration, indicating that phosphate had been precipitated probably as calcium phosphate. Kuzawa et al. (2006) showed that addition of $CaCl_2$ to desorbed phosphate solution can form calcium phosphate and hydroxyapatite compounds which have good fertiliser value. Midorikawa et al. (2008) also proposed a phosphate removal and recovery system with recycling of the alkaline desorbing solution similar to the method reported by Kuzawa et al. (2006). Recently this system was successfully tested in pilot plants in Japan and the United States (Midorikawa et al., 2008; Fitzpatrick et al., 2011). If phosphate removed from the water is economically recovered, it can partly overcome the perceived future scarcity of P when natural phosphate rock reserves will be exhausted (Loganathan et al., 2014).

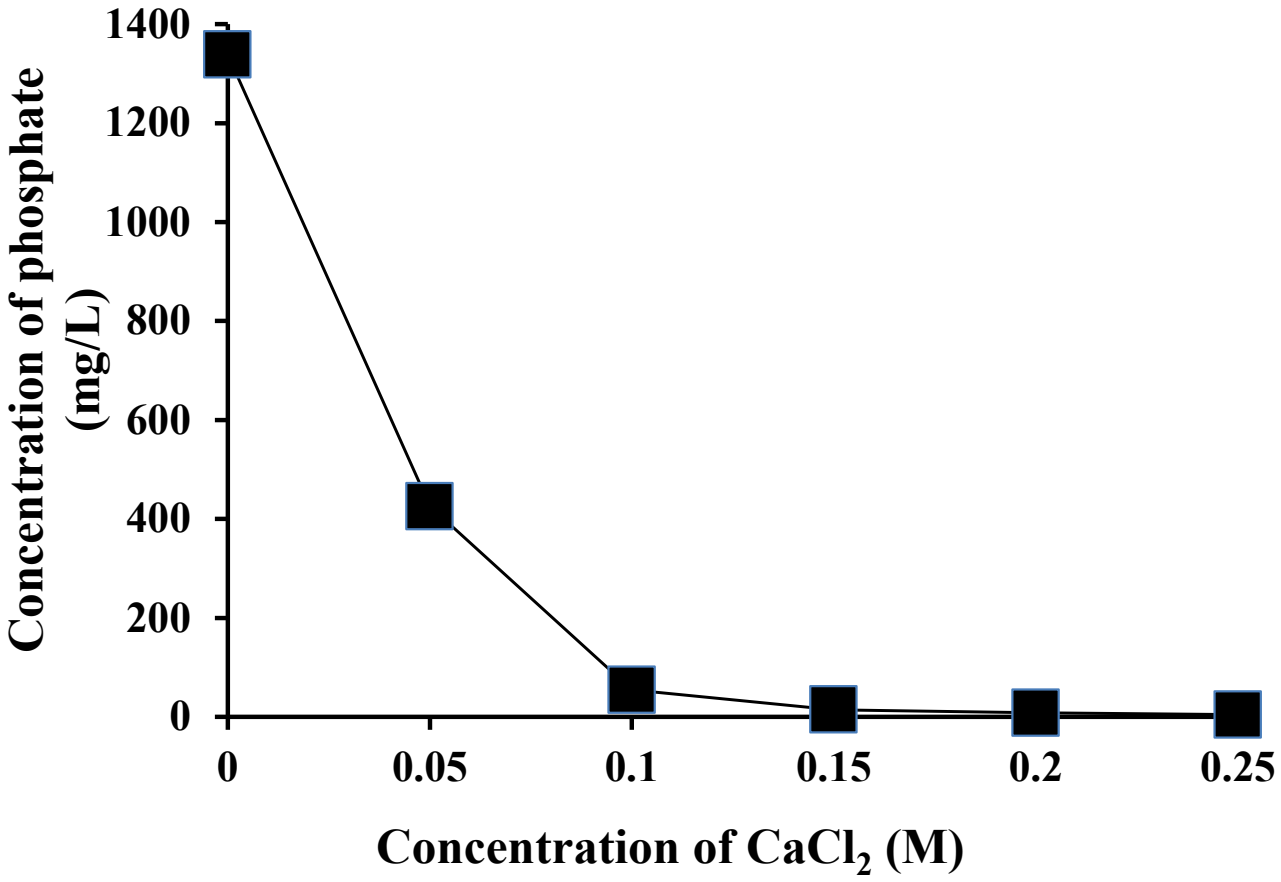

Figure 6.11. Supernatant concentrations of phosphate after $CaCl_2$ addition to the solution obtained by 1M NaOH leaching of Purolite FerrIX A33E resin after phosphate adsorption.

6.4. Conclusions

Fixed-column experimental results showed that Purolite FerrIX A33E is a potential adsorbent for removing phosphate from aqueous solutions compared with two other adsorbents. Three empirical models, Bohart-Adams, Thomas and Yoon-Nelson models and a numerical model based on advection-dispersion equation satisfactorily described phosphate adsorption behaviour in a fixed-bed column containing Purolite FerrIX A33E. The phosphate adsorption capacity of the column was estimated by Thomas model to be 22.7 mg P/g and by breakthrough curve calculation to be 16.3 mg/g at the inlet concentration of 30 mg P/L, 12 cm bed height and 10 m/h filtration velocity. The Purolite FerrIX A33E resin could be regenerated by leaching the adsorbed phosphate with 1 M NaOH solution and reused for at least four times without significantly reducing the adsorption capacity. Finally, phosphate could be recovered from the exhausted desorption solution as calcium phosphate by adding $CaCl_2$. Therefore, it can be concluded that Purolite FerrIX A33E is a potential adsorbent and can be used in a cost effective manner to remove phosphate from water.

CHAPTER 7

PHOSPHORUS RECOVERY AS STRUVITE AND HYDROXYAPATITE

Chapter 7

Phosphorus recovery as struvite and hydroxyapatite

7.1. Introduction

As discussed in Chapter 2, the recovery of phosphorus from phosphorus-containing wastewater is essential for developing an alternative source that can help overcome the global challenge of phosphorus scarcity. The technology to help remove phosphorus from wastewater consists of reusable compounds such as struvite ($MgNH_4PO_4 \cdot 6H_2O$) and hydroxyapatite [$(Ca_{10}(PO_4)_6(OH)_2$] which have attracted considerable research interest as both of them have been identified as fertilisers. The best way to capture phosphorus from wastewater is to use adsorbents with high phosphorus capacity in a fixed-bed or column-type configuration and then desorb the adsorbed substance using NaOH. The desorbed solution containing a high concentration of phosphorus can be converted into struvite and hydroxylapatite (Cordell, 2011; Loganathan et al., 2014). Very few studies have reported the recovery of phosphate through the adsorption process using wastewater (Sengupta and Pandit, 2011). Wendling et al. (2012) added $Ca(NO_3)_2.4H_2O$ or a mixture of $MgSO_4.7H2O$ and NH_4Cl to a solution containing phosphate desorbed from an anion exchange resin and recovered the phosphorus either as high-purity $Ca_3(PO_4)_2$ or struvite ($MgNH_4PO_4$) fertiliser.

Struvite precipitation has in the past decade become increasingly important as a method of phosphorus recovery (Doyle et al., 2003). Struvite has been commercialised in Japan as a fertiliser for growing rice and vegetables (Ueno and Fujii, 2001). Struvite

formation depended on the influence of pH of crystallisation, mixing energy, induction time, molar ratio of the metal constituents and temperature (Le Corre et al., 2009).

Depending on the solution composition and pH, and the molar ratio of calcium and phosphate following the addition of lime to wastewater, several different calcium phosphates may be formed including: hydrated dicalcium phosphate, monetite, octacalcium phosphate, amorphous calcium phosphate, hydroxyapatite and tricalcium phosphate. Considering the results of both phosphorus solubility in 2% citric acid and phosphorus uptake from phosphorus containing minerals contained in ryegrass, phosphorus availability to plants is expected to decrease in the following order: hydrated dicalcium phosphate > hydroxyapatite > hydrated tricalcium phosphate > apatite (Romer, 2006).

Very few studies have been reported on precipitation of struvite and hydroxyapatite from phosphorus desorbed after removing phosphorus from wastewaters using adsorbents. This chapter presents a study on the recovery of phosphorus as struvite and hydroxyapatite from solutions containing phosphorus which was desorbed from an iron oxide impregnated with a strong base anion exchange resin, Purolite FerrIX A33E. This resin was employed earlier to remove phosphorus from water via the adsorption process. The adsorption of phosphate by this ion exchange resin was described in Chapter 6. After adsorption of phosphate, the resin was regenerated by desorbing the adsorbed phosphate using 1M NaOH.

The objectives of this study presented in this chapter were to: (i) develop a suitable method for struvite and hydroxyapatite formation that considered the effects of molar ratio of the chemical elements, pH, temperature and experimental duration for; (ii) investigate the feasibility of struvite and hydroxyapatite formation from phosphorus

desorbed from the Purolite FerrIX A33E used to remove phosphorus from water; and (iii) characterise the recovered struvite and hydroxyapatite materials using XRD, FTIR and chemical analysis.

7.2. Material and methods

7.2.1. Struvite precipitation

A series of batch investigations were conducted examining the influence of a number of chemical factors on struvite crystallisation. Magnesium chloride ($MgCl_2.6H_2O$), ammonium sulphate ($(NH_4)_2SO_4$) and monopotassium phosphate (KH_2PO_4) were mixed in de-ionised water to obtain phosphate, ammonium and magnesium in molar ratios of 1:0.5:0.5, 1:1:0.5, 1:0.5:1, 1:1:1, 1:1:2, 1:2:1, 1:0.5:2, 1:2:0.5 and 1:2:2. All reagents used were of Analar grade. The experiments were conducted in a set of glass flasks containing 200 mL of solution and the solutions were agitated in a flat shaker at a shaking speed of 150 rpm for 3 h at room temperature (24 ± 1^{o}C). During the struvite reaction, the pH of the samples was adjusted to the desired value by adding sodium hydroxide (NaOH). When the reaction time had elapsed the pH was measured and the precipitate that had formed was collected by filtration through a 0.2 mm membrane filter. The precipitates were kept in an oven to dry at 40°C, 100°C or at air temperature for 24 h.

After creating the best scenario for struvite formation out of the above experiments, the experiments were repeated using the best conditions to produce struvite from the regeneration solution obtained from the column adsorption experiment that utilised Purolite FerrIX A33E. The phosphate was enriched through the adsorption process was

then desorbed by NaOH and recovered as struvite ($NH_4MgPO_4.\ 6H_2O$) by adding magnesium chloride ($MgCl_2.6H_2O$), and ammonium sulphate ($(NH_4)_2SO_4$).

7.2.2. Hydroxyapatite precipitation

A series of batch investigations examined the influence of a number of chemical factors on hydroxyapatite precipitation. Calcium hydroxide ($Ca(OH)_2$) and monopotassium phosphate (KH_2PO_4) were added to obtain the required phosphorus to calcium molar ratios of 1:0.2, 1:0.5, 1:1, 1:2 and 1:3. All reagents used were of Analar grade. The experiments were conducted in a set of glass flasks containing 150 mL of solution and the solutions were agitated in a flat shaker at a shaking speed of 150 rpm for 3 h at room temperature (24 ± 1°C). The pH of the solutions ranged from 6.7 to 7.0. The precipitate formed was collected by filtration through a 0.2 mm membrane filter and dried at room temperature for 24 h.

The best scenario for creating hydroxyapatite obtained in the earlier experiments was used to produce hydroxyapatite from the regeneration solution obtained from the column adsorption experiment using Purolite FerrIX A33E. The enriched phosphate gained through the adsorption process was then desorbed by the regeneration solutions and recovered as hydroxyapatite by adding calcium hydroxide ($Ca(OH)_2$).

7.2.3. Total phosphorus in struvite and hydroxyapatite

Total phosphorus in struvite and hydroxyapatite was measured by placing 0.1- 0.7 g of precipitate samples in a set of beakers containing 100 – 200 ml of 1% (w/w) nitric acid solution and agitating the suspension in a magnetic stirrer for 30 min at room

temperature (24 ± 1°C). Concentrations of phosphate in aqueous samples were measured after filtration through a 0.2 mm membrane filter.

7.2.4. Citric acid solubility of struvite and hydroxyapatite

Citric acid solubility of hydroxyapatite was determined by placing 0.30 g recovered materials in a set of glass flasks containing 100 mL of 2% (w/w) citric acid solution and agitating the suspensions in a flat shaker at a shaking speed of 120 rpm for 2 h at room temperature (24 ± 1°C). Concentrations of phosphate in aqueous samples were measured after filtration through a 0.2 mm membrane filter.

7.2.5. Chemical analysis

The phosphate concentration in solutions was measured using a Metrohm ion chromatograph (model 790 Personal IC) equipped with an auto sampler and conductivity cell detector. Separation of anions was achieved using an A SUPP column 3 (150 mm x 4 mm). Na_2CO_3 (3.2 mmol/L) and $NaHCO_3$ (1.0 mmol/L) were used as mobile phase with a flow rate of 0.9 mL/min. The concentration of calcium and magnesium were measured employing Microwave Plasma - Atomic Emission Spectroscopy. Measuring the ammonium concentration was carried out using the cell test method (Spectroquant, Merck) and a photometer (NOVA 60, Merck). The pH was measured using a HQ40d portable pH Meter.

7.2.6. Characterisation of recovered materials

Dried precipitate produced in the experiments was examined using X-ray diffraction (XRD) and Fourier transform infrared (FTIR) spectroscopy analysis. X-ray diffraction (XRD) was conducted with a XRD Shimadzu S6000 (Japan) diffractometer on powder samples of the dried precipitate. The X-ray diffraction unit (Theta/2Theta) was equipped with a Cu target operated at 40 kV and 30 mA with a setting of 5-45° 2-theta, step time 2° min-1, 25° C. FTIR pattern was recorded using: a Nicolet 6700 FT-IR Spectrometer equipped with a room temperature DLaTGS detector; and a Nicolet FT-IR Smart System with Smart Accessories using a Diamond crystal HATR.

7.3. Results and discussion

7.3.1. Struvite production

7.3.1.1. Effect of pH

To determine the effect of pH on struvite production in synthetic water, an experiment was conducted at two different pHs (7.0 and 9.5). No precipitation was formed at pH 7.0 when magnesium and ammonium salts were added to phosphate solution. However, at pH 9.5 significant amounts of precipitates were found (Table 7.1). This result is similar to those documented in previous studies which stated that the formation of struvite generally rose above pH 9.0 and decreased below pH 9.0 (Doyle et al., 2002). Therefore, the pH was fixed for the rest of the experiments at 9.5. Increased precipitate at higher pHs is due to the de-protonation of HPO_2^- at high pHs, $H_2PO_4^-$ and H_3PO_4 species are favoured at higher pH levels. Hence, the availability of free phosphate

ions increases when pH also increases, which leads to more supersaturation of magnesium ammonium phosphate (Seckler et al., 1996).

7.3.1.2. Effect of experimental duration

Two sets of experiments were done at two different shaking periods, these being 3 h and 5 h. The results showed that the phosphate contents of the precipitates formed were almost the same at the two durations (Table 7.1). For this reason the shaking period was fixed at the smaller duration time of 3 h for all subsequent experiments.

7.3.1.3. Effect of drying method

Three sets of experiments were carried out at different drying temperatures (air drying, 40ºC and 100ºC). After drying the precipitates the phosphate contents were measured and it emerged that the best scenario for struvite precipitation was drying at 40ºC in an oven for 24 h (Table 7.1).

7.3.1.4. Effect of mixing speed

Two sets of experiments were done at two different shaking speed, these being 100 rpm and 150 rpm. The results showed that the phosphate contents of the precipitates formed were highest for the 150 rpm (Table 7.1). For this reason the shaking speed was fixed at 150 rpm for all subsequent experiments.

7.3.1.5. Effect of molar ratio

Previous studies have demonstrated that the molar concentration of phosphate, ammonium and magnesium played an important role in struvite formation (Ohlinger et al., 1998; Uludag-Demirer and Othman, 2009). Nine molar ratios of phosphate, ammonium and magnesium (1:0.5:0.5, 1:1:0.5, 1:0.5:1, 1:1:1, 1:1:2, 1:2:1, 1:0.5:2, 1:2:0.5 and 1:2:2) were used in the experiment and the concentrations of phosphate, ammonium and magnesium in the precipitate formed are presented in Figure 7.1 and Table 7.2.

The concentration of phosphate was fixed to be equal to the concentration in the regeneration solution obtained in the Purolite FerrIX A33E adsorption experiment (Chapter 6). Only the molar ratio of ammonium and magnesium was changed to determine the effect of the chemical constituents' molar ratio on struvite formation. It was discovered that the concentrations of phosphate, ammonium and magnesium were highest at the molar ratio of 1:1:1 which proved to be very similar to the theoretical composition of struvite (Durrant et al., 1999). When the magnesium concentration declined compared to those for phosphate and ammonium, the concentration of phosphate in the struvite precipitate also decreased. On the other hand, the concentration of recovered phosphate in the precipitate increased with the molar concentration of magnesium which is similar other reported results (Mùnch and Burr, 2001; Uludag-Demirer, 2008; Liu, 2009).

On the other hand, the increase in the molar ratio of ammonium to phosphate and magnesium had very little effect on the concentration of phosphate in the struvite. High purity struvite was formed at an initial molar ratio of ammonium to phosphate of 1:1 which was also similar to the results reported in the literature (Uludag-Demirer and Othman, 2009).

7.3.1.6. Struvite precipitation from regeneration solution of adsorption experiment

After considering all the results from the above experiments, the experiment on struvite formation from regeneration solution of Purolite FerrIX A33E was done at the molar concentration ratio of phosphate, ammonium and magnesium of 1:1:1 at pH 9.5 in a batch experiment for 3h. After the experiment the precipitate was dried in an oven at 40º C for 24 h. The concentrations of phosphate, ammonium and magnesium in the precipitate are presented in Table 7.3. They are 41.73%, 10.95% and 12.61%, respectively which closely matched the theoretical composition of struvite of phosphate, ammonium and magnesium (38.8%, 7.3% and 9.8%), respectively (Durrant et al., 1999).

Table 7.1. Effect of experimental conditions on the phosphorus content (mean ± standard errors) in the recovered precipitate of struvite (initial concentrations of PO_4^{3-}: NH_4^+: Mg = 0.066 M: 0.066 M: 0.066 M).

Different parameters	pH		Experimental duration		Drying temperature			Mixing speed	
	7.0	9.5	3 h	5 h	Air temperature	Oven dry 40º C	Oven dry 100º C	100 rpm	150 rpm
Phosphorus content (%)	No precipitate	12.5 ± 0.24	12.5 ± 0.24	12.6 ± 0.24	9.1 ± 1.37	12.5 ± 0.24	9.2 ± 0.05	8.9 ± 0.12	12.2 ± 0.05

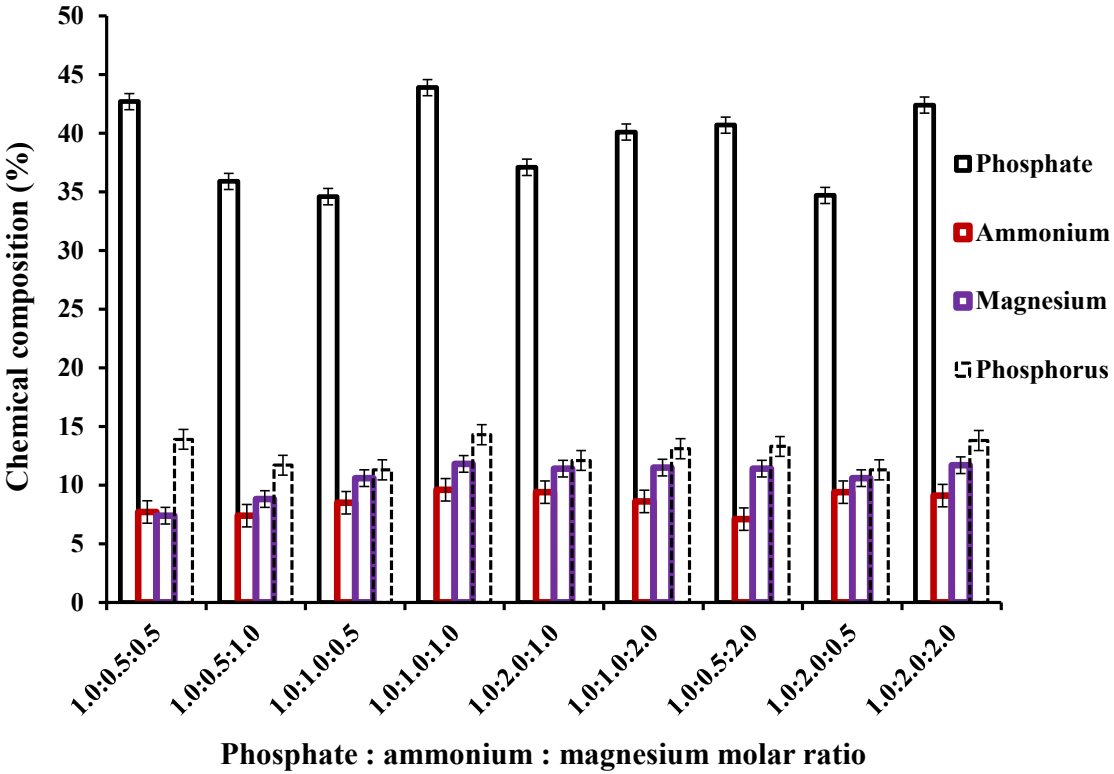

Figure 7.1. Chemical composition of the recovered struvite at different molar ratios of initial phosphate, ammonium and magnesium in synthetic water (The fixed phosphate concentration = 0.066 M).

Table 7.2. . Chemical compositions of the recovered struvite precipitate from the regenerated solution in the Purolite FerrIX A33E adsorption experiment (The initial phosphate concentration 0.02 M).

Molar ratio (PO_4^{3-}:NH_4^+:Mg^{2+})	Chemical composition of the recovered struvite precipitate, wt (%)			
	Phosphate (PO_4^{3-})	Ammonium (NH_4^+)	Magnesium (Mg^{2+})	Phosphorus (P)
1.0:1.0:1.0	41.7 ± 0.29	10.9 ± 0.68	12.6 ± 0.55	14.0 ± 0.78

7.3.1.7. Characterisation of struvite

The XRD pattern of the recovered precipitate is presented in Figure 7.2. The position of the peaks matched well with the standard data of struvite for the position and intensity of the peaks (JCPDS database, No. 3-863 and 21-1272). The peaks reported by others also matched the position and intensity of the peaks for the recovered precipitate (Song et al., 2011; Liu et al., 2011; Foletto et al., 2013; Crutchik et al., 2013). The mean peaks in the experiment were at 2θ = 15.1º, 23.2º, 31.3º and 38.1º (Figure 7.2). Liu et al. (2011), Song et al. (2011), Crutchik et al. (2013) and Foletto et al. (2013) also reported peaks at 2θ = 15.195º, 21.658º, 32.141º and 38.465º for the struvite they prepared in their experiments.

The FTIR spectra of the recovered precipitate are shown in Figure 7.3. The absorption peak at 3449 cm^{-1} corresponds to the O-H and N-H stretching vibrations reported by Bindu and Thambi (2012). The absorption band corresponding to 1640 cm^{-1} is assigned to N-H bending vibrations and the sharp band corresponding to 1462 cm^{-1} is caused by N-O asymmetric stretching vibration. These bands were also reported for struvite prepared by others (Kurtus and Tas, 2011; Bindhu and Asai Thambi, 2012). Chauhan and Joshi (2008 and 2011) also obtained peaks at the same wavelengths for struvite in their experiments. The absorption peak occurring at 1063 cm^{-1} is assigned to ionic phosphate and those at 882 cm^{-1} are assigned to ammonium – water H bonding, which was similar to the results obtained by Kurtus and Tas, (2011) in their struvite experiments.

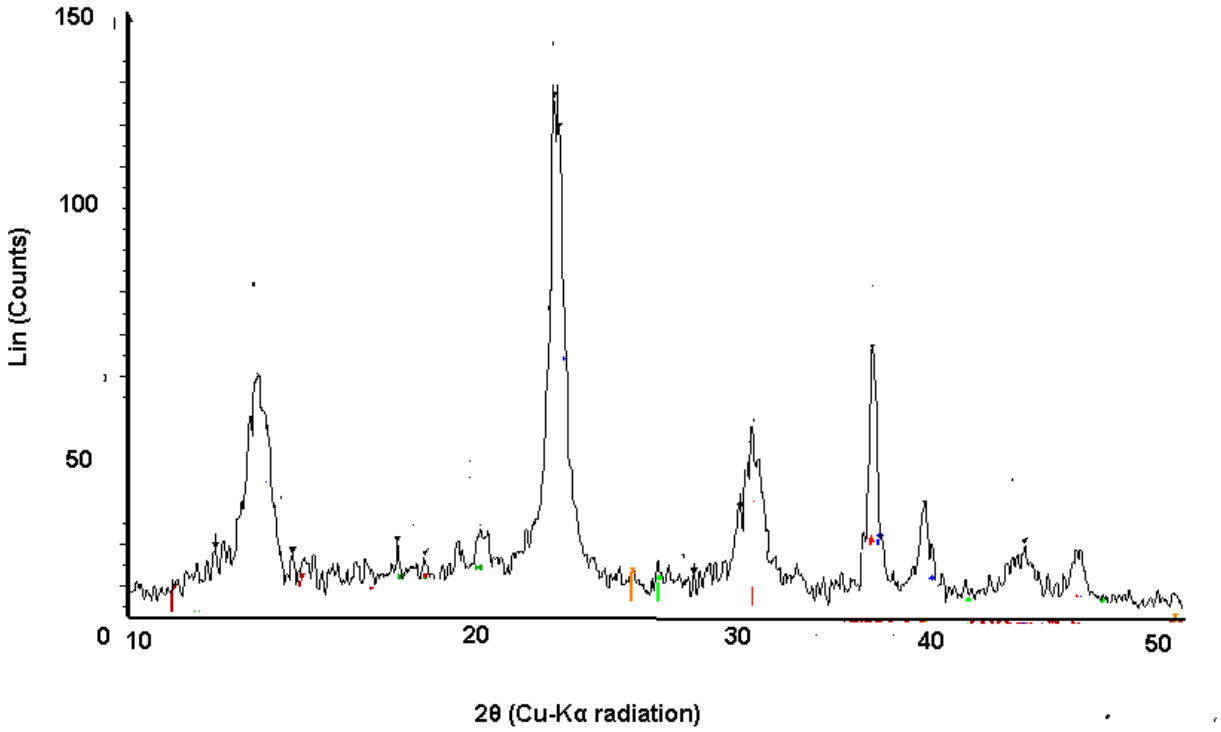

Figure 7.2. XRD pattern of precipitated struvite.

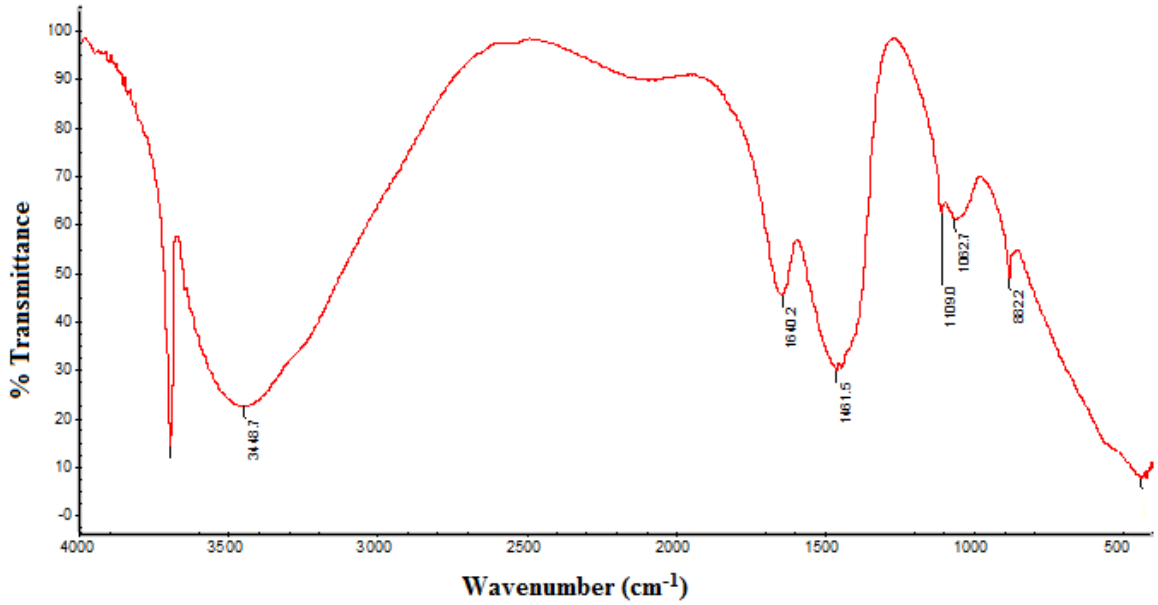

Figure 7.3. FTIR spectra of precipitated struvit

7.3.2. Hydroxyapatite production

7.3.2.1. Effect of experimental duration

Hydroxyapatite experiments were conducted at two different shaking periods of 3 h and 5 h. The results showed that the phosphate concentration of the two precipitates was almost the same at the two durations (Table 7.4). For this reason the shaking period was fixed at the smaller duration of 3 h for future experiments.

7.3.2.2. Effect of drying temperature

Three sets of experiments were carried out at different drying temperatures, namely air drying, oven drying at 40ºC and 100ºC, and all for duration of 24 h. After drying, the phosphate concentrations of all precipitates were measured and it was found that the highest phosphate content was obtained for the hydroxyapatite precipitation at air temperature (Table 7.4).

7.3.2.3. Effect of mixing speed

Two sets of experiments were done at two different shaking speed, these being 100 rpm and 150 rpm for the hydroxyapatite production. The results showed that the phosphate contents of the precipitates formed were highest for the 150 rpm (Table 7.2). For this reason the shaking speed was fixed at 150 rpm for all subsequent experiments**.**

7.3.2.4. Effect of molar ratio

To determine the best molar ratio of phosphate and calcium for the precipitation of hydroxyapatite, five molar ratios of phosphate to calcium such as 1: 0.2, 1: 0.5, 1: 1, 1: 2 and 1: 3 were tested in the experiment. The concentrations of phosphate and calcium in the precipitate formed at the various molar ratios are presented in Figure 7.4. The concentration of phosphate was fixed at all the molar ratios, staying similar to that in the regeneration solution of the adsorption experiment. The amount of phosphate and calcium in the precipitate increased gradually in tandem with an increase in the molar ratio. Their ratios were nearly the same, i.e. 1: 0.5 to 1: 3 (see Figure 7.4).

7.3.2.5. Hydroxyapatite precipitation from the adsorption experiment's regeneration solution

Having described the results in the previous section, the experiment on hydroxyapatite formation from phosphate in the regeneration solution of Purolite FerrIX A33E experiment was done at the molar concentration ratio of phosphate to calcium of 1: 0.5 and 1: 2 at pH 7.0. The precipitate formed was dried in an oven at air temperature for 24 h. The amount of phosphate in the precipitate was 45.73% and 39.95% while on the other hand, the calcium content in the recovered materials was 36.95% and 37.23% at the molar ratio 1: 0.5 and 1: 2, respectively (Table 7.6). The phosphorus content of the precipitate was 12.8% and 14.8% for phosphorus to calcium ratio of 1: 0.5 and 1: 2, respectively which are within the range of values reported in the literature for natural phosphate rocks (8.9 - 17.2%) (Loganathan et al., 2003). The citric-soluble phosphorus contents of the precipitates were 41% and 43% of total P, respectively which were higher than the recommended values suggested for reactive phosphate rock (< 30%, Bolan et al.,

1993), indicating that the precipitate could be used as a phosphate fertiliser (FAO, 2004). These values suggest that the recovered precipitate has potential to be used as a fertiliser precursor.

Table 7.3. Effect of experimental conditions on the phosphorus content (mean ± standard errors) in the recovered precipitate of hydroxyapatite (initial PO_4^{3-}: NH_4^+: Mg = 0.066 M: 0.066 M: 0.066 M).

Different parameters	Experimental duration		Drying temperature			Mixing speed	
	3 h	5 h	Air temperature	Oven dry 40º C	Oven dry 100º C	100 rpm	150 rpm
Phosphorus content (%)	11.4 ± 0.49	11.9 ± 0.67	11.4 ± 0.49	9.8 ± 0.96	10.1 ± 0.85	8.4 ± 0.49	11.4 ± 0.49

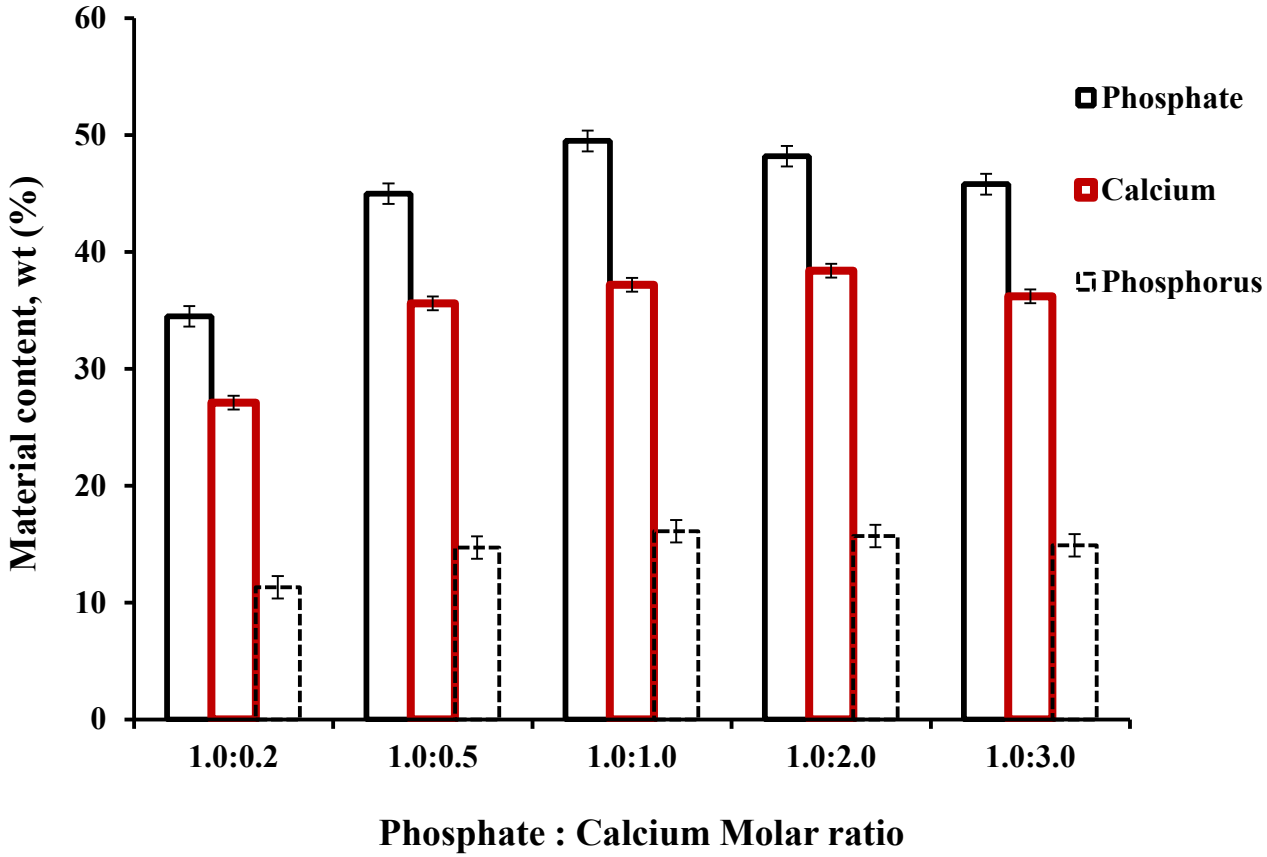

Figure 7.4. Chemical composition of the recovered hydroxyapatites at different molar ratios of initial phosphate to calcium (The fixed phosphate concentration = 0.066 M).

Table 7.4. Chemical compositions of the recovered precipitate (mean ± standard errors) for the precipitation of hydroxyapatite from the regenerated solution of Purolite FerrIX A33E (The initial phosphate concentration 0.02 M)

Molar ratio Phosphate : Calcium (PO_4^{3-} : Ca)	Chemical composition of struvite precipitate, wt (%)		
	Phosphate (PO_4^{3-})	Calcium (Ca^{2+})	Phosphorus (P)
1.0: 0.5	45.2 ± 0.38	37.1 ± 0.67	14.7 ± 0.58
1.0: 2.0	39.2 ± 0.78	38.2 ± 0.95	12.8 ± 0.89

7.3.2.6. Characterisation of hydroxyapatite

Figure 7.5 presents the X-ray diffraction (XRD) patterns of the recovered precipitate. The diffraction lines matched with those characteristics of hydroxyapatite (Midorikawa et al., 2008; Mobasherpour et al., 2007; Bayraktar and Tas, 1999; Ungureanu et al., 2011; Sobczak et al., 2009) and those from the standard database (ICDD PDF No.: 9-432 for $Ca_{10}(PO_4)_6(OH)_2$). The XRD patterns indicated that hydroxyapatite was the only crystalline phase and no impurity peak was observed in the recovered materials. The major phase, as expected, was hydroxyapatite, which was further confirmed by comparing data obtained with the ICDD - PDF2 card: 00-009-0432 (The International Centre for Diffraction Data, 2013). The main peaks in the experiment were at $2\theta = 25.1^{\circ}$, 39.5° and 53.3° (Figure 7.2). Midorikawa et al. (2008), Mobasherpour et al. (2007), Bayraktar and Tas (1999), Ungureanu et al. (2011), and Sobczak et al. (2009) also reported peaks at $2\theta = 28.195^{\circ}$, 32.85°, 39.73° and 52.16° for the hydroxyapatite they prepared in their experiments.

The FTIR spectra of the recovered material is presented in Figure 7.6 and it is quite similar to previous results reported for hydroxyapatite (Prakash et al., 2006; Sammons et al., 2007; Furuzono et al., 2001; Palard et al., 2008). As observed in Figure 7.6, one of the most intensive bands 1038 cm^{-1} is in the range of 1047–1095 cm^{-1} which corresponded to the stretching vibration mode of P - O which was also reported by Prakash et al. (2006), Sammons et al. (2007), Furuzono et al. (2001) and Palard et al. (2008) in their hydroxyapatite experiments. These researchers also reported that the band at the wavelength around 601-561 cm^{-1} in this experiment was due to the O–P–O bonds, whereas a small band at around 470 cm^{-1} is ascribed to the O-P-O bending mode. The low-intensity bands at 1427 cm^{-1} observed for the material obtained in the preliminary

calcination could correspond to the stretching vibrations of CO_3^{2-}. The broad asymmetric bands in the range of 3431 to 3010 cm^{-1} together with an absorption band centred at approximately 1634 cm^{-1} are assigned to the presence of adsorbed water molecules on the hydroxyapatite crystallite surface (Palard et al., 2008; Kannan et al., 2005).The absorption band at around 874 cm^{-1} has also been assigned to the presence of CO_3^{2-} substitution which was also noted by Siddharthan et al. (2005), Raynaud et al. (2002) and Heughebaert (1977).

Raynaud et al. (2002) reported that the band at 875 cm^{-1} was due to the presence of HPO_4^{2-}, which suggested the formation of calcium deficient hydroxyapatite.

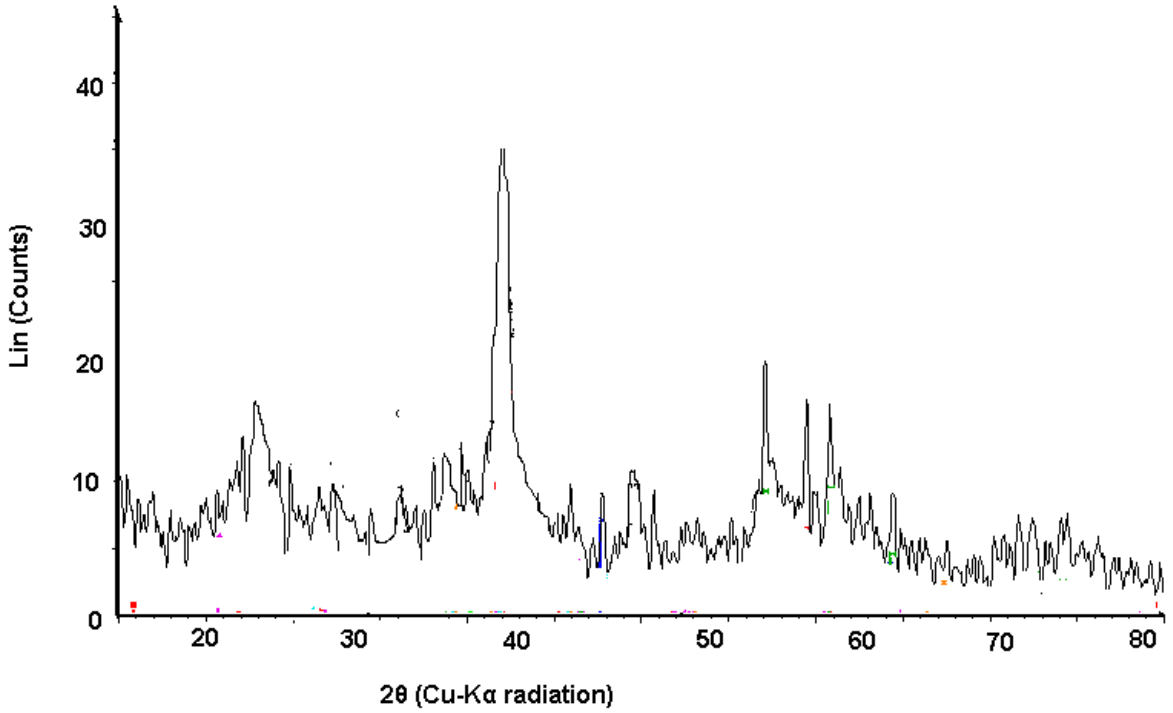

Figure 7.5. XRD pattern of precipitated hydroxyapatite

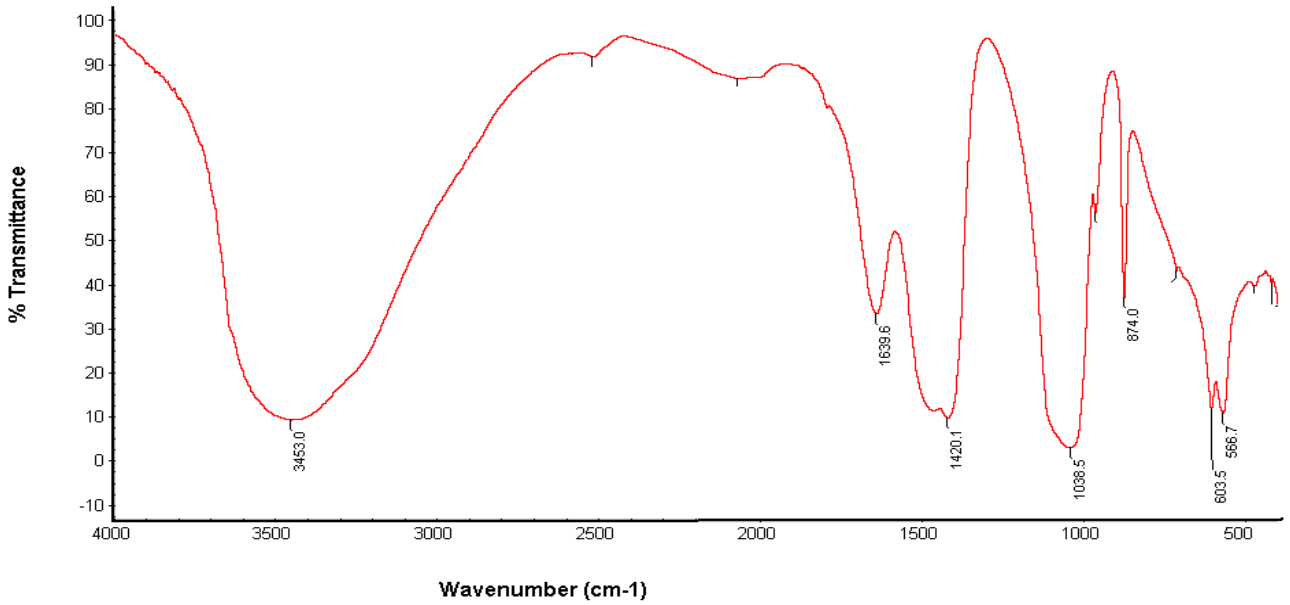

Figure 7.6. FTIR spectra of precipitated hydroxyapatite

7.4. Conclusions

Struvite precipitation was obtained by the reaction of magnesium chloride ($MgCl_2.6H_2O$), ammonium sulphate ($(NH_4)_2SO_4$) and monopotassium phosphate (KH_2PO_4). The effects of varying reaction conditions such as molar ratio of phosphate, ammonium and magnesium, pH, duration of reaction and drying temperature of the precipitate were important. They showed that the optimum conditions as assessed by the highest P content of the precipitate were molar ratio of phosphate, ammonium and magnesium of 1:1:1 at pH 9.5 and drying method at 40ºC in an oven.

In an earlier experiment described in Chapter 6, Purolite FerrIX A33E resin was used to remove phosphorus from water and the exhausted adsorbent was regenerated by leaching the adsorbed phosphorus with 1 M NaOH solution, which resulted in a substantial amount of phosphorus in the regeneration solution. This phosphorus was recovered from the exhausted desorption solution as struvite at the molar ratio of phosphate, ammonium and magnesium of 1:1:1 at pH 9.5 and drying temperature at 40ºC for 24 h. The XRD and FTIR analysis confirmed the recovered precipitate existed as pure struvite. The phosphorus content of the precipitate was 12-14% which was similar to the phosphorus content of commercial struvite. It can be concluded from these results that the recovered struvite is usable as a phosphate fertiliser.

Phosphorus was also recovered from the exhausted desorption solution as hydroxyapatite at the molar ratio of phosphate to calcium of 1: 0.05 and 1: 2 at pH 7.0 and drying at air temperature for 24 h. The XRD and FTIR analysis confirmed the recovered precipitate as pure hydroxyapatite. The phosphorus content of the precipitate was 12-14% which was similar to the phosphorus content of commercial hydroxyapatite.

Both struvite and hydroxyapatite produced from the regeneration solution satisfactorily matched with the corresponding commercial fertilisers. The technique developed in this study needs to be tested in pilot plant scale. If this proves to be successful it can potentially be applied to commercial scale production of phosphate fertilisers from waste water. This may help alleviate future global shortages of phosphorus.

CHAPTER 8

FLUORIDE ADSORPTION USING A HYDROUS FERRIC OXIDE

Chapter 8

Fluoride adsorption using a hydrous ferric oxide*

8.1. Introduction

It was discussed earlier in Chapter 2 that fluoride contamination of drinking water is one of the world's most serious health problems (Amini et al., 2008; WHO, 1996). A low concentration of fluoride in drinking water (0.4–1.0 mg/L) has beneficial effects on teeth especially for young children as it promotes calcification of dental enamel and protects teeth against tooth decay. On the other hand, excessive intake of fluoride leads to various diseases such as osteoporosis, arthritis, brittle bones, cancer, infertility, brain damage, Alzheimer syndrome and thyroid disorder (Chinoy,1994; Harrison, 2005; Tripathy et al., 2006). Owing to these adverse effects, the World Health Organization (WHO) has recommended a maximum allowable fluoride concentration of 1.5 mg/L in drinking water (WHO, 1996).

In view of the toxic effects of fluoride on human health, many treatment methods which were discussed in Chapter 2, such as electrodialysis, membrane and adsorption processes and chemical precipitation have been developed for the removal of excess fluoride from drinking water (Bhatnagar et al., 2011b; Loganathan et al., 2013a). Of these methods, adsorption is generally considered to be the most effective and suitable one due to its simplicity, effectiveness and relatively low cost (Bhatnagar et al., 2011b; Loganathan et al., 2013a). As we discussed in Chapter 2, a wide variety of natural and synthetic adsorbents has been tested and applied for the removal of fluoride ions from

***A major part of this chapter was published in "T. Nur, P. Loganathan, T.C. Nguyen, S. Vigneswaran, J. Kandasamy, Batch and column adsorption and desorption of fluoride using hydrous ferric oxide: Solution chemistry and modeling, Chemical Engineering Journal 247 (2014) 93–102".**

aqueous solution (Bhatnagar et al., 2011b; Loganathan et al., 2013a). Of these adsorbents, multivalent metal (Al, Fe, La, Zr) oxides and hydroxides (Loganathan et al., 2013a) and metals incorporated activated carbon (Leyva-Ramos et al., 1999; Daifullah et al., 2007), and calcium phosphate compounds such as bone char (Abe et al., 2004; Leyva-Ramos et al., 2010; Tovar-Gómez et al., 2013) were reported to have high fluoride removal capacities.

Most studies on fluoride removal by adsorbents have been performed in batch experiments and only a few have been reported in fixed bed column systems which are more relevant to real operating systems on natural waters (Bhatnagar et al., 2011b; Loganathan et al., 2013a). Moreover, many previous studies on adsorptive removal of fluoride have not considered desorption of fluoride after the adsorbent is saturated with fluoride. Easy desorption of fluoride is important for multiple reuse of the adsorbent as this reduces operational costs. The species of fluoride in solution and the surface charge on the adsorbent are controlled by solution pH and therefore pH has been reported to influence fluoride adsorption (Kumar et al., 2009; Dey et al., 2004). Natural water contains anions such as $H_2PO_4^{2-}$, PO_4^{3-}, SO_4^{2}-, Cl^-, NO_3^- which can compete with fluoride for adsorption (Loganathan et al., 2013a; Kumar et al., 2009; Dey et al., 2004), therefore in any fluoride removal studies the effect of these co-ions also need to be considered.

The objectives of this research were to: (i) compare the fluoride removal percentages of seven adsorbents expected to have high adsorption capacities and justify the selection of hydrous ferric oxide (HFO) for a detailed study; (ii) model equilibrium and kinetic batch isotherm data of fluoride adsorption; (iii) determine the effect of pH and complementary anions on fluoride adsorption and evaluate the mechanisms of adsorption using zeta potential data; (iv) model the breakthrough curves of fluoride adsorption in

column experiments; and (v) develop a suitable method to regenerate the adsorbent for reuse. The novelty of the research is modelling of fluoride adsorption in fixed-bed column under different experimental conditions by applying an artificial neural network approach and determining the mechanism of fluoride adsorption using solution and solid/solution interface chemistry.

8.2. Material and Methods

8.2.1. Adsorbents

Four ion exchange resins, Purolite A520E, Purolite A502PS, Purolite FerrIX A33E and Dowex 21k and three multivalent metal oxide adsorbents, HFO (iron (iii) oxide $HFeO_2$), Zirconium (IV) hydroxide (H_4O_4Zr) and α-Alumina (Al_2O_3) were used to compare their removal efficiencies of fluoride from water. The basis for the selection of these adsorbents is that a recent review on fluoride adsorption reported that multivalent metal oxides and some ion exchange resins have high fluoride adsorption capacities (Loganathan et al. 2013 a). The characteristics of Purolite A520E, Purolite A500PS, Dowex 21k XLT and Purolite FerrIX were described in Chapter 3, 4 and 5.

These ion exchange resins were reported to have very high adsorption capacities for arsenic or phoaphate (Johir et al., 2011) and therefore they are expected to also have high adsorption capacities for fluoride, since fluoride like arsenate/arsenite and phosphate, is specifically adsorbed (inner-sphere complexation) on many adsorbents (Loganathan et al., 2013a). The Purolite and Dowex resins were obtained from Purolite Company (USA) and Dow chemical company (USA), respectively. The metal oxide/hydroxide adsorbents were obtained from Sigma Aldrich (USA).

8.2.2. Characterisation of adsorbents

X-ray diffraction (XRD) was conducted using a XRD Shimadzu S6000 (Japan) diffractometer on powder samples of the inorganic adsorbents, HFO, zirconium hydroxide and alpha-alumina. The X-ray diffraction unit (Theta/2Theta) was equipped with a Cu target operated at 40 kV and 30 mA with a setting of 5–45° 2-theta, step time 2° min-1, 25 °C. As HFO was used for the detailed adsorption study, scanning electron microscopy (SEM), Fourier transform infrared (FTIR) spectroscopy, surface area, and porosity measurements were conducted only for this adsorbent. For the SEM analysis, the samples were imaged, uncoated, in a Zeiss Evo LS15 SEM using its variable pressure mode and an accelerating voltage of 15 kV. FTIR pattern was recorded using a Nicolet 6700 FT-IR Spectrometer equipped with a room temperature DLaTGS detector and a Nicolet FT-IR Smart System with Smart Accessories using a Diamond crystal HATR. Surface area and porosity were determined by nitrogen-sorption measurements carried out at 77 K with a Micromeritics 3Flex surface characterization analyzer. The BET method was used to calculate the specific surface area. The pore size distribution was derived from the adsorption branch of the isotherm by using the Barrett–Joyner–Halenda (BJH) method

8.2.3. Fluoride analysis

The fluoride analysis was carried out using a Metrohm ion chromatograph (model 790 Personal IC) equipped with an auto sampler and conductivity cell detector. The separation of anions was achieved using an A SUPP column 3 (150 mm x 4 mm). Na_2CO_3 (3.2 mmol/L) and $NaHCO_3$ (1.0 mmol/L) were used as mobile phase with a flow rate of 0.9 mL/min. In the initial experiments the measured fluoride concentrations were

compared with those determined using a Thermo Scientific Orion® 9609BNWP Fluoride Combination Ion Selective Electrode, after addition of Orion 940909 TISAB II solution to the test solutions. As the measured concentrations were not significantly different between the two methods, the ion chromatograph method was used for the rest of the experiments. The reason for selecting ion chromatographic method was that this method was rapid for the analysis of a large number of samples.

8.2.4. Zeta potential measurement

Zeta potential is the electrical potential close to a particle surface where adsorption of ions from solution phase occurs and it is positively related to the surface charge. Higher the positive zeta potential the higher the anion exchange capacity which results in higher amounts of anions such as fluoride adsorption. Suspensions of 1 mg/L HFO in deionised water or 10^{-2} M $NaNO_3$ were prepared and the pH was adjusted from 2.8 to 10 using 0.1 M NaOH or 0.1 M HNO_3 solutions using a HQ40d portable pH Meter Package with PHC 301 pH electrode. The suspensions were agitated in a flat shaker at a shaking speed of 120 rpm at room temperature (24 ± 1^{o}C). The final pH values were measured and zeta potential was measured using a Zetasizer nano instrument (Nano ZS Zen3600, Malvern, UK). For each sample, the instrument automatically made triplicate measurements, and a mean value was recorded. Measurements for zeta potential were undertaken twice for each sample and a mean value of the two measurements were taken as a result.

8.2.5. Batch adsorption experiments

Equilibrium adsorption isotherm and adsorption kinetics experimental methods are also the same as those described in Chapter 3.

8.2.6. Adsorption modelling

8.2.6.1. Batch adsorption equilibrium modelling

The data for batch adsorption at different adsorbent doses were treated with Langmuir and Freundlich isotherm models, the details of which were discussed in Chapter 2. The equations of the models and the graphical methods used to calculate the model parameters are explained in Chapter 3.

8.2.6.2. Batch adsorption kinetic modelling

The batch adsorption kinetic data are analysed by pseudo-first-order and pseudo-second-order kinetics models which were also discussed earlier in Chapter 2**.** The equations for the pseudo-first-order and pseudo-second-order kinetic models and the methods of calculating the model parameters were presented in Table 3.3.

8.2.7. Effect of pH

Of the seven adsorbents, HFO had the highest fluoride adsorption capacity. Therefore, the effect of pH of the medium and the influence of complementary ions were investigated on HFO only. For the effect of pH on the adsorption of fluoride, samples

prepared for zeta potential measurements were used. The effect of pH was also studied with 1g of HFO at the pH ranges from 4 to 10 at a nitrate concentration of 10 mg F/L in a set of glass flasks containing 100 mL of fluoride solution. The suspensions were agitated in a flat shaker at a shaking speed of 120 rpm for 6 h at room temperature (24 ± 1^{o}C). The aqueous samples were taken at different time intervals and the concentrations of fluoride were measured

8.2.8. Effect of other co-ions

Natural water and wastewater may contain many anions at different concentrations which can compete with fluoride for adsorption. The extent of the competition depends on the relative concentrations of the ions and their affinity for the adsorbent. Therefore, the effect of complementary anions (Cl^-, SO_4^{2-}, NO_3^- and PO_4^{3-}) on fluoride adsorption by HFO was studied at a constant initial fluoride concentration of 10 mg/L, adsorbent dose of 1 g/L, and pH 7 by varying anion concentrations from 25 to 200 mg/L using NaCl, Na_2SO_4, KNO_3 and KH_2PO_4.

8.2.9. Fixed-bed column studies

The description of the fixed-bed column studies is similar to that presented in Chapter 3.

8.2.10. Fixed-bed column modelling

Three empirical models, Bohart-Adams model (1920), Thomas model (1944), Yoon and Nelson (1984) and a hybrid model based on Thomas model and artificial neural

networks (ANN) were used to analyse the column breakthrough data which we discussed earlier in Chapter 2. The methods of calculation of the model parameters are presented in Table 3.4.

8.2.11. Fluoride desorption and adsorbent regeneration

Desorption of fluoride that had previously been adsorbed to HFO was studied in batch and column experiments. In the batch experiment, HFO was saturated with fluoride by shaking a 50 mL fluoride solution (10 mg/L) with HFO at a dosage of 5 g/L for 72 h, followed by filtering and drying the fluoride -loaded HFO at room temperature. The adsorbed fluoride was then desorbed using 0.1 M NaCl, NaOH or Na_2SO_4 solution. Desorption was carried out by shaking the fluoride -saturated HFO with 50 ml of the reagents in a flat shaker at a shaking speed of 150 rpm for 30 min. The desorbed solutions were analysed for fluoride concentrations.

Since 0.1 M NaOH was found to be the most efficient reagent in desorbing fluoride in the batch experiment, this reagent was used in the column desorption study. Initially, fluoride was saturated on HFO in a 24 cm length column containing 20% HFO by passing a fluoride solution of 30 mg/L at pH 5 through the column at a velocity of 2.5 m/h until complete breakthrough of the solution occurred. Then the column was washed with distilled water followed by 0.1 M NaOH at a velocity 10 m/h for 30 min and the leachate was analysed for fluoride to determine the amount of fluoride desorbed. Fluoride adsorption was carried out on the regenerated HFO as previously described, after the column was washed several times with distilled water until the pH in the effluent reached 6.5. The adsorption/desorption cycle was continued three times in total.

8.3. Results and discussion

8.3.1. Characteristics of HFO

X-ray diffraction analysis showed that HFO (Figure 8.1) and zirconium hydroxide (data not shown) were poorly crystalline (amorphous) whereas alpha-alumina was crystalline and having diffraction peaks conforming to its structure (data not shown). For HFO, two broad diffraction peaks at 2θ values of 34-36° and 61-64° with the corresponding d-spacing values of 0.253-0.267 Å and 0.152-0.158 Å were obtained. These peaks match with those of the poorly ordered ferrihydrite mineral (Zhang et al., 2009; Hofmann et al., 2004).

The SEM images showed that the surface morphology of the HFO particles was irregular and it did not change significantly after fluoride adsorption at a fluoride concentration of 50 mg/L and HFO dose of 10g/L (Figure 8.2).

The FTIR spectra of HFO before and after adsorption of fluoride at 50 mg F/L and 10 g/L dose of HFO show two major adsorption peaks (Figure 8.3). The peaks at 3418 and 3445 cm^{-1} are for the the stretching vibration mode of lattice water and hydroxyl groups and those at 1621 and 1636 cm^{-1} are for OH^- bending vibration mode of adsorbed water molecules (Biswas et al., 2009; Sujanaa et al., 2013). The spectra shows that these band intensities were significantly reduced after fluoride adsorption indicating that the structural hydroxyl group and water molecules had an important role in fluoride adsorption. The BET surface area of HFO was 148 m^2/g. The total pore volume and pore diameter were 0.214 cm^3/g and 5.4 nm, respectively.

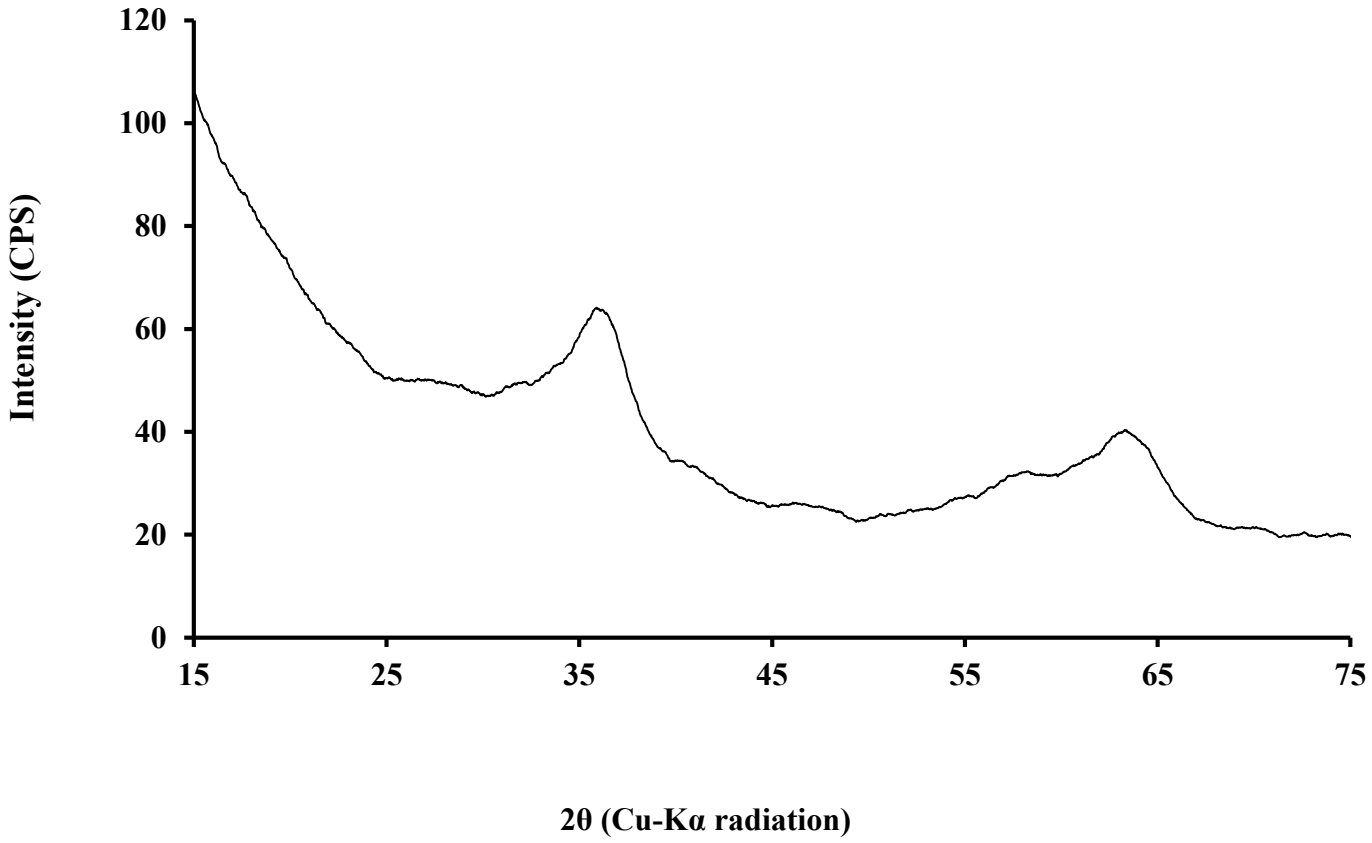

Figure 8.1. XRD patterns of HFO.

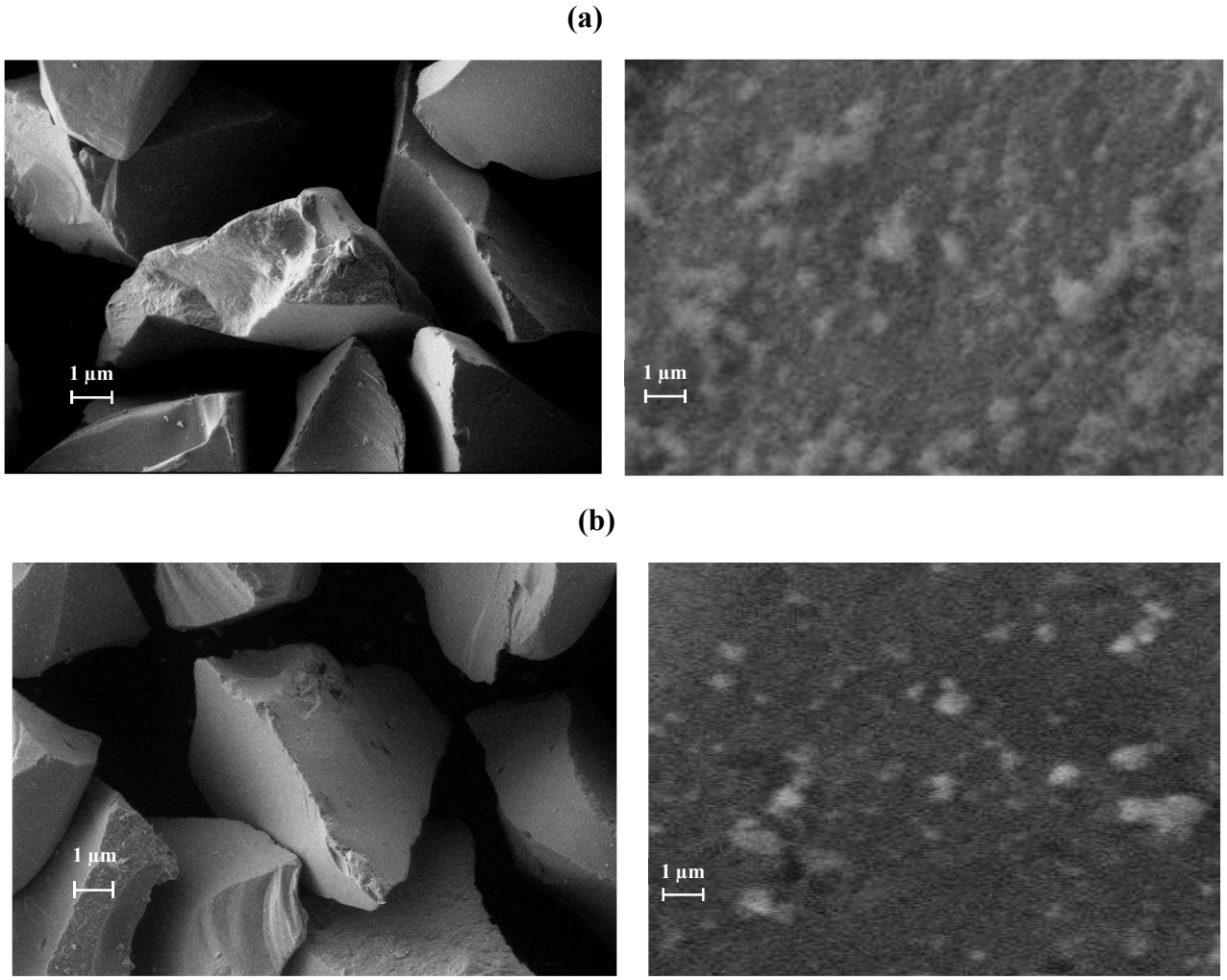

Figure 8.2. The SEM images of (a) HFO and (b) HFO+F (with magnification of 100X (Left hand side) and 5000X (right hand side).

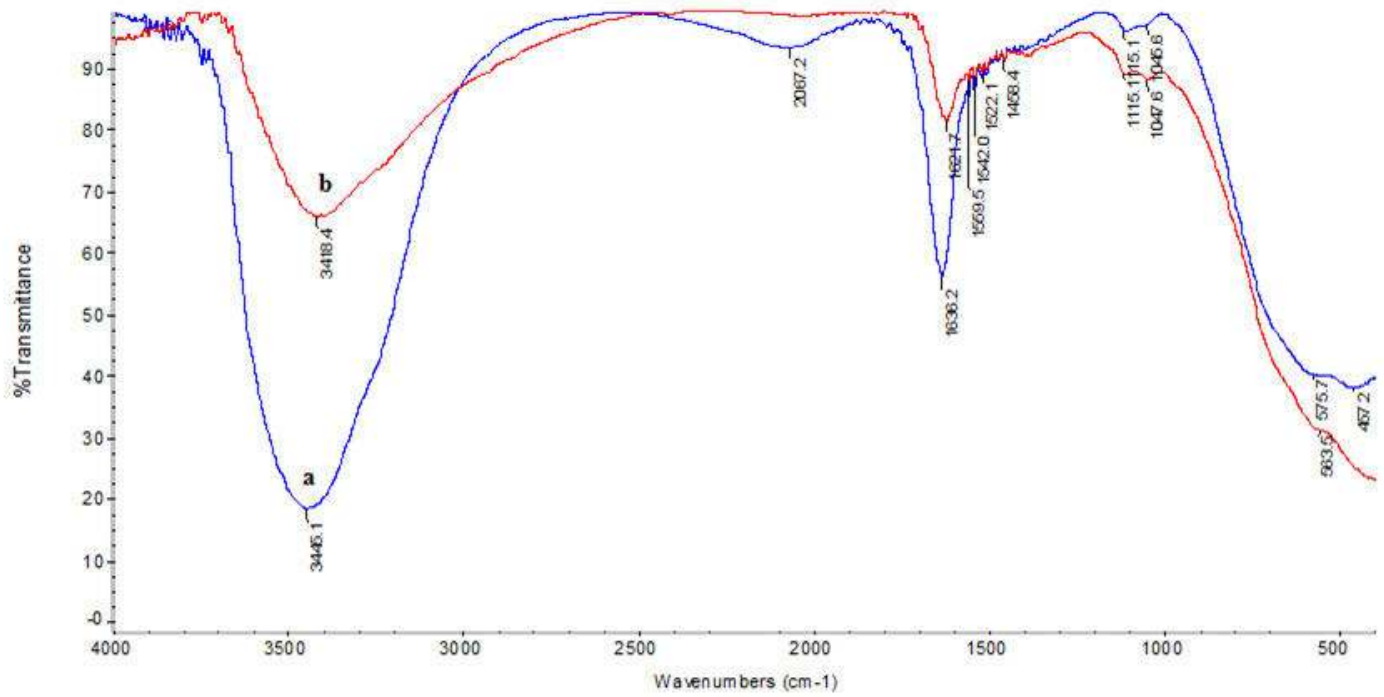

Figure 8.3. FTIR spectra of HFO (a) before and (b) after fluoride adsorption.

8.3.2. Batch adsorption studies

8.3.2.1. Batch equilibrium adsorption

Initially, batch equilibrium experiments were conducted with seven adsorbents, four ion exchange resins namely Purolite A500PS, Purolite A520E, Purolite FerrIX A33E and Dowex 21K and three multivalent metal oxides such as HFO (iron (iii) oxide $HFeO_2$), Zirconium (IV) hydroxide and aluminium oxide. The batch adsorption experiments show that the removal efficiency of fluoride increased with increased adsorbent dosage as expected due to the availability of increased number of adsorption sites which was similar to fluoride absorption on other adsorbents (Lv et al., 2006). Of the seven adsorbents tested, HFO produced the highest removal efficiency at all dosages of adsorbents for an initial fluoride concentration 10 mg/L from a solution volume of 100 mL (Figure 8.4a).

The removal efficiency was 94-97% for HFO dosages of 3-10 g/L. After HFO, the highest removal efficiency of fluoride was shown by Dowex 21K (86%) and Zirconium (IV) hydroxide (84%) at resin dose of 10 g/L (Figure 8.4a). Purolite A500PS, Purolite A520E and Purolite FerrIX A33E showed the same removal efficiency 81%, 70% and 52% respectively and aluminium oxide had the lowest removal efficiency (29%) in the equilibrium experiment. The results of the batch equilibrium adsorption experiment indicated that the removal efficiency of fluoride improved with increased resin dose due to increased availability of surface area for adsorption.

8.3.2.2. Batch kinetic adsorption

The kinetics of fluoride adsorption at an initial fluoride concentration of 10 mg/L and HFO dosage of 1 g/L showed that the adsorption capacity increased with contact time up to approximately 60 min and became steady afterword (Figure 8.4b). Among the seven adsorbents, HFO had the highest fluoride removal efficiency (56%) followed by Dowex 21k (52%), Zirconium (IV) hydroxide (38%), Purolite A502PS (35%), Purolite FerrIX A33E (29%) and Purolite A520E (25%) within 120 min. The lowest removal efficiency was found for Alumina (4%). Of the seven adsorbents tested, consistent with the batch equilibrium adsorption data, HFO produced the highest removal efficiency at all dosages of adsorbents for an initial fluoride concentration 10 mg/L from a solution volume of 100 mL.

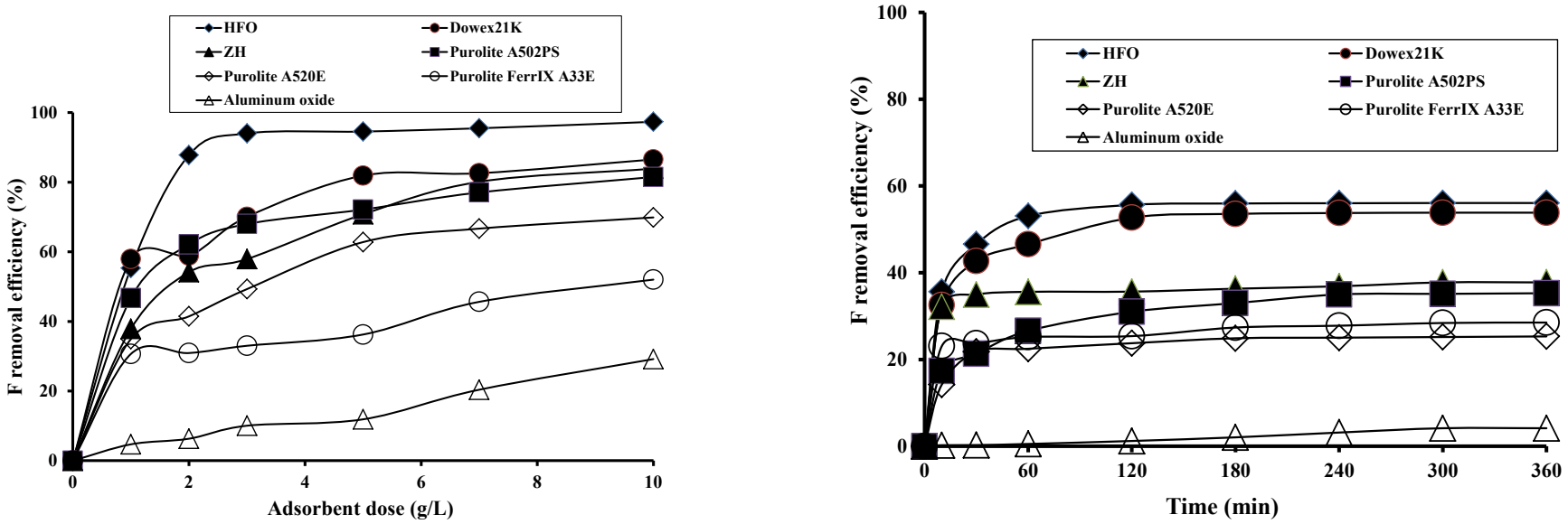

Figure 8.4. Effect of (a) resin dose and (b) contact time on the removal of fluoride (initial fluoride concentration 10 mg F/L) by seven adsorbents (adsorbent dose 1g/L).

8.3.2.3. Batch equilibrium adsorption modelling

The adsorption data for all seven adsorbents satisfactorily fitted to Freundlich adsorption model (R^2 = 0.66-0.98). Consistent with the removal percentage data (Figure 8.4a), HFO had the highest Freundlich constant K_F that is related to the adsorption capacity (Table 8.1). However, only the data for HFO satisfactorily fitted to the Langmuir adsorption model with positive value for the adsorption maximum (R^2 = 0.91). The adsorption maxima for the other adsorbents were either negative or where positive values were obtained the R^2 values were < 0.10. Negative maximum adsorption values were also reported for other adsorbents and adsorbates in literature (Öztürk and Bektas, 2004). The fit of the data to Langmuir model for HFO indicates that the adsorption sites on HFO were homogeneous with monolayer adsorption coverage. The Freundlich model fit to the other adsorbents indicates a hetrogenity of the adsorbent surfaces with different energies of adsorption.

The adsorption maximum calculated from the Langmuir model for HFO was 6.71 mg F/g. This adsorption capacity is approximately equal to the maximum adsorption capacity of 7 mg F/g at pH 6-7 obtained by Kumar et al. (2009) for a ferric oxide that had similar chemical characteristics as the HFO used in this study. The Langmuir adsorption capacity obtained for HFO is among the highest adsorption capacities reported for adsorbents (Loganathan et al., 2013a).

8.3.2.4. Batch kinetic adsorption modelling

The adsorption data showed that for all adsorbents, except Alumina, the pseudo-second-order kinetic model described the experimental data better than the pseudo-first-

order model (R^2 = 0.99 for pseudo-second-order model compared to R^2 = 0.65-0.97 for pseudo-first order model) (Table 8.2). Furthermore, the values of q_e calculated from pseudo-second-order kinetic model were approximately equal to the experimental values of q_e, while the pseudo-first-order model values of q_e were much lower than the experimental values of q_e (Table 8.2) confirming the better applicability of the pseudo-second-order model for describing the experimental data for all adsorbents except Alumina. The better fit of data to pseudo-second-order model suggests that chemisorption process could be the rate-limiting step in the adsorption (Yan et al., 2010). Fluoride adsorption on other adsorbents has also been reported to fit better to this model than pseudo-first order model (Tovar-Gómez et al., 2013; Tor et al., 2009).

Table 8.1.

Freundlich isotherm parameters for fluoride adsorption on seven adsorbents.

Parameters	Purolite A520E	Purolite A500PS	Purolite A33E	Dowex21K	Aluminum oxide	ZH	HFO
K_F (mg F/g) (L/mg F)$^{1/n}$	0.11	0.26	0.0008	0.56	0.0004	0.48	2.69
n	0.57	0.57	0.25	0.74	0.22	0.94	1.63
R^2	0.94	0.98	0.66	0.81	0.84	0.90	0.80

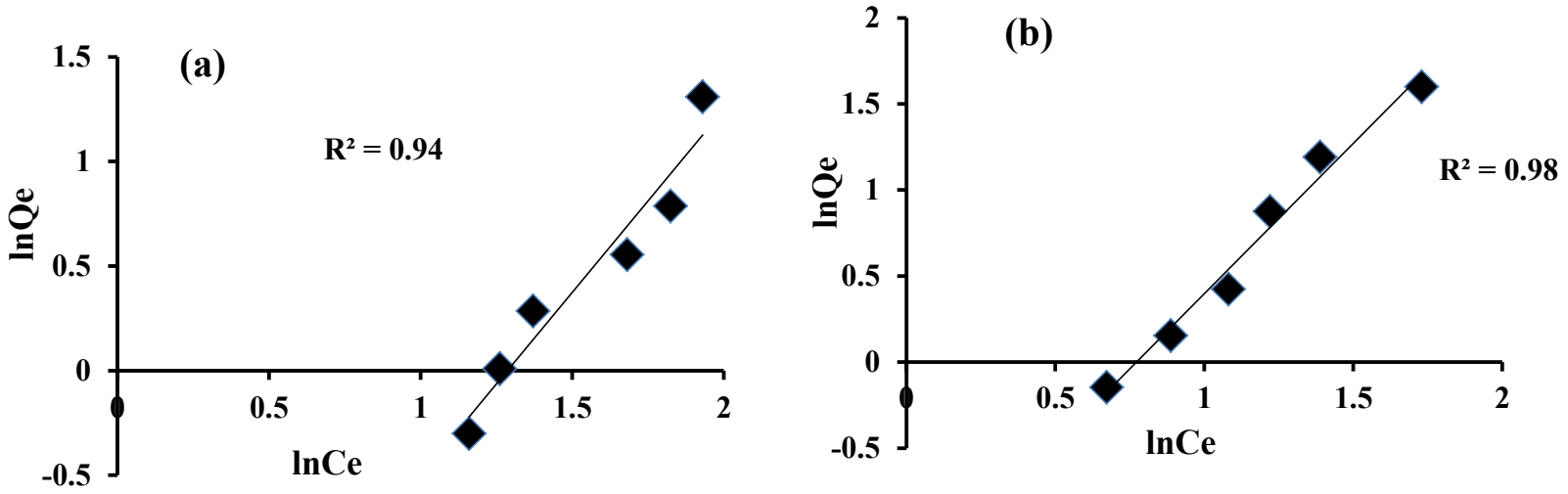

Figure 8.5. Isotherm Freundlich.modelling of fluoride adsorption on (a) Purolite A520E (b) Purolite A500PS.

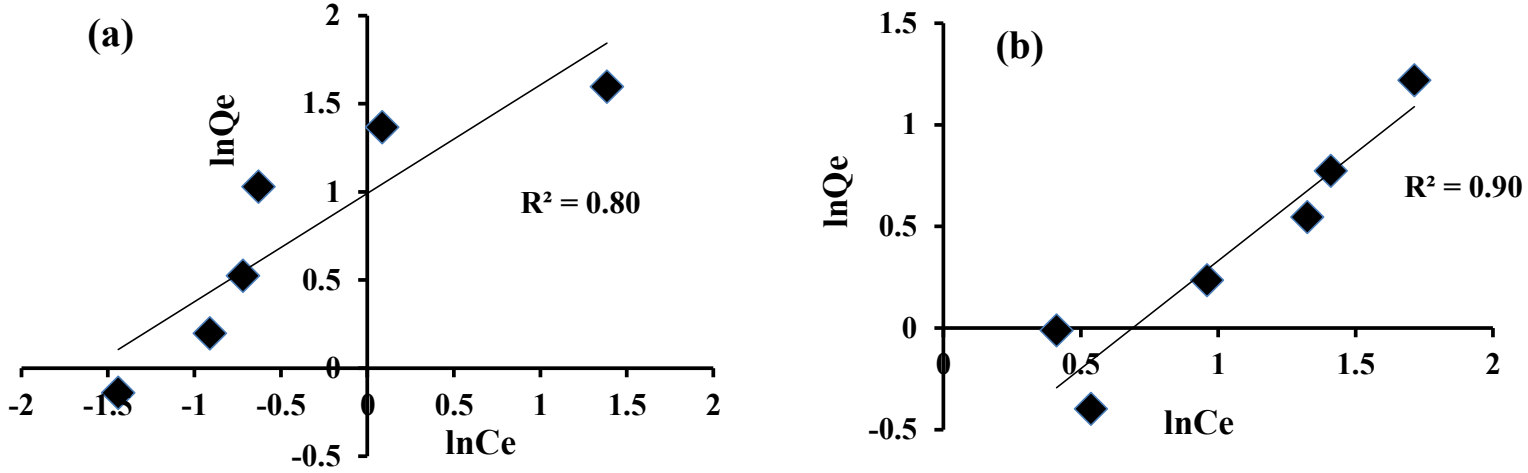

Figure 8.6. Isotherm Freundlich.modelling of fluoride adsorption on (a) HFO (b) ZH.

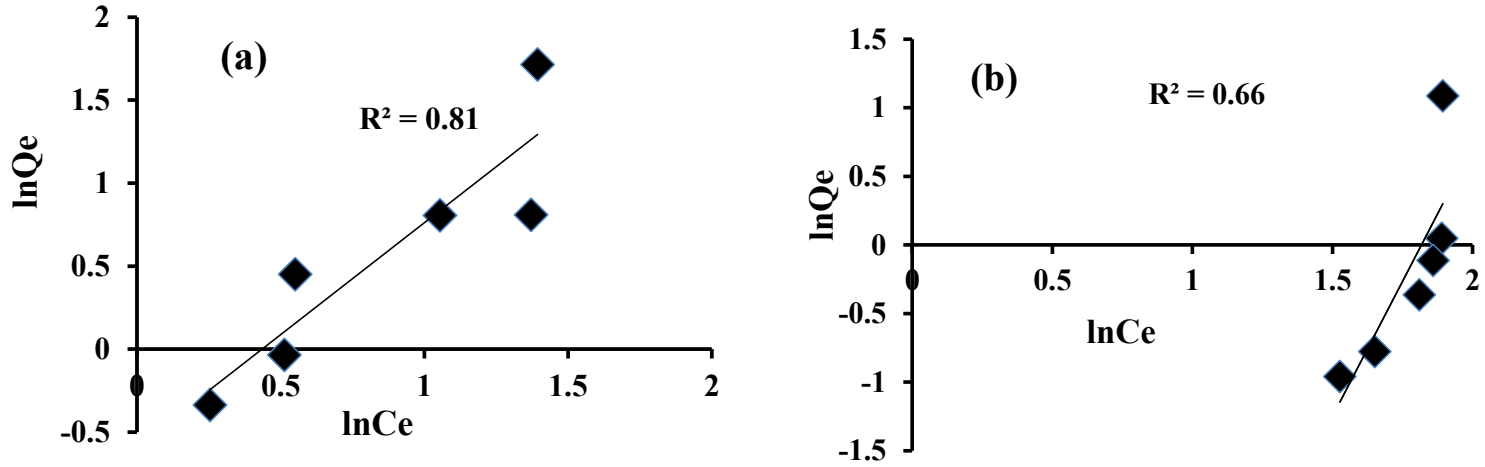

Figure 8.7. Isotherm Freundlich.modelling of fluoride adsorption on (a) Dowex 21K XLT (b) FerrIX A33E.

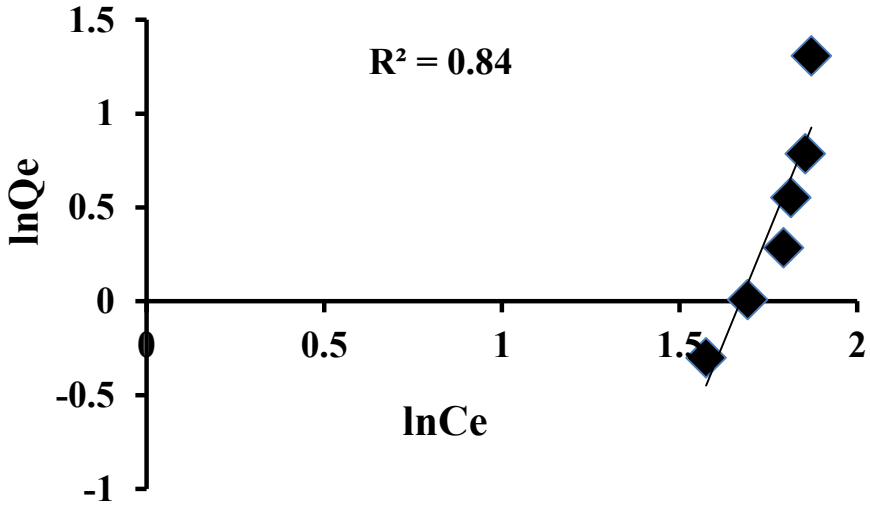

Figure 8.8. Isotherm Freundlich.modelling of fluoride adsorption on α-Alumina

Table 8.2.

Batch adsorption kinetic parameters of pseudo-first-order and pseudo-second-order kinetics models for the adsorption of fluoride on seven adsorbents.

Adsorbent		Pseudo-first-order model			Pseudo-second-order model		
	q_e experimental (mg F/g)	q_e (mg F/g)	k_1 x 10^{-2} (min^{-1})	R^2	q_e (mg F/g)	k_2 x 10^{-2} (g/mg. min)	R^2
Purolite A520E	2.32	0.93	0.1	0.65	1.81	7.00	0.99
Purolite A502PS	2.87	1.38	0.4	0.90	2.62	1.90	0.99
Purolite FerrIX A33E	2.96	0.74	0.3	0.96	2.78	4.30	0.99
HFO	5.55	2.34	1.5	0.97	5.68	2.40	0.99
ZH	3.40	0.51	0.9	0.94	3.4	6.60	0.99
Dowex21K	4.90	1.59	1.4	0.91	5.08	1.80	0.99
Aluminium oxide	0.73	0.42	0.2	0.96	-4.36	0.01	0.02

8.3.2.5. pH changes during adsorption

During adsorption the pH of the suspension changed. At low pH values (equilibrium final pH, pH_f < 4.0) the pH increased from the initial value (pH_i) resulting in positive values for $pH_f - pH_i$ (Figure 7.6). At high pH values (pH_f > 4.0) the pH decreased during adsorption leading to negative values for $pH_f - pH_i$. Similar results were reported for fluoride adsorption on HFO (Dey et al., 2004), nano-hydroxyapatite/chitosan (Sundaram et al., 2008) and manganese oxide–coated alumina (Teng et al., 2009) and phosphate adsorption on nano-sized magnetite (Zach-Maor et al., 2011). The explanation for the increase in the final pH at low pH values may be the liberation of OH^- from HFO during fluoride adsorption by ligand exchange process (inner-sphere complexation) (Dey et al., 2004) as described in Equation 8.1 .

$$HFO\text{---}OH + F^- = HFO\text{----}F + OH^- \quad (8.1)$$

At high pH values the final pH decreased from the initial pH probably due to Na^+ added in NaOH for pH alteration might have exchanged with H^+ electrostatically adsorbed (outer-sphere complexation) onto the increasingly negatively charged HFO (Dey et al., 2004) as described in Equation 8.2.

$$HFO^-(H^+) + F^- + Na+ = HFO^-(Na^+) + F^- + H^+ \quad (8.2)$$

When the ionic strength of the solution was increased to 10^{-2} M by adding $NaNO_3$ the values of $pH_f - pH_i$ increased (Figure 8.5) due to enhanced exchange of H^+ by the additional Na^+ supplied by $NaNO_3$. At pH_f = 4.0, $pH_f = pH_i$. This pH is, therefore, the

point of zero charge (PZC) of HFO in the presence of fluoride (Sundaram et al., 2008; Zach-Maor et al., 2011).

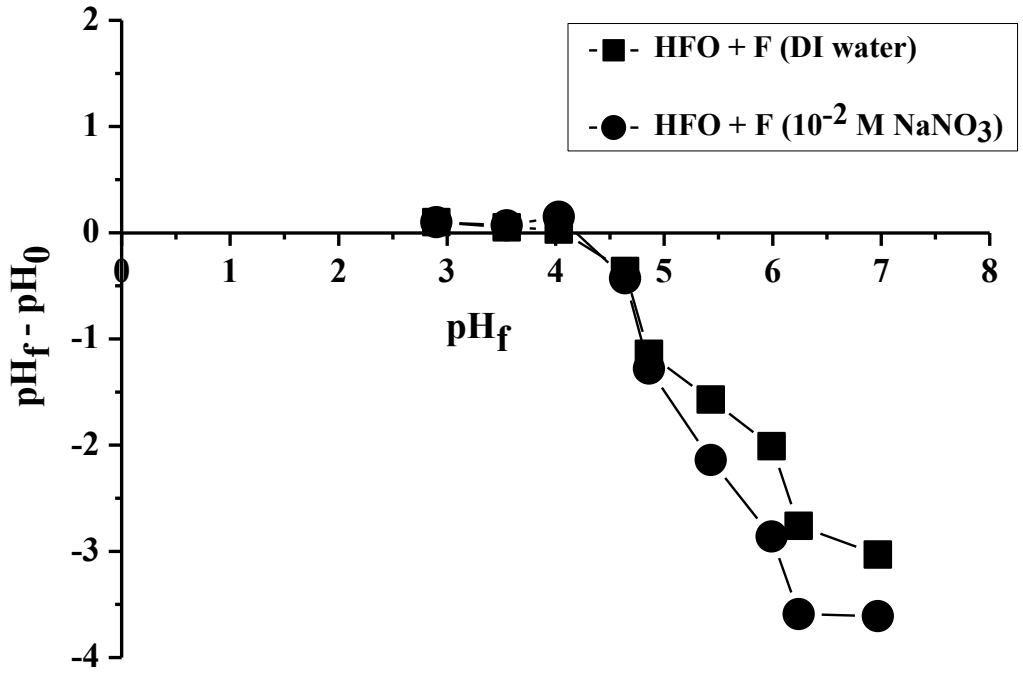

Figure 8.9. Changes in solution pH during fluoride adsorption on HFO.

8.3.2.6. Effect of pH on fluoride adsorption

Fluoride adsorption continued to decrease as pH_f increased from 3 to 7 (pH_i 3.5 to 9.0) (Figure 8.6a). The decrease in adsorption is due to an increase in the surface negative charges on HFO with increased pH (Figure 8.6b) causing repulsion of the negatively charged fluoride ions. It is also due to the increased concentration of OH^- ions at higher pH values that competed with fluoride for adsorption. Adsorption is favoured at low pH because of the presence of more hydroxylated sites for ligand exchange with fluoride than at high pH. The decline in fluoride adsorption as pH increased was also observed by other studies on HFO (Dey et al., 2004) and other adsorbents (Tor et al., 2009; Teng et al., 2009). The actual pH where the fluoride adsorption starts to decrease depends on the surface chemical characteristics of the adsorbent especially the PZC (Loganathan et al., 2013a). There was very little difference in fluoride adsorption between the two ionic strengths (water and 10^{-2} M $NaNO_3$) of the solutions. This shows that fluoride was adsorbed by forming inner-sphere complexation on HFO (Hiemstra and Van Riemsdijk, 2000).

Zeta potential curves at the two ionic strengths intersected close to zero zeta potential because when the net surface charge is zero the ionic strength has no effect (Figure 8.6b). The pH at which the intersection occurs is the PZC (Wang et al., 2009). Therefore, based on the zeta potential data, fluoride is adsorbed mainly by the ligand exchange mechanism (specific adsorption or inner-sphere complexation (Loganathan et al., 2013a). Figure 8.6 (b) shows that zeta potential at the HFO particle surface was more negative in the presence of fluoride at all pH values. The PZC decreased from pH 5.0 in the absence of fluoride to pH 4.0 when fluoride was added consistent with the PZC determined using pH change data (Figure 8.6b). Thus, fluoride adsorption created

negative surface charges on the HFO thereby shifted the PZC to a lower pH, which was consistent with the inner-sphere adsorption mechanism. When the ionic strength of the solution was increased by the addition of $NaNO_3$, the zeta potential became less negative when pH was above the PZC, whereas it behaved oppositely at pH values below the PZC. This pattern of ionic strength effects was also reported for fluoride adsorption on alumina (Bahena et al., 2002) and phosphate adsorption on variable charge soils (Wang et al., 2009).

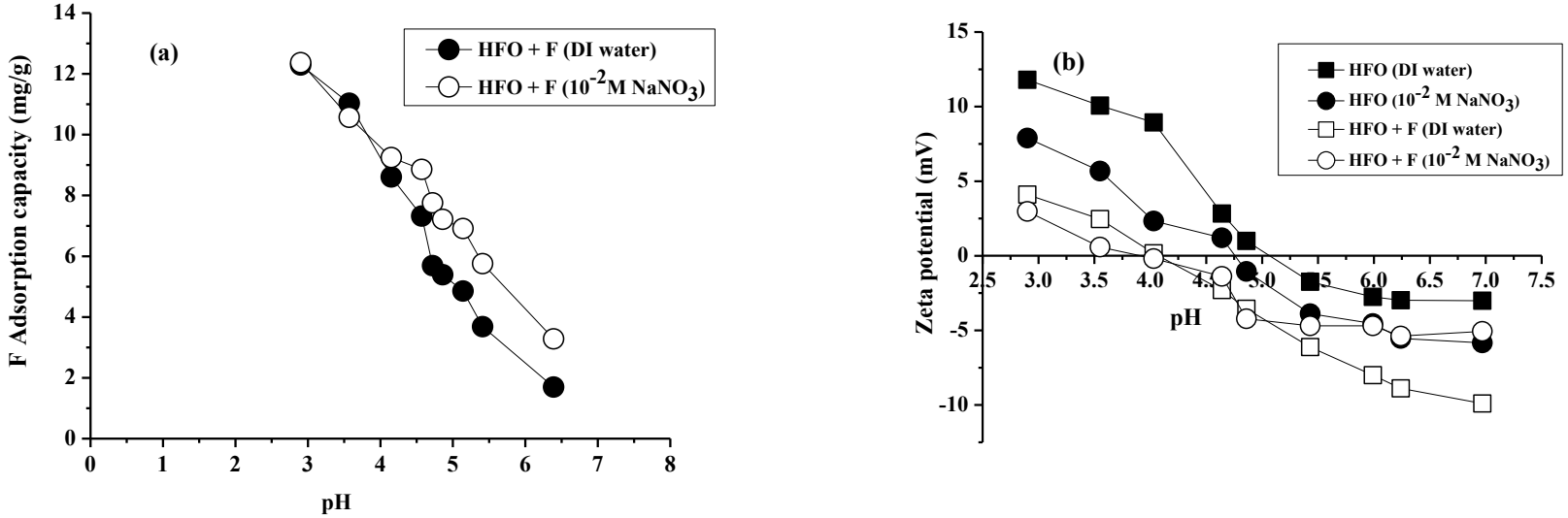

Figure 8.10. Influence of final pH of HFO suspension on (a) fluoride adsorption and (b) zeta potential at the HFO/solution interface

8.3.2.7. Effect of complementary ions

The ratios of the anions concentrations in natural water and wastewater are widely different and therefore such ratios need to be considered in assessing the extent of competition. For example, PO_4^{3-} concentrations are generally much lower than the concentrations of other anions. Figure 8.7 shows that even with the lower concentration of PO_4^{3-}, this anion can exert a higher degree of competition with fluoride than the other anions. Effects of SO_4^{2-}, PO_4^{3-}, Cl^- and NO_3^- on fluoride adsorption showed that the presence of these anions at concentrations ranging from 25 to 200 mg/L at pH 6.7 reduced the adsorption of fluoride appreciably with the increase in initial concentration of these anions (Figure 8.7). The order of fluoride adsorption reduction by these anions was $PO_4^{3-} > SO_4^{2-} > NO_3^- > Cl^-$. These results can be explained based on the adsorption mechanisms of these anions. Phosphate is known to be strongly adsorbed on high valent metal oxides and hydroxides by specific adsorption (inner-sphere complexation) (Loganathan et al., 2014). Therefore, it is able to compete easily with fluoride which is also specifically adsorbed (Loganathan et al., 2014).

NO_3^- and Cl^- which are non-specifically adsorbed (outer-sphere complexation) to metal oxides and therefore unable to compete well with fluoride at equal concentrations. Sulphate, on the other hand, can be adsorbed specifically and non-specifically and therefore it competed with fluoride better than Cl^- and NO_3^- but weaker than PO_4^{3-} (Tang et al., 2009). The decreased order of competition observed in this study ($PO_4^{3-} > SO_4^{2-} > NO_3^- > Cl^-$) is consistent with the findings in other studies on iron oxides/hydroxides ($PO_4^{3-} > SO_4^{2-} > NO_3^- > Cl^-$ (Kumar et al., 2009); $PO_4^{3-} > SO_4^{2-} > Cl^-$ (Dey et al., 2004), and on other adsorbents ($SO_4^{2-} > NO_3^- > Cl^-$ (Kamble et al., 2007); $PO_4^{3-} > SO_4^{2-} > NO_3^-$ (Sujana et al., 1998).

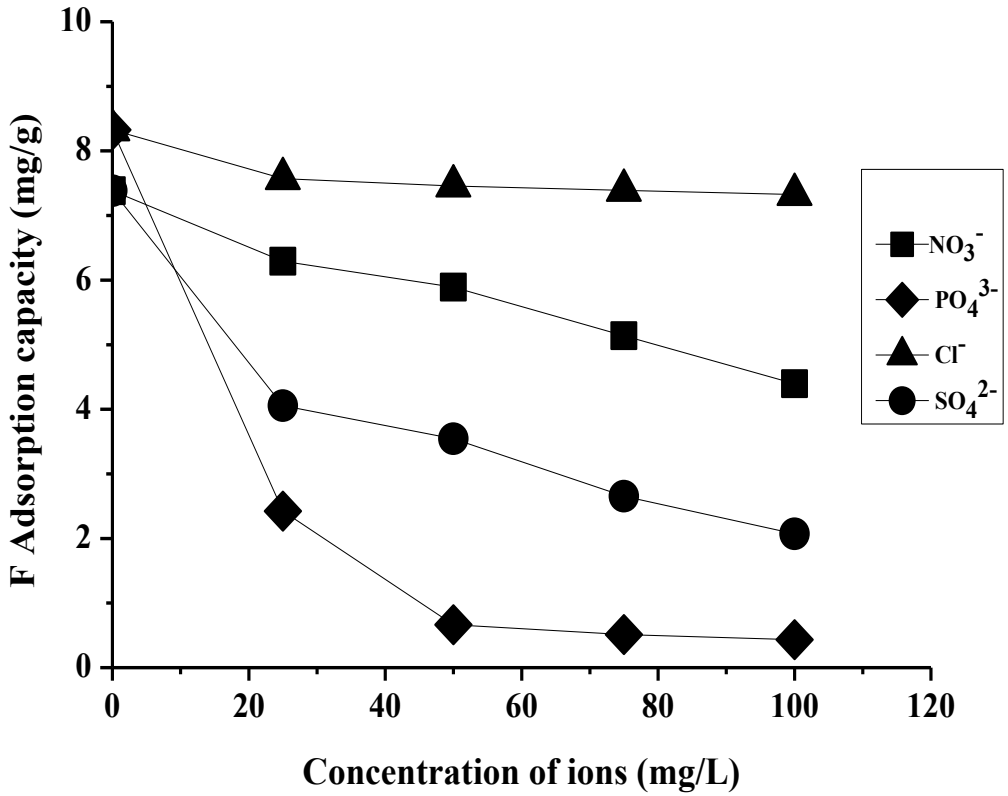

Figure 8.11. Effect of complementary anions on the adsorption of fluoride by HFO (initial fluoride concentration 10 mg F/L and adsorbent dose 1g/L).

8.3.3. Fixed-bed column experiments

8.3.3.1. Breakthrough curves

Adsorption of fluoride by HFO is presented in the form of breakthrough curves (Figure 8.8). When the HFO got exhausted in its ability to adsorb fluoride, the fluoride concentration in the effluent (C_t) became equal to the influent concentration (C_0). The breakthrough curves became less sharp when the mass transfer rates were decreased (Cloutier et al., 1985). Since mass transfer rates were finite, the breakthroughs were diffused and exhibited an S-shape pattern. Effects of bed height, influent fluoride concentration and pH on the breakthrough curves are presented in Figure 8.8.

The effect of bed height was investigated at bed heights of 12 and 24 cm, at a constant filtration velocity 2.5 m/h, inlet fluoride concentration 10 mg/L, and pH 7. The results show that at the lower bed height, the breakthrough occurred faster than that at the higher bed height. This pattern of breakthrough is similar to the findings of fluoride adsorption on manganese oxide coated alumina (Teng et al., 2009; Maliyekkal et al., 2006). The contact time of fluoride with the adsorbent is shorter at lower bed height resulting in faster exhaustion of the HFO bed and less volume of treated water. The empty bed contact time available for fluoride at the depths of 12 cm and 24 cm were 2.89 min and 5.76 min, respectively.

The effect of pH on the adsorption of fluoride on HFO was investigated by comparing the breakthrough curves at pHs 5 and 7 at a constant adsorbent bed height 24 cm, constant filtration velocity 2.5 m/h and inlet concentration 10 mg F/L. The fluoride breakthrough generally occurred faster and the breakthrough curve was steeper at pH 7 than at pH 5 (Figure 7.9). The time to reach the plateau of C_t/C_0 (equal to 0.98) was significantly higher at a lower pH level. The plateau of C_t/C_0 occurred at 5 and 12 h for

the pH of 7.0 and 5.0, respectively. This is due to the higher fluoride adsorption capacity of HFO at acidic pH than at neutral pH, as found in the batch study. Ku et al. (2002) also reported faster breakthrough and steeper breakthrough curves for fluoride adsorption on an Amberlite resin at pH 6.7 than at pH 5.5.

The effect of increase in the influent fluoride concentration from 10 to 30 mg F/L on breakthrough curves is also shown in Figure 7.9. The breakthrough time occurred faster and the breakthrough curves were sharper with the higher influent fluoride concentration which was similar to the findings of fluoride adsorption on other adsorbents (Tovar-Gomez et al., 2013). These results are also consistent with the findings on column adsorption on other adsorbents and adsorbates (Hekmatzadeh et al., 2012). These results demonstrate that the change of concentration gradient in the solid/solution interface affects the saturation rate and breakthrough time, or in other words, the fluoride diffusion process is concentration dependent. As the influent concentration increases, fluoride loading rate increases, so does the driving force for mass transfer, and decreases in the adsorption zone length which was also reported in other column studies on other adsorbents (Tovar-Gomez et al., 2013). The extended breakthrough curve (slower exhaustion of the HFO column) at the lower influent concentration indicates that a higher volume of solution can be treated.

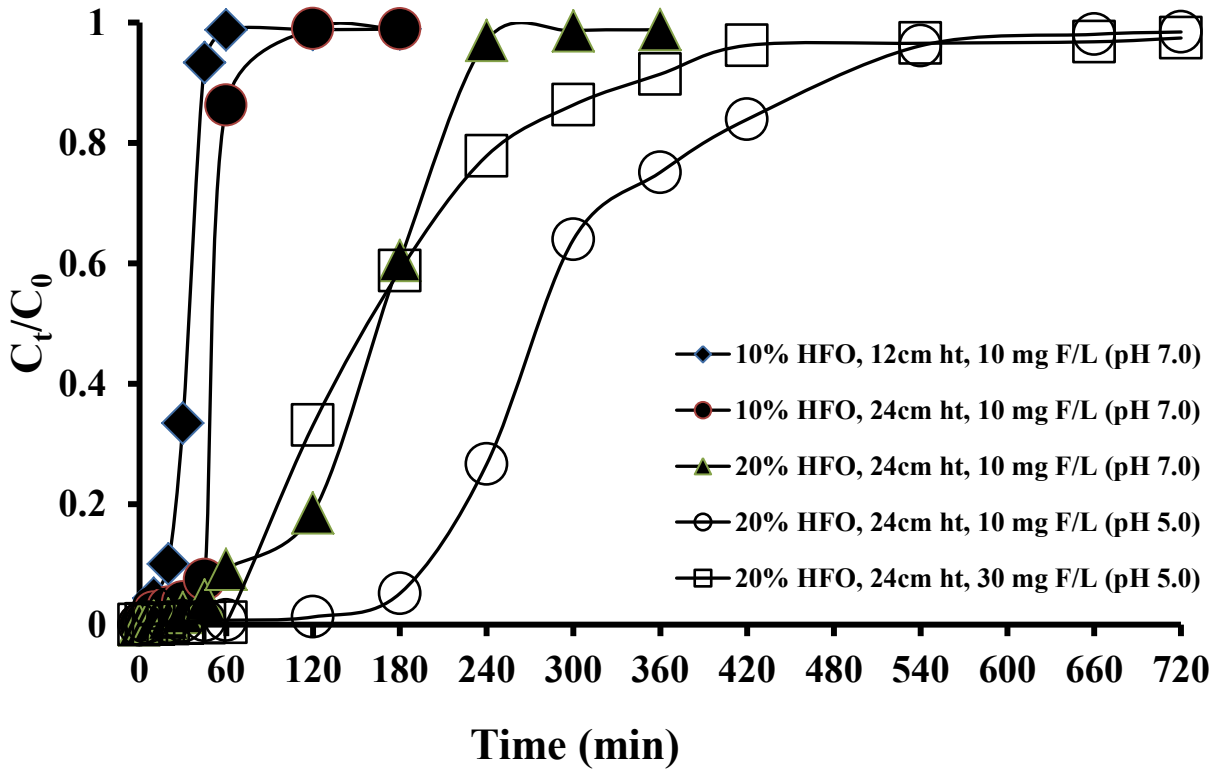

Figure 8.12. Breakthrough curves for different bed heights, pH and inlet fluoride concentrations (initial fluoride concentration 10 mg F/L, HFO dose 20% and filtration velocity 2.5 m/h).

8.3.3.2. Column adsorption modeling

8.3.3.2.1. Bohart-Adams model

The experimental data fitted satisfactorily to Bohart-Adams model for both the bed heights ($R^2 \geq 0.79$) and for the higher pH and higher influent fluoride concentration ($R^2 \geq 0.84$) (Tables 8.3). The data fit, however, was only marginally satisfactorily for the lower pH and higher influent concentration ($R^2 = 0.47$). The values of the rate constant, k_{AB} calculated from the model decreased when the inlet fluoride concentration and the bed height increased. In contrast to the value of k_{AB} the value of N_o that is related to the fluoride adsorption capacity increased with the increasing inlet fluoride concentration and bed height, but decreased with increasing pH of the influent. The fluoride concentration and bed height effects on Bohart-Adams model constants are similar to those observed for other adsorbates and adsorbents (Aksu and Gonen, 2004).

8.3.3.2.2. Thomas model

The Thomas model fitted very well to the experimental data as shown by the high R^2 values (0.79-0.97) (Tables 8.3). The model prediction of the column adsorption capacity (q_o) increased with increases in inlet fluoride concentration and decreased with increased pH and bed height. The values obtained for q_o from the model are approximately equal to those calculated from the breakthrough curves, except for the initial fluoride concentration of 30 mg/L at the bed height 24 cm and HFO dosage 20% at pH 7, where the breakthrough capacity was 7.06 mg F/g and q_0 was 12.7 mg F/g. The above adsorption capacities were the highest estimated by Thomas model in the experiments. The breakthrough adsorption capacity of 7.06 mg F/g is approximately equal to the Langmuir

adsorption capacity of 6.71 mg F/g observed in the batch study. Similar to the results of Bohart-Adams model, the increase of bed height and influent concentration decreased k_{Th} and increase of pH increased k_{Th}.

8.3.3.2.3. Yoon–Nelson model

The experimental data also fitted satisfactorily to Yoon-Nelson model for the two fluoride concentrations, pHs and bed heights (R^2 = 0.75-0.95) (Tables 8.3). The rate constant k_{YN} increased and the 50% breakthrough time (τ) decreased when both pH and inlet concentration increased, but the opposite trend occurred with increasing bed height. With the increase of bed height, τ rose while k_{YN} fell.

Considering the values of R^2 for the models fits to the experimental data and breakthrough curves, it can be concluded that all three models can be used reasonably well to describe the behaviour of the adsorption of fluoride on HFO in the fixed-bed columns, except for the lower pH and higher influent concentration where Bohart-Adams model fit to the data was only marginal.

8.3.3.2.4. ANN Model

The Thomas model fitted faily well to the experimental data as shown by the moderate to high R^2 values (0.79-0.97) (Tables 8.3). However, the hybrid ANN + Thomas model fit to the data was better for all scinerios (Tables 8.3, Figure 8.9), especially for inlet fluoride concentration 30 mg/L, 24 cm column height, pH 5, and HFO 20% where the R^2 value for Thomas model was 0.79 but for the hybrid model it was 0.98. The column adsorption capacity (q_o) predictions by both the Thomas and hybrid models increased

with increases in inlet fluoride concentration and decreased with increased pH and bed height.

The values obtained for q_o from the models are approximately equal to those calculated from the breakthrough curves, except for the initial fluoride concentration of 30 mg/L at the bed height 24 cm and HFO dosage 20% at pH 7, where the breakthrough capacity was 7.06 mg F/g (similar to the Langmuir adsorption capacity of 6.71 mg F/g observed in the batch study) but q_0 predicted by both models was 12.7 mg F/g. The above adsorption capacities were the highest estimated by the models in the experiments. Higher column adsorption capacity obtained in the models for 30 mg F/L inlet concentration than the Langmuir adsorption maximum in batch study is probably because of the lower initial fluoride concentration of 10 mg F/L used in the batch study which would have further decreased at equilibrium due to adsorption. In the column study the solution concentration was always maintained at 30 mg F/L with the passage of fresh influent solution. Higher solution fluoride concentration is expected to produce higher fluoride adsorption.

Table 8.3.

HFO column adsorption model parameters and breakthrough adsorption capacities for different bed heights, pHs and influent fluoride concentrations (filtration velocity 2.5 m/h).

Models and parameters	Bed height (cm) (C_0 10 mg F/L, pH 7, HFO 10%)		pH (Bed height 24 cm, C_0 10 mg F/L, HFO 20%)		Influent fluoride concentration, C_0 (mg F/L) (Bed height 24 cm, pH 5, HFO 20%)	
	12	24	5.0	7.0	10	30
Bohart-Adams Model						
k_{AB} (L/mg F. min) $x10^{-3}$	16.9	5.3	0.98	6.5	0.98	0.60
N_o (mg F/L)	115	165	926	167	926	2012
R^2	0.83	0.79	0.47	0.94	0.47	0.84
Thomas Model						
k_{Th} (mL/min.mg F)	17.0	9.7	1.38	3.38	1.38	0.37
q_o (mg F/g HFO)	1.2	1.1	3.43	1.47	3.43	12.7
R^2	0.97	0.83	0.95	0.95	0.95	0.79

Table 8.3 (continued).

Models and parameters	Bed height (cm) (C_0 10 mg F/L, pH 7, HFO 10%)		pH (Bed height 24 cm, C_0 10 mg F/L, HFO 20%)		Influent fluoride concentration, C_0 (mg/L) (Bed height 24 cm, pH 5, HFO 20%)	
	12	24	5.0	7.0	10	30
ANN-Thomas Model						
k_{Th} (mL/min.mg F)	16.73	9.3	1.28	3.27	1.28	0.36
q_o (mg F/g HFO)	1.18	1.10	3.57	1.47	3.57	12.72
R^2	0.999	0.979	0.996	0.998	0.996	0.982
Breakthrough adsorption capacity, q_e (mg F/g HFO)	1.01	0.90	2.12	1.28	2.12	7.06

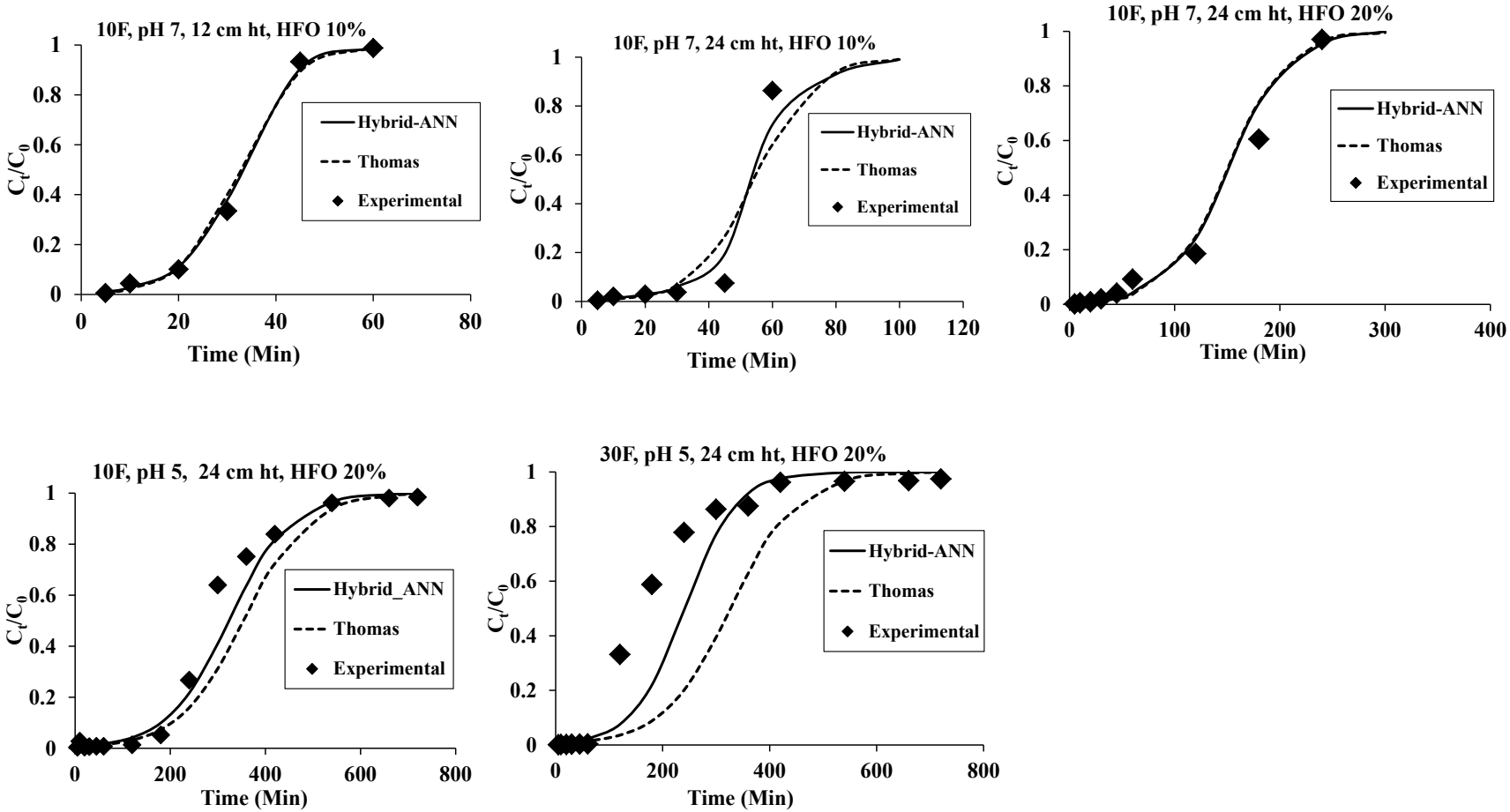

Figure 8.13. Breakthrough curves for different inlet fluoride concentrations, pHs, bed heights, and HFO% (filtration velocity 2.5 m/h). Experimental values are shown by data points, and model predictions are represented by lines.

8.3.4. Fluoride desorption and HFO regeneration

Of the reagents tested in the batch study to desorb fluoride that was already adsorbed on HFO, 0.1M NaOH was found to be the most suitable one (Figure 8.10). The high effectiveness of 0.1 M NaOH in desorbing fluoride is due to the lowest fluoride adsorption at very high pHs (Figure 8.10a) produced by this alkaline reagent. In the study on the effect of complementary anions on fluoride adsorption it was observed that the anions Cl^- and SO_4^{2-} did not significantly reduce fluoride adsorption because of the stronger ability of fluoride adsorption compared to these two anions. This is the likely explanation for the inability of 0.1 M Na_2SO_4, and 0.1 M NaCl to significantly desorb fluoride from HFO. Dey et al. (2004) also reported that among four reagents tested, the largest percentage of fluoride desorption (80%) from a fluoride-rich HFO was observed for NaOH and the least (15%) was for NaCl.

The column study results showed that almost 97% of the previously adsorbed fluoride was desorbed by 0.1 M NaOH in 30 min (21 bed volumes) and HFO was regenerated for reuse (Figure 8.10b). The fluoride removal percentage of the regenerated HFO declined to 62% (a decrease in fluoride adsorption capacity from 5.90 mg/g for the virgin HFO to 3.63 mg/g for the regenerated HFO) (Figure 8.10b).

The fluoride adsorption capacity of HFO further fell to 3.43 and 3.26 mg/g, after the second and the third cycles of adsorption/desorption, respectively, as found by others (Dey et al. 2004). The reduction in adsorption capacity with continued reuse of adsorbents may be due to the chemisorption of previously adsorbed fluoride, part of which was not desorbed (Dey et al. 2004) and/or the use of the highly concentrated NaOH which might have modified the adsorbent surface. Reduced adsorption capacity when HFO was reused

three times was still much higher than that of many other adsorbents (Loganathan et al., 2014). Therefore, HFO is proved to be a potential adsorbent for the removal of fluoride.

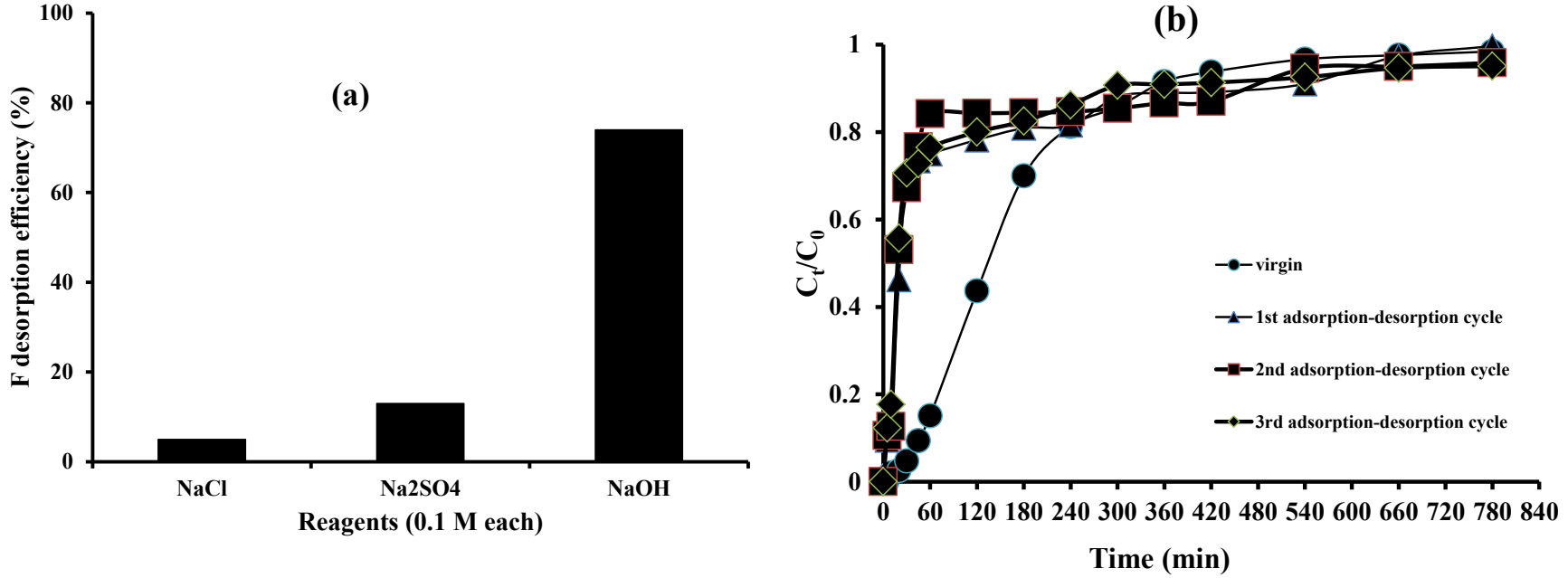

Figure 8.14. (a) Desorption of fluoride using three reagents in batch experiments and (b) breakthrough curves for fluoride before and after desorption of fluoride using 0.1 M NaOH in column experiments (bed height 24 cm, initial fluoride concentration 10 mg/L, filtration velocity 2.5 m/h).

8.4. Conclusions

Batch and fixed-bed column (10 or 20% HFO + 90 or 80% anthracite) experimental results showed that HFO is an efficient adsorbent for removing fluoride from aqueous solutions. The batch adsorption was satisfactorily explained using both the Langmuir and Freundlich isotherms while the column adsorption data fitted reasonably well to Thomas model but by using an artificial neural network approach the model's capability was improved. The Langmuir maximum adsorption capacity at pH 6.5 was 6.71 mg F/g and the highest column breakthrough adsorption capacity was 7.06 mg F/g at the inlet concentration of 30 mg F/L, 12 cm bed height, pH 5 and 2.5 m/h filtration velocity. The adsorption capacity predicted by the Thomas model was also highest (12.7 mg F/g) for these experimental conditions. The kinetic data on fluoride adsorption on HFO was better described by pseudo-second-order model than pseudo-first-order model.

Solution pH had a strong effect on fluoride adsorption which decreased continuously from pH 3 to 7. Fluoride adsorption decreased the PZC of HFO. Phosphate and SO_4^{2-} reduced fluoride adsorption whereas NO_3^- and Cl^- had little effect on fluoride adsorption. Consistent with this data 0.1 M NaCl and 0.1 M Na_2SO_4 failed to desorb fluoride from HFO whereas 0.1 M NaOH was able to desorb nearly all adsorbed fluoride. Data on zeta potential and PZC of HFO and complementary ions effects on fluoride adsorption and desorption showed that fluoride was specifically adsorbed by HFO by an inner-sphere complexation mechanism. Finally, the HFO could be regenerated by leaching the adsorbed fluoride with 0.1 M NaOH solution and reused for at least three times but the fluoride adsorption capacity decreased with repeated use.

CHAPTER 9

CONCLUSIONS

AND

RECOMMENDATIONS

Chapter 9

Conclusion and recommendations

9.1. Conclusions

The main objective of the research was to determine the most suitable and efficient adsorbents which can be used to effectively remove nitrate, phosphate and fluoride from water. Initially various adsorbents were used for each of these contaminants and the adsorbent having the highest adsorption capacity was selected for detailed analysis.

9.1.1. Nitrate adsorption

The nitrate selectivity of adsorption and adsorption capacity were higher for Purolite A520E than these other anion exchange resins (Purolite A520E, Purolite A500PS, Purolite FerrIX A33E and Dowex 21k) tested in batch studies. The Langmuir adsorption capacity was 33 mg N/g for Purolite A520E and the highest column adsorption capacity was 21.3 mg N/g at the inlet concentration of 20 mg N/L, 12 cm bed height and 2.5 m/h filtration velocity. The kinetics of nitrate adsorption by Purolite A520E in the batch study was satisfactorily described using pseudo-first-order, pseudo-second-order and HSDM models. The presence of co-ions such as F^- and PO_4^{3-} had very little effect on this resin's nitrate adsorption capacity even at high concentrations. However, Cl^- and SO_4^{2-} reduced the effectiveness of the resin's ability to adsorb nitrate at high concentrations. Moreover, at all nitrate-to-phosphate ratios in solution, the ratio of nitrate to phosphate adsorbed was higher for Purolite A520E which suggested that the nitrate

selectivity for adsorption was higher than phosphate. Finally, solution pH had little effect on nitrate adsorption in the pH range 5-8.

The empirical Thomas model and a numerical model based on advection-dispersion equation adequately described nitrate adsorption behaviour in a fixed-bed column containing Purolite A520E at two filtration velocities. The breakthrough curve was steeper and breakthrough occurred more rapidly for the higher filtration rate. The experimental and Thomas model predicted breakthrough adsorption capacities (12.0-13.5 mg N/g and 8.2-9.7 mg N/g, respectively) agreed fairly well. Moreover, Purolite A520E can be regenerated by leaching with 1M NaCl and used at least three times without significantly reducing adsorption capacity. It can therefore be concluded that Purolite A520E is a potential nitrate adsorbent with high adsorption capacity which is cost-effective and will remove nitrate from water, even in the presence of moderate concentrations of other anions.

9.1.2. Phosphate adsorption

Of the six adsorbents tested (Purolite A520E, Purolite A502PS, Purolite FerrIX A33E, Dowex 21k XLT, HFO (iron (iii) oxide $HFeO_2$) and Zirconium (IV) hydroxide (H_4O_4Zr)) in a batch study, Purolite FerrIX A33E had the highest phosphate removal capacity. The batch adsorption isotherm data for Purolite FerrIX A33E was satisfactorily explained using the Langmuir, Freundlich and Tempkin isotherm models while the kinetic adsorption data fitted reasonably well to the pseudo-second-order, Elovich and intraparticle diffusion models. Freundlich adsorption constant related to adsorption capacity was highest for Purolite FerrIX A33E among the six adsorbents. The high adsorption capacity for this adsorbent is probably due to the functional groups and the

presence of nano-sized iron oxide particles in the adsorbent. The Langmuir adsorption capacity of Purolite FerrIX A33E was 48 mg P/g which constituted one of the highest phosphorus adsorption capacities reported in the literature for adsorbents. Therefore Purolite FerrIX A33E is a potential adsorbent for removing phosphate from aqueous solutions.

pH had little effect on phosphate adsorption on Purolite FerrIX in the pH range 4 – 10. Furthermore, Cl^-, NO_3^- and F^- did not have much effect on phosphate adsorption but SO_4^{2-} reduced phosphate adsorption at equal concentrations of the anions. At high concentration of the co-ions, the decreasing order of competition of the anions was as follows: $SO_4^{2-} > Cl^- > NO_3^- > F^-$. Fixed-column experimental results showed that Purolite FerrIX A33E is a potential adsorbent for removing phosphate from aqueous solutions compared to the other two adsorbents. Three empirical models - Bohart-Adams, Thomas and Yoon-Nelson models and a numerical model based on advection-dispersion equation - satisfactorily described phosphate adsorption behaviour in a fixed-bed column containing Purolite FerrIX A33E at different bed heights, initial phosphate concentrations and filtration velocities.

The phosphate adsorption capacity of the column was estimated by the Thomas model to be 22.7 mg P/g and by the breakthrough curve calculation to be 16.3 mg/g at the inlet concentration of 30 mg P/L, 12 cm bed height and 10 m/h filtration velocity. The Purolite FerrIX A33E resin could be regenerated by leaching the adsorbed phosphate with 1 M NaOH solution and reused for at least four times without significantly reducing the adsorption capacity.

9.1.3. Fluoride adsorption

Hydrous ferric oxide (HFO) had the highest fluoride adsorption capacity of seven adsorbents (Purolite A520E, Purolite A502PS, Purolite FerrIX A33E, Dowex 21k, HFO (iron (iii) oxide $HFeO_2$), Zirconium (IV) hydroxide (H_4O_4Zr) and α-Alumina (Al_2O_3)) and therefore it was selected for detailed investigations in batch and column study. The batch adsorption data was satisfactorily explained using both the Langmuir and Freundlich isotherms while the column adsorption data fitted reasonably well to the Thomas model but by using an artificial neural network approach this particular model's capability did improve. The Langmuir maximum adsorption capacity at pH 6.5 was 6.71 mg F/g and the highest column breakthrough adsorption capacity was 7.06 mg F/g at the inlet concentration of 30 mg F/L, 12 cm bed height, pH 5 and 2.5 m/h filtration velocity. The adsorption capacity predicted by the Thomas model was also highest (12.7 mg F/g) for these experimental conditions. The kinetic data on fluoride adsorption on HFO was better described by the pseudo-second-order model than the pseudo-first-order model.

Solution pH had a strong effect on fluoride adsorption which decreased continuously from pH 3 to 7. Fluoride adsorption decreased the PZC of HFO. PO_4^{3-} and SO_4^{2-} reduced fluoride adsorption whereas NO_3^- and Cl^- had little effect on fluoride adsorption. Consistent with this data 0.1 M NaCl and 0.1 M Na_2SO_4 failed to desorb fluoride from HFO whereas 0.1 M NaOH was able to desorb nearly all adsorbed fluoride. Data on zeta potential and PZC of HFO and complementary ions' effects on fluoride adsorption and desorption showed that fluoride was specifically adsorbed by HFO by an inner-sphere complexation mechanism. Finally, the HFO could be regenerated by leaching the adsorbed fluoride with 0.1 M NaOH solution and reused for at least three times but the fluoride adsorption capacity declined with repeated use.

9.1.3. Phosphorus recovery

The Purolite FerrIX A33E resin used in the phosphate adsorption study was regenerated by leaching the adsorbed phosphorus with 1 M NaOH solution which resulted in a substantial amount of phosphorus existing in the regeneration solution. This phosphorus was recovered from the regeneration solution as struvite by adding magnesium chloride ($MgCl_2.6H_2O$) and ammonium sulphate ($(NH_4)_2SO_4$) at the molar ratio of phosphate, ammonium and magnesium of 1:1:1. Phosphorus was also recovered as hydroxyapatite by adding calcium hydroxide ($Ca(OH)_2$) to the regeneration solution at the molar ratio of phosphate and calcium of 1:0.5 and 1:2. The XRD and FTIR analysis confirmed the recovered precipitate as pure struvite and hydroxyapatite. The phosphorus content of these precipitates was 12-14% which proved to be similar to the phosphorus contents of commercial struvite and hydroxyapatite. Citric acid solubility of hydroxyapatite was 43% of total P. Based on these results, it was concluded that the recovered struvite and hydroxyapatite could serve as alternative sources of phosphorus and used as fertilisers to alleviate future shortages of phosphorus.

9.2. Recommendations for future studies

The following recommendations are made for any future study on this important topic:

- Future research needs to explore highly efficient, low cost adsorbents such as industrial and agricultural wastes for the removal of nitrate, phosphate and fluoride that have good adsorption capacities.

- The majority of studies reported have been conducted in batch trials on synthetic waters. These trials need to be extended to continuous mode column trials which have more relevance to real operating systems on natural waters containing other ions as well. To remove these anions in continuous column mode, adsorbents need to have good hydraulic conductivity to prevent filters clogging.
- Surface modifications of the adsorbents can be explored to increase the capacity and strength of adsorption without significantly increasing the cost of such modification.
- More regeneration studies need to be done for nitrate, phosphate and fluoride adsorbents to reduce the costs of the water treatment process.
- The technique developed in this study for the production of struvite and hydroxyapatite from phosphate desorbed from adsorbents that were used in removing phosphate from water needs to be tested in pilot plant scale. If this proves to be successful it has the potential to be be applied to commercial scale production of phosphate fertilisers from waste water.

REFERENCES

Abdul, J.M., Vigneswaran, S., Shim, W. G., and Kandasamy, J. (2010). Removal of metsulfuron methyl by granular activated carbon adsorption, Desalination and Water Treatment 21: 247 - 254.

Abe, I., Iwasaki, S., Tokimoto, T., Kawasaki, N., Nakamura, T., and Tanada, S. (2004). Adsorption of fluoride ions onto carbonaceous materials, Journal of Colloid and Interface Science 275: 35 - 39.

Abou-Shady, A., Peng, C., Bi, J., Xu, H., and Juan Almeria, O. (2012). Recovery of Pb (II) and removal of NO_3^- from aqueous solutions using integrated electrodialysis, electrolysis, and adsorption process, Desalination 286: 304 - 315.

Agyei, N.M., Strydom, C.A., and Potgieter, J.H. (2002). The Removal of Phosphate ions from Aqueous Solution by Fly Ash, Slag, Ordinary Portland cement and Related Blends, Cement and Concrete Research 32: 1889 - 1897.

Aharoni, C., and Ungarish, M. (1977). Kinetics of activated chemisorption. Part 2 - Theoretical models, Journal of the Chemical Society, Faraday Transactions I 73: 456 - 464.

Ahmad, A.A., and Hameed, B.H. (2010). Fixed bed adsorption of reactive azo dye onto granular activated carbon prepared from waste, Journal of Hazardous Materials 175: 298 - 303.

Ahmad, R.T., Nguyen, T.V., Shim, W.G., Vigneswaran, S., Moon, H., and Kandasamy, J. (2012). Effluent organic matter removal by Purolite®A500PS: experimental performance and mathematical model, Separation and Purification Technology 98: 46 - 54.

Ahn, S.C., Oh, S.-Y., and Cha, D.K. (2008). Enhanced reduction of nitrate by zero-valent iron at elevated temperatures, Journal of Hazardous Materials 156: 17 - 22.

Akhurst, D.J., Jones, G.B., Clark, M., and McConchie, D. (2006). Phosphate removal from aqueous solutions using neutralised bauxite refinery residues (BauxsolTM0), Environmental chemistry 3: 65 - 74.

Aksu, Z., and Gonen, F. (2004). Biosorption of phenol by immobilized activated sludge in a continuous packed bed: prediction of breakthrough curves, Process Biochemistry 39: 599 - 613.

Allen, S.J., McKay, G. and Khader, K.Y.H. (1989). Intraparticle Diffusion of a Basic Dye during Adsorption onto Sphagnum, Peat and Environmental Pollution 56 (39 - 50): 1989 - 1995.

Alowitz, M.J., and Scherer, M.M. (2002). Kinetics of nitrate, nitrite, and Cr(VI) reduction by iron metal, Environmental Science and Technology 36: 299 - 306.

Amini, M., Mueller, K., Abbaspour, K.C., Rosenberg, T., Afyuni, M., Møller, K.N., Sarr, M., and Johnson, C.A. (2008). Statistical modeling of global geogenic fluoride contamination in groundwater, Environmental Science and Technology 42: 3662 - 3668.

Amuda, O.S., and Ibrahim, A.B. (2006). Industrial waste water treatment using natural material as adsorbent, African Journal of Biotechnology 5(16): 1483 - 1487.

ANZECC (2000). National Water Quality Management Strategy: An Introduction to the Australian and New Zealand Guidelines for Fresh and Marine Water Quality. Australian Government Department of Sustainability, Environment, Water, Population and Communities, Canberra, Australia.

Arami, M., Yousefi Limaee, N., and Mahmoodi, N.M. (2008). Evaluation of the adsorption kinetics and equilibrium for the potential removal of acid dyes using a biosorbent, Chemical Engineering Journal 139 (1): 2 - 10.

Awual, R., Jyo, A., El-Safty, S.A., Tamada, M., and Seka, N. (2011). A weak-fibrous anion exchanger effective for rapid phosphate removal from water, Journal of Hazardous Materials 188: 164 - 171.

Bae, B., Jung, Y., Han, W., and Shin, H. (2002). Improved brine recycling during nitrate removal using ion exchange, Water Research 36: 3330 - 3340.

Bahena, J.L.R., Cabrera, A.R., Valdivieso, A.L., and Urbina, R.H. (2002). Fluoride adsorption onto a-Al_2O_3 and its effect on the zeta potential at the alumina–aqueous electrolyte interface, Separation and Purification Technology 37: 1973 - 1987.

Bastin, O., Janssens, F., Dufey, J., and Peeters, A. (1999). Phosphorus removal by a synthetic iron oxide - gypsum compound. Ecological Engineering 12: 339 - 351.

Bayraktar, D., and Tas, A.C. (1999). Chemical Preparation of Carbonated Calcium Hydroxyapatite Powders at 37ºC in Urea-containing Synthetic Body Fluids, Journal of the European Ceramic Society 19: 2573 - 2579.

Benyoucef, S., and Amrani, M. (2011a). Adsorption of phosphate ions onto low cost Aleppo pine adsorbent, Desalination 275: 231 - 236.

Beverloo, W.A., Pierik, G.M., and Lubyen, A.M.K.Ch. (1984). Adsorption rate of organics from aqueous solutions onto granular GAC, in: A.L. Myers, G. Belfort (Eds.), Fundamentals of Adsorption, The Engineering Foundation, NewYork, 95 - 104.

Bhatnagar, A., and Sillanpää, M. (2011a). A review of emerging adsorbents for nitrate removal from water, Chemical Engineering Journal 168: 493 - 504.

Bhatnagar, A., Kumar, E., and Sillanpää, M. (2011b). Fluoride Removal from Water by adsorption – A review, Chemical Engineering Journal 171: 811 - 840.

Bilgili, M.S. (2006). Adsorption of 4-chlorophenol from aqueous solutions by XAD-4 resin: isotherm, kinetic, and thermodynamic analysis, Journal of Hazardous Materials 137: 157 - 164.

Bindhu, B., and Thambi, T.A. (2012). Formation and Microanalysis Of Struvite Urinary Calculi, International Journal of Engineering Research and Applications (IJERA) 2 (4): 1480 - 1485.

Biswas, K., Gupta, K., and Ghosh, U.C. (2009). Adsorption of fluoride by hydrous iron (III) – tin (IV) bimetal mixed oxide from the aqueous solutions Chemical Engineering Journal 149: 196 - 206.

Blanchard, G., Manuaye, M., and Martin, G. (1984). Removal of heavy metals from waters by means of natural zeolites, Water Research 18: 1501 - 1507.

Blaney, L.M., Cinar, S., and Sengupta, A.K. (2007). Hybrid anion exchanger for trace phosphate removal from water and wastewater, Water Research 41: 1603 - 1613.

Bohart, G.S., and Adams, E.Q. (1920). Behaviour of charcoal towards chlorine, Journal of the Chemical Society 42: 523 - 529.

Bolan N.S., Hedley, M.J., and Loganathan, P. (1993). Preparation, forms and properties of controlled- release phosphate fertlizers, Fertilizer Research 35: 13 - 24.

Booker, N.A., Priestley, A.J., and Fraser, I.H. (1999). Struvite formation in wastewater treatment plants: opportunities for nutrient recovery, Environmental Technology 20: 777 - 782.

Boumediene, M., and Achour, D. (2004). Denitrification of the underground waters by specific resin exchange of ion, Desalination 168: 187 - 194.

Bowden, L.I., Jarvis, A.P., Younger, P.L., and Johnson, K.L. (2009). Phosphorus removal from waste waters using basic oxygen steel slag, Environmental Science and Technology 43: 2476 - 2481.

Brown, P.N., and Byrne, G.D., and Hindmarsh, A.C. (1989). VODE: a variable coefficient ODE solver, SIAM Journal on Scientific Computing (SISC) 10: 1038 - 1051.

Bulgariu, L., Ceica, A., Lazar, L., Cretescu, I., and Balasanian, I. (2010). Equilibrium and Kinetics Study of Nitrate Removal from Water by Purolite A100 Resin, Revista de Chimie 61: 1136 - 1141.

Bulusu, K.R., Sundaresan, B.B., Pathak, B.N., Nawlakhe, W.G., Kulkarni, D.N., and Thergaonkar, V.P. (1979). Fluorides in water, defluoridation methods and their limita-tions, Journal of the Institution of Engineers (India) Environmental Engineering Division 60: 1 - 25.

Burge, S., and Halden, R. (1999). Report on Environmental Restoration Division, Lawrence Livermore National Laboratory, UCRL-ID-135639, University of California, Livermore.

Cambardella, C.A., Moorman, T.B., Jaynes, D.B., Hatfield, J.L., Parkin, T.B., Simpkins, W.W., and Karlen, D.L. (1999). Water quality in Walnut Creek watershed: nitrate–

nitrogen in soils, subsurface drainage water, and shallow groundwater, Journal of Environmental Quality 28 (1): 25 - 34.

Canter, L.W. (1997). Nitrates in Groundwater, CRC Press, Boca Raton

Carucci, A., Ramadori, R., Rossetti, S., and Tomei, M.C. (1996). Kinetics of denitrification reactions in single sludge systems, Water research 30 (1): 51 - 56.

Cavas, L., Karabay, Z., Alyuruk, H., Dogan, H., and Demir, G.K. (2011). Thomas and artificial neural network models for the fixed-bed adsorption of methylene blue by a beach waste Posidonia oceanica (L.) dead leaves, Chemical Engineering Journal 171: 557 - 562.

Cengelo˘glu, Y., Kir, E., Ersöz, M. (2002). Removal of fluoride from aqueous solution by using red mud, Separation and Purification Technology 28: 81 - 86.

Cengelo˘glu, Y., Tor, A., Ersoz, M., Arslan, G. (2006). Removal of nitrate from aqueous solution by using red mud, Separation and Purification Technology 51: 374 - 378.

Chartres, C., and Williams, J. (2006). Can Australia Overcome its Water Scarcity Problems?, Journal of Developments in Sustainable Agriculture 1: 17 - 24.

Chatterjee, S., Woo, S.H. (2009). The removal of nitrate from aqueous solutions by chitosan hydrogel beads, Journal of Hazardous Materials 164: 1012 - 1018.

Chaturvedi, A.K., Yadava, K.P., Pathak, K.C., Singh, V.N. (1990). Defluoridation of water by adsorption on fly ash, Water, Air, and Soil Pollution 49: 51 - 61.

Chaudhari, N., Pereira, E., Landin, A.M. and Roper, S.D. (2003). Immunodetecting a candidate umami receptor, taste-mGluR4, in taste cells. Chemical Senses 28: 559 - 565.

Chauhan, C.K., Joshi, M.J. (2008). Growth and characterization of struvite crystals, Indian journal of Pure and Applied physics 46: 507 - 512.

Chauhan, C.K., Joshi, M.J. (2011). In vitro crystallization, characterization and growth inhibition study of urinary type struvite crystals, Journal of Crystal growth 362 (1): 330 - 337.

Chen, Y.M., Li, C.W., Chen, S.S. (2005). Fluidized zero valent iron bed reactor for nitrate removal, Chemosphere 59: 753 - 759.

Cheng, I.F., Muftikian, R., Fernando, Q., Korte, N. (1997). Reduction of nitrate to ammonia by zero valent iron, Chemosphere 35: 2689 - 2695.

Cheng, X., Huang, X., Wang, X., Zhao, B., Chen, A., and Sun, D. (2009). Phosphate adsorption from sewage sludge using zinc-aluminum layered double hydroxides, Journal of Hazardous Materials 169: 958 - 964.

Chien, S.H., and Clayton, W.R. (1980). Application of Elovich equation to the kinetics of phosphate release and sorption in soils, Soil Science Society of America Journal 44: 265 - 268.

Chimenos, J. M., Fernandez, A. L., Villalba, G., Segarra, M., Urruticoechea, A., Artaza, B. and Espiell, F. (2003) Removal of ammonium and phosphates from wastewater resulting from the process of cochineal extraction using MgO-containing by-product. Water Research 37 (7): 1601 - 1607.

Chinoy, N.J. (1991). Effects of fluoride on physiology of animals and human beings, Indian Journal of Environment and Toxicology 1: 17 - 32.

Chinoy, N.J. (1994) Effect of fluoride on physiology of some animals and human beings. Indian Journal of Environment and Toxicology 1: 17 - 32.

Chiu, H.-F., Tsai, S.-S., and Yang, C.Y. (2007). Nitrate in drinking water and risk of death from bladder cancer: An ecological case-control study in Taiwan, Journal of Toxicology and Environmental Health A 70: 1000 - 1004.

Chitrakar, R., Tezuka, S., Sonoda, A., Sakane, K., Ooi, K., and Hirotsu, T. (2006a). Phosphate adsorption on synthetic goethite and akaganeite, Journal of Colloid and Interface Science 298: 602 - 608.

Chitrakar, R., Tezuka, S., Sonoda, A., Sakane, K., Ooi, K., and Hirotsu, T. (2006b). Selective adsorption of phosphate from sea water and wastewater by amorphous zirconium hydroxide, Journal of Colloid and Interface Science 297: 426 - 433.

Chu, J.C., Kalil, J., and Wetteroth, W. A. (1953). Mass Transfer in a fluidized bed, Chemical Engineering Progress 49: 141 - 149.

Cloutier, J.N., Leduy, A., and Ramalho, R.S. (1985). Peat adsorption of herbicide 2, 4-D from wastewater, The Canadian Journal of Chemical Engineering 63: 250 - 257.

Collins, J.J. (1967). Chemical Engineering Programing Symposium Series, 63: 31.

Cordell, D., Drangert, J.-O., and White, S. (2009). The Story of Phosphorus: Global food security and food for thought. Global Environmental Change 19: 292 - 305.

Cordell, D., Rosemarin, A., Schröder, J.J., and Smit, A.L. (2011). Towards global phosphorus security: A systems framework for phosphorus recovery and reuse options. Chemosphere 84: 747 - 758.

Crittenden, J.C., Luef, P., and Hand, D.W. (1985). Prediction of multicomponent equilibria in background mixtures of unknown composition, Water Research 19: 1537 - 1548.

Crutchik, D., Sánchez, A., and Garrido, J.M. (2013). Simulation and experimental validation of multiple phosphate precipitates in a saline industrial wastewater, Separation and Purification Technology 118: 81 - 88.

Daifullah, A.A.M., Girgis, B.S., and Gada, H.M.H.A. (2004). A study of the factors affecting the removal of humic acid by activated carbon prepared from biomass material, Colloids and Surfaces A: Physicochemical and Engineering Aspects 235: 1 - 10.

Daifullah, A.A.M., Yakout, S.M., and Elreefy, S.A. (2007). Adsorption of fluoride in aqueous solutions using KMnO4-modified activated carbon derived from steam pyrolysis of rice straw, Journal of Hazardous Materials 147: 633 - 643.

Danny, D.K., Ko, K.F., Porter, J.F., and McKay, G. (2001). Film pore diffusion model for the fixed-bed sorption of copper and cadmium ions onto bone char, Water Research 35: 3876 - 3886.

Das, D.P., Das, J., and Parida, K. (2003). Physicochemical characterization and adsorption behaviour of calcined Zn/Al hydrotalcite-like compound (HTlc) towards removal of fluoride from aqueous solution, Journal of Colloid and Interface Science 261: 213 - 220

Demiral, H., and Gunduzo˘glu, G. (2010). Removal of nitrate from aqueous solutions by activated carbon prepared from sugar beet bagasse, Bioresource Technology 101: 1675 - 1680

De-Bashan, L.E. and Bashan, Y. (2004). Recent advances in removing phosphorus from wastewater and its future use as fertilizer, Water Research 38: 4222 - 4246.

Delaney, P., McManamon, C., Hanrahan, J. P., Copley, M. P., Holmes, J. D., and Morris, M. A. (2011). Development of chemically engineered porous metal oxides for phosphate removal, Journal of Hazardous Materials 185: 382 - 391.

Delgado, J.M.P.Q. (2006). Heat and Mass Transfer 42 (4): 279 - 310.

Deliyanni, E.A., Peleka, E.N., and Lazaridis, N.K. (2007). Comparative study of phosphates removal from aqueous solutions by nanocrystalline akaganéite and hybrid surfactant-akaganéite, Separation and Purification Technology 52: 478 - 486.

Della Rocca, C., Belgiorno, V., and Meriç, S. (2007). Overview of in-situ applicable nitrate removal processes, Desalination 204 (1-3): 46 - 62.

Dey, S., Goswami, S., and Ghosh, U.C. (2004). Hydrous Ferric Oxide (HFO) - A scavenger for fluoride from contaminated water. Water Air Soil Poll 158: 311 - 323.

Dissanayake, C. B. (1991). The fluoride problem in the groundwater of Sri Lanka – environmental management and health, International Journal of Environmental Studies 19: 195 - 203.

Do, D.D. (1998). Adsorption Analysis: Equilibrium and Kinetics, Imperial College Press, UK.

Donnert, D., and Salecker, M. (1999a). Elimination of phosphorus from waste water by crystallization, Environmental Technology 20: 735 - 742.

Donnert, D., and Salecker, M. (1999b). Elimination of phosphorus from municipal and industrial waste water. Water Science and Technology 40: 195 - 202.

Doyle, J.D., and Parsons, S.A. (2002). Struvite formation, control and recovery, Water Research 36: 3925 - 3940.

Doyle, J.D., Oldring, K., Churchley, J., Price, C., and Parsons, S.A. (2003). Chemical control of struvite precipitation Journal of Environmental Engineering (ASCE) 129: 419 - 426.

Driver J, Lijmbach D, and Steen I. (1999). Why recover phosphorus for recycling, and how? Environmental Technology 20 (7): 651 - 662.

Durrant, A.E., Scrimshaw, M.D., Stratful, I., and Lester, J.N. (1999). Review of the feasibility of recovering phosphate from wastewater for use as a raw material by phosphate industry, Environmental Technology 20 (7): 749 - 758.

El Midaoui, A., Elhannouni, F., Taky, M., Chay, L., Sahli, M.A.M., Echihabi, L., and Hafsi, M. (2002). Optimization of nitrate removal operation from ground water by electrodialysis, Separation and Purification Technology, 29: 235 - 144.

Elzinga, E.J., and Sparks, D.L. (2007). Phosphate adsorption onto hematite: An insitu ATR-FTIR investigation of the effects of pH and loading level on the mode of phosphate surface complexation, Journal of Colloid and Interface Science 308: 53 - 70.

EPA (2009). National Primary Drinking Water Standards, http://water.epa.gov/drink/ contaminant/index.cfm#list.

European Commission (2009). Guidance Document on Eutrophication Assessment. Common Implementation Stractegy for the Water Framework Directive (2000/60/EC) Guidance.

FAO (2004). Use of phosphate rocks for sustainable agriculture. Fertilizer and plant nutrition Bulletin 13, Food and Agriculture Organization of the United Nations, http://www.fao.org/docrep/007/y5053e/y5053e06.htm (accessed July 28, 2010).

Faur, C., Cogunaud, A., Dreyfus, G., and Cloirec, P.L. (2008). Modelling the breakthrough of activated carbon filters by pesticides in surface waters with static and recurrent neural networks, Chemical Engineering Journal 145: 7 - 15.

Faust, S.D., and. Aly, O.M. (1987). Adsorption processes for water treatment; Butterworth, 1987.

Fawell, J., Bailey, K., Chilton, E., Dahi, E., Fewtrell, L., and Magara, Y. (2006). Fluoride in Drinking Water, World Health Organization, IWA Publishing, UK.

Fewtrell, L. (2004). Drinking-water nitrate, methemoglobinemia, and global burden of disease: a discussion. Environ Health Perspect 112:1371 - 1374

Fitzpatrick, J., Aoki, H., Koh, S., deBarbadillo, C., Midorikawa, I., Miyazaki, M., Omori, A., and Shimizu, T. (2011). Phosphorus recovery with ultra-low adsorption process, Water Environment Federation/IWA Nutrient Recovery Management Conference: 778 - 789.

Foletto, E.L., dos Santos, W.R.B., Mazutti, M.A., Jahn, S.L., and Gündel, A. (2013). Production of struvite from beverage waste as phosphorus source, Material Research 16 (1): 242 - 245.

Ford, R.G. (2006). Structural dynamics of metal partitioning to mineral surfaces. In: Hamon, R., McLaughlin, M., and Lombi, E. (eds.), Natural Attenuation of Trace Element Availability in Soils. CRC Taylor and Francis Group, New York, 73 - 88.

Freundlich, H. (1926). Colloid and capillary Chemistry, Methuen, London.

Fritz W. and Schtunder E. U. (1981) Competitive adsorption of two dissolved organics onto activated carbon, Chemical Engineering Science 36: 721 - 730.

Furuzono, T., Walsh, D., Sato, K., Sonoda, K., and Tanaka, J. (2001). Effect of reaction temperature on the morphology and size of hydroxyapatite nanoparticles in an emulsion system, Journal of Materials Science Letters (20): 111 - 114.

Fytianos, K., Voudrias, E., and Kokkalis, E. (2000). Sorption-desorption behavior of 2, 4-dichlorophenol by marine sediments, Chemosphere, 40(1): 3 - 6.

Gavagnin, R., Biasetto, L., Pinna, F., and Strukul, G. (2002). Nitrate removal in drinking waters: the effect of tin oxides in the catalytic hydrogenation of nitrate by Pd/SnO_2 catalysts, Applied Catalysis B: Environmental 38: 91 - 99.

Genz, A., Kornmüller, A., and Jekel, M. (2004). Advanced phosphorus removal from membrane filtrates by adsorption on activated aluminium oxide and granulated ferric hydroxide, Water Research 38: 3523 - 3530.

Ghorai, S., and Pant, K.K. (2005). Equilibrium, kinetics and breakthrough studies for adsorption of fluoride on activated alumina, Separation and Purification Technology 42: 265 - 271.

Goel, J., Kadirvelu, K., Rajagopal, C., and Garg, V.K. (2005). Removal of lead (II) by adsorption using treated granular activated carbon: batch and column studies. Journal of Hazardous Materials 125: 211 - 220.

Gong, G., Ye, S., Tian, Y., Wang, Q., Ni, J., and Chen, Y. (2009). Preparation of a new sorbent with hydrated lime and blast furnace slag for phosphorus removal from aqueous solution, Journal of Hazardous Materials 166: 714 - 719.

Goswami, S., and Ghosh, U.C. (2005). Studies on Adsorption Behaviour of Cr (VI) onto Synthetic Hydrous Stannic Oxide, Water SA 31 (44): 57 - 60.

Greenburg, A.E., Levin, G., and Kauffman, W.J. (1955). The effect of phosphorus removal on the activated sludge process, Sewage and industrial wastes 27: 227 - 232.

Greenan, C.M., Moorman, T.B., Kaspar, T.C., Parkin, T.B., and Jaynes, D.B. (2006). Comparing carbon substrates for denitrification of subsurface drainage water**,** Journal of Environmental Quality 35 (3): 824 - 829.

Gu, B., Ku, Y-K., and Jardine, P.M. (2004). Sorption and binary exchange of nitrate, sulphate and uranium on an anion exchange resin, Environmental Science and Technology 38: 3184 - 3188.

Gupta, V.K., Carrott, J.M., Carrott, M.M.L.R., and Suhas (2009). Low-cost adsorbents: Growing approach to wastewater treatment – a review, Critical Reviews in Environmental Science and Technology 39 (10): 783 - 842.

Gupta, M.D., Loganathan, P., and Vigneswaran, S. (2012). Adsorptive removal of nitrate and phosphate from water by a Purolite ion exchange resin and hydrous ferric oxide columns in series, Separation Science and Technology 47: 1785 - 1792.

Guo, W.S., Shim, W.G., Vigneswaran, S., Ngo, H. H. (2005). Effect of operating parameters in a submerged membrane adsorption hybrid system: experiments and mathematical modelling, Journal of Membrane Science 247: 65 - 67.

Hameed, B.H., Din, A.T.M., and Ahmad, A.L. (2007). Adsorption of methylene blue onto bamboo-based activated carbon: Kinetics and equilibrium studies, Journal of Hazardous Materials 141: 819 - 825.

Harrison, P.T.C. (2005). Fluoride in water: a UK perspective, Journal of Fluorine Chemistry 126: 1448 - 1456.

Haugen, K.S., Semmens, M.J., and Novak, P.J. (2002). A novel in-situ technology for the treatment of nitrate contaminated groundwater, Water Research 36: 3497 - 3506.

Healy, M.G., Rodgers, M., and Mulqueen, J. (2006). Denitrification of a nitrate-rich synthetic wastewater using various wood-based media materials, Journal of Environmental Science and Health 41 (5): 779 - 788.

Hell, F., Lahnsteiner, J., Frischherz, H., and Baumgartner, G. (1998). Experience with full-scale electrodialysis for nitrate and hardness removal, Desalination, 117: 173 - 180.

Helferich, F. (1995). Ion Exchange, Dover Publication Inc., USA.

Hekmatzadeh, A.A., Karimi - Jashani, A., Talebbeydokhti, N., and Klove, B. (2012). Modeling of nitrate removal for ion exchange resin in batch and fixed bed experiments, Desalination 284: 22 - 31.

Heughebaert, J.C. (1977). Contribution à l'étude de l'évolution des orthophosphates de calcium précipités amorphes en orthophosphates apatitiques, Thesis, Institute National Polytechnique, Toulouse, France.

Hiemstra, T., and Riemsdijk, W.H.V. (2000). Fluoride adsorption on goethite in relation to different types of surface sites, Journal of Colloid and Interface Science 225: 94 - 104.

Ho, Y.S., and McKay, G. (1998). Sorption of dye from aqueous solution by peat, Chemical Engineering Journal 70: 115 - 124.

Hoek, J.P., Hoek, W.F., and lapwijk, A. (1988). Nitrate removal from ground water—use of a nitrate selective resin and a low concentrated regenerant, Water, Air, and Soil Pollution 37: 41 - 53.

Hofmann, A., Pelletier, M., Michot, L., Stradner, A., Schurtenberger, P., and Kretzschmar, R. (2004). Characterization of the pores in hydrous ferric oxide aggregates formed by freezing and thawing, Journal of Colloid and Interface Science 271: 163 - 173.

Huang, C.P., Wang, H.W., and Chiu, P.C. (1998). Nitrate reduction by metallic iron, Water Research 32: 2257 - 2264.

Huang, Y.H., and Zhang, T.C. (2002). Kinetics of nitrate reduction by iron at near neutral pH, Journal of Environmental Engineering 128: 604 - 611.

Huang, Y.H., and Zhang, T.C. (2004). Effects of low pH on nitrate reduction by iron powder, Water Research 38: 2631 - 2642.

Hussain, S., Aziz, H.A., Isa, M.H., Ahmad, A., Leeuwen, J.V., Zou, L., Beecham, S., and Umar, M. (2011). Orthophosphate removal from domestic wastewater using limestone and granular activated carbon, Desalination 271: 265 - 272.

Hutchinson, D.H., and Robinson, C.W. (1990). A microbial regeneration process for granular activated carbon−II. regeneration studies, Water Research 24: 1209 - 1215.

Islam, M., and Patel, R. (2009). Nitrate sorption by thermally activated Mg/Al chloride hydrotalcite-like compound, Journal of Hazardous Materials 169 (2009): 524 - 531.

Islam, M., Mishra, P.C., and Patel, R. (2010). Physicochemical characterization of hydroxyapatite and its application towards removal of nitrate from water, Journal of Environmental Management 91: 1883 - 1891.

Islam, M., and Patel, R. (2010). Synthesis and physicochemical characterization of Zn/Al chloride layered double hydroxide and evaluation of its nitrate removal efficiency, Desalination 256: 120 - 128.

Islam, M., and Patel, R. (2011). Thermal activation of basic oxygen furnace slag and evaluation of its fluoride removal efficiency, Chemical Engineering Journal 169: 68 - 77.

IUPAC (1985). International Union of Pure and Applied Chemistry Technical Reports and Recommendations.

Jagtap, S., Yenkie, M.K., Labhsetwar, N., and Rayalu, S. (2012) Fluoride in drinking water and defluoridation of water, Chemical Reviews: 2454 - 2466.

Jinadasa, K.B.P.N., Weerasooriya, S.W.R., and Dissanayake, C.B. (1988). A rapid method for the defluoridation of fluoride-rich drinking waters at village level, International Journal of Environmental Studies 31: 305 - 312.

Johansson, L., and Gustafsson, J.P. (2000). Phosphate removal using blast furnace slags and opoka-mechanisms, Water Research 34: 259 - 265.

Johir, M.A.H., George, J., Vigneswaran, S., Kandasamy, J., and Grasmick, A. (2011). Removal and recovery of nutrients by ion exchange from high rate membrane bio-reactor (MBR) effluent, Desalination 275: 197 - 202.

Jorgensen, S.E., and Williams, W.D. (2001). Water Quality: The Impact of Eutrophication, United Nations Environment Program.

Jourak, A., Herrmann, I., Frishfelds, V., Lundström, T.S., and Hedström, A. (2011). Modeling of Phosphate Removal by Filtra P in Fixed-bed Columns, 2nd International Conference on Environmental Science and Technology (ICEST), 241 - 248.

Kamble, S.P., Jagtap, S., Labhsetwar, N.K., Thakare, D., Godfrey, S., Devotta, S., Rayalu, S.S. (2007). Defluoridation of drinking water using chitin, chitosan and lanthanum-modified chitosan, Chemical Engineering Journal 129: 173 - 180.

Kapoor, A., and Viraraghavan, T. (1997). Nitrate removal from drinking water - review, Journal of Environmental Engineering 123: 371 - 380.

Kannan, S., Lemos, I.A.F., Rocha, J.H.G., and Ferreira, J.M.F. (2005). Synthesis and characterization of magnesium substituted biphasic mixtures of controlled hydroxyapatite/β-tricalcium phosphate ratios, Journal of Solid State Chemistry (178): 3190 - 3196.

Khadhraoui, M., Watanabe, T., and Kuroda, M. (2002). The effect of the physical structure of a porous Ca-based sorbent on its phosphorus removal capacity, Water Research 36: 3711 - 3718

Koilraj, P., and Kannan, S. (2010). Phosphate uptake behaviour of ZnAlZr ternary double hydroxides through surface precipitation, Journal of Colloid and Interface Science 341: 289 - 297.

Kostraba, T.N., Gay, E.C., Rewers, M., and Hamman, R.F. (1992). Nitrate levels in community drinking waters and risk of IDDM. An ecological analysis, Diabetes Care 15: 1505 - 1508.

Ku, Y., and Chiou, H. (2002). The adsorption of fluoride ion from aqueous solution by activated alumina, Water, Air, and Soil Pollution 133: 349 - 360.

Kumar, E., Bhatnagar, A., Minkyu, J., Jung, W., Lee, S., Kim, S., Lee, G., Song, H., Choi, J., Yang, J., and Jeon, B. (2009). Defluoridation from aqueous solutions by granular ferric hydroxide (GFH), Water Research 43: 490 - 499.

Kuroda, A., Takiguchi, N., Gotanda, T., Nomura, K., Kato, J., Ikeda, T., and Ohtake, H. (2002). A simple method to release polyphosphate from activated sludge for phosphorus reuse and recycling, Biotechnology and Bioengineering 78: 333 - 338.

Kurtulus, G., and Tas, A.C. (2011). Transformations of neat and heated struvite ($MgNH_4PO_4.6H_2O$), Materials Letters 65: 2883 - 2886.

Kuzawa, K., Jung, Y., Kiso, Y., Yamada, T., Nagai, M., and Lee, T. (2006). Phosphate removal and recovery with a synthetic hydrotalcite as an adsorbent, Chemosphere 62: 45 - 52.

Lai, Y.D., and Liu, J.C. (1996). Fluoride removal from water with spent catalyst, Separation Science and Technology 31: 2791 - 2803.

Lagergren, S. (1898). Zur theorie der sogenannten adsorption gelˆster stoffe, Kungliga Svenska Vetenskapsakademiens, Handlingar 24 (4): 1 - 39.

Langmuir, I. (1918). The adsorption of gases on plane surfaces of glass, mica and platinum, Journal of American Chemical Society 40 (9): 1361 - 1403.

Le Corre, K.S., Valsami-Jones, E., Hobbs, P., and Parsons, S.A. (2009). Phosphorus recovery from wastewater by struvite crystallization: a review, Critical Reviews in Environmental Science and Technology 39: 433 - 477.

Lee, S.H. (1995). Phosphorus removal mechanism in soil and slag media, PhD thesis, University of Technology Sydney (UTS), Australia.

Lee, S.I., Weon, S.Y., Lee, C.W., and Koopman, B. (2003). Removal of nitrogen and phosphate from wastewater by addition of bittern, Chemosphere 51: 265 - 271.

Lee, S., Lee, K., Rhee, S., and Park, J. (2007). Development of a new zero-valent iron zeolite material to reduce nitrate without ammonium release, Journal of Environmental Engineering 133: 6 - 12.

Levin, G.V., and Shapiro, J., 1965. Metabolic uptake of phosphorus by wastewater organisms. Journal Water Pollution Control Federation 37 (6): 800 - 821.

Leyva-Ramos, R., and Ovalle-Turrubiartes, J. (1999). Adsorption of Fluoride from Aqueous Solution on Aluminum-Impregnated Carbon. Carbon 37 (4): 609 - 617.

Leyva-Ramos R., Rivera-Utrilla J., Medellin-Castillo N.A., and Sanchez-Polo M. (2010). Kinetic modeling of fluoride adsorption from aqueous solution onto bone char, Chemical Engineering Journal 158: 458 - 467.

Li, Z.H., and Bowman, R.S. (2001). Retention of Inorganic Oxyanions by Organo-kaolinite, Water Resources 35: 3771 - 3776.

Li, Y.H., Wang, S., Zhang, X., Wei, J., Xu, C., Luan, Z., Wu, D., and Wei, B. (2003). Removal of fluoride from water by carbon nanotube supported alumina, Environmental Technology 24: 391 - 398.

Li, Y., Liu, C., Luan, Z., Peng, X., Zhu, C., Chen, Z., Zhang, Z., Fan, J., and Jia, Z. (2006). Phosphate removal from aqueous solutions using raw and activated red mud and fly ash, Journal of Hazardous Materials 137: 374 - 383.

Liang, S., Mann, M.A., Guter, G.A., Kim, O., and Hardan, D.L. (1999). Nitrate removal from contaminated ground water, Journal - American Water Works Association 91: 79 - 91.

Liao, X., and Shi, B. (2005). Adsorption of fluoride on zirconium (IV)-impregnated collagen fiber, Environmental Science and Technology 39: 4628 - 4632.

Lin, S.H., and Wu, C.L. (1996). Removal of nitrogenous compounds from aqueous solution by ozonation and ion exchange, Water Research 30: 1851 - 1857.

Liou, Y.-H., Lo, S.L., Lin, C.J., Hu, C.Y., Kuan, W.H., and Weng, S.C. (2005). Methods for accelerating nitrate reduction using zerovalent iron at near-neutral pH: effects of H2-reducing pretreatment and copper deposition, Environmental Science and Technology 39: 9643 - 9648.

Liu, J.C. (2009). Recovery of phosphate and ammonium as struvite from semiconductor wastewater, Separation and Purification Technology 64: 368 - 373.

Liu, Y.H., Kwag, J.H., Kim, J.H., and Ra, C.S. (2011). Recovery of nitrogen and phosphorus by struvite crystallization from swine wastewater, Desalination 277: 364 - 369.

Loganathan, P., Hedley, M.J., Grace, N.D., Lee, J., Cronin, S.J., Bolan, N.S., and Zanders, J.M. (2003). Fertiliser contaminants in New Zealand grazed pasture with special reference to cadmium and fluorine – a review, Australian Journal of Soil Research 41: 501 - 532.

Loganathan, P., Vigneswaran, S., Kandasamy, J., and Naidu, R. (2013a). Defluoridation of drinking water using adsorption processes, Journal of Hazardous Materials (248 – 249): 1 - 19.

Loganathan, P., Vigneswaran, S., and Kandasamy, J. (2013b). Enhanced removal of nitrate from water using surface modification of adsorbents ‐ A review, Journal of Environmental Management 131: 363 - 374.

Loganathan, P., Vigneswaran, S., Kandasamy, J., and Bolan, N.S. (2014). Removal and recovery of phosphate from water using sorption, Critical Reviews in Environmental Science and Technology, 44: 847 - 907.

Lohumi, N., Goasin, S., Jain, A., Gupta, V.K., and Verma, K.K. (2004). Determination of nitrate in environmental water samples by conversion into nitrophenols and solid phase extraction−spectrophotometry, liquid chromatography or gas chromatography mass spectrometry, Analytica Chimica Acta 505: 231 - 237.

Long, F., Gong, J., Zeng, G., Chen, L., Wang, X., Deng, J., Niu, Q., Zhang, H., and Zhang, X. (2011). Removal of phosphate from aqueous solution by magnetic Fe-Zr binary oxide. Chemical Engineering Journal 171: 448 - 455.

Lüdtke, K., Peinermann, K., Kasche, V., and Behling, R. (1998). Nitrate removal of drinking water by means of catalytically active membranes, Journal of Membrane Science 151: 3 - 11.

Luo, F., and Inoue, K. (2004). The removal of fluoride ion by using metal (III)-loaded Amberlite resins, Solvent Extraction and Ion Exchange 22: 305 - 322.

Lv, L., He, J., Wei, M., Evans, D.G., and Duan, X. (2006). Factors influencing the removal of fluoride from aqueous solution by calcined Mg-Al-CO3 layered double hydroxides, Journal of Hazardous Materials B133: 119 - 128.

Ma, J., Lenhart, J.H., and Tracy, K. (2011). Orthophosphate adsorption equilibrium and breakthrough on filtration media for storm-water runoff treatment Journal of Irrigation and Drainage Engineering (ASCE) 137: 244 - 250.

Mahmudov, R., and Huang, C.P. (2011). Selective adsorption of oxyanions on activated carbon exemplified by Filtrasorb 400 (F400), Separation and Purification Technology 77: 294 - 300.

Majumdar, D., and Gupta, N. (2000). Nitrate pollution of groundwater and associated human health disorders**,** Indian journal of environmental health 42: 28 - 39.

Maliyekkal, S.M., Sharma, A.K., and Philip, L. (2006). Manganese-oxide-coated alumina: a promising sorbent for defluoridation of water, Water Research 40: 3497 - 3506.

Mall, I.D., Srivastava, W., and Argawal, K. (2006). Removal of orange G and Methyl Violet Dyes by Adsorption onto Bagasse Fly Ash-Kinetic Study and Equilibrium Isotherm Analyse, Dyes and Pigments 69: 210 - 223.

Manes, M. (1980). The Polanyi adsorption potential theory and its application to adsorption from water solution onto activated carbon. In: Suffet, I.H., McGuire, M.J. (Eds.), Activated Carbon Adsorption of Organics from the Aqueous Phase. Ann Arbor Science, Michigan, 43 - 63.

Marshall, W.E., and Wartelle, L.H. (2004). An anion exchange resin from soybean hulls, Journal of Chemical Technology and Biotechnology 79: 1286 - 1292.

Martin, B.D., Parsons, S.A., and Jefferson, B. (2009). Removal and recovery of phosphate from municipal wastewaters using a polymeric anion exchanger bound with hydrated ferric oxide nanoparticles, Water Science and Technology 60: 2637 - 2645.

Masukume, M., Eskandarpour, A., Onyango, M.S., Ochieng, A., and Otieno, F. (2011).Treating high nitrate groundwater using surfactant modified zeolite in fixed bed column, Separation Science and Technology 46: 1131 - 1137.

Matsui, H., Randell, S.H., Peretti, S.W., Davis, C.W., and Boucher, R.C. (1998). Coordinated clearance of periciliary liquid from airway surfaces, Journal of Clinical Investigation 102: 1125 - 1131.

McKay, C.P. (1996). Elemental composition, solubility, and optical properties of Titan's organic haze, Planetary and Space Science 44: 741 - 747.

Meenakshi, and Maheshwari, R.C. (2006). Fluoride in drinking water and its removal, Journal of Hazardous Materials B137: 456 - 463.

Meenakshi, S., and Viswanathan, N. (2007). Identification of selective ion-exchange resin for fluoride sorption, Journal of Colloid and Interface Science 308: 438 - 450.

Midorikawa, I., Aoki, H., Omori, A., Shimizu, T., Kawaguchi, Y., Katsusai, K., and Murakami, T. (2008). Recovery of high purity phosphorus from municipal wastewater secondary effluent by a high-speed adsorbent, Water Science and Technology 58: 1601 - 1607.

Miyahara, M., and Okazaki, M. (1993). Correlation of Concentration-Dependent Surface Diffusivity in Liquid Phase Adsorption, Journal of Chemical Engineering of Japan 5: 510 - 516.

Mishra, S.P., Das, M., and Dash, U.N. (2010). Review on adverse effects of water contaminants like arsenic, fluoride and phosphate and their remediation, Journal of scientific and industrial research 69: 249 - 253.

Mobasherpour, I., Soulati Heshajin, M., Kazemzadeh, A., and Zakeri, M. (2007). Synthesis of nanocrystalline hydroxyapatite by using precipitation method. Journal of Alloys and Compounds 430: 330 - 333.

Mondal, M.K. (2009). Removal of Pb (II) ions from aqueous solution using activated tea waste: adsorption on a fixed-bed column, Journal of Environmental Management 90: 3266 - 3271.

Mori, H. (1996). Characterization of a Potential Catalytic Residue, Asp-133, in the High Affinity ATP-binding Site of Escherichia coli SecA, Translocation ATPase, Journal of Biological Chemistry 271 (17): 439 - 444.

Moriyama, K., Kojima, T., Minawa, Y., Matsumoto, S., and Nakamachi, K. (2001). Development of artificial seed crystal for crystallization of calcium phosphate, Environmental Technology 22: 1245 - 1252.

Mortul, M., Gubbons, M., and Gagnon, G.A. (2007). Phosphorus adsorption by naturally occuring materials and industrial by-products, Journal of Environmental Engineering and Science 6: 157 - 164.

Morse, G.K., Brett, S.W., Guy, J.A., and Lester, J.N. (1998). Review: Phosphorus removal and recovery technologies, Science of the Total Environment 212: 69 - 81.

Mueller, D.K., and Helsel, D.R. (1996). Nutrients in the Nation's Waters--Too Much of a Good Thing? , U.S. Geological Survey Circular 1136: 24 - 30.

Munch, E.V., and Barr, K. (2001). Controlled struvite crystallisation for removing phosphorus from anaerobic digester sidestreams, Water Research 35: 151 - 159.

Murray, J.J. (1986). Appropriate Use of Fluorides for Human Health, World Health Organisation, Geneva.

Nagamine, S., Ueda, T., Masuda, I., Mori, T., Sasaoka, E., and Joko, I. (2003). Removal of phosphorus from wastewater by crystallization on the surface of macroporous TiO_2 with a fibrous microstructure, Industrial and Engineering Chemistry Research 42: 4748 - 4752.

Najm, I.N. (1996). Mathematical modeling of PAC adsorption processes, Journal - American Water Works Association 88: 79 - 89.

Namasivayam, C., and Sangeetha, D. (2004). Equilibrium and kinetic studies of adsorption of phosphate onto $ZnCl_2$ activated coir pith carbon. Journal of Colloid and Interface Science 280: 359 - 365.

Namasivayam, C., and Holl, W.H. (2005). Quaternized biomass as an anion exchanger for the removal of nitrate and other anions from water, Journal of Chemical Technology and Biotechnology 80: 164 - 168.

National Health and Medical Research Council, (2011). Australia drinking water guidelines 6. In: National Water Quality Management Strategy, vol. 1. Commonwealth of Australia, Canberra.

Nawlakhe, W.G., Kulkarni, D.N., Pathak, B.N., and Bulusu, K.R. (1975). Defluoridation of water with alum by Nalgonda technique, Indian journal of environmental health 17: 26 - 65.

Nelson, N.O., Mikkelsen, R.L., and Hesterberg, D.L. (2003). Struvite precipitation in anaerobic swine lagoon liquid: effect of pH and Mg:P ratio and determination of rate constant. Bioresource Technology 89: 229 - 236.

Nemade, P.D., Vasudeva Rao, A., and Alappat, B.J. (2002). Removal of fluorides from water using low cost Adsorbents, Water Science and Technology: Water Supply 2: 311 - 317.

Noll, K.E., Gounaris, V., and Hou, W.S. (1992). Adsorption Technology for Air and Water Pollution Control, Lewis Publishers, Inc., Michigan.

Nwabanne, J.T., and Igbokwe, P.K. (2012). Adsorption performance of packed bed column for the removal of lead (II) using oil palm fibre, International Journal of Applied Science and Technology 2: 106 - 115.

Oguz, E. (2005). Sorption of phosphate from solid/liquid interface by fly ash. Colloids and Surfaces A: Physicochemical and Engineering Aspects 262: 113 - 117.

Oguz, E., and Ersoy, M. (2010). Removal of Cu2+ from aqueous solution by adsorption in a fixed bed column and Neural Network Modelling, Chemical Engineering Journal 164: 56 - 62.

Ohlinger, K.M., Young, T.M., and Schroeder, E. (1998). Predicting struvite formation in digestion, Water Research 26: 2229 - 2232.

Onyango, M.S., Kojima, Y., Aoyi, O., Bernardo, E.C., and Matsuda, H. (2004). Adsorption equilibrium modelling and solution chemistry dependence of fluoride removal from water by trivalent-cation-exchanged zeolite F-9, Journal of Colloid and Interface Science 279: 341 - 350.

Onyango, M.S., Kojima, Y., Kumar, A., Kuchar, D., Kubota, M., and Matsuda, H. (2006). Uptake of fluoride by Al^{3+} pretreated low-silica synthetic zeolites: adsorption equilibrium and rate studies, Separation Science and Technology 41: 683 - 704.

Orlando, U.S., Baes, A.U., Nishijima, W., and Okada, M. (2002). Preparation of Agricultural Residue Anion Exchangers and its Nitrate Maximum Adsorption Capacity, Chemosphere 48: 1041 - 1046.

Oscik, J. (1982). Adsorption at the solid/liquid interface. In Adsorption (ed. J. Oscik), Ellis Horwood, Chichester, 109 - 175.

Ozacar, M. (2003). Adsorption of Phosphate from Aqueous Solution onto Alunite, Chemosphere, 51: 321 - 327.

Öztürk, N., and Bektaş, T.E. (2004). Nitrate removal from aqueous solution by adsorption onto various materials, Journal of Hazardous Materials B112: 155 - 162.

Padmesh, T.V.N., Vijayaraghavan, K., Sekaran, G., and Velan, M. (2005). Batch and column studies on biosorption of acid dyes on fresh water macro alga Azolla filiculoides Journal of Hazardous Materials B 125: 121 - 129.

Palard, M., Champion, E., and Foucaud, S. (2008). Synthesis of silicated hydroxyapatite $Ca_{10}(PO_4)_6$-x(SiO_4)x$(OH)_2$-x, Journal of Solid State Chemistry (181): 1950 - 1960.

Panday, K.K., Prasad, G., and Singh, V.N. (1986). Mixed adsorbents for Cu(II) removal from aqueous solutions, Environmental Technology Letters, 7 (1-12): 547 - 554.

Paulson, E.G. (1977). Reducing fluoride in industrial wastewater, Chemical Engineering (New York), 84 (22): 89 - 94.

Peleka, E.N., and Deliyanni, E.A. (2009). Adsorptive removal of phosphates from aqueous solutions, Desalination 245: 357 - 371.

Peel, J.W., Reddy, K.J., Sullivan, B.P., and Bowen, J.M. (2003). Electrocatalytic reduction of nitrate in water, Water Resources 37: 2512 - 2519.

Phillips, D.H., Gu, B., Watson, D.B., and Parmele, C.S. (2008). Uranium removal from contaminated groundwater by synthetic resins, Water Research 42: 260 - 268.

Pintar, A., Batista, J., and Levec, J. (2001). Integrated ion exchange/catalytic process for efficient removal of nitrates from drinking water, Chemical Engineering Science 56: 1551 - 1559.

Pradhan, J., Das, J., Das, S., and Thakur, R.S. (1998). Adsorption of phosphate from aqueous solution using activated red mud, Journal of Colloid and Interface Science 204: 169 - 172.

Prakash, K.H, Kumar, R., Ooi, C.P., Cheang P, and Khor K.A. (2006). Conductometric study of precursor compound formation during wet-chemical synthesis of nanocrystalline hydroxyapatite. The Journal of Physical Chemistry B 110 (24): 457 - 462.

Primo, O., Rivero, M., Urtiaga, A., and Ortiz, I. (2009). Nitrate removal from electro-oxidized landfill leachate by ion exchange, Journal of Hazardous Materials 164: 389 - 393.

Prosnansky, M., Sakakibara, Y., and Kuroda, M. (2002). High-rate denitrification and SS rejection by biofilm-electrode reactor (BER) combined with microfiltration, Water Research 36 (19): 4801 - 4810.

Raichur, A.M., and Basu, M.J. (2001). Adsorption of fluoride onto mixed rare earth oxides, Separation and Purification Technology 24: 121 - 127.

Rawn, A.M., Perry Banta, A., and Pomeroy, R. (1937). Multiple-stage sewage sludge digestion, American Society of Civil Engineers 2116: 93 - 132.

Raynaud, S., Champion, E., Bernache-Assollant, D., and Thomas, P. (2002). Calcium phosphate apatites with variable Ca/P atomic ratio I. Synthesis, characterisation and thermal stability of powders, Biomaterials (23): 1065 - 1072.

Riahi, K., Thayer, B.B., Mammou, A.B., Ammar, A.B., and Jaafoura, M.H. (2009). Biosorption characteristics of phosphates from aqueous solution onto *Phoenix dactylifera* L. date palm fibers, Journal of Hazardous Materials 170: 511 - 519.

Romer, W. (2006). Plant availability of P from recycling products and phosphate fertilizers in a growth-chamber trial with rye seedlings, Journal of Plant Nutrition and Soil Science 169: 826 - 832.

Roques, H., Nugroho-Jeudy, L., and Lebugle, A. (1991). Phosphorus removal from wastewater by half-burned dolomite, Water Research 25: 959 - 965.

Ruthven, D.M. (1984). Principles of Adsorption and Adsorption Processes, John Wiely and Sons, New York.

Saha, B., Chakraborty, S., and Das, G. (2009). A mechanistic insight into enhanced and selective phosphate adsorption on a coated carboxylated surface, Journal of Colloid and Interface Science 331: 21 - 26.

Sakadevan, K., and Bavor, H.J. (1998). Phosphate adsorption characteristics of soils, slags and zeolite to be used as substrates in constructed wetland systems, Water Research 32: 393 - 399.

Samatya, S., Kabay, N., Yuksel, U., Arda, M., and Yuksel, M. (2006a). Removal of nitrate from aqueous solution by nitrate selective ion-exchange resins, Reactive and Functional Polymers 66: 1206 - 1214.

Samatya, S., Yuksel, U., Arda, M., Kabay, N., and Yuksel, M. (2006b). Investigation of selectivity and kinetic behaviour of strong-base ion exchange Purolite A520E for nitrate removal from aqueous solution, Separation Science and Technology 66: 1206 - 1214.

Samatya, S., Yuksel, U., Yuksel, M., and Kabay, N. (2007). Removal of fluoride from water by metal ions (Al3+, La3+ and ZrO2+) loaded natural zeolite, Separation Science and Technology 42: 2033 - 2047.

Sammons R.L., Thackray, A.C., Ledo, H.M., Marquis, P.M., Jones, I.P., Yong, P., and Macaskie, L.E. (2007). Characterisation and sintering of nano phase hydroxyapatite synthesised by a species of Serratia, Journal of Physics: Conference Series (93): 1-7.

Sansalone, J. L., and Ma, J. (2009). Parametric evalution of batch equilibria for stormwater phosphorus adsorption on aluminum oxide media, Journal of Environmental Engineering ASCE 135: 737 - 746.

Schoeman, J.J., and Steyn, A. (2003). Nitrate removal with reverse osmosis in a rural area in South Africa, Desalination 155: 15 - 26.

Seckler M. M., Bruinsma O. S. L. and Van Rosmalen G. M. (1996) Calcium phosphate precipitation in a fluidized bed in relation to process conditions: a black box approach, Water Research 30: 1677 - 1685.

Sengupta, S., and Pandit, A. (2011). Selective removal of phosphorus from wastewater combined with its recovery as a solid-phase fertilizer, Water Research 45: 3318 - 3330.

Shim, W.G., Abdul, J.M., Mohammad, T., Vigneswaran, S., Ngo, H.H., and Kandasamy, J. (2012). Biofilter in leachate treatment processes, Desalination and Water Treatment 41: 249 - 257.

Siddharthan, A., Seshadri, S.K., and Sampath Kumar, T.S.S. (2005). Rapid synthesis of calcium deficient hydroxyapatite nanoparticles by microwave irradiation, Trends in Biomaterials and Artificial Organs (18): 110 - 113.

Sigma-Aldrich (2013). www.sigmaaldrich.com. Accessed March 2013.

Sincero, A. P., and G. A. Sincero (2003). Physical-Chemical Treatment of Water and Wastewater, CRC Press, Boca Raton, Florida.

Sivasamy, A., Singh, K.P., Mohan, D., and Maruthamuthu, M. (2001). Studies on defluoridation of water by coal-based sorbents, Journal of Chemical Technology and Biotechnology 76: 717 - 722.

Sparks, D.L. (1989). Kinetics of Soil Chemical Processes, Academic Press Inc., New York.

Sparks, D.L. (2001). Elucidating the fundamental chemistry of soils: past and recent achievements and future frontiers, Geoderma 100: 303 - 319.

Soares, M.I.M. (2000). Biological denitrification of groundwater, Water, Air and Soil Pollution, 123: 183 - 193.

Sobczak, A., Kowalski, Z., and Wzorek, Z. (2009). Preparation of hydroxyapatite from animal bones, Acta of bioengineering and biomechanics 11: 23 - 28.

Socias-Viciana, M.M., Urena-Amate, M.D., Gonzalez-Pradas, E., Garcia- Cortes, M.J., and Lopez-Teruel, C. (2008). Nitrate removal by calcined hydrotalcite-type compounds, Clays and Clay Minerals 56: 2 - 9.

Solangi, I.B., Memon, S., and Bhanger, M.I. (2010). An excellent fluoride sorption behaviour of modified amberlite resin, Journal of Hazardous Materials 176: 186 - 192.

Song, Y.-H., Qiua, G.-L., Yuana, P., Cui, X.-Y., J.-F. Peng, Zeng, P., Duan, L., Xiang, L.-C., and Qian, F. (2011). Nutrients removal and recovery from anaerobically

digested swine wastewater by struvite crystallization without chemical additions, Journal of Hazardous Materials 190: 140 - 149.

Srinath, E. G., Sastry, C. A. and Pillai, S. C. (1959). Rapid removal of phosphorus from sewage by activated sludge, Experientia 15: 339 – 340

Srivastava, V.C., Prasad, B., Mishra, I.M., Mail, I.D., and Swamy, M.M. (2008). Prediction of breakthrough curves for sorptive removal of phenol by bagasse fly ash packed bed, Industrial and Engineering Chemistry Research 47: 1603 - 1613.

Stratful, I., Brett, S., Scrimshaw, M.B., and Lester, J.N. (1999). Biological phosphorus removal, its role in phosphorus recycling, Environmental Technology 20: 681 - 695.

Strickland T. (1999). Perspectives for phosphorus recovery offered by enhanced biological P removal, Environmental Technology 20 (7): 721 - 725.

Su., C., and Puls, R. (2004). Nitrate reduction by zerovalent iron: effects of formate, oxalate, citrate, chloride, sulfate, borate, and phosphate, Environmental Science and Technology 38: 2715 - 2720.

Sujana, M.G., Thakur, R.S., and Rao, S.B. (1998). Removal of fluoride from aqueous solution by using alum sludge, Journal of Colloid and Interface Science 206: 94 - 101.

Sujana, M.G., Pradhan, H.K., and Anand, S. (2009). Studies on sorption of some geomaterials for fluoride removal from aqueous solutions, Journal of Hazardous Materials 161: 120–125.

Sujanaa, M.G., Mishrab, A., and Acharyaa, B.C. (2013). Hydrous ferric oxide doped alginate beads for fluoride removal: adsorption kinetics and equilibrium studies, Applied Surface Science 270: 767 - 776.

Suksabye, P., Thiravetyan, P., and Nakbanpote W. (2008). Column study of chromium (VI) adsorption from electroplating industry by coconut coir pith, Journal of Hazardous Materials 160: 56 - 62.

Sundaram, C.S., Viswanathan, N., and Meenakshi, S. (2008). Uptake of fluoride by nanohydroxyapatite/ chitosan, a bioinorganic composite, Bioresource Technology 99: 8226 - 8230.

Suzuki, T. (1990). Adsorption engineering, Kodansha, Tokyo, Japan.

Tan, T.W., and Ng, H.Y. (2008). Influence of mixed liquor recycle ratio and dissolved oxygen on performance of pre-denitrification submerged membrane bioreactors, Water research 42 (4-5): 1122 – 1132.

Tang, Y., Guanc, X., Wang, J., Gaob, N., Mcphaild, M.R., and Chusuei, C.C. (2009). Fluoride adsorption onto granular ferric hydroxide: effects of ionic strength, pH, surface loading, and major co-existing anions, Journal of Hazardous Materials 171: 774 - 779.

Tate, C.H. and Arnold, K.F. (1990). Health and Aesthetic Aspects of Water Quality, Water Quality and Treatment, a Handbook of Community Water Supplies, Fourth Edition, F.W. Pontius, Editor, AWWA, McGraw-Hill, New York.

Teng, S., Wang, S., Gong, W., Liu, X., and Gao, B. (2009). Removal of fluoride by hydrous manganese oxide-coated alumina: performance and mechanism, Journal of Hazardous Materials 168: 1004 - 1011.

Tetsuji, C., Ning, T., Masamoto, T. and mashahiro, T. (1997). An ecotechnological removal system for fluoride in water by activated alumina, in Proceedings of 4th Asian Symposium on Ecotechnology, 30 September.

Thomas, H.C. (1944). Heterogeneous ion exchange in a flowing system, Journal of the American Chemical Society 66: 1466 - 1664.

Tien, C. (1994). Adsorption Calculations and Modeling. Butterworth- Heinemann, Boston.

Till, B.A., Weathers, L.J., and Alvarez, P.J.J. (1998). Fe (0)-supported autotrophic denitrification, Environmental Science and Technology 32: 634 - 639.

Tokunaga, S., Haron, S.A., Wasay, S.A., Wong, K.F., Laosangthum, K., and Uchiumi, A. (1995). Removal of fluoride ions from aqueous solutions by multivalent metal compounds, International Journal of Environmental Studies 48: 17 - 28.

Tor, A., Danaoglu, N., Arslan, G., and Cengeloglu, Y. (2009). Removal of fluoride from water by using granular red mud: batch and column studies, Journal of Hazardous Materials 164: 271 - 278.

Tovar-Gomez, R., Moreno-Virgen, M.R., Dena-Aguilar, J.A., Hernandez-Montoya, V., Bonilla-Petriciolet, A., and Montes-Moran, M.A. (2013). Modeling of fixed-bed adsorption of fluoride on bone char using a hybrid neural network approach, Chemical Engineering Journal 228: 1098 - 1109

Tripathy, S.S., Bersillon, J.L., and Gopal, K. (2006). Removal of fluoride from drinking water by adsorption onto alum-impregnated activated alumina, Separation and Purification Technology 50: 310 – 317.

Trivedi, P., and Axe, L. (2006). Long-term fate of metal contaminants in soils and sediments: role of intraparticle diffusion in hydrous metal oxides. In: Hamon, R., McLaughlin, M., and Lombi, E. (eds.), Natural Attenuation of Trace Element Availability in Soils. CRC Taylor and Francis Group, New York, 57 - 71.

Tseng, C., Potter, T.G., and Koopman, B. (1998). Effect of influent chemical oxygen demand to nitrogen ration on a partial nitrification/complete denitrification process, Water research 32 (1): 165 - 173.

Ueno, Y., and Fujii, M. (2001). Three years' experience of operating and selling recovered struvite from full-scale plant, Environmental Technology 22: 1373–1381.

Uludag-Demirer, S., and Othman, M. (2009). Removal of ammonium and phosphate from the supernatant of anaerobically digested waste activated sludge by chemical precipitation, Bioresource Technology 100: 3236 - 3244

Ungureanu, D. N., AngelescuRodica, N., Ion, M., Stoian, E.V. (2011). Synthesis and characterization of hydroxyapatite nanopowders by chemical precipitation, Proceeding of 10th WSEAS international conference on electronics, hardware, wireless and optical communications, and 10th WSEAS international conference on signal processing, robotics and automation, and 3rd WSEAS international conference on nanotechnology, and 2nd WSEAS international conference on Plasma-fusion-nuclear physics, 296 - 301.

Urano, K., Tachikawa, H., and Kitajima, M. (1992). Process development for removal and recovery of phosphorus from wastewater by a new adsorbent. 1. Preparation

method and adsorption capability of a new adsorbent, Industrial and Engineering Chemistry Research 30: 1893 - 1896.

U.S. Public Health Service, (1962). US Public Health Service Drinking Water Standards, US Government Printing Office, Department of Health Education and Welfare, Washington DC.

Valincius, G., Niaura, G., Kazakevicˇieneu,` B., Talaikyteu,`Z., Kazˇemeu` kaiteu,` M., Butkus, E., and Razumas, V. (2004). Anion effect on mediated electron transfer through ferrocene-terminated self-assembled monolayers, Langmuir 20: 6631 - 6638.

van Rijn, J., Tal, Y., and Schreier H.J. (2006). Denitrification in recirculating systems: Theory and applications, Aquacultural Engineering 34: 364 - 376.

van Rensburg, P., Musvoto, E.V., Wentzel, M.C., and Ekama, G.A. (2003). Modelling multiple mineral precipitations in anaerobic digester liquor, Water Research 37 (13): 3087 - 3097.

Verma, D.K., Hasan, S.H., Ranjan, D., and Banik, R.M. (2014). Modified biomass of *Phanerochaete chrysosporium* immobilized on luffa sponge for biosorption of hexavalent chromium, International Journal of Environmental Science and Technology, doi:10.1007/3/3762-013-0345-6.

Vermeulen T., Klein G., and Heister N. K. (1973). Adsorption and ion exchange, In Chemical Engineers Handbook, 5th edition (Edited by Perry R. H. and Chilton C. H.), Chap. 16. McGraw Hill, New York, USA.

Vigneswaran, S., and Visvanathan, C. (1995). Water Treatment Processes. Simple Options, CRC Press, Inc., Florida.

Vigneswaran, S., and Moon, H. (1999). Phosphorus removal by slag: experiments and mathematical modelling. In: Adsorption and its applications in industry and environmental protection, vol.2. Elsevier, Amsterdam.

Villadsen, J., and Stewart, W.E. (1967). Solution of boundary value problems by orthogonal collocation, Chemical Engineering Science 22: 1483 - 1501.

Villadsen, J., and Michelsen, M. L. (1978). Solution of Differential Equation Models by Polynomial Approximation, Prentice-Hall, New Jersey.

Viswanathan, N., and Meenakshi, S. (2010). Selective fluoride adsorption by a hydrotalcite/ chitosan composite, Applied Clay Science 48: 607 - 611.

Wang, Y., Gao, B.-Y., Yue, W.-W., and Yue, Q.-Y. (2007). Preparation and utilization of wheat straw anionic sorbent for the removal of nitrate from aqueous solution, Journal of Environmental Sciences 19: 1305 - 1310.

Wang, J., Zhang, Y., Feng, C., Li, J., and Li, G. (2009). Adsorption capacity for phosphorus comparison among activated alumina, silica sand and anthracite coal. Journal of Water Resource and Protection 4: 260 - 264.

Ward, M.H., de Kok T.M., Levallois, P., Brender, J., Gulis, G., Nolan, B.T., and VanDerslice, J. (2005). Workgroup report: drinking-water nitrate and health—recent findings and research needs, Environmental Health Perspectives 113: 1607 - 1614.

Wasik, E., Bohdziewicz, J., and Blasszezyk, M. (2001). Removal of nitrates from ground water by a hybrid process of biological denitrification and microfiltration membrane, Process Biochemistry 37: 57 - 64.

Weber, W.J., and Morris, J.C. (1963). Kinetics of adsorption on carbon from solution, Journal of the Sanitary Engineering Division - American Society of Civil Engineers 89: 31 - 60.

Weber, T.W., and Chakravorti, P.K. (1974). Pore and solid diffusion models for fixed bed adsorbent. Journal of American Institution of Chemical Engineers 20: 228 - 252.

Wendling, L.A., Douglas, G.B., Coleman, S., Yuan, Z. (2012). Nutrient and dissolved organic carbon removal from water using mining and metallurgic by-products, Water Research 46 (8): 2705 - 2717.

Westerhoff, P. (2003). Reduction of nitrate, bromate, and chlorate by zero valent iron (Fe0), Journal of Environmental Engineering 129: 10 - 16.

WHO (1996). Guidelines for Drinking water Quality, Volume 2, Health Criteria and Other Supporting Information, 2nd ed., World Health Organisation, Geneva.

WHO (2003). Guidelines for Drinking Water Quality, 3rd ed., World Health Organization, Geneva.

Wilke, C.R., and Chang, P. (1955). Correlation of Diffusion Coefficients in Dilute Solutions, AIChE Journal (1): 264 - 270.

Williams, S. (1999). Struvite precipitation in thesludgestreamat Slough wastewater treatment plant and opportunities for phosphorus recovery, Environmental Technology 20: 743 - 747.

Woods N.C., Sock S.M. and Daigger G.T. (1999). Phosphorus recovery technology modeling and feasibility evaluation for municipal wastewater treatment plants, Environmental Technology 20 (7): 663 - 679.

Wu, Y.Y., Bai, H.M., Zhou, J.Z., Chen, C.X., Xu, X., Xu, Y.F., and Qian, G.R. (2009). Thermal and chemical stability of Cu-Zn-Cr-LDHs prepared by accelerated carbonation, Applied Clay Science 42: 591 - 596.

www.aquascotland.com/_product_33602/Ion_Exchange_Ferr.

www.purolite.com-Purolite FerrIX A33E , Technical data, ISO 9002.

Xing, X., Gao, B.-Y., Zhong, Q.-Q., Yue, Q.-Y., and Li, Q. (2011). Sorption of nitrate onto aminecrosslinked wheat straw: characteristics, column sorption and desorption properties, Journal of Hazardous Materials 186: 206 - 211.

Xu, Y., Dai, Y., Zhou, J., Xu, Z.P., Qian, G., and Lu, G.Q.M. (2010a). Removal efficiency of arsenate and phosphate aqueous solution using layered double hydroxide materials: intercalation vs. precipitation, Journal of Materials Chemistry 20: 4684 - 4691.

Xu, X., Gao, B.-Y., Yue, Q.-Y., and Zhong, Q.-Q. (2010b). Preperation of agricultural by-product based anion exchanger and its utilization for nitrate and phosphate removal, Bioresource Technology 101: 8558 - 8564.

Xu, X., Gao, B., Yue, Q., and Zhong, Q. (2011). Sorption of phosphate onto giant reed based adsorbent: FTIR, Raman spectrum analysis and dynamic sorption/desorption properties in filter bed, Bioresource Technology 102: 5278 - 5282.

Xue, Y., Hou, H., and Zhu, S. (2009). Characteristics and mechanisms of phosphate adsorption onto basic oxygen furnace slag, Journal of Hazardous Materials 162: 973 - 980.

Yahaya, N.K.E.M., Abustan, I., Latiff, M.F.P.M., Bello, O.S., and Ahmad, M.A. (2011). Fixed–bed column study for Cu (II) removal from aqueous solutions using rice husk based activated carbon, International Journal of Engineering and Technology 11: 248 - 252.

Yan, L., Xu, Y., Yu, H., Xin, X., Wei, Q., and Du, B. (2010). Adsorption of phosphate from aqueous solution by hydroxyl-aluminum, hydroxyl-iron and hydroxyl-ironaluminium pillared bentonites, Journal of Hazardous Materials 179: 244 - 250.

Yang, R.T. (1986). Gas Separation by Adsorption Processes, Butterworths, Boston.

Yeoman, S., Stephenson, T., Lester, J.N., and Perry, R. (1988). The removal of phosphorus during wastewater treatment: A review. Environmental Pollution 49: 183 - 233.

Yi, W.G., and Lo, K.V. (2003). Phosphate recovery from greenhouse wastewater, Journal of Environmental Science and Health, Part B 38: 501 - 509.

Yoon, Y.H., and Nelson, J.H. (1984). Application of gas adsorption kinetics. I. A theoretical model for respirator cartridge service life, American Industrial Hygiene Association Journal 45: 509 - 516.

Yoshida, H., and Galinada, W.A. (2002). Equilibria for adsorption of phosphates on OH-type strongly basic ion exchanger, AIChE Journal 48: 2193 - 2202.

Young, D.M., and Crowell, A.D. (1962). Physical Adsorption of Gases, Butterworths, London.

Young, G.K., Bungay, H.R., Brown, L.M., and Parson, W.A. (1964). Chemical reduction of nitrate in water, Journal of the Water Pollution Control Federation 36: 395 - 398.

Zach-Maor, A., Semiat, R, and Shemer, H. (2011). Synthesis, performance, and modeling of immobilized nano-sized magnetite layer for phosphate removal, Journal of Colloid and Interface Science 357: 440 - 446.

Zagorodni, A.A. (2007). Ion exchange materials properties and applications. Elsevier BV, Amsterdam.

Zeng, L., Li, X., and Liu, J. (2004). Adsorptive removal of phosphate from aqueous solutions using iron tailings, Water Research 38: 1318 - 1326.

Zevenbergen, C., van Reeuwijk, L.P., Frapporti, G., Louws, R.J., and Schuiling, R.D. (1996). A simple method for defluoridation of drinking water at village level by adsorption on Ando soil in Kenya, Science of the Total Environment 188: 225 - 232.

Zhao, D., and Sengupta, A.K. (1998). Ultimate removal of phosphate from wastewater using a new class of polymeric ion exchangers, Water Resources 32: 1613 - 1625.

Zhan, Y., Lin, J., and Zhu, Z. (2011). Removal of nitrate from aqueous solution using etylpyridinium bromide (CPB) modified zeolite as adsorbent, Journal of Hazardous Materials 186: 1972 - 1978.

Zhang, J., and Stanforth, R. (2005). Slow adsorption reaction between arsenic species and Goethite (α-FeOOH): diffusion or heterogeneous surface reaction control, Langmuir 21: 2895 - 2901.

Zhang, G., Liu, H., Liu, R., and Qu, J. (2009). Removal of phosphate from water by a Fe–Mn binary oxide adsorbent, Journal of Colloid and Interface Science 335: 168 - 174.

Zhou, Y., Yu, C., and Shan, Y. (2004). Adsorption of fluoride from aqueous solution on La3+ impregnated crosslinked gelatin, Separation and Purification Technology 36: 89 - 94.